istituto nazionale di fisica nucleare
laboratori nazionali di frascati

# 2014
# ANNUAL REPORT

# ATLAS

P. Albicocco, M. Antonelli(Resp.),
M.M. Beretta, H. Bilokon, C. Brutti,

S. Cerioni (Tech.), V. Chiarella, M. Curatolo,
R. Di Nardo(Ass. Ric.), M. Dreucci, B. Esposito, M. Gatta (Tech.), C. Gatti,
P.F. Laurelli, C. La Storia(laur.), S. Lauciani(Tech.),
G. Maccarrone, A. Martini, G. Mancini(dott.), G. Nicoletti, G. Pileggi (Tech.),
B. Ponzio(Tech.), V. Russo(Tech.), A. Sansoni,
M. Testa, P. P. Valentini, T. Vassilieva (Tech.), E. Vilucchi.

In collaboration with:
Centro di Calcolo:
M. Pistoni, D. Spigone

May 6, 2015

# 1 Introduction

The activity of the ATLAS LNF group is focused on five items: Higgs four leptons analysis (R. Di Nardo is the group convener), Paricle Flow, PF, and Missing Transverse Energy reconstruction, MET, (M. Testa is the group convener), computing activity includin the PRIN tasks on Proof on Demand (the LNF Tier2 has been moved in the new computing room), Fast TracK (FTK) upgrade phase 1 activity, new Small Wheel for the upgrade of the muon system (G. Maccarrone is the INFN coordinator).

## 1.1 Properties of the Higgs boson

In the spirit of fully characterize the properties of the Higgs boson, discovered in 2012 at CERN by the ATLAS and CMS collaboration, during the 2013 and 2014 the Frascati group was fully involved in several measurements of the Higgs boson properties expoiting the $H \to ZZ* \to 4\ell$ decay channel. In particular the Frascati group gave an important contribution for the updated measurement of the Higgs boson mass, the differential cross section measurements in the $H \to ZZ* \to 4\ell$ channel performed for several observables related to the Higgs boson production and decay, the determination of the off-shell Higgs boson signal strength in the high-mass ZZ final state, the measurements of Higgs boson production and couplings in the four-lepton channel.

### 1.1.1 Higgs boson mass measurement with the $H \to ZZ^* \to 4\ell$ and $H \to \gamma\gamma$ decay channels

In order to measure the Higgs boson mass, a fit to the invariant mass spectra in the $H \to ZZ^* \to 4\ell$ and $H \to \gamma\gamma$ decay channels has been performed. In both channels the signal appears as a narrow peak resonance over a smooth background and the typical experimental resolutions in both channels ranges between 1.6–2 GeV for an Higgs boson mass of about 125 GeV. The mass is extracted from the invariant mass spectra fit without assumpions on the signal production and decay. With respect to the previous measurement [**?**], the $H \to \gamma\gamma$ channel profits of an improved calibration of the electron and photons energy measurements, resulting in a considerable reduction of the systematic uncertainties on their energy scales. In the $H \to ZZ^* \to 4\ell$ channel, a multivariate discriminant designed to increase the signal-to-background separation is used to reduce the expected statistical uncertainty while the systematic uncertainty are reduced with respect to the previous measurement [**?**] thanks to the improved electron energy calibration and the reduction of the muon momentum scale uncertainty. Fig. 1 shows the four-lepton (a) and the diphoton (b) invariant mass spectra for the selected candidates of the combined 7 TeV and 8 TeV data samples compared with MC expectations, and the value of the minus-two-log-likelihood as a function of $m_H$ for the individual $H \to \gamma\gamma$ and $H \to ZZ* \to 4\ell$ channels and their combination (c). In the combination the signal strengths for the two channels are allowed to vary independently The

combined mass measurement is $mH = 125.36 \pm 0.37(\text{stat}) \pm 0.18(\text{sys})$ GeV.

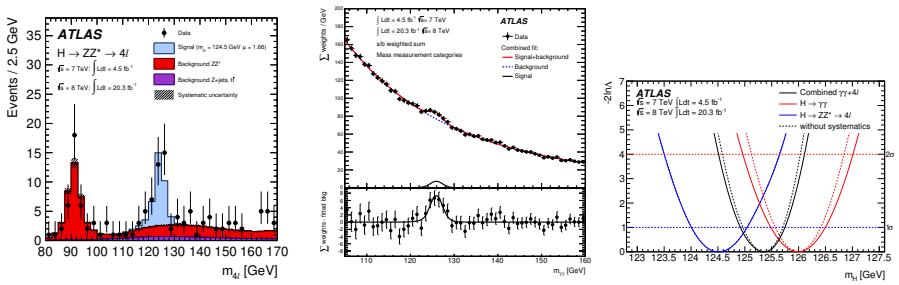


(a) (b) (c)

Figure 1: (a) Distribution of the four-lepton invariant mass for the selected candidates in the combined 7 TeV and 8 TeV data samples. Superimposed are the expected distributions of a SM Higgs boson signal for $m_H$=124.5 GeV normalized to the measured signal strength, as well as the expected $ZZ^*$ and reducible backgrounds. (b) Invariant mass distribution in the $H \to \gamma\gamma$ analysis for 7 TeV and 8 TeV data samples combined, showing weighted data points with errors, and the result of the simultaneous fit to all categories. The bottom plot shows the difference between the summed weights and the background component of the fit. (c) Value of the minus-two-log-likelihood as a function of $m_H$ for the individual $H \to \gamma\gamma$ and $H \to ZZ* \to 4\ell$ channels and their combination, where the signal strengths for the two channels are allowed to vary independently. The dashed lines show the statistical component of the mass measurements.

### 1.1.2 Fiducial and differential cross sections of Higgs boson production measured in the four-lepton decay channel at $\sqrt{(s)} = 8$ TeV

The differential measurements are performed for several observables related to the Higgs boson production and decay using an integrated luminosity of 20.3 fb[1] of pp collisions at $\sqrt{s} = 8$ TeV :

- the transverse momentum $p_{T,H}$ of the Higgs boson, that is sensitive to its production mechanisms as well as spin/CP quantum numbers, and can be used to test perturbative QCD predictions;
- the rapidity $|y_H|$ of the Higgs boson that is sensitive to the parton distribution functions (PDFs) of the proton;
- the invariant mass of the subleading lepton pair $m_{34}$ and the $\cos(\theta^*)$, being $\theta^*$ the decay angle of the leading lepton pair in the four-lepton rest frame with respect to the beam axis, that are sensitive to the Lagrangian structure of Higgs boson interactions (spin/CP,quantum numbers and higher-dimensional operators)

- the number of jets $n_{jets}$ and the transverse momentum of the leading jet $p_{T,jet}$ that are sensitive to QCD radiation effects and to the relative rates of Higgs boson production modes.

  In order to obtin these differential distribution, the measured signal yields, obtained after the background subtraction, are corrected for detector efficiency and resolution effects using correction factors obtained from simulated SM signal samples. Figure 2 shows the differential cross sections as a function of $p_{T,H}$ and $m_{34}$. The theoretical calculations are normalized to the most precise SM inclusive cross-section predictions currently available. The p-values quantifying the compatibility between data and predictions have been computed and no significant discrepancy is observed.

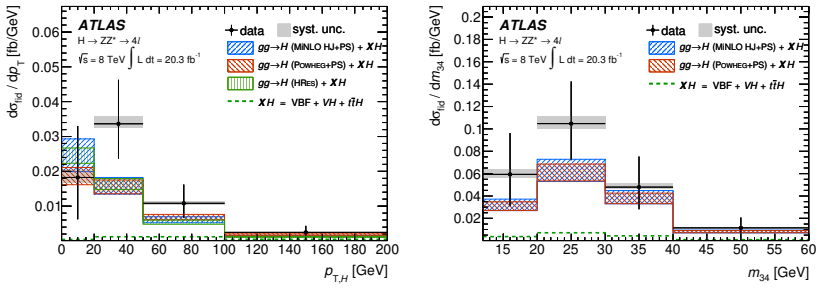


(a) (b)

Figure 2: Differential unfolded cross sections for the transverse momentum $p_{T,H}$ and the invariant mass of the subleading lepton pair $m_{34}$ in the $H \to ZZ^* \to 4\ell$ decay channel compared to different theoretical calculations of the ggF process: Powheg, Minlo and HRes2. The contributions from VBF, ZH/WH and ttH are added to the ggF distributions. All theoretical calculations are normalized to the most precise SM inclusive cross-section predictions currently available. The error bars on the data points show the total (stat. $\oplus$ syst.)uncertainty, while the grey bands denote the systematic uncertainties. The bands of the theoretical prediction indicate the total uncertainty.

## 2 Particle Flow Reconstruction and PileUp suppression

The increase of luminosity for for RunII, corresponding to up to 80 mean interaction per bunch crossing, will induce serious degradation of the jets and $\not{E}_T$ resolutions and increase in fake rate contamination from Pileup jets.
Standard ATLAS reconstruction exploits several techniques to mitigate Pileup effects in the jets and in the $\not{E}_T$ reconstruction. These techniques are aimed to improve resolution and reduce the fake rate of jet and $\not{E}_T$.

One well established approach is calorimeter based and uses the "Jet Area" method[**?**], which basically evaluates the average energy Pileup contribution under the area of the jet and subtract it. This approach has the intrinsic limitation to not be able to capture local Pileup fluctuations, limiting therefore the resolution improvements and the rejection of Pileup jets. Other local approaches based on tracks have been develop to reduce Pileup jets rate. They exploit the possibility of extrapolating the tracks to the interaction vertex and therefore to identify a signal jet coming from the hard scatter vertex from the Pileup Jets coming from other Pileup vertices[**?**]. Even if those techniques are track-based, the constituents of the jets are calorimeter clusters. Therefore, no improvement in the resolution of jets is expected and signal jets will still suffer resolution degradation from Pileup contamination.

To face the future unprecedented Pileup conditions a Particle-Flow reconstruction has been revisited and developed within the collaboration. This kind of reconstruction can maximally mitigate Pileup effects by exploiting the correlations among the inner detector and the calorimeter. Through the association between tracks and calorimeter deposits and the track pointing to the interactions vertices, calorimeter energy deposits coming from Pileup interactions can be removed in the jets and $\not{E}_T$ reconstruction. Large improvements in resolutions and fake rate reduction can be therefore achieved. Figure 3 (top) shows the fractional $p_T$ resolution of calorimeter based standard jets (red and ligh blue[1]), calorimeter based standard jets with improved average track-based calibration (blue) and Particle-Flow jets, based on tracks and calorimeter signals. The bottom of figure 3 shows the resolution on the $\eta$ and $\phi$ jet directions versus the truth $p_T$ of the jet.

# 3 Performances of the ATLAS High Level Trigger using a Particle Flow algorithm based on FTK tracks for $ZH \to \nu\bar{\nu}b\bar{b}$

The $H \to b\bar{b}$ decay is fundamental to study the coupling of the Higgs-boson to down-type quarks. It has not been yet observed at ATLAS. Because of the overwhelming QCD background, this decay can be observed only if the Higgs boson is produced in association with $W/Z$ bosons or top-quarks pairs. In particular the $ZH \to \nu\bar{\nu}b\bar{b}$ is one of the most sensitivity channel. It relies on a trigger on $\not{E}_T$ with a threshold which was 70 GeV during RunI and that will be raised to 90 GeV during RunII, to face the increased pile-up conditions. The increase of threshold induces a dangerous loss of signal efficiency, which can be mitigated using alternative $\not{E}_T$ reconstruction and/or trigger chains.

[1] using Local Hadron and electronmagnetic calibrations respectively

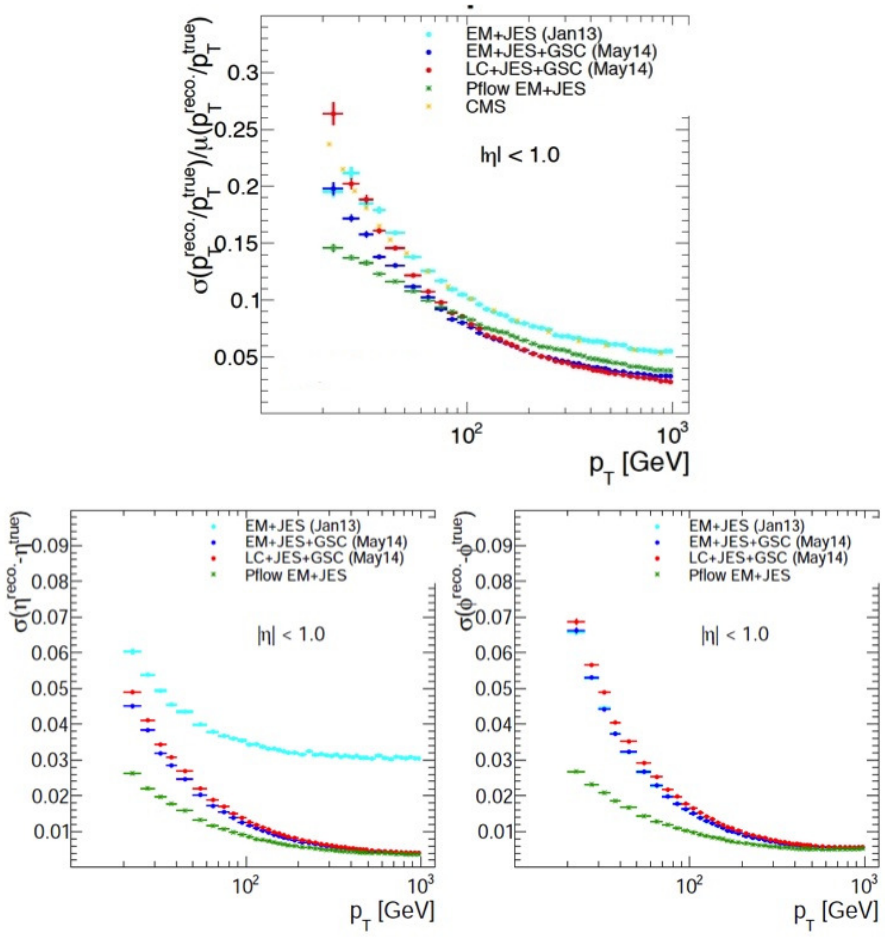


Figure 3: Fractional resolution on jet $p_T$ (top) and on the $\eta$ and $\phi$ directions (bottom) of calorimeter based standard jets (red and ligh blue curves), calorimeter based standard jets with improved average track-based calibration (blue curve) and Particle-Flow jets (green curve), based on tracks and calorimeter signals.

We studied new High Level Trigger (HLT) chains to select $ZH \to \nu\bar{\nu}b\bar{b}$ events, using FTK tracks [**?**] in combination with the particle-flow algorithm to reconstructed $\not\!\!E_T$ and jets. In Figure 4 the HLT efficiency is shown vs $E_T^{miss,truth}$ for different configurations: for the black curve the fully calorimeter $\not\!\!E_T$ reconstruction is used (as for RunI)[2], for the red

[2]due to the small statistics of the samples, a cut at 80 GeV instead that at 90 GeV has been used

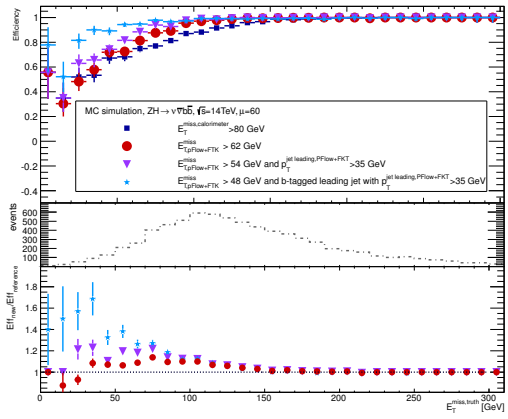


Figure 4: Efficiencies to select $ZH \rightarrow \nu\bar{\nu}b\bar{b}$ events vs $E_T^{miss,truth}$ for different $\not\!\!E_T$ reconstruction and trigger chains (see text)

curve the $\not\!\!E_T$ is reconstrued using the particle-flow algorithm with FTK tracks, for the violet and azure curves additional requirements on the $p_T$ and the b-tagging of the leading jet are applied. All the configurations give the same HLT rate. Using the best configuration (azure curve) an average increase on the HLT signal efficiency of 8% , up to 20% at low $E_T^{miss,truth}$, has been obtained.

# 4 Large Eta Studies for Phase-II upgrade

After the "Phase-I" upgrade in 2018, the LHC will undergo a "Phase-II" upgrade in 2023, to deliver the instantaneous luminosity o $5{\times}10^{34} cm^{-2} s^{-1}$, a factor 10 beyond its design value, corresponding to unprecedented PileUp conditions with an a average of 140 interactions per crossing. The ATLAS detector will undergoes upgrades to maintain its capabilities. In particular the Inner Detector (ID) will be substituted by a new, all-silicon Inner Tracker (ITk), whose default layout extends maximally to $|\eta|$ =2.7. Currently important studies are on going to evaluate the benefits of extending in $\eta$ the ITk, considering either longer pixel barrel layers and/or additional pixel disks or rings [**?**]. There is tremendous potential for improved performance for jets and $\not\!\!E_T$ in the very forward region. Tracking information can be used by tagging pile-up jets in the forward region as has been done in the central region for Run I. Forward pile-up rejection induces an improvement in $\not\!\!E_T$ as well. The variable used to study the forward pile-up jet tagging is $R_{pT} = \frac{\Sigma_k p_T^{trk_k}(PV_0)}{p_T^{jet}}$ which computes the scalar sum of the $p_T$ of the charged tracks associated with a particular jet, which are also

associated with the primary vertex (PV0 ), and normalizes this to the $p_T$ of the relevant jet. Small values of $R_{pT}$ correspond to jets with very small charged fraction associated with the primary vertex, and hence very likely to be pileup jet. The studies performed so far used smearing functions to mimic reconstructed tracks from generated truth particles. After applying a requirement that $R_{pT} > 0.2$, a rejection of pileup jets by roughly a factor of 100 for $|\eta| > 2.5$ is achievable with an inefficiency for the signal jets from the primary vertex of only about 10% (Figure 5, left). Although this performance is somewhat worse than for $|\eta| < 2.5$, it is still a very powerful incentive to make more detailed studies. The effect of forward pile-up jets suppression in $\not\!\!E_T$ resolution can be seen in Figure 5,right. It is apparent that the use of forward tracks for the soft component of $\not\!\!E_T$ does not affect the resolution (blue/red vs black/orange curve), while the use of $R_{pT}$ to suppress forward pileup jets results in an improvement in $\not\!\!E_T$ resolution of about 30% (red/orange vs blue/black curves)

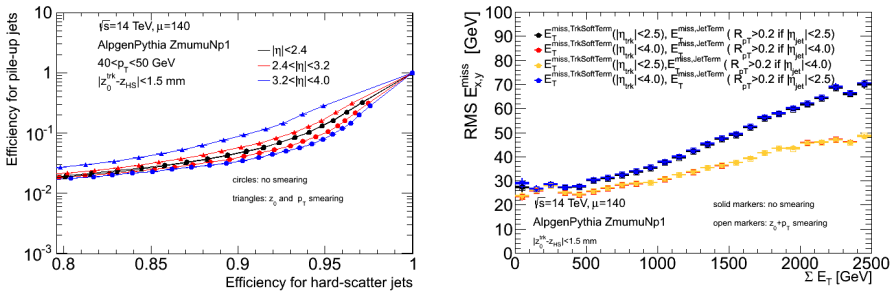


Figure 5: Top: the rejection for the background pileup jets versus the efficiency for the signal jets. Bottom: $\not\!\!E_T$ resolution with and without soft forward tracks and forward pile-up jet rejection

# 5 Tier-2

## 5.1 Activity during 2014

During the year 2014 the Frascati Tier-2 successfully and continuously performed all the typical activities of an ATLAS Tier-2: Monte Carlo production and users and physics groups analysis, as we can see from the chart in fig.6 left, which highlights the different activities performed in the Tier-2 in 2014.

Moreover, the efficiency of the site was always maintained above 90share of data consistent with its size. fig.6 shows the overall wall clock consump-

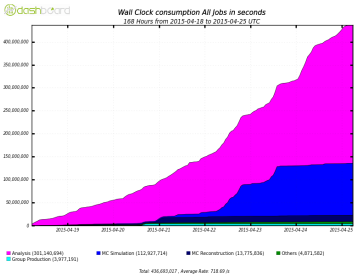


Figure 6: Wall clock time of all the jobs at LNF Tier-2 in 2014

tions of all the jobs at Frascati Tier-2, while the number of all the jobs run at Frascati Tier-2 is reported in fig.7.

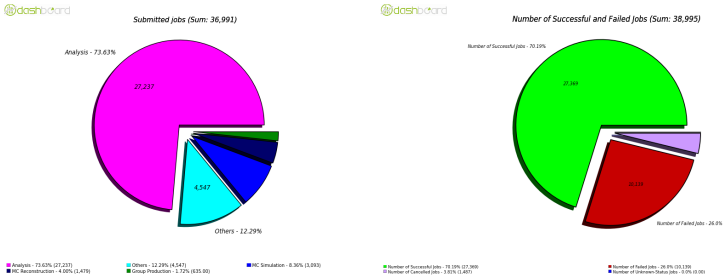


Figure 7: Jobs run at Frascati Tier-2 in 2014. Left: Submitted jobs. Right: successful and failed jobs

Among the most significant activities that involved the Tier-2 and Tier-3 staff we can mention the participation in the INFN computing PRIN, with the test activity of the analysis tool PROOF on Demand (PoD). This activity started in 2012 in collaboration with CERN developers and the other ATLAS Italian Tier-2s, and continued in 2014 in order to test PoD with the new ATLAS Prodsys2 workload management system and the new PROOF features of dynamic workers addition: the addition of new enabled workers to an already started PROOF-based analysis,
About the participation of the Tier-2 staff in the ATLAS computing activities, we should mention the role of the VO manager assumed by the Tier-2 responsiblle. This activity is of primary importance for the experiment, in fact, it is recognized as in kind contribution of the Italian group. Finally, we should mention that the Tier-2 farm was successfully moved in a new computing room thanks to the efforts of many members of the LNF ATLAS group: engineers, researchers and technologists. This will allow a future expansion beyond the current provisions of the experiment, as well as the possibility to open the Tier-2 to the calculation of other experiments.

### 5.2 Collaboration with INAF-OAR for CTA computing

The CTA project will involve INFN and INAF in the coming years. It is considered strategic, for both institutions, to develop, in synergy, the aspects of the project related to calculation. To integrate different skills and experiences in developing scientific software for data analysis and simulations, the approach is the gradual evolution of the commitment in the project through a modular development that addresses in succession, the need for calculation for:

- CTA Prototype Small Size Dual Mirror Telescope (SST-2M);
- Mini Array of Small Size Dual Mirror Telescope in the context of CTA;
- CTA Data Center.

The goal for the CTA data center is to get to an Italian solution that combines experiences in the management of large computing infrastructures (INFN) and implementation of softwares for data analysis and management of archives and astronomy databases (INAF).
The choice for the Laboratories of Frascati depends on the proximity to the INAF structure that develops and coordinates the software, the archive and the database.
In the light of the experience gained in this first phase, we will proceed, then, to integrate the archive and analysis system mini array of SST-2M, that will be installed at the site on the south of the observatory CTA. The software and the archive are developed by INAF - Astronomical Observatory of Rome, Monte Porzio Catone - and its integration into the computing system of the Tier-2 at LNF is expected.

## 6 Test of Micromegas chambers at the LNF BTF

During the second week of July 2014 we performed tests at the Dafne test-beam facility (BTF) with a particular type of micormegas chamber. This chamber, QF in the following, was constructed with resistive strips not aligned to the readout strips with the pourpose of understanding the impact on position measurement. QF has four different sectors: a sector with resistive strips aligned with readout strips; a sector with resistive strip shifted by half pitch with respect to readout strips; two sectors with resistive strips inclined by 1 and 2 degrees with respect to the readout

strips. The test was done using three standard micromegas as a reference tracker. The chambers, mounted on a frame, were put upon a remotable table to perform a scan by changing the relative position of the frame with respect to the beam (left panel of Fig. 8). On the right panel of Fig. 8 we show an example of reconstructed event. The chamber strip-planes are represented by blue segments. The QF is rotated by thirty degrees to study its performance in the micro-TPC mode. We performed several

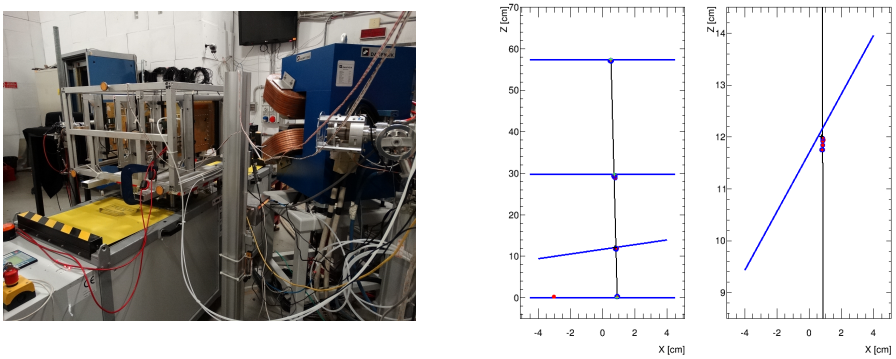


Figure 8: Left: Experimental setup of the test beam. Four micromegas chamber are mounted on a frame and put upon the remotable table just in front of the beam exit point. Right: Example of recontructed track. In the QF chamber, inclined by 30 degrees, the track is reconstructed using the microTPC technique. Blue points represent the hits on the strips while black markers represent the cluster centroid on the strip plane. Electrons enters from the bottom.

scans of the four QF regions, with QF at 0 and 30 degrees inclination, taking data for about 7 days. After analyzing data we observed for the first time the impact of the peculiar QF geometry on the reconstruction of the position in micro-TPC mode. These results have been discussed in our Collaboration. Further studies are ongoing.

# 7 Test of Micromegas prototypes with cosmic rays

We put in operation and succesfully tested our first prototype of a micromegas quadruplet. The tests to determine prototype performance were done both with an external tracker and in a standalone way. On the left panel of Fig. 9 we show the setup during a test with no reference tracker. The four strip-planes are instrumented with four apv-chips each, for a total of about 500 strips readout per plane. An example of reconstructed

event is shown in the right panel of Fig. 9. The blue points represent the hits on the strips while black markers represent the cluster centroid on the strip plane.

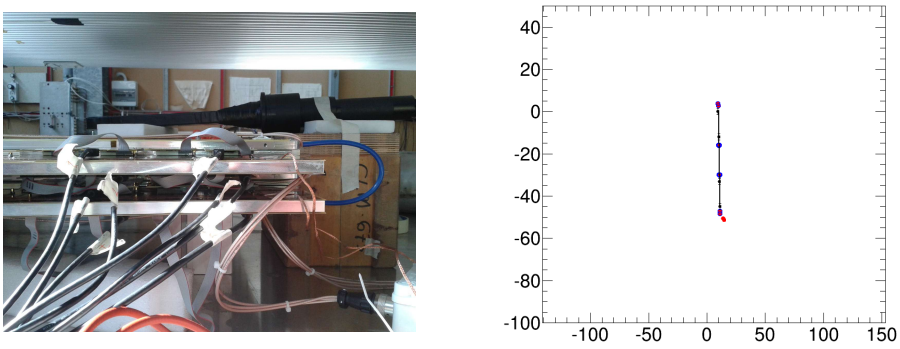


Figure 9: Left: Detail of the micromegas quadruplet with the four planes instrumented with four apv-chips each, during a test with cosmic rays. Right: Example of reconstructed track. Blue points represent the hits on the strips while black markers represent the cluster centroid on the strip plane. Axes values are in millimeters. Cosmic rays arrives from top.

# 8 FTK

The trigger is a fundamental part of any experiment at hadron colliders. It is needed to select on-line the interesting low cross-section physics from the huge QCD background. Experience at high luminosity hadron collider experiments shows that controlling trigger rates at high instantaneous luminosity can be extremely challenging. As the luminosity increases, physics goals change in response to new discoveries, and detector aging. It is thus essential that the trigger system be flexible and robust, and redundant and significant operating margin. Providing high quality track reconstruction over the full ATLAS Inner Detector by the start of processing in the level-2 computer farm can be an important element in achieving these goals. With the goal to improve and make more robust the ATLAS trigger, during summer 2007 the group joined the Fast-Track (FTK) proposal for A hardware track finder for the ATLAS trigger. This is a proposal to build a hardware track finder as an upgrade to the ATLAS trigger. It will provide global reconstruction of tracks above 1 GeV/c in the silicon detectors, with high quality helix parameters, by the beginning of level-2 trigger processing. FTK can be particularly important for the

selection of 3rd-generation fermions (b and ?). These have enormous background from QCD jets, which can be quickly rejected in level-2 if reconstructed tracks are available early. This RD proposal was completed with the submission of the FTK Technical Proposal that was finally approved by the ATLAS collaboration meeting in June 2011. We are continuing the design and prototyping RD aiming to prepare the FastTrack Technical Design Report to be submitted in Spring 2013. The FTK processor performs pattern recognition with a custom device called the Associative Memory (AM). It is an array of VLSI chips that stores pre-calculated trajectories for a ultra-fast comparison with data. The first way to reduce the combinatorial at high luminosity is to work with better resolution in the AM. In order to do that, we will need a new AM chip with a high density of patterns, so that all possible tracks with a thinner resolution can be stored in the AM. Even with better resolution the number of candidate tracks that the AM will find at these high instantaneous luminosities will be very large. For this reason we redesigned the FTK architecture to increase the internal parallelism and data-flow to accommodate a larger flux of data. For this purpose it was essential a new ideas. The efficiency curves for patterns is slowly increasing for efficiencies above 70%. This is due to the fact that many low probability patterns are needed to gain the missing efficiency. This is a consequence of the fact that the AM performs pattern recognition with a fixed resolution. We developed the idea of variable resolution patterns that increases the equivalent number of pattern per AMchip by a factor 3-5 with a corresponding reduction in hardware size [doi:10.1109/ANIMMA.2011.6172856]. In the beginning of 2014 we have completed the design of the AMchip05 whose aim was testing the final AM chip architecture. This chip has all the features of the final AMchip but, as prototype is small in area and has less memory banks. Moreover it contains two different architectures of the memory cell layer to be tested. The first architecture, designed by LNF, is based on a analog mixed digital approach to minimize the power consumption. Power reduction is reached minimizing the bit line parasitic capacitance, and reducing the power supply voltages to less than 1V. The price of this approach is an increasing in the silicon area of the memory layer of about 15% compared with standard memory layer, and an increasing in power distribution complexity inside the chip due to lots of different power domains. The second architecture is based on a fully digital architecture, it is proposed by INFN Milan. Even in this case the goal is the reduction of the power consumption, and is reached optimizing all the parasitic capacitance. The AMchip05 was submitted to foundry in March. Due to the high occupancy of the IBL ATLAS pixel layer, the previous version of the FTK IM board based on Xilinx Spartan6 FPGA could not process all the data coming from the detector. We have developed this board together with FTK japanese group of Waseda University. As responsible of this board the FTK collaboration ask us to develop a new version of the FTK IM based on a Xilinx Artix7 FPGA 1. This is a more recent and powerfull

FPGA. The design last June and July with me and a full time technician from LNF Electronic Service. The first prototype arrive at LNF in the September and was tested in October and November.

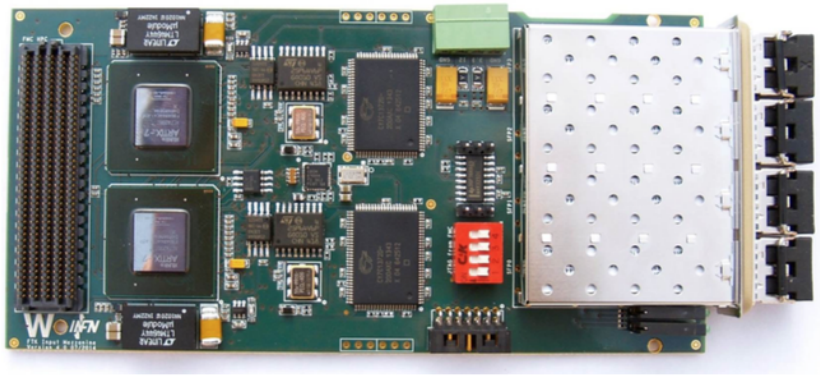

Figure 10: New version of the FTK IM with Artix7

In the same period of the development of the new FTK IM we developed also the test board of the AMchip05 that was submitted in March. This board allow the access all the input and output pins of the AMchip05 from a test board on which an FPGA is mounted. The programmable logic act as pattern generator and logic analyzer. The first prototype of this board was ready to be used in July when the chip arrive from foundry. In October we have developed also a new version of the board in which we have included the power supply part for the chip with the single supply current measurement through an SPI analog to digital converter. As responsible of the test procedure for the AMchip, in the last part of the year we have started to develop a test procedure for the final version of the chip basing on the results obtained for the AMchip05 tests that we have performed even in LNF.

**Public presentations:**

– G.Mancini,"Introduction to Higgs differential cross-section measurements", ATLAS Higgs Workshop, Rome 14th-18th April 2014.

– G.Mancini,"Differential cross section measurements of the Higgs boson in the $H \to ZZ^* \to 4l$ and $H \to gg$ decay channels" (Poster),presented at IFAE 2014,L' Aquila, 9th-11th April 2014.

– R.Di Nardo,"ATLAS Higgs off-shell and interferometry in Run 1 and wish list for Run 2", Higgs (N)NLO MC and Tools Workshop for LHC RUN-2, 17-19 December 2014, CERN

– R.Di Nardo,"Introduction to the Higgs session ", ATLAS-Italy Workshop on physics and upgrade for HL-LHC program, January 13-16 2014, Bologna

– R.Di Nardo,"SM Higgs results: bosonic channels", ATLAS Week, 15-20 June 2014, Sibiu/Hermannstadt

– R.Di Nardo,"Results, precision and performances achieved with Run1 data", $H \to ZZ^*$ Workshop, 18-19 October 2014 , CERN

– ATLAS Collaboration, "Pile-up Suppression in Missing Transverse Momentum Reconstruction in the ATLAS Experiment in Proton-Proton Collisions at $\sqrt{s} = 8$ TeV", ATLAS-CONF-2014-019

– Annovi A., Antonelli M., Beretta M., Testa M. et al. "Fast TracKer (FTK) Performance", ATL-COM-DAQ-2014-011

– C. Lastoria, "Performances of the ATLAS High Level Trigger using a Particle Flow algorithm based on FTK tracks of $ZH \to v\bar{v}b\bar{b}$"

– M.Testa for the ATLAS Collaboration, "ATLAS Higgs to diboson", Higgs Hunting 2014

**Publications and internal documents:**

– "Fiducial and differential cross sections of Higgs boson production measured in the four-lepton decay channel in pp collisions at $\sqrt{s} = 8$ TeV with the ATLAS detector", Physics Letters B 738 (2014) 234-253, 14th August 2014.

– "Measurement of the Higgs boson mass from the $H \to \gamma\gamma$ and $H \to ZZ^* \to 4\ell$ channels with the ATLAS detector using 25 fb$^{-1}$ of $pp$ collision data," Phys. Rev. D **90**, no. 5, 052004 (2014)

– "Determination of the off-shell Higgs boson signal strength in the high-mass ZZ and WW final states with the ATLAS detector", submited to EPJC 2015/03/03

– "Measurements of Higgs boson production and couplings in the four-lepton channel in pp collisions at center-of-mass energies of 7 and 8 TeV with the ATLAS detector," Phys. Rev. D **91** (2015) 1, 012006

– PoD-2012R. Di Nardo et al., Enabling data analysis la PROOF on the Italian ATLAS Tier-2s using PoD J. Phys.: Conf. Ser. 396 (2012) 032043, [http://iopscience.iop.org/1742-6596/396/3/032043/].

– PoD-2013E. Vilucchi et al., "PROOF-based analysis on the ATLAS Grid facilities: first experience with the PoD/PanDa plugin", 2014 J. Phys.: Conf. Ser. 513 032102, [http://iopscience.iop.org/1742-6596/513/3/032102].
– PoD-2015R. Di Nardo et al, "PROOF-based analysis on ATLAS Italian Tiers with Prodsys2 and Rucio", accepted poster at CHEP 2015 workshop.
– gridE. Vilucchi, "GRID", talk at "1st Synergy LNF-OAR Workshop", Frascati (RM), INFN-Laboratori Nazionali di Frascati, 16-17 aprile 2014, [https://agenda.infn.it/getFile.py/access?contribId=12&sessionId=3&resId=0&mater

# *BABAR*

R. de Sangro, G. Finocchiaro (Resp.), S. Martellotti (post-doc), B. Oberhof (post-doc)
I. Peruzzi (ass.), M. Piccolo (ass.), M. Rama, A. Zallo (ass.)

## 1 Introduction

The *BABAR* experiment has been running at the PEP-II asymmetric $B$ factory of the SLAC National Laboratory (Stanford, USA) from 2000 to 2008, collecting a data sample corresponding to approximately $0.5\,\mathrm{ab}^{-1}$. Analysis of this large data set is still ongoing, and resulted in about 20 papers published in 2014.

Members of the LNF group have contributed to the writing of the "Physics of $B$ Factories Book", a joint effort of the *BABAR* and Belle collaborations. The book, a comprehensive description of the $B$-factory experiments, of the data taking, the analysis techniques, and the physics results obtained has been published in 2014.

A PhD student member of the group has completed his doctoral thesis "Measurement of radiative leptonic $\tau$ decays $\tau \to \ell\gamma\nu\bar{\nu}$ ($\ell = e, \mu$) at *BABAR*", discussed in the following section.

## 2 Measurement of radiative $\tau$ decays at *BABAR*

Leptonic decays are generally well suited to investigate the Lorentz structure of electroweak interactions in a model-independent way. In particular, leptonic radiative decays $\tau \to \ell\gamma\nu\bar{\nu}$, where the charged lepton ($\ell$) is either an electron ($e$) or a muon ($\mu$), have been studied for a long time because they are sensitive to the anomalous magnetic moment of the $\tau$ lepton. At tree level, these decays can proceed through three Feynman diagrams depending on whether the photon is emitted by the incoming $\tau$, the outgoing charged lepton, or the intermediate W boson. The amplitude for the emission of the photon by the intermediate boson is suppressed by a factor $(m_\tau/M_w)^2$ with respect to a photon from the incoming/outgoing fermions and is thus negligible with respect to next-to-leading order QED radiative corrections. Both branching fractions have been measured by the CLEO collaboration. CLEO obtained $BF(\tau \to \mu\gamma\nu\bar{\nu}) = (3.61 \pm 0.16 \pm 0.35) \times 10^{-3}$, and $BF(\tau \to e\gamma\nu\bar{\nu}) = (1.75 \pm 0.06 \pm 0.17) \times 10^{-2}$ for a minimum photon energy of 10 MeV in the $\tau$ rest frame.

In our work we also perform a measurement of $\tau \to \ell\gamma\nu\bar{\nu}$ branching fractions for a minimum photon energy of 10 MeV in the $\tau$ rest frame.

The analysis uses data recorded by the *BABAR* detector at the PEP-II asymmetric-energy $e^+e^-$ storage rings operated at the SLAC National Accelerator Laboratory. The data sample consists of 431 fb of $e^+e^-$ collisions (about $400 \times 10^6$ $\tau$ pairs) recorded at the center-of-mass energy (CM) of 10.58 GeV. With our analysis we find $BF(\tau \to \mu\gamma\nu\bar{\nu}) =$

$(3.69 \pm 0.0 \pm 0.10)10^{-3}$, and $BF(\tau \to e\gamma\nu\bar{\nu}) = (1.847 \pm 0.015 \pm 0.052) \times 10^{-2}$, where the first error is statistical and the second is systematic. These results are more precise by a factor of three compared to previous experimental measurements. Our results are in agreement with the Standard Model values at tree level, $BF(\tau \to \mu\gamma\nu\bar{\nu}) = 3.67 \times 10^{-3}$, and $BF(\tau \to e\gamma\nu\bar{\nu}) = 1.84 \times 10^{-2}$, and with current experimental bounds.

**Conference Talks by LNF authors in 2014**

1. **"Measurement of the branching fractions of radiative leptonic tau decays $\tau \to \ell\gamma\nu\bar{\nu}$ $(\ell = e, \mu)$ at *BABAR*"**
   B. Oberhof
   The 13th International Workshop on Tau Lepton Physics Aachen, Germany, 15-19 September, 2014.

2. **"Measurement of radiative leptonic $\tau$ decays $\tau \to \ell\gamma\nu\bar{\nu}$ $(\ell = e, \mu)$ at *BABAR*"**
   B. Oberhof
   100° congresso SIF Pisa, Settembre 2014 http://www.sif.it/attivita/congresso/100.

3. **"Measurement of branching fractions of radiative leptonic $\tau$ decays $\tau \to \ell\gamma\nu\bar{\nu}$ $(\ell = e, \mu)$ at *BABAR*"**
   B. Oberhof
   Meeting KEK-FF & B2TIP - http://kds.kek.jp/conferenceDisplay.py?confId=15873.

**Conference papers by LNF authors in 2014**

1. **"Direct observation of time-reversal violation in $B^0$ decays"**
   B. Oberhof
   Proceedings of Tau 2014, Nuclear and Particle Physics Proceedings (2015), pp. 12-15
   DOI information: 10.1016/j.nuclphysbps.2015.02.003

**Papers published by *BABAR* in 2014**

In 2014 the *BABAR* collaboration published 16 papers on Phys. Rev. D, three papers on Phys. Rev. Lett. and one on Eur. Phys. J. The complete list can be retrieved from the inspire database (http://inspirehep.net).

# Belle II

Composition of the group: R. de Sangro (staff, resp), Erika De Lucia (staff), Giuseppe Finocchiaro (staff), Benjamin Oberhof (post doc), Piero Patteri(staff), Ida Peruzzi (ass.) , Marcello Piccolo (ass.).
In collaboration with: Alessandro Russo (tec), Andrea Zossi (tec).

## Introduction

The BABAR and Belle experiments recorded a total of over a billion Y(4S)→B $\bar{B}$ events (at the B-factories PEP-II at SLAC and KEKB at KEK, respectively), and were extremely successful in discovering CP violation effects in B decays and understanding the nature of heavy quarks and leptons.
Our group worked on BABAR since the original proposal in 1995, and successively participated in the SuperB project, aimed at the construction of an $e^+e^-$ collider with 100 times the PEP-II luminosity.
Once SuperB was cancelled for lack of adequate funding, we decided to carry on the same line of research at KEK, where the local accelerator was being upgraded in order to reach similar performances. This choice was in line with LNF's long standing tradition in playing an important role in electron positron colliders Physics. Our group was accepted into the BELLE-II collaboration in July 2013, together with eight other INFN Institutions, for a total of about 50 physicists.
The KEK-B machine, now called SuperKEKB, has undergone substantial modifications which were almost completed in 2014: the magnetic lattice has been re-designated to reduce the emittance, the final focus has been redone, a new beam pipe has been installed, the RF system has been modified and a new damping ring and positron target built. Fig. 1 shows the new machine layout. The design luminosity is $8x10^{35}$ $cm^{-2}$ $s^{-1}$ with a projected integrated luminosity of 50 $ab^{-1}$ by 2022-23.
Because of the increased level of background, the Belle II detector has to cope with higher occupancy and radiation damage than the Belle detector. Furthermore the increased event rate puts high demands on trigger, data acquisition, and computing. To be able to operate at the conditions at the SuperKEKB collider, the components of the Belle detector are either upgraded or replaced by new ones.

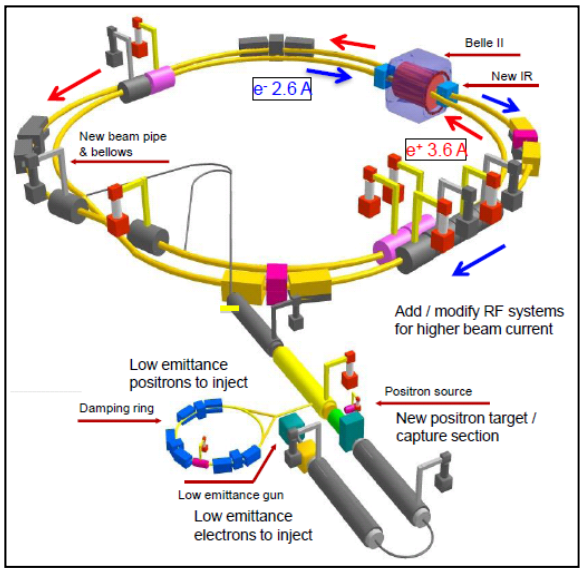


*Fig, 1. The SuperKEKB layout: grey indicates recycled parts; in color are the new ones.*

A new vertex detector is being built, a new drift chamber with smaller cell size was completed in 2014, the particle identification system will include a new Time Of Propagation (TOP) detector. The barrel CsI crystals, thallium doped, EM calorimeter will be provided with new readout electronics; studies are being carried on for the end caps upgrade. This is the area of interest of our group, and details are provided in the following. In the KL and muon detector only the outer barrel layers of glass RPCs will be re-used, the remaining will be substituted with scintillation counters. A sketch of the BELLE II detector is shown in Fig. 2.

The SuperKEKB upgrade is almost completed, and commissioning will start in 2016; all the new, or upgraded, Belle II sub-detectors are in advanced stage of preparation, and the data acquisition has been integrated. The present schedule calls for first Physics in 2017.

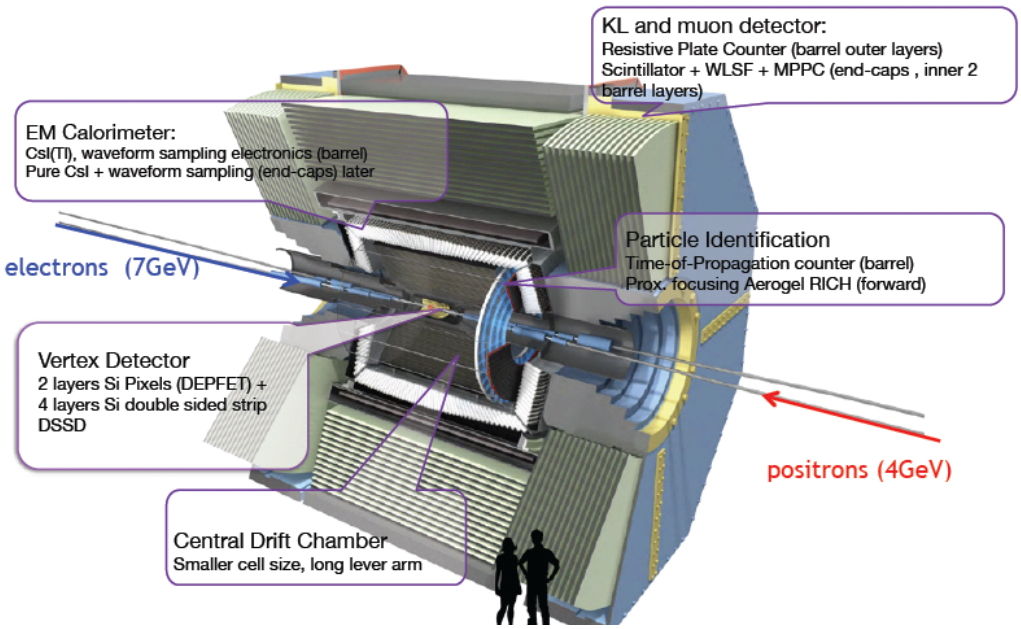


*Fig 2. The Belle II detector; major upgrades or new parts are indicated*

The Belle II Physics program is very rich and will complement the flavor studies carried on at the LHC by the LHCb detector; even though BABAR and Belle have been very successful, several fundamental questions remain unanswered in the flavor sector of quarks and leptons. The origin of hierarchy in the measured CKM matrix elements is still a mystery; it may indicate that some hidden mechanism, e.g. some new flavor symmetry, exists at a higher energy scale. Many TeV new physics scenarios almost inevitably introduce new flavor mixing that can be detected with precision measurements at the energy scale of B factories. Information obtained from flavor physics experiments is thus essential to uncover the details of the physics beyond the Standard Model, even after energy frontier machines discover new particles.

The Belle II program in which we participate is the upgrade of the EM calorimeter in the forward end cap. For the Thallium-doped CsI crystals used by Belle, the concern exists of radiation damage and of high pileup levels, especially at small polar angles. For this reason, at least part of the crystals in the forward region might be replaced with pure CsI crystals. Non doped CsI has in fact improved radiation hardness, and much faster light decay time (6/35 ns for the two main components, compared to 1.2 μs in Cs(Tl)).

Pure CsI yields, however, much less light, and has the emission peak of the fast components at 310-420 nm wavelengths. The PIN photodiodes reading the present Cs (Tl) crystals must therefore be replaced by photo detectors best matching these characteristics, that is having large internal gain and good efficiency in the near-UV region.

We also have an active role in the revision of the software for the EM calorimeter, which is necessary because the expected data rate and size of Belle II is much higher than Belle, and of the same order, or even higher, than the one of an LHC experiment.

Hereafter is a description of our group's main activities during 2014.

## R&D on Avalanche Photo Diodes

The present baseline envisages a 2-inch photo pentode for its large signal. This device is however quite sensitive to the magnetic field, would offer no redundancy in the event of failure and, due to its relatively large size, would require to redesign and rebuild the supporting structure for the electronics. An alternative readout option, which would address these two issues, could be the use of much more compact devices such as Avalanche Photo Diodes (APDs).

Based on simulation studies of the expected background rates in the Belle II forward end cap calorimeter, in order to have a negligible electronic noise contribution with respect to the pile-up noise, the Equivalent Noise Energy (ENE) should be kept below 1 MeV.

Our group made extensive R&D studies specifically on a device, the C30739ECERH2 from Excelitas Technologies, which features high gain, G = 200, at the nominal bias voltage Vnom, small capacitance (≈60 pF), very small dark current (≤1nA) and good spectral response at the relevant wavelengths of $\lambda \geq 310$ nm. As the photo detector active area is relatively small (5.6×5.6 $mm^2$), the crystals must be instrumented with more than one APD; we used four in our research. The setup used to study the APD response to the light emitted by pure CsI crystals – of size 5×5×30 $cm^3$, similar to those used in the Belle calorimeter – included a light-tight box with monitored and controlled relative humidity (RH≈15%) and temperature (within 2°C), and a simple cosmic-ray telescope assembled with a pair of scintillation counters placed above and below the crystal under study. The photo sensors were then readout with a low-noise commercial amplifier and the signals recorded by a digital oscilloscope with 1GS/s sampling frequency.

A typical recorded waveform from a cosmic ray muon traversing the crystal in the setup is shown in Fig. 3 (left). The right-hand plot of the same figure shows the signal amplitude spectrum after shaping the waveform with a semigausssian CR-$(RC)^4$ filter with 75 ns time constant to reduce fluctuations.

We measured the dependence of the APD gain on the bias voltage, $\Delta G/G = (5.2 \pm 0.2)\%$ /V, and on the temperature, $\Delta G/G = (4.5 \pm 0.2)\%$ /°C (part of the latter, about 1.5%/°C, is due to the light yield variation in the CsI crystal).

The equivalent noise energy is proportional to the RMS of the pedestal. The energy scale is set by the position of the signal peak, which corresponds to the average energy released by a cosmic ray

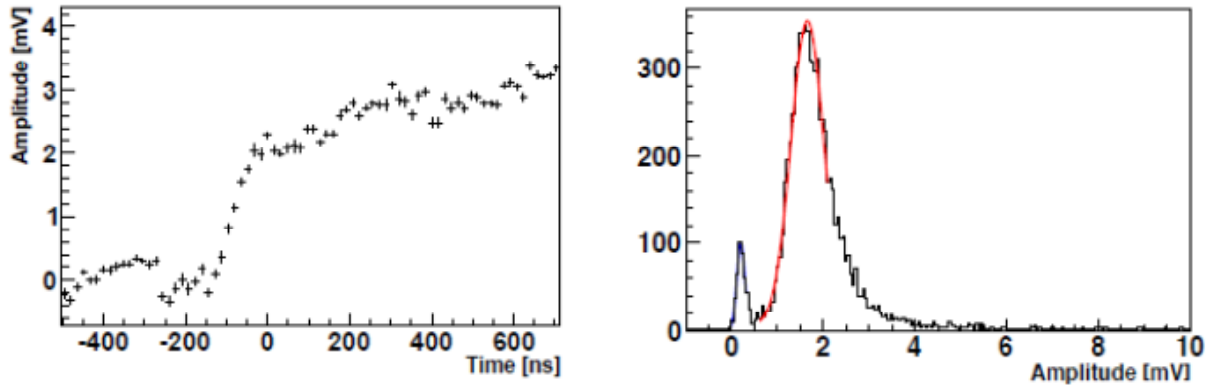


*Fig.3. Left: sample waveform from APD reading a pure CsI crystal; right: signal amplitude after a CR-$(RC)^4$ shaping with t= 75 ns.*

muon in the 5 cm thick crystal (30 MeV). We perform fits to the distribution in Fig. 3 to measure position and width of the pedestal peak (the blue curve superimposed to the histogram), and the position of the signal peak (red curve).

For the sum of four APDs we get a pedestal noise σ = (174 ± 8) μV and an average signal of (5.35 ± 0.02) mV, corresponding to a S/N ratio of 31 ± 1 and equivalent noise energy (0.98 ± 0.05) MeV. Similar studies were conducted on one more APD, the S0S86641010 from Hamamatsu Photonics. The active area of the latter is relatively large (10 × 10 $mm^2$), and we used only two of them to readout the crystal light. The two devices show similar performances within our experimental uncertainty, and both meet the requirement ENE ≤ 1 MeV.

## Radiation Hardness Studies

One concern regarding the use for the Belle II experiment of the Belle calorimeter without any changes, and therefore crucial to the decision about whether the end cap calorimeter should be upgraded to a pure CsI one, is the possible damage to the CsI(Tl) crystals due to the radiation dose received during the expected Belle II lifetime.

The light yield of the CsI(Tl) crystals has been monitored during the ten years lifetime of the Belle experiment. These measurements, reported in the Belle II Technical Design Report, have shown a light yield reduction of about 7% in the barrel and 13% in the end cap, for the integrated dose of low energy (~1 MeV) photons of about 100 rad in the barrel and 400 rad in the end cap.

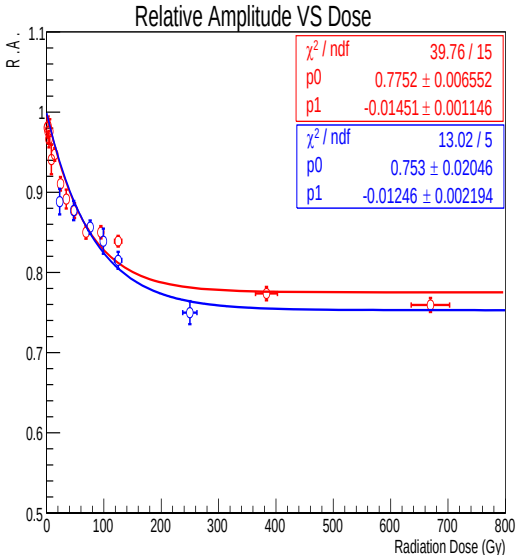


*Fig.4 Relative light yield, (1-L/L₀), in two CsI(Tl) crystals, as a function of dose measured with cosmic rays.*

At SuperKEKB, the dose over the 10 years lifetime of the experiment is expected to exceed these values by one order of magnitude or more. Radiation hardness studies done in the past (see D.M. Beylin,et al. Nucl. Instrum. Meth. Phys. Res. A 541, 501 (2005)) on a sample of several crystals from different manufacturers, have shown decreases in light yield as high as ~30% for an irradiation dose of ~3.7 Gy, with large variations between crystals from different manufacturers.

However it is not clear from these measurements, whether the radiation damage does or does not continue to increase for doses above 4000 rad, nor if there is a breakdown at some higher dose. Since Monte Carlo predictions of expected doses in Belle II are affected by large errors, and may well be higher than the doses covered by this previous study, we have decided to repeat these measurements extending the dose range up to several hundred Gy.

We have conducted this study in close collaboration with the group of ENEA Casaccia at the Calliope irradiation facility, where we irradiated two spare CsI(Tl) crystals from the Belle experiment using the intense $^{60}Co$ source. The light yield was monitored measuring the energy deposit of cosmic ray particles

traversing the crystals, using a pair of scintillator counters to trigger the events. This measurement greatly extends the range of dose of previous ones, and clearly shows a saturation of the damage to the crystals. The results are shown in Fig. 4, which are in agreement, at a low dose, with the results from the previous study.

At a higher dose, the data clearly shows that the damage due to irradiation, apparent in the loss of light yield, saturates to values near ~20-25% and that there is no breakdown of the crystals observed up to doses of few hundred Gy, several times those expected to be integrated by Belle II.

The light yield was also monitored over a period of several weeks after the last irradiation and, as Fig. 5 shows, it remains stable with time, and does not show any recovering, confirming existing literature.

These crucially important results have led our Belle II Canadian collaborators to repeat these tests using additional Thallium doped CsI crystals in order to increase the statistical significance of the result.

If confirmed, we shall conclude that from the point of view of the radiation damage there would be no need to replace the existing crystals, and therefore the final decision about whether to upgrade from CsI(Tl) to a pure CsI end cap calorimeter will have to be based on other considerations, such as for example the radiation resistance of the photo-sensors (PIN diodes) and the effect on key physics channels of the increased pile up noise at higher luminosity, both of which are under study.

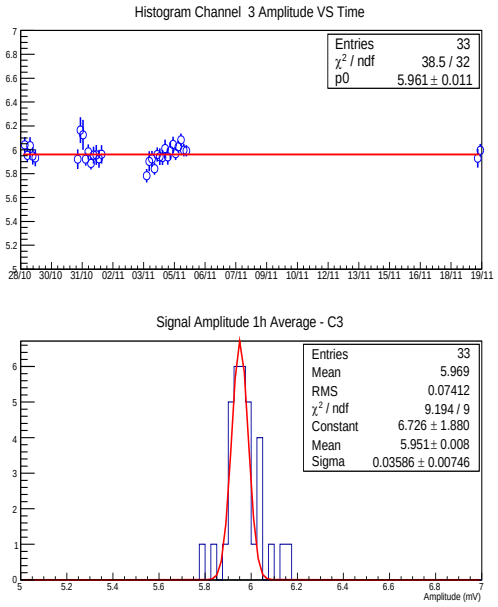


*Fig. 5 Light yield as a function of time after irradiation. The overall time span is 22 days.*

## Software developments

In order to cope with higher expected background conditions, not only sub-detector upgrades but also upgrades of the data acquisition and offline computing systems are foreseen. Both systems use a common software framework with ROOT as persistency layer, allowing the efficient use of modern multicore machines. The Belle II software system, *basf2* acronym of *Belle AnlaysiS Framework 2,* uses $C^{++}$ object oriented software. The framework consists of functional objects called modules involving event generation, Monte Carlo (MC) simulation, track and cluster reconstruction, particle identification and physics analysis. *Basf2* uses dynamic module loading, with the steering of the framework done via python, and has capabilities of parallel processing.

Our group is presently involved in the revision of the EM Software and its optimization in view of the expected higher machine background level compared to the previous Belle configuration. A new version of the Digitizer module, used in Monte Carlo to reproduce the signal shaping from the new calorimeter hardware configuration, has been written and the group is validating it within the official Belle II reconstruction framework. Next steps will include the study of the clustering procedure and its optimization in terms of background rejection, based on time and energy information. The correct

matching of the MC information to the data-like reconstructed quantities, identifying signal and background processes, represents a key ingredient for reconstruction optimization and is one of the tasks assigned to the LNF group.

The revision of the reconstruction software is fundamental to understand the expected performance of new hardware configurations on benchmark physics channels, $B \to \tau\nu$ and $B \to K^{(*)}\nu\bar{\nu}$ ,and to take the final decision on the upgrade of the forward calorimeter. To this extent, the group is going to simulate several crystal-photo sensor configurations presently under scrutiny, using also measurements from laboratory test bench and test-beam results.

# BESIII

M. Anelli (Tecn.), R. Baldini Ferroli (ass.), M. Bertani (Resp.), A. Calcaterra, J. Dong (ass.),
G. Felici, S. Pacetti (Perugia), P. Patteri, D. Pierluigi (Tecn.),
A. Russo (Tecn.), E. Tskhadadze (FAI fellowship) , Y. Wang (borsista), A. Zallo (ass.)
and in collaboration with:
LNF Spas: S. Cerioni,
LNF SEA: M. Gatta,
LNF Reparto Allineamento (Div. Acc.): M. Paris, F. Putino
INFN-Roma1 Servizio progettazione meccanica: A. Pelosi

## 1 The BESIII experiment

The BESIII experiment is successfully taking data since 2009 at the Beijing Electron Positron Collider BEPC-II, at the Institute of High Energy Physics, IHEP, and it will continue taking data until at least 2022. The BESIII detector is designed to study $\tau$- charm physics and collected the world largest samples of $J/\psi$, $\psi(3686)$, $\psi(3770)$, $\psi(4040)$, $Y(4260)$ and $Y(4360)$. BESIII discovered the first unambiguous four-quark states, the charged $Zc(3900)^+$ and $Zc(4020)^-$.

The maximum instantaneous luminosity reached in 2014 is $\mathcal{L} = 0.8 \times 10^{33}$ cm$^{-2}$ s$^{-1}$. In 2014 the experiment has taken data for a precise R-scan of 104 energy points between 3.85 and 4.59GeV, $1.0fb^{-}1$ at 4.42GeV, $0.1fb^{-}1$ at 4.47 GeV and 4.53 GeV for line shape, $0.04fb^{-}1$ at 4.575 GeV (around the threshold of $\Lambda_c$), $0.5fb^{-}1$ at 4.60GeV.

In 2012 the LNF group started to work on the proposal of upgrading the inner BESIII traking chamber, which is suffering early ageing due to the increase of the luminosity, with a new Cylindrical GEM (CGEM) detector. The project has gone ahead and a Conceptual Design Report has been drafted in 2014 with the contribution of the whole Italian BESIII group. The project, that since 2014 also includes groups from Mainz, Uppsala and IHEP, has been recognized as a Great Relevance Project within the Executive Program for Scientific and Technological Cooperation between Italy and P.R.C. for the years 2013-2015 and it has been selected as one of the projects funded by the European Commission within the call H2020-MSCA-RISE-2014.
The group is involved in the analysis of physics procesess mainly involving nucleons and light hadrons.

## 2 Physics analysis

The INFN component of the BESIII Collaboration (BESIII-IT), represented by the LNF, INFN-Torino, INFN-Ferrara and INFN-Perugia groups, has contributed to the 2014 BESIII activities in terms of proposals and data analyses concerning the following topics.

### 2.1 Measurement of the relative phase between strong and electromagnetic vector charmonium decay amplitudes

Two years ago BESIII-IT proposed an energy scan below, above and at the $J/\psi$ to measure the phase between strong and electromagnetic (EM) decay amplitudes, in a model independent way, from the interference between the $J/\psi$ and the continuum for as much as possible processes. It turned out that this phase, in modulus (i.e., apart the sign), is close to 90 degrees [1)], at odd with the 0 degree expectation. This result has also been achieved looking to the $VP$ decays, where

$V$ and $P$ stand for vector and pseudoscalar mesons, in a model dependent way, as shown in Tab 1, as well as looking to $PP$ decays, updating the various $J/\psi$ branching ratios [2)].

| Parameter | Fit |
|---|---|
| $SU_3$ strong amplitude $g$ | $7.22 \pm 0.38$ |
| $SU_3$ breaking strange $s$ | $0.18 \pm 0.04$ |
| $SU_3$ breaking OZI $r$ | $-0.04 \pm 0.02$ |
| EM amplitude $e$ | $0.75 \pm 0.04$ |
| Relative phase $\phi$ (degree) | $82 \pm 7$ |

| Decay | Amplitude | PDG ($10^{-4}$) | PDG ($10^{-4}$) | $\Delta\chi^2$ |
|---|---|---|---|---|
| $\rho^0\pi^0$ | $ge^{i\phi} + e$ | $169.0 \pm 15.0$ | 133.00 | 1.13 |
| $K^{*+}K^-$ | $g(1-s)e^{i\phi} + e$ | $51.2 \pm 3.0$ | 51.5 | 0.01 |
| $K^{*0}K^0$ | $g(1-s)e^{i\phi} - 2e$ | $43.9 \pm 3.1$ | 48.5 | 0.48 |
| $\omega\eta$ | $(gX + d)e^{i\phi} + eX$ | $17.4 \pm 2.0$ | 18.5 | 0.06 |
| $\phi\eta$ | $\left[g(1-2s)Y + d\right]e^{i\phi} - 2eY$ | $7.5 \pm 0.8$ | 3.9 | 4.02 |
| $\rho\eta$ | $3eX$ | $1.9 \pm 0.2$ | 2.2 | 0.30 |
| $\omega\pi$ | $3e$ | $4.5 \pm 0.5$ | 4.1 | 0.11 |
| $\omega\eta'$ | $(gX' + d')e^{i\phi} + eX'$ | $7.0 \pm 7.0$ | 11.9 | 0.10 |
| $\phi\eta'$ | $\left[g(1-2s)Y' + d'\right]e^{i\phi} - 2eY'$ | $4.0 \pm 0.7$ | 6.1 | 1.87 |
| $\rho\eta'$ | $3eX'$ | $1.1 \pm 0.2$ | 1.1 | 0.04 |

Table 1: Fit results for the $SU_3$ parameterization of the $J/\psi \to VP$ decay rate.

In short, if the relative phase between strong and EM vector charmonium is different from zero, something important is lacking in the present charmonium description. We have put forward a proposal to extend this measurement to the $\psi(2S)$ [3)].

Perturbative QCD (pQCD) regime is supposed to be valid in the $J/\psi$ decay, as also proven by the small decay width. As a consequence, in such a regime, all the decay amplitudes, i.e., the amplitudes for any decay channel, are expected to be real. Accordingly a simple relationship is established between EM decay and continuum amplitude, which is supposed to be almost real as well. On the other hand, no phase between decay amplitudes is foreseen in a description of vector charmonium by means of a Breit-Wigner (BW). In particular, unitarity would be violated in the case of a simple BW description, if strong partial amplitudes would be imaginary. We have proposed a model to explain this phase anomaly [4)]. Assuming this model the PANDA [5)] experiment, for instance, making a scan of the total hadronic cross section should see the $J/\psi$ as a dip instead of a peak [6)].

The $\psi(3770)$ width is greater than the accelerator energy spread. Such a meson decays mostly in $D\bar{D}$ and the aforementioned interference affects the peak value. In this way the phase can be achieved and it turns out that it is close to $-90$ degrees [3)]. Conversely, present data on $\psi(2S) \to VP$ decay indicate a phase close to 180 degrees, as shown in Tab. 2, while decay into $PP$ channels indicate a phase with modulus close to 90 degrees. Even $\psi(2S) \to p\bar{p}$, $n\bar{n}$ decays, as measured by BESIII-IT [7)], do not agree with the 90 degree found in the case of $J/\psi$ (also measured by the BESIII-IT [8)]). As it has been anticipated, because of that, the BESIII-IT has put forward a proposal for a $\psi(2S)$ scan [3)], which has been approved by the BESIII Collaboration and it will be done hopefully during the 2015-2016 data taken.

| Parameter | Fit |
|---|---|
| $SU_3$ strong amplitude $g$ | $0.49 \pm 0.04$ |
| $SU_3$ breaking strange $s$ | $-0.04 \pm 0.13$ |
| $SU_3$ breaking OZI $r$ | $-0.04 \pm 0.08$ |
| EM amplitude $e$ | $0.18 \pm 0.02$ |
| Relative phase $\phi$ (degree) | $159 \pm 12$ |

| Decay | Amplitude | PDG ($10^{-4}$) | PDG ($10^{-4}$) | $\Delta\chi^2$ |
|---|---|---|---|---|
| $\rho^0\pi^0$ | $ge^{i\phi} + e$ | $0.32 \pm 0.13$ | 0.28 | 0 |
| $K^{*+}K^-$ | $g(1-s)e^{i\phi} + e$ | $0.17 \pm 0.08$ | 0.19 | 0 |
| $K^{*0}K^0$ | $g(1-s)e^{i\phi} - 2e$ | $1.09 \pm 0.20$ | 1.15 | 0.04 |
| $\omega\eta$ | $(gX + d)e^{i\phi} + eX$ | $0.00 \pm 0.11$ | 0.08 | 0.06 |
| $\phi\eta$ | $\big[g(1-2s)Y + d\big]e^{i\phi} - 2eY$ | $0.28 \pm 0.90$ | 0.24 | 0.10 |
| $\rho\eta$ | $3eX$ | $0.22 \pm 0.06$ | 0.15 | 0.22 |
| $\omega\pi$ | $3e$ | $0.11 \pm 0.06$ | 0.26 | 0.10 |
| $\omega\eta'$ | $(gX' + d')e^{i\phi} + eX'$ | $0.32 \pm 0.25$ | 0.03 | 0.23 |
| $\phi\eta'$ | $\big[g(1-2s)Y' + d'\big]e^{i\phi} - 2eY'$ | $0.31 \pm 0.16$ | 0.29 | 0.02 |
| $\rho\eta'$ | $3eX'$ | $0.19 \pm 0.17$ | 0.08 | 0.11 |

Table 2: Fit results for the $SU_3$ parameterization of the $\psi(2S) \to VP$ decay rate.

### 2.2 Measurement of the $e^+e^- \to \Lambda_c^+\overline{\Lambda}_c^-$ cross section close to the production threshold

Many unexpected features has been observed, mostly by BaBar by means of the initial state radiation technique, in the measurement of $e^+e^- \to p\bar{p}$ cross section close to the production threshold: a sudden jump in the total cross section, likely related to a Coulomb enhancement, followed by a flat behavior and a form factor at threshold close to unity [10].
The angular distribution is not isotropic, while isotropy at threshold is demanded by form factor analyticity. In other words the electric and magnetic form factors, $G_E$ and $G_M$, are not equal each other at threshold. Unfortunately, this last result has been achieved integrating the cross section on a finite energy interval, to have enough statistics. Actually the interpretation of BaBar data is controversial. A measurement of $e^+e^- \to \Lambda_c^+\overline{\Lambda}_c^-$ cross section in the $e^+e^-$-center of mass can be done even exactly at threshold, because of the weak decay into lighter particles, and BESIII can check and eventually confirm these features in the case of a heavy baryon. For this reason we have proposed [9] to the BESIII Collaboration to perform the measurement of the $e^+e^- \to \Lambda_c^+\overline{\Lambda}_c^-$ cross section close to the production threshold and in part has been performed by BESIII at the end of the 2014 data taken.
It can be anticipated that they have indeed been observed. As a consequence, first principles assumptions, like analyticity, have to be revisited. Before claiming for these discoveries, we have asked for a higher amount of integrated luminosity at the threshold, likely to be delivered in the 2015-2016 data taken [9].

The measurement of baryon pair cross sections close to their thresholds, charged and neutral (unexpected to be different from zero, as measured by BESIII [11]), emphasized by us [12] several times, is driven the present BESIII data collection at low energies.

## 3 CGEM-IT related activities

The BESIII group has completed in 2014 the $2^{nd}$ year of the Program of Great Relevance PGR00136, a 3-year joint project of INFN, IHEP, and the Italian Ministry of Foreign Affairs. The objective of this program, started in 2013 and ending with 2015, is a prototype of a cylindrical layer of detector, built with the technique of Cylindrical Gas Electron Multiplier (CGEM) developed in Frascati for the KLOE2 Inner Tracker.

This prototype layer has 2 roles: it will help the BESIII group to understand and test construction details differing from KLOE, and it will be finally incorporated, once proven functional, in the 3-layer Inner Tracker for the BESIII experiment at IHEP, whose Inner Drift Chamber is starting to show signs of degradation by excessive backgrounds. This second requirement has complicated much the task, because the connections for all services, HV, gas, anchoring points, needed an ampunt of planning that usually may be overlooked in a prototype. In fig.1-top a sketch of the BESIII Inner Tracker around the BESIII beam pipe.

### 3.1 BESIII CGEM innovations

The experience achieved with the KLOE2 CGEM detector [21], [22] allows us to replicate what has worked best with KLOE2 and also to introduce new innovative concepts in the design and construction of the BESIII CGEM-IT detector.

The main innovation with respect to the KLOE2-IT is in the readout: for the KLOE-IT the readout was digital, while for the BES3 CGEM-IT, destined to operate in a magnetic field twice as high as the KLOE one, will be analogic. The goal is to be able to compute hit coordinates by weighing the charge collected on adjacent anode strips, and thus to recover the resolution lost because of the charge drift in the higher magnetic field. A new anode has been designed with two-dimensional readout: X-strips, $570\mu m$-wide parallel to the CGEM axis which provide $\rho\phi$ coordinates, and V-strips, $130\mu m$-wide and with a stereo angle with respect to the X-strip, giving the $z$ coordinate. The strip pitch is $650\mu m$ for both X- and V-strips, and the space between the readout and the ground plane will be filled by a Rohacell structure. A "jagged" configuration (fig.1-bottom) has been studied to minimize the inter-strip capacitance, in which the overlap region between the strips is reduced by decreasing the size of the X-strips on the intersections. Additional studies on the anode are being studied with Garfield simulations and with tests on a small planar prototype. In order to achieve the required $100\mu m$ spatial resolution an analogue readout ASIC is beeing designed by INFN-Turin investigating the UMC $0.11\mu m$ technology.

Moreover, a new Rohacell based tecnique, instead of standard Honeycomb, will be adopted to manufacture the anode and the cathode electrodes in order to minimize the material budget [23].

In 2014 large GEM foils needed for construction have been manufactured by the CERN TS-DEM-PMT laboratory at CERN and delivered to LNF, here they have been tested, and identified a few defects, that have been corrected at CERN. The fixed foils have been tested again in Frascati, and passed all selection criteria.

We have designed, ordered and received a new Al table, carrying precisely-drilled holes and holding fixtures for positioning and gluing 2 individual GEM foils of 3 different sizes into 3 bigger GEM foils, for subsequent wrapping in a cylindrical shape; the KLOE glueing table had dimensions incompatible with BES3 cylinders.

We have designed, ordered and received the 5 cylindrical Al molds necessary for converting the glued planar GEM sheets into cylindrical ones. This has been done in the LNF clean room with a laser measuring system supervised by M. Paris, head of the LNF Alignment Department (Accelerator Division) assisted by F. Putino. This system (see Fig. 2) takes many measurement of points on the mold's surface and fits them all to a cylindrical surface, giving RMS deviations from it. All our molds had surfaces cylindrical within a few tens of microns. Starting from the

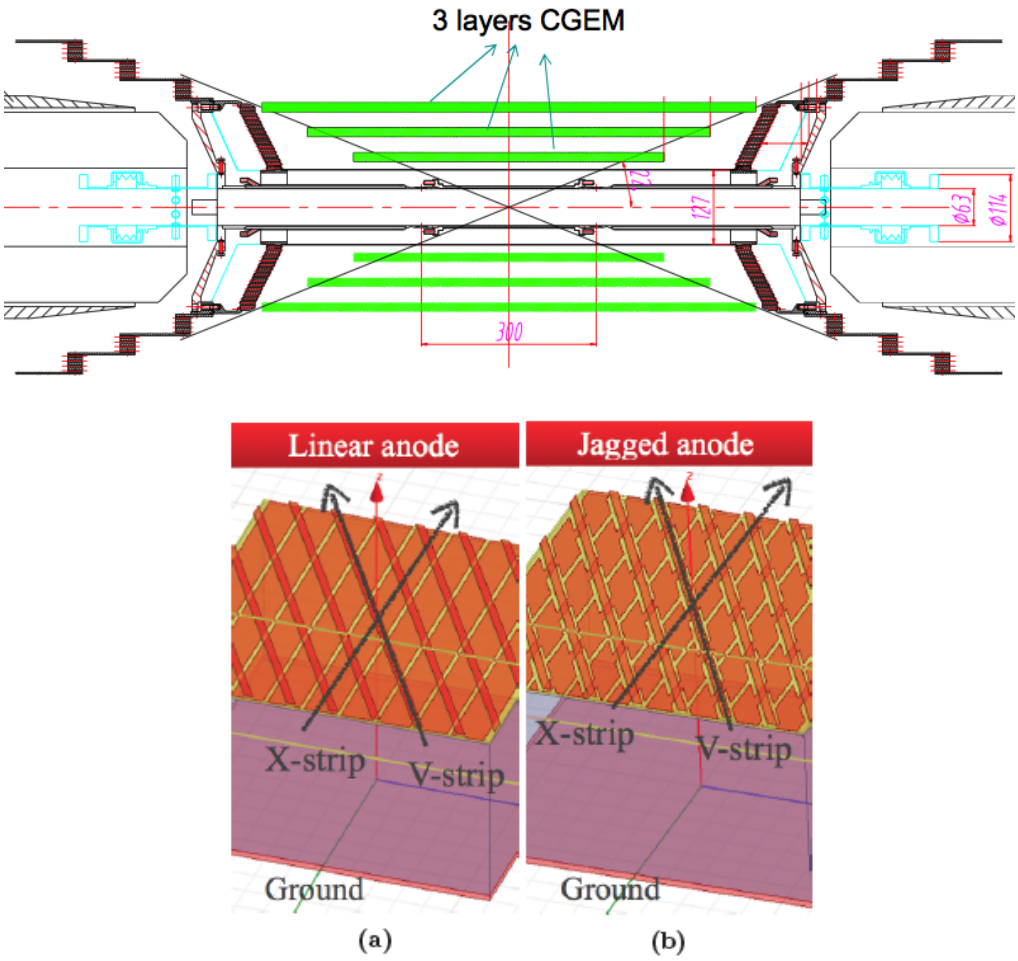


Figure 1: Top: longitudinal drawing of the BESIII three layers CGEM detector (green lines) along the BEPCII beam pipe,
bottom: anode layout for XY strips with straight (a) and jagged (b) configuration.

beginning of 2015 the first complete CGEM layer will be constructed and by the end of the year it will be tested with a provisional readout system.

Figure 2: The laser measurement of the 5 Al molds. The laser head is shown in front

### 3.2 Cosmic Ray Test Setup

The group has continued to run the cosmic ray telescope described in the 2013 Activity Report, which is constituted by 2 scintillators, 4 small (10x10cm$^2$) KLOE trackers, and a 10x10cm$^2$ BESIII-like chamber, with the object of understanding as much as possible the properties of the new type of anode sheets, made lately at the CERN workshop, that differ from the ones used for the KLOE-IT. This apparatus, formerly read digitally with GASTONE electronics, was converted in 2014 to use an analogical readout, based on the SRS system in use at CERN, developed in the cadre of the RD51 group of detector developers. This setup has the primary purpose to keep the hardware ready to operate at a test beam, although it can also be used for some measurement of its own, with the limitations due to the unknown momenta of cosmic rays, and the systematics due to cosmic showers and multiple scattering.

### 3.3 CERN Test Beam

In December 2014 we have run a 3-week beam test at SPS H4 beam line at CERN, within the RD51 Collaboration, using the same apparatus tested in cosmic rays, with the main purpouses of measuring efficiency at different gains, cluster size and resolution as function of the magnetic field, signal to noise ratio, test of the analog readout in magnetic field. The planar BESIII chamber has been tested with two different gap sizes (3 and 5 mm) and two gas mixtures (Argon-CO2 70-30 and Argon C2H10 90-10). The H4 beam line at the SPS has a secondary extracted beam of muons and pions with momentum up to 400GeV/c, the facility has a dipole magnet (GOLIATH) capable of reaching B field values of 1.5T. A schematic drawing and a picture of the setup are shown in fig.3 top part.

To exploit the features of the GEM detectors fully analog readout, both the tracking and the test chambers have been instrumented by means of a front-end chain based on the APV25 hybrid boards. These boards provide a 25 ns sampling of the input signals then allowing a coarse

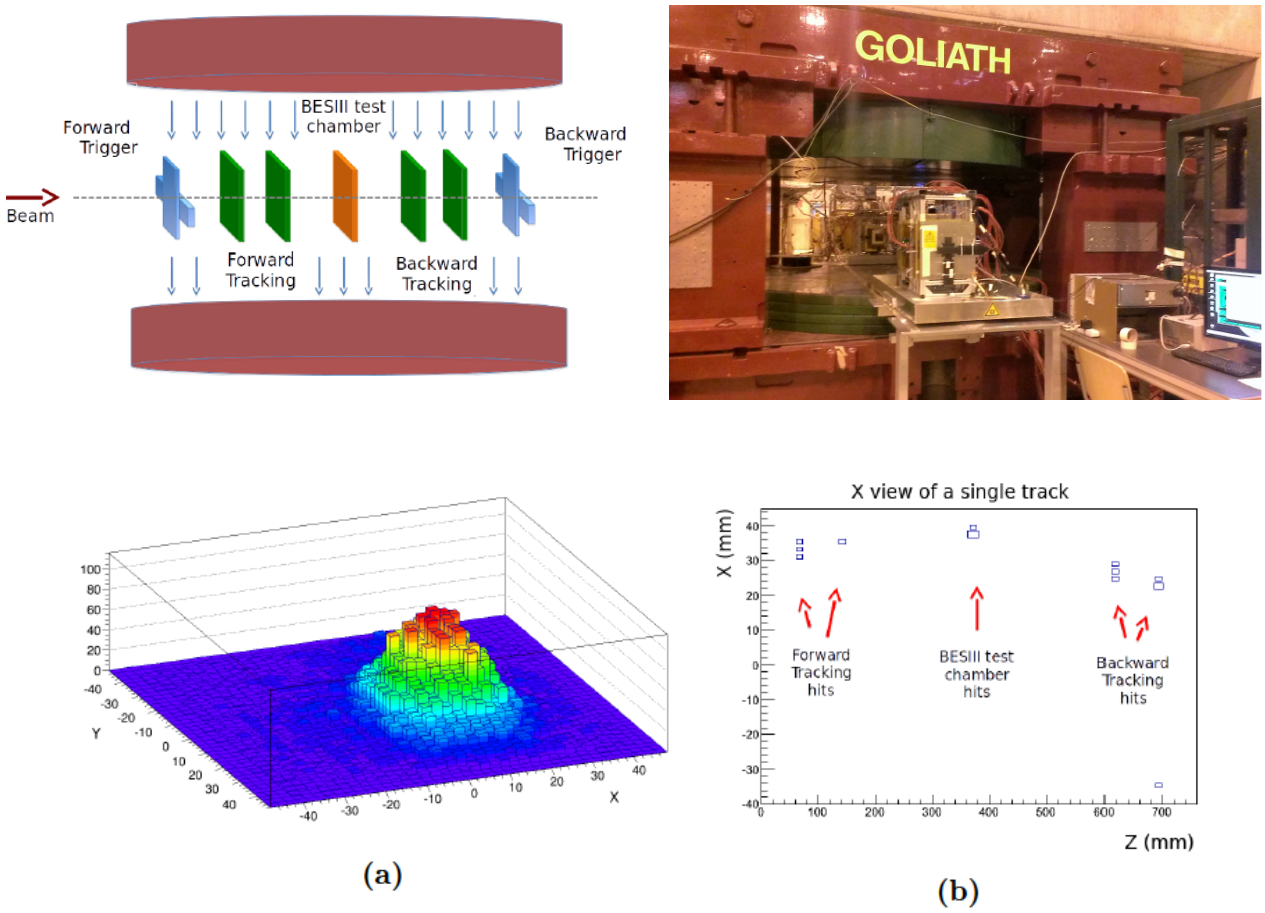


Figure 3: top left: drawing of the Beam Test setup, particles going from left to right. The BESIII test chamber (yellow) in-between the four trackers (green) the four trigger bars (blue). The whole setup is placed in the magnet (purple). top right: picture of the whole setup inside the GOLIATH magnet at Cern SPS H4 beam line. Bottom:(a) beam profile obtained from the BESIII test chamber, (b) $x$ view of a single track without alignement.

reconstruction of the signal shape. The output data can be used for simple charge centroid measurements or, by means of a more complex analysis, to define the arrival time of the signals then allowing to implement the so called $\mu$TPC readout. The $\mu$TPC method is very powerful as it allows to avoid the worsening of spatial resolution measurements carried out by means of the charge centroid method in presence of strong (1 T) magnetic fields. The complete Test Beam chain was made of 12 APV boards (for a total amount of 768 channels) and a FADC-SRS card readout through a GBD transceiver. The HV was provided by commercial CAEN system instrumented with CAEN A1550 power supply and distributed to the GEM electrodes by a custom distribution system. Singular current monitoring was provided by a nano-amperometer.

In fig.3 bottom part are shown the beam profile obtained by plotting all the clusters of the BESIII test chamber during one run (a) and the $x$-view of a reconstructed track, before alignement (b). Overall the data from this test beam are very satisfactory and its analysis just started.

## References


1. BAM-128 Y. Wang *et al.*, under review for publication on Phys. Rev. Lett.;
   BAM-106 M. Destefanis *et al.*, under review for publication on Phys. Rev. Lett.
2. K. A. Olive *et al.* [Particle Data Group Collaboration], Chin. Phys. C **38** (2014) 090001.
3. BESIII-IT, BESIII Collaboration Meeting, Beijing, June 2014.
4. BESIII-IT, BESIII Physics and Software Meeting, Beijing, February 2013.
5. PANDA Experiment website: http://www-panda.gsi.de/.
6. BESIII-IT, PANDA Meeting, Frascati, September 2014.
7. BAM-126 K. Zhu *et al.*, under review for publication on Phys. Rev. Lett..
8. M. Ablikim *et al.* [BESIII Collaboration], Phys. Rev. D **86** (2012) 032014.
9. BESIII-IT, BESIII Collaboration Meeting, Jinan, June 2014.
10. J. P. Lees *et al.*, Phys. Rev. D **87** (2013) 092005.
11. X. Zhou *et al.*, under review for publication on Phys. Rev. Lett..
12. BESIII-IT, BESIII Collaboration Meeting, Beijing, June 2013.
13. B. Aubert *et al.* [BaBar Collaboration] Phys. Rev. Lett. **95** (2005) 142001
14. C.Z. Yuan *et al.* [Belle Collaboration] Phys. Rev. Lett. **99** (2007) 182004
15. Z.Q.. Liu *et al.* [Belle Collaboration] Phys. Rev. Lett. **110** (2013) 252002
16. G. Lopez Castro, J. L. Lucio M. and J. Pestieau, AIP Conf. Proc. **342** (1995) 441.
17. R. Baldini, M. Bertani, C. Bini, R. Calabrese, A. De Falco, M. L. Ferrer, P. Gauzzi and E. Luppi *et al.*, "Measurement of $J/\psi \to N\bar{N}$ branching ratios and estimate of the phase of the strong decay amplitude," Phys. Lett. B **444** (1998) 111.
18. S. J. Brodsky and G. P. Lepage, Phys. Rev. D **24** (1981) 2848.
19. B. Aubert, *et al.* [BaBar Collaboration], Phys. Rev. D **76** (2007) 092006.

20. L. Yan, Report on BESIII Winter Collaboration Meeting 2013 "$\Lambda\overline{\Lambda}$ at threshold".

21. F.Archilli *et al.* [KLOE2 Collaboration], "technical design report of the inner trackerfor the KLOE2 experiment" arXiv:1002.2572 (2010)

22. G.Morello, on behalf of the KLOE2-IT group, "Construction and commissioning of the KLOE2 Inner Tracker", TIPP2014 proceeding (2014)

23. I. Garzia, on behalf of the BESIII CGEM-IT group, "A cylindrical GEM detector with analog readout for the BESIII experiment", TIPP2014 proceeding (2014)

**CMS**

L. Benussi, S. Bianco, M.A. Caponero (Ass.) F.L. Fabbri (Ass.), M .Ferrini (Ass.),
M. Parvis (Ass.), L. Passamonti (Tecn.), D. Piccolo (Resp.)
D. Pierluigi (Tecn.), G. Raffone, A. Russo (Tecn.), G. Saviano (Ass.), A. Lalli (Laureando.)

In collaboration with:
A.Cecchetti (SPECAS), D.Orecchini (SPECAS),

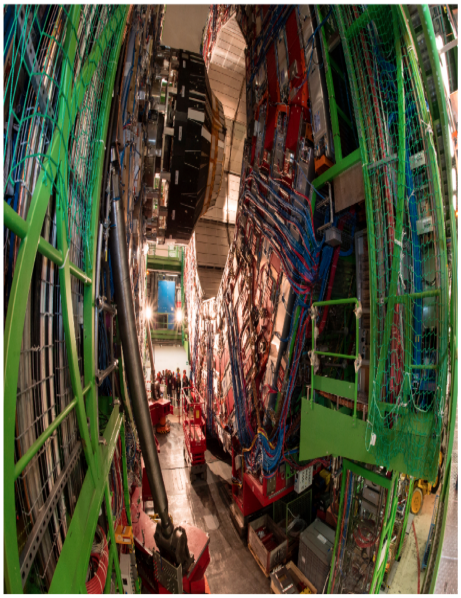

In 2015 The Compact Muon Solenoid (CMS) experiment [1) 2)], after the discovery of the Higgs Boson [3)], will start to explore the new energy regime of 13 TeV collisions to improve the precision on the Higgs boson parameters and to search for new physics beyond the standard model. The key element of the CMS detector is the highly performing and redundant muon system. Drift tubes and Resistive Plate Chambers (RPC) in the Barrel and Cathode Strip Chambers and RPCs in the endcap are used for both triggering and tracking of muon particles. The activity of the CMS Frascati group is centered on various responsibilities in the construction, operations and monitoring of the RPC detector, as well as in the quality control of data and physical data analysis. In view of the high luminosity LHC upgrades of phaseII, the group is also highly involved in studies of longevity of the present system and in the development of GEM detectors for the completion of the muon system at high $\eta$.

## 1 Activity of the CMS Frascati group in 2014

The Frascati group is involved in the muon project of the CMS experiment since 2005. The group has been responsible of the construction and of the maintenance of the Gas Gain Monitor system and is well integrated in all the activities both during the running periods and during the last years shutdown efforts. Several responsibilities have been covered by members of the group during these years: In 2010 and 2011 the RPC DPG (Detector Performance Group) coordinator was a Frascati charge; In 2011 and 2012 the RPC Run coordination. Since 2013 the CMS GEM hardware coordination were covered by Frascati;

For the period 2013-14 a member of the group (Stefano Bianco) is the RPC national responsible.

In 2014 the main efforts of the group were devoted to the support to the shutdown activities of CMS and on studies and R&Ds for the future muon upgrades at high eta.

During the shutdown period the completion of the muon system has been planned [4)] and a new station of RPC detectors is under installation in the endcap regions to improve the muon trigger performances.

In view of the Phase II of LHC an extension of the muon system has been scheduled and GEM detectors have been proposed [5)] in order to cope with the high background and hostile environment expected in the next years of LHC operations.

### 1.1 Long Shutdown 1 activities and RE4

A total number of 144 new RPC chambers will cover the outermost station of the muon endcap system (RE4) (see figure 1 for a schematic layout of the muon system with indications in the dashed box of future planned upgrades as well) in view of the LHC Run 2 operations. The RE4 endcap installation has been succesfully completed in september 2014 (fig. 2).

Frascati physicists and technicians have been involved in the preparations of the RPC chambers at CERN before the installation and in the tests of the HV and readout system for this new set of chambers. This work had the Frascati group involved with contributions in terms of physicists and technicians both in installations and commissioning activities.

### 1.2 GEM chamber assembling at Frascati

CMS is planning an upgrade of the muon system with the installation of GEM detectors in the high eta region (GE1/1 chambers). These chambers will improve the muon trigger performance allowing to maintain low pt thresholds at Level 1 trigger level. Frascati will be one of the GEM assembling sites in view of the full production. The dimensions of these chambers will be of the order of 80 x 120 $cm^2$ a size very big with respect to previews experiences. During 2014 several activities have been completed and now the the laboratory is ready to assemble these large size GEM chambers for the final production.

### 1.3 GEM R&Ds

In view of the upgrade of CMS with GEM detectors, the Frascati group started an R&D program in order to study few critic issues important for the CMS GEM program: The R&D items, aimed to both the phase 2 Technical Proposal and the GE1/1 TDR and funded by INFN comprise studies

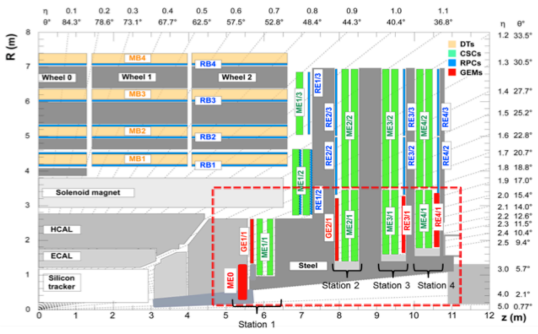


Figure 1: CMS muon system layout. In the dashed box are shown the upgrades proposed for the Muon system

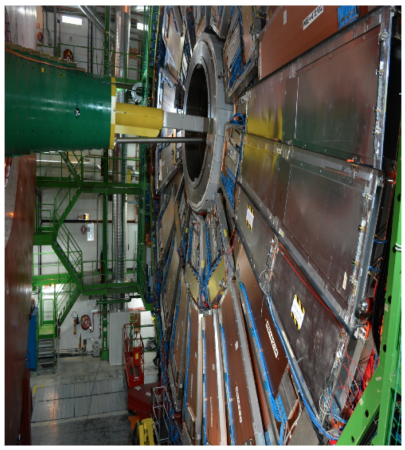

Figure 2: Completion of the first RE4 station installation.

on GEM gas mixtures studies, GEM materials analysis and stretching of the GEM foils. All these tasks address important challenges that need to be solved for the TDR.

### *1.3.1 GEM gas mixture R&D*

The choice of the gas mixture is fundamental to keep an high detection efficiency in parallel to a time resolution of the order of ns. At moment the CMS GEM detectors have been operated with a mixture of $Ar/CO_2/CF_4$ in the ratios 45/15/40. With this gas mixture a time resolution of about 4-5 ns is reached, enough to maintain high efficiency detection inside the LHC time window of 25 ns. Nevertheless the European Community has prohibited the production and use of gas mixtures with Global Warming Power (GWF) above 150. Gas mixtures used by GEMs (and RPCs as well) contains $CF_4$ (and $C_2H_2F_4$ for RPCs) with GWF=5800 and 1430 respectively so an R&D to find new eco-friendly gas mixtures with same performance as the previews one is necessary.

### *1.3.2 GEM foil tensioning R&D*

The goal is to develop a simple, cost-effective, mass production tools to assess both planarity and parallelism of GEM foils within 100 $\mu$m over the 1 mm gap. This task addressed a specific question raised by the Apollinari review committee set-up by CMS in March 2013. Solution proposed is based on optical tools based on Moiré interferometry (Fig.3). Preliminary results show clear fringes with patterns sensible to 100 $\mu$m deviations from planarity. A factor of 5 improvement using phase-shift techniques is expected. The second goal is to discover if an *in situ* monitoring of stretching and planarity is possible. The solution being studied is based on the use of optical sensors installed on GEM films/frames. For both items the studies carried on by the Frascati group demonstarted the relaibility for the new technology adobted by the CMS - GEM collaboration for the GE1/1 chamber. The results obtained deomstarted taht the three folis are correctly stretched up the the

final planar position with respect to the drift board. Those results have been succesfully reported to the Apollinari review committee and published on the GE1/1 TDR (in publication).

### *1.3.3 GEM materials aging R&D*

In order to guarantee safe operation of a GEM detector made of composite materials over 20 years, in harsh high-radiation environment, a detailed programme aimed to the full characterization of materials pre- and post-irradiation was funded and started (kapton, glue, gas, etc). Initial studies on the deployment of eco-friendly gases to replace R134a and $CF_4$ were also initiated. Results (Fig.4) on first measurement of $H_2O$ absorption in kapton and GEM films, and on measurement of tensile properties of dry/humid kapton/GEM films were presented at Siena 2013 Conference.

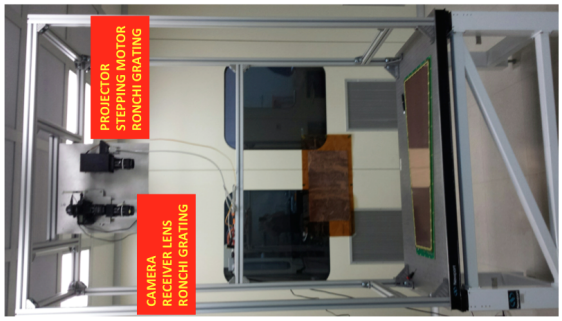


Figure 3: Moiree setup mounted in the Frascati Laboratory

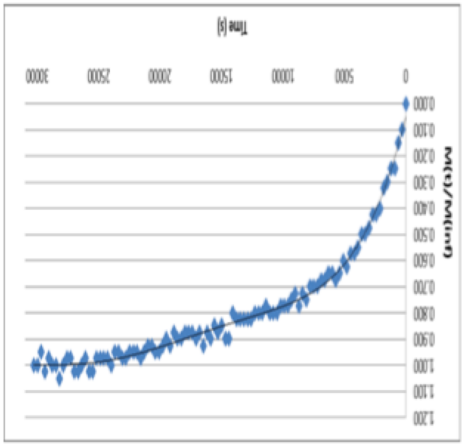

Figure 4: First results of $H_2O$ absorption coefficient inside the GEM kapton foil, before irradiation at GIF. Measurements will be repeated in 2014 after full irradiation

## 1.4 GGM maintenance and data analysis

The Gas Gain Monitoring construction has been the first contribution of the Frascati group to the RPC collaboration. The system monitors the changes in working point due to gas variations, by means of monitoring of anodic charge in small RPC gaps in a cosmic ray telescope. During 2014 few hardware intervention have been necessary to fix a leaky chamber and some electronic channel. The full data sample collected during 2011 and 2012 has been analyzed offline and final results have been organized in view of the RPC 2014 conference where a talk has been dedicated to this work. Figure 5 shows anodic charge collected in different chambers of the GGM system and the ratios to factorize out environmental contributions. Signs of gas mixture variation, due to a $SF_6$ gas flowmeter fault, is clearly spotted in the trend and marked in the circle.

## 1.5 RPC longevity analysis

Studies of the present RPC system longevity in view of High Luminosity LHC (HL-LHC) operations have started in 2013 and are coordinated by Frascati member. The goal is to analyze the

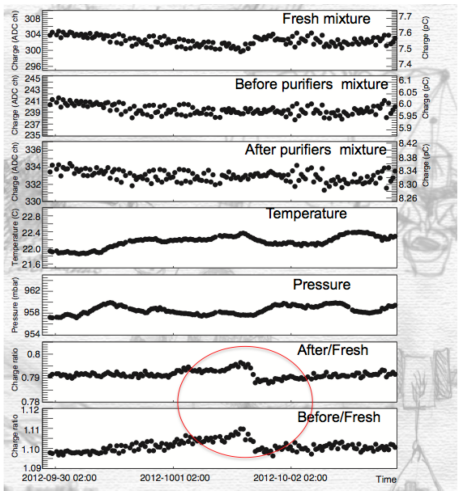


Figure 5: GGM performance during 2011 and 2012. Anodic charge collected in different chambers and ratio between charges coming from recirculated and fresh gas flowed RPCs. Clear sign of warning is spotted inside the circle due to a $SF_6$ gas flowmeter fault.

performance of the system from different point of view (detection efficiency, dark current, intrinsic noise) to correlate the results and to spot possible aging effects, background dependent, or weak points that could generate failures on the long term. Up to now no visible signs of aging have been identified but smaller effects are under study. In parallel the background rate on the RPCs have been systematically studied and clear extrapolations for the HL-LHC scenarios have been extracted . The conclusions of such studies will drive R&D programs to be carried out in the near future in local laboratories and at GIF++ at CERN.

### 1.6 Physics analysis: single top production

In LHC the top quark can be produced both in pairs or as a single top via Electroweak mechanism. The single top production is possible through three different diagrams: t-channel [6], tW channel [7] and s-channel, each of them sensible to different possible effects of new physics. The precise measurement of the cross section of the single top production is so an important standard model check and a window for new physics. The Frascati group joined in 2012 the group of Analysis of the single top and was mainly involved in two main activities: study of the hadronic cross-trigger efficiency and study of selection for the s-channel cross section measurement.

## 2 Activity planned for 2015

Frascati group will support the activities with contribution of physicists and technicians in the commissioning and installation phases in P5. At the same time the GEM collaboration is progressing very fast to realize a system based on GEM detectors for the coverage of the high $\eta$ region of the CMS muon system [5]. A technical design report is under preparation and should be ready for the summer. Frascati is involved in this effort with a several years plan of R&D activities started in 2012 and to be carried on in Frascati.

From the R&D point of view the Frascati group will finalize the tensioning studies of the GEM foils inside the CMS chambers and the studies of gas mixture. The layout that is under development in the Frascati lab will permit to plan a systematic study of several ecological gas mixtures in parallel on GEM and RPC detectors. The analysis of the materials used in the GEM chambers, after irradiation at GIF, will be completed and will be part of the TDR document which is presently under final review before printing.

A new and improved mechanical prototype of CMS GEM chamber has been ordered at cern and will be mounted and tested in Frascati to exercise and standardize the production and quality control capabilities of our laboratory in view of the large scale production.

Additional contributions of the group will cover the development of software tools for the monitoring of the RPC performance and for longevity studies that is a task under Frascati responsibility.

## 3 Status of the CMS experiment

In 2014 have been succesfuly completed severl interventions to consolidate the present system fixing hardware failures. It has benn also totally installed the fourth station of the muon system in the endcap composed by CSC and RPC chambers. The system has been also prepared for the tracker colder operations and for installation of pixels tracker in 2016-17. The successful completion of Long Shutdown 1 (LS1) activities has been the top priority of CMS, however, Technical

From the physics analysis point of view many new analysis have been finalized by CMS during 2014. The Higgs analysis group produced several new results including the search for ttH with H decaying to ZZ, WW, $\tau\tau$+bb where an excess of $2.5\sigma$ is observed in the like-sign di-muon channel, and new searches for high-mass Higgs bosons. Search for invisible Higgs decays have also been performed both using the associated and the VBF production channels. A combined limit on the invisible decay branching fractions have been set to BR(H$\rightarrow$invisible) of $\leq$52% (at 95% confidence level). The final Run 1 VH(bb) search, which sees a $2.1\sigma$ excess consistent with the SM Higgs boson has been submitted to a journal. The final Run 1 H(WW), H(ZZ), H($\tau\tau$) analyses have been approved and are in the final stages of preparing for journal submission. The SUSY seraches continued harvesting the 8 TeV dataset in the search for "natural" SUSY. New results include searches for sbottom and stop by gluino-induced production by using the razor variable and specific (1,2,3 leptons + b jet) topologies as well as searches for gluinos decaying to top-pairs and neutralinos. The lower limits on the gluino mass have been pushed up to 1350 GeV at a 95% CL. A new series of searches with Higgs in the final state have started to appear, such as searches for stop pair production or electroweak partner pair production with Higgs bosons in the decay chain. Chargino and neutralinos masses are probed up to about 200 GeV in the latter search.

One of the most prominent results of this year has been the first observation of the B0$\rightarrow \mu\mu$ decay by both the CMS and the LHCb collaborations after a 25-year-long relay race of different facilities to establish this rare decay. The measured decay rate by CMS experiment is $(3.0 \pm 1.0) \times 10^{-9}$. The combination with LHCb gives a decay rate of $(2.9 \pm 0.7) \times 10^{-9}$. In good agreement with SM predictions.

More results have been obtained in Exotica, Standard Model and QCD analysis.

## 4 Status of the RPC Muon system

In 2014 the two main activities of the RPC project were the preparation and maintenance of the present system and the construction and to finalize the installation of the RE4 system. One copleted the RE4 installation the full system have been completely tested with cosmic rays for commissioning. Presently the system is fully operative and it is successfuly participating to the LHC RUN2 commissioning period.

## 5 Conference Talks by LNF Authors

1. L. Benussi *et al.* [CMS Collaboration], "Performance of the gas gain monitoring system of the CMS RPC muon detector," JINST **10**, no. 01, C01003 (2015) talk presented by L. Benussi at RPC2104 conference, Beijin, China, February 2014.

## 6 Papers

1. For the listing of CMS papers in 2014 see /www.slac.stanford.edu/spires/
2. M. Tytgat, M. Abbas, M. Abbrescia, A. A. Abdelalim, M. Abi Akl, W. Ahmed, W. Ahmed and P. Altieri *et al.*, PoS TIPP **2014** (2014) 065.
3. D. Abbaneo, M. Abbas, M. Abbrescia, A. A. Abdelalim, M. Abi Akl, W. Ahmed, W. Ahmed and P. Altieri *et al.*, arXiv:1412.0228 [physics.ins-det].

4. D. Abbaneo, M. Abbrescia, M. A. Akl, C. Armaingaud, P. Aspell, Y. Assran, S. Bally and Y. Ban *et al.*, JINST **9** (2014) 01, C01053.

5. D. Abbaneo, M. Abbas, M. Abbrescia, A. A. Abdelalim, M. A. Akl, W. Ahmed, W. Ahmed and P. Altieri *et al.*, JINST **9** (2014) 10, C10036.

6. D. Abbaneo, M. Abbrescia, M. A. Akl, C. Armaingaud, P. Aspell, Y. Assran, S. Bally and Y. Ban *et al.*,

7. D. Abbaneo, M. Abbrescia, M. A. Akl, C. Armaingaud, P. Aspell, Y. Assran, S. Bally and Y. Ban *et al.*, JINST **9** (2014) C04022.

8. D. Abbaneo, M. Abbrescia, M. A. Akl, W. Ahmed, C. Armaingaud, P. Aspell, Y. Assran and S. Bally *et al.*, JINST **9** (2014) C03052. Conf. 60 16010

**References**

1. CMS Collaboration home page is /cms.cern.ch/.

2. R. Adolphi *et al.*, "The CMS experiment at the CERN LHC," JINST **3** (2008) S08004

3. S. Chatrchyan et al., "Observation of a new boson at a mass of 125 GeV with the CMS experiment at the LHC", Phys. Lett. B 716 (2012) 30

4. M. Tytgat, *et al.*, "The Upgrade of the CMS RPC System during the First LHC Long Shutdown," PoS RPC **2012** (2012) 063 [JINST **8** (2013) T02002] [arXiv:1209.1979 [physics.ins-det]].

5. D. Abbaneo, *et al.*, "A GEM Detector System for an Upgrade of the High-eta Muon Endcap Stations GE1/1 + ME1/1 in CMS," arXiv:1211.1494

6. S. Chatrchyan et al., "Measurement of the single-top-quark t-channel cross section in pp collisions at $sqrts = 7$ TeV " Phys. Lett. B 716 (2012) 30

7. S. Chatrchhyan et al., "Evidence for associated production of a single top quark and W boson in pp collisions at sqrt(s) = 7 TeV " Phys. Rev. Lett. **110** (2013) 022003

**GMINUS2**

A. Anastasi (Dott.)[1], D. Babusci, G. Corradi (Tecn.), S. Dabagov, C. Ferrari (Ass.)[2], A. Fioretti (Ass.)[2], C. Gabbanini (Ass.)[2], D. Hampai, M. Lobello(Tecn.), G. Venanzoni (Resp)

[1] *Also Dipartimento di Fisica e di Scienze della Terra dell'Universitá di Messina, Messina, Italy*
[2] *Also Istituto Nazionale di Ottica del C.N.R., UOS Pisa, via Moruzzi 1, 56124, Pisa, Italy*

## 1 The $g-2$ experiment at Fermilab

The new $g-2$ experiment at Fermilab (E989) plans to measure the muon anomaly $a_\mu = (g-2)/2$ to an uncertainty of $16 \times 10^{11}$ (0.14 ppm), derived from a 0.10 ppm statistical error and roughly equal 0.07 ppm systematic uncertainties on $\omega_a$ and $\omega_p$. The proposal efficiently uses the unique properties of the Fermilab beam complex to produce the necessary flux of muons, which will be injected and stored in the (relocated) muon storage ring. To achieve a statistical uncertainty of 0.1 ppm, the total data set must contain more than $1.8 \times 10^{11}$ detected positrons with energy greater than 1.8 GeV, and arrival time greater than 30 $\mu$s after injection into the storage ring.

With a higher expected beam rate, more rapid filling of the ring, and even more demanding goals in systematic uncertainties, the collaboration has had to devise improved instrumentation. The ring kicker-system will be entirely new, optimized to give a precise kick on the first turn only, to increase the storage fraction. The magnetic field will be even more carefully prepared and monitored. The detectors and electronics are entirely new, and a state-of-the-art calibration system will ensure critical performance stability throughout the long data taking periods. New in situ trackers will provide unprecedented information on the stored beam. The first physics data-taking is expected in early 2017.

## 2 The Laser Calibration system

The $g-2$ experiment will require a continuous monitoring and re-calibration of the detectors, whose response may vary on both a short timescale of a single beam fill, and a long one of accumulated data over a period of more than one year. It is estimated that the detector response must be calibrated with relative accuracy at sub-per mil level to achieve the goal of the E989 experiment to keep systematics contributions due to gain fluctuations at the sub-per mil level on the beam fill scale (0-700s) and at the sub per cent level over the longer data collection period. This is a challenge for the design of the calibration system because the desired accuracy is at least one order of magnitude higher than that of all other existing, or adopted in the past, calibration systems for calorimetry in particle physics.

As almost 1300 channels must be kept calibrated during data taking, the proposed solution is based on the method of sending simultaneous light calibration pulses onto the silicon photo-multiplier (SiPM) photo-detectors, through the active crystals (made of $PbF_2$) that make up the calorimeter. Light pulses should be stable in intensity and timing in order to correct systematic effects due to drifts in the response of the crystal readout devices. A suitable photo-detector system must also be included in the calibration architecture to monitor any fluctuation in time of the light source intensity and beam pointing as well as any fluctuation of the transmitted light along the optical path of the light distribution system, which could occur due to mechanical vibrations or to aging of the optics.

Some guidelines are defined to select the light source(s) and to design the geometry of the light distribution and monitoring; the following criteria are adopted to select the light source type:

- light wavelength must be in the spectral range accepted by the detector and determined by the convolution of the spectral density of the Cherenkov signal produced by electrons in $PbF_2$ crystals with the spectral transmission of the crystals, and with the spectral Q.E. of the photo-detector; Q.E. is peaked around 420 nm for SiPMs.

- the luminous energy of the calibration pulses must be in the same range of that produced by the conversion of the electron energy in the crystals, typically 1-2 GeV, into light [?]. This corresponds to a luminous energy on each tower of a calorimeter station of about 0.01 pJ, or to about 0.013 nJ for simultaneous excitation of all calorimeter readout channels (1300). The numbers quoted above are merely indicative of the order of magnitude and are derived by assuming that the readout of each crystal will produce about 1.5 photo-electrons per MeV with 35% P.D.E. (Particle Detection Efficiency) for SiPMs and with 23% coverage of the crystal readout face.

- the pulse shape and time width must be suitable to infer on the readout capability in pile-up event discrimination: pulse rise/trailing time should be of the order of some hundred of picoseconds, the total pulse width should be of the order of 1 ns. However, as the SiPM detectors in the planned experiment give temporal tails of several ns, the time width requirements are less stringent.

- the pulse repetition rate must be of the order of 10 kHz; this value will be tuned to obtain the best compromise between the need of having enough calibration statistics in the time interval when the maximum rate is achieved in the readout devices and the need to avoid saturation.

Among many different types of pulsed lasers commercially available, pulsed diode lasers in the blue seem to best address all the criteria listed above and are considered as a source for the calibration pulses. The light pulses will be distributed to the calorimeters in a way that will be defined after the completion of all tests required to qualify, in terms of light transmission and time stability, all other optical elements of the calibration system.

## 3 GMINUS2 Activity in 2014

The LNF activity in 2014 has been focused on:

- Choice of the laser source. After reviewing different models, the PicoQuant LDH-P-C-405M pulsed diode laser has been chosen to drive the calibration system. It featured a pulse width $<$600 ps at a wavelength of $405 \pm 10$ nm. The power stability over 12 hours in an environment with temperature stability $\Delta$T (ambient) $<$3 K is quoted as 1 % RMS and 3 % peak-to-peak, a performance we verified in the field. The maximum energy per pulse is $\sim$500 pJ. For the final system, where an energy of few nJ is requested a multilaser system (like the 8-channel PicoQuant SEPIA II) will be used.

- Choice of the distribution system. The integrating sphere has been compared with respect to an engineered diffuser. For the sphere our results show that a short laser pulse produces spatial illumination fluctuations in the output ports below 0.2 %, when integrated over windows of 1 squared mm area (i.e. of the order of the optical fiber surface). This is obtained at the price of a temporal lengthening of the laser pulse up to a few ns, depending on the number of open ports of the sphere. This is however not a problem for the $g-2$ experiment, as the pulse width remains below the SiPM response time [?]. Laser pulses are also severely attenuated by the sphere when used to couple light into a fiber bundle, resulting in a measured transmission of the order of $10^{-5}$ in a single fiber of 200 $\mu$m diameter and an estimated

Figure 1: *(a)* Front view of the array of 28 $pb^{-1}$ crystals. Elements 1 – 16 are wrapped in white Millipore paper, while elements 17 – 28 are wrapped in black Tedlar. *(b)* Schematic diagram of the laser calibration system used. Light from each fiber in the distributed bundle is directed through a lens into the front face of a single crystal.

one of $2.5 \times 10^{-4}$ into a 1 mm one. Nevertheless, such a system is able to uniformly split a single laser pulse into more than 100 optical fibers simultaneously, with a good long-term mechanical stability, and an estimated total transmission coefficient of the order of 2 %.
The test has also shown that it is possible to achieve even higher transmission coefficient for each fiber when using a system based on an engineered diffuser, at the expense of a lower uniformity and long-term stability. The diffuser has the advantage of leaving unaltered the temporal profile of the laser.
The final choice for the light distribution system of the $g-2$ experiment calibration will be done by considering several issues, including the total required laser power.

- Test of a calorimeter prototype made of 28 crystals together with SiPM bias power supply and a laser diode based monitoring system at the SLAC National Accelerator Laboratory (SLAC) test beam facility **?)** (see Fig. **??**, (a)). A high-performance calibration system was used to set the gains of the individual crystal/SiPM elements as well as to monitor the gain stability of each detector throughout the test beam period. Several prototype elements of the overall optical system being designed for the $g-2$ experiment were tested, including a suite of out-of-beam pin diode monitors, which measured the laser shot-to-shot intensity fluctuations. The studies reported here relied on a subset of these tools including the light source, a system to precisely control its intensity by attenuation, and a distribution system to direct light separately to each of the 28 detector elements (see Fig. **??**, (b)). Results from this test beam were submitted for publication **?)**

All the work above was performed in close connection with the National Institute of Optics (INO) Section in Pisa.

## 4 List of Conference Talks, Posters by LNF Authors in Year 2014

1. G. Venanzoni "The New Muon g-2 experiment at Fermilab (E989)", 37th International Conference on High Energy Physics (ICHEP2014), 2-9 July 2014, Valencia (Spain).

2. A. Anastasi, "Results from the test beam of a g-2 electromagnetic calorimeter prototype at SLAC", $100^o$ Congresso Nazionale della Societá Italiana di Fisica, 22-26 September 2014, Pisa (Italy).

3. C. Ferrari, "The calibration system of the muon g2 experiment at Fermilab", $100^o$ Congresso Nazionale della Societá Italiana di Fisica, 22-26 September 2014, Pisa (Italy).

4. A. Anastasi "The New Muon g-2 experiment at Fermilab (E989)", International Conference on Dark Matter, Hadron Physics and Fusion Physics (DHF14), September 24-26 2014, Messina (Italy).

5. A. Anastasi, "The calibration system of the new g-2 experiment at Fermilab", Poster at MesonNet meeting, 29 September-1 October 2014, INFN-Laboratori Nazionali di Frascati, Frascati (Italy).

6. A. Fioretti, "The calibration system of the new g-2 experiment at Fermilab", Poster at INO meeting, 1-3 October 2014, Brescia (Italy).

## 5 List of Papers/Proceeding

1. G. Venanzoni *et al.*, "The New Muon g-2 experiment at Fermilab", proceedings of ICHEP2014, to appear on Nuclear Physics B - Proceedings Supplements (NUPHBP).
2. A. Anastasi *et al.*,"The Muon g-2 experiment at Fermilab", proceedings of DHF14, to appear on EPJ Web of Conferences.

## References

1. A. T. Fienberg, L. P. Alonzi, A. Anastasi, R. Bjorkquist, D. Cauz, R. Fatemi, C. Ferrari and A. Fioretti *et al.*, Nucl. Instrum. Meth. A **783** (2015) 12

# KLOE-2

The KLOE-2 Collaboration at the LNF

D. Babusci, G. Bencivenni, C. Bloise (Resp.), F. Bossi, G. Capon (Ass.), P. Ciambrone, E. Dané (Art. 23), E. De Lucia, A. De Santis (Art.23), P. De Simone, D. Domenici (Art. 23), G. Felici, G. Fortugno (Tec.), S. Giovannella, F. Happacher, M. Iannarelli (Tec.), J. Lee-Franzini (Ass), M. Martini (Ass)*, M. Mascolo (PostDoc), S. Miscetti, A. Palladino (PostDoc), G. Pileggi (Tec.), B. Ponzio (Tec.), R. Rosellini (Tec.), P. Santangelo, I. Sarra (PostDoc), F. Sborzacchi (Tec.), E. Turri (Tec.), G. Venanzoni.

In collaboration with "LNF-SEA"
A. Balla, G. Corradi, U. Denni, A. Frani, M. Gatta, C. Paglia, G. Papalino

*Also Dipartimento di Scienze e Tecnologie applicate,"Guglielmo Marconi" University, Rome, Italy*

## 1 The operation at DAΦNE

First commitment of the Collaboration was the commissioning of the upgrades of the KLOE detector installed in 2013, together with the maintenance of the drift chamber and calorimeters and of all the subsystems needed for the data taking. Improvements on the data taking and especially on the procedures to control and set the operational parameters of the detectors and front end electronics went on all year long. Software development for the encoding, reconstruction and simulation of the new detectors is in progress. Unfortunately, a number of incidents forced to stop the $DA\Phi NE$ complex for several months delaying till November the start of data taking. During a run at the end of the year lasting 31 days KLOE-2 was able to collect about 120 pb$^{-1}$ of integrated luminosity in reasonable background conditions relating to an uptime of about 60%. Total uptime of $DA\Phi NE$ and KLOE without any cut on the background conditions in the same period exceeded 80%. These are considered promising starting point data even if not yet conclusive for the feasibility of a long run to collect 5 fb$^{-1}$.

## 2 Physics results published in year 2014

Progress in data analysis leaded to the publication of i) the most sensitive test in the quark sector of CPT and Lorentz invariance, from the study of quantum interference of neutral kaon pairs [1)], ii) the precision measurement of the branching fraction, BR($K^+ \to \pi^+\pi^-\pi^+(\gamma)$ ) $= 0.05565 \pm 0.00031_{stat} \pm 0.00025_{syst}$ [2)], and iii) the exclusion region for dark–photon production from the analysis of the $\mu\mu\gamma$ final state [3)]. Other analyses are being finalised and presented to international conferences, as a) the precision measurements of the transition form factors of the $\phi$ meson to the pseudoscalars, $\pi^0$ and $\eta$, b) the dalitz plot of the $\eta \to \pi^+\pi^-\pi^0$, an isospin–breaking process sensitive to the light quark masses; c) the searches for dark forces in the final states $e^+e^-\gamma$ and $\mu\mu$ plus missing energy.

### 2.1 CPT and Lorentz invariance test with entagled neutral kaon pairs

CPT and Lorentz invariance tests are considered a probe for physics at the Planck scale, where natural mechanisms of CPT violation are expected in connection with modifications in the space–time structure relating to quantum theory of the gravity. Space–time modifications could naturally

lead to Lorentz–invariance breaking that, in the low–energy regime accessible to experiments, are described by effective field theories, such as the Standard Model Extension, SME, widely used in CPT tests from a broad class of physics sectors, from atomic to particle physics, to cosmology. In year 2014 KLOE obtained the best sensitivity ever reached in the quark sector on CPT and Lorentz invariance, based on 1.7 fb$^{-1}$ of integrated luminosity. The test was performed on the entangled neutral kaon pairs, in the $\phi \to K_S K_L \to \pi^+\pi^-\pi^+\pi^-$ final state, studying the interference pattern as a function of sidereal time and particle direction in celestial coordinates (fig. 1). Due to the fully–destructive quantum interference at $\Delta\tau$=0, the distribution is very sensitive to CPT–violating effects, especially for decays near the IR.

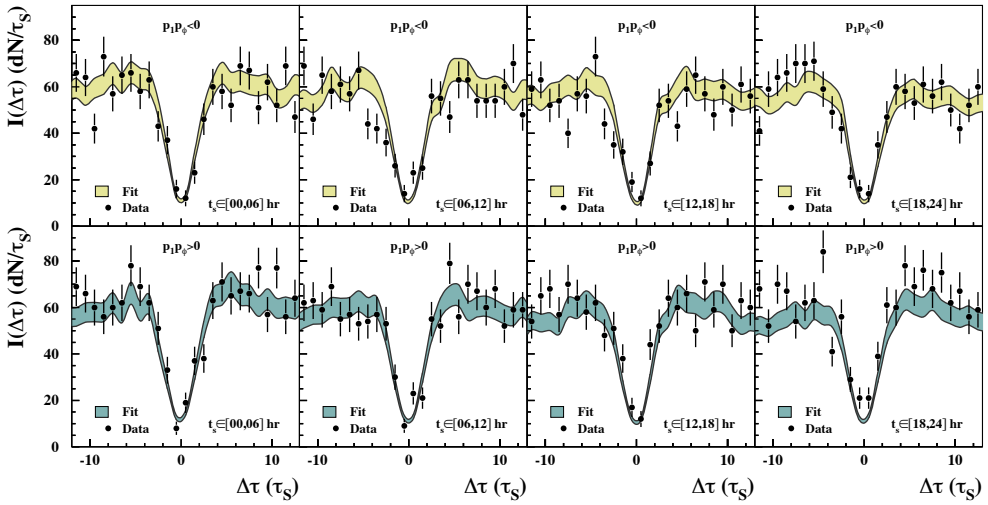


Figure 1: Fit to the distribution of the difference in proper time of neutral kaons as a function of sidereal time and particle direction in celestial coordinates [1].

The result is the measurement of all four CPT-violating parameters in the kaon sector of the SME [4]. In this context, $\Delta a_\mu$ parametrization of CPT–violation is used:

$$\delta_k \sim i \sin\phi_{\rm SW} e^{i\phi_{\rm SW}} \gamma_{\rm K} (\Delta a_0 - \vec{\beta_{\rm K}} \cdot \Delta\vec{a})/\Delta m \,, \tag{1}$$

where $\gamma_{\rm K}$ and $\vec{\beta_{\rm K}}$ are the kaon $\gamma$ factor and velocity in the laboratory frame, $\phi_{\rm SW} = \arctan(2\Delta m/\Delta\Gamma)$ is the so-called *superweak* phase, $\Delta m = m_{\rm L} - m_{\rm S}$, $\Delta\Gamma = \Gamma_{\rm S} - \Gamma_{\rm L}$ are the mass and width differences of the neutral kaon mass eigenstates. The neutral kaon system is expressed by:

$$|{\rm K_{S,L}}\rangle \propto (1+\epsilon_{S,L})|{\rm K^0}\rangle \pm (1-\epsilon_{S,L})|\bar{\rm K}^0\rangle, \quad with\ \epsilon_{\rm S,L} = \epsilon_{\rm K} \pm \delta_k. \tag{2}$$

Data reduction is based on two decay vertices with only two tracks each. For each vertex, invariant mass $|m_{\rm rec} - m_{\rm K}| < 5$ MeV, missing mass $\sqrt{E^2_{\rm miss} + |\vec{p}_{\rm miss}|^2} < 10$ MeV, -50 MeV$^2$ $< m^2_{\rm miss} < 10$ MeV$^2$, and kaon momenta compatible with the 2–body decay hypothesis are required, the missing momentum being obtained from the analysis of Bhabha scattering events. A global likelihood function is built in order to kinematically constrain the event and to improve on the vertex resolution.

Main background source is the kaon regeneration on the spherical beam pipe, suppressed by selecting events with both $K_S$ and $K_L$ decaying inside the beam pipe, that give a final contamination at the 2–3% level. Background contributions and analysis selection efficiencies are derived from MC simulation to which corrections from real data are applied. Full analysis chain was repeated several times varying all the cuts for the evaluation of the systematic uncertainties. The

sum in quadrature of all the effects ranges between 30% and 40% of the statistical error. The results [1] are the most sensitive measurements in the quark sector:

$$\begin{aligned}
\Delta a_o &= (-6.0 \pm 7.7_{stat} \pm 3.1_{syst}) \times 10^{-18}\, GeV; \\
\Delta a_x &= (\ 0.9 \pm 1.5_{stat} \pm 0.6_{syst}) \times 10^{-18}\, GeV; \\
\Delta a_y &= (-2.0 \pm 1.5_{stat} \pm 0.5_{syst}) \times 10^{-18}\, GeV; \\
\Delta a_z &= (\ 3.1 \pm 1.7_{stat} \pm 0.5_{syst}) \times 10^{-18}\, GeV.
\end{aligned} \tag{3}$$

For comparison, the accuracy reached by similar measurements in B and D systems is of $O(10^{-13})$ GeV [4].

### 2.2 The $K^+ \to \pi^+\pi^-\pi^+(\gamma)$ branching fraction

The measurement of the branching fraction (BR) of $K^+ \to \pi^+\pi^-\pi^+(\gamma)$ completes the KLOE program of precision measurements of the dominant kaon branching fractions, fully inclusive of radiation effects [5, 6, 7]. It is based on an integrated luminosity of $\int \mathcal{L}\, dt \simeq 174$ pb$^{-1}$ that corresponds to ∼17 million tagged $K^+$ mesons. The availability of tagged kaons enables the precision measurement of absolute BRs providing the normalization sample. The analysis procedure consists of i) the selection of $K^+$ candidates (tagging procedure) by the identification of $K^- \to \pi^-\pi^0$ and $K^- \to \mu^-\nu$ samples, independently treated; ii) the reconstruction of the $K^+$ path from the kinematical constraints given by the $K^-$ momentum and $\phi$ momentum (from Bhabha–scattering events); iii) the backward extrapolation of any charged track not belonging to the $K^-$ decay chain; iv) the reconstruction of the $K^+$ decay vertex radial position ($\rho_{xy}$) and the closest–approach distance ($CAd_i$) between the track and the $K^+$ flight path; v) the selection of events with at least two tracks with $CAd_i \leq 3$ cm and $\rho_{xy} \leq 26$ cm, outside the drift chamber (DC) sensitive volume (for a better control of systematics from tagging procedure); vi) the measurement of the missing–mass distribution, $M^2_{miss} = (\Delta E_{K^+-\pi\pi})^2$ - $|\Delta \mathbf{P}_{K^+-\pi\pi}|^2$ (fig.2). The analysis is fully inclusive of radiative decays. The tagging procedure affects the selection efficiency of the $K^+ \to \pi^+\pi^+\pi^-$ sample

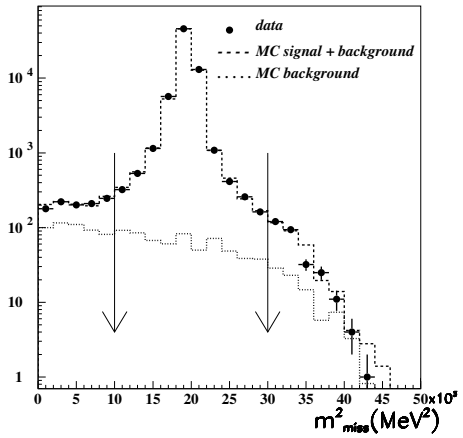


Figure 2: MC (dashed) and data (points) missing mass spectrum of the selected events. The arrows show the missing mass window for signal counting [2].

introducing a bias (tag–bias) on the BR measurement that has been evaluated from Monte Carlo simulation and used as a correction factor for the BR. Relating systematic error is estimated by changing the selection criteria of the tagging procedure. The other sources of systematics are the

analysis cuts and the uncertainty on the kaon lifetime [8]. All of the contributions give a systematic uncertainty of 0.6% [2]. In a sample of 12,065,087 (5,171,239) $K^- \to \mu^- \bar{\nu}$ ($K^- \to \pi^- \pi^0$ ) tagging decays we found $N_{K\to 3\pi} = 48,032 \pm 286$ $(20,063 \pm 186)$ signal events, from which we derive fully consistent measurements of the absolute branching fractions:

$$BR(K^+ \to \pi^+\pi^-\pi^+(\gamma))|_{TagK_{\mu 2}} = 0.05552 \pm 0.00034_{stat} \pm 0.00034_{syst}; \quad (4)$$

$$BR(K^+ \to \pi^+\pi^-\pi^+(\gamma))|_{TagK_{\pi 2}} = 0.05587 \pm 0.00053_{stat} \pm 0.00033_{syst}. \quad (5)$$

The average, $BR(K^+ \to \pi^+\pi^-\pi^+(\gamma)) = 0.05565 \pm 0.00031_{stat} \pm 0.00025_{syst}$ [2] has a 0.72% accuracy, that is a factor ∼5 better with respect to the previous measurement [9].

### 2.3 Dark photon searches

Some models of physics beyond the SM predict the existence of light neutral vector particles (the dark photon or U–boson) mediator of new gauge interactions under which ordinary matter is uncharged [10, 11]. Motivated by astrophysical arguments, their mass, $M_U$, is expected to be of order 1 GeV or lighter [12, 13]. Dark photon coupling to SM could arise from kinetic mixing with the $\gamma$/Z boson [14] and regulated by a dimensionless parameter $\epsilon$ expected to be of $O(10^{-3})$ or lower. These new particles can be observed as a sharp resonance at $M_U$ in the invariant mass distribution of charged lepton or pion pairs, in $e^+e^- \to l^+l^-\gamma$ or $V \to Pl^+l^-$ reactions, where $V$ ($P$) stands for any vector (pseudoscalar) meson, and $l^\pm$ for muons, electrons or charged pions. KLOE has searched for U boson production using both, $\phi \to \eta e^+e^-$ events (a), and $e^+e^- \to \mu^+\mu^-\gamma$ events (b). As for reaction (a), the papers of reference [15, 16] have been published in which the $\eta$ meson was identified from $\pi^+\pi^-\pi^0$ and $\pi^0\pi^0\pi^0$ decays in a sample of 1.7 fb$^{-1}$ of integrated luminosity at the $\phi$ peak. We obtained an excluded region at 90% CL in the $M_U$–$\epsilon^2$ plane that rules out kinetic mixing above 8 $10^{-6}$ in the mass range from 50–210 MeV (fig. 3). Reaction (b) was studied on the sample used for the measurement of the ratio $R = \sigma(e^+e^- \to \pi^+\pi^-)/\sigma(e^+e^- \to \mu^+\mu^-)$ exploiting the precision MC simulation and data analysis chain of the QED process $e^+e^- \to \mu\mu\gamma$ published in reference [26].

A $\mu\mu\gamma$ candidate must have two tracks of opposite charge, with the point of closest approach to the $z$ axis within a cylinder of radius 8 cm and length 15 cm centered at the IR. We require two tracks at large polar angle, $50^\circ < \theta < 130^\circ$, and one undetected photon. The separation between tracks and photon regions greatly reduces the contamination from both, the resonant $e^+e^- \to \phi \to \pi^+\pi^-\pi^0$, and FSR processes, $e^+e^- \to \pi^+\pi^-\gamma_{\rm FSR}$ and $e^+e^- \to \mu^+\mu^-\gamma_{\rm FSR}$. Electron, pion and muon pairs are identified by the mass obtained assuming an $e^+e^- \to x^+x^-\gamma$ process. In addition, a pseudo–likelihood estimator based on time-of-flight and calorimeter information is used for improving on the separation of electrons from pions and muons. Residual contamination and analysis efficiency is evaluated from MC simulations that have been controlled with real data samples. The differential $\mu\mu\gamma$ cross section is in excellent agreement with the expectations from the NLO PHOKHARA generator [27]. The exclusion plot for $e^+e^- \to$U$\gamma \to \mu^+\mu^-\gamma$ is obtained using the CL$_{\rm S}$ technique. It covers the mass region $520 < M_U < 980$ MeV (fig. 3), with upper limits at 90% CL on $\epsilon^2$ from 8.6 $10^{-7}$ to 1.6 $10^{-5}$.

## 3 Conclusions

KLOE obtained several results on kaon and hadron physics, and performed dark photon searches in the mass range from 20–980 MeV. Further studies on the interference pattern of neutral kaon pairs are in progress to improve on the sensitivity of quantum–mechanics tests with entangled

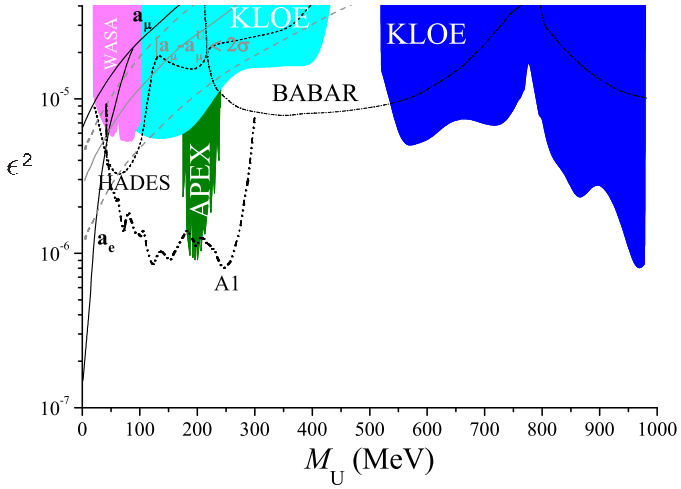


Figure 3: Exclusion plot at 90% CL in the $M_U$–$\epsilon^2$ plane obtained from the analysis of $\phi \to \eta e^+e^-$ (cyan) and the $e^+e^- \to \mu^+\mu^-\gamma$ (blue) final states [3]. Current limits from the A1 (dash–double dotted [17, 18]), Apex (green [19]), WASA (magenta [20]), and HADES (dashed [21]) experiments are also shown. The dash–dotted line is an estimate using BaBar data [22, 23, 24]. The solid lines are the limits from muon and electron anomaly [25]. Gray line shows values that could explain the $a_\mu$ discrepancy.

meson systems. As for the dark photon searches, the ongoing analysis of the $e^+e^- \to U\gamma \to e^+e^-\gamma$ process will extend the sensitivity to low masses, in the 2–200 MeV range, and the studies of the final state with two muons plus missing energy are investigating dark photon production through dark–higgsstrahlung, $e^+e^- \to Uh'$, assuming $m_{h'} < m_U$. In order to extend the KLOE physics program [28], the innermost part of the detector has been upgraded including tagger stations for $\gamma$–$\gamma$ physics, an inner tracker to improve on vertex resolution near the IR, and calorimeters both, to increase the acceptance at low polar angle, and to instrument the $DA\Phi NE$ focusing region. The commissioning of the new detectors and their integration in the KLOE DAQ and Control system is progressing towards the goal to enter in a smooth, stable data taking period with good quality data for physics, integrated at a rate exceeding 300 pb$^{-1}$ per month.

## References


1. D. Babusci et al. (KLOE-2), Phys. Lett. B **730**, 89 (2014)
2. D. Babusci et al. (KLOE/KLOE-2), Phys. Lett. B **738**, 128 (2014)
3. D. Babusci et al. (KLOE-2), Phys. Lett. B **736**, 459 (2014)
4. V.A. Kostelecky, N. Russell, Rev. Mod. Phys. **83**, 11 (2011)
5. F. Ambrosino et al. (KLOE), Phys. Lett. B **632**, 76 (2006)
6. F. Ambrosino et al. (KLOE), J. High Energy Phys. **02**, 098 (2008)
7. A. Aloisio et al. (KLOE), Phys. Lett. B **597**, 139 (2004)

8. F. Ambrosino et al. (KLOE), J. High Energy Phys. **01**, 073 (2008)
9. I. Chiang et al., Phys. Rev. D **6**, 1254 (1972)
10. P. Fayet, Phys. Lett. B **95**, 285 (1980)
11. B. Batell, M. Pospelov, A. Ritz, Phys. Rev. D **80**, 095024 (2009)
12. N. Arkani-Hamed, N. Weiner, J. High. Energy Phys. **12**, 104 (2008)
13. M. Pospelov, A. Ritz, M.B. Voloshin, Phys. Lett. B **662**, 53 (2008)
14. B. Holdom, Phys. Lett. B **166**, 196 (1986)
15. F. Archilli et al. (KLOE-2), Phys. Lett. B **706**, 251 (2012)
16. D. Babusci et al. (KLOE-2), Phys. Lett. B **720**, 111 (2013)
17. H. Merkel et al. (A1), Phys. Rev. Lett. **106**, 251802 (2011)
18. H. Merkel et al., Phys. Rev. Lett. **112**, 221802 (2014)
19. S. Abrahamyan et al. (APEX), Phys. Rev. Lett. **107**, 191804 (2011)
20. P. Adlarson et al. (WASA-at-COSY), Phys. Lett. B **726**, 187 (2013)
21. G. Agakishiev et al. (HADES), Phys. Lett. B **731**, 265 (2014)
22. M. Reece, L.T. Wang, J. High Energy Phys. **07**, 051 (2009)
23. J.D. Bjorken, R. Essig, P. Schuster, N. Toro, Phys. Rev. D **80**, 075018 (2009)
24. B. Aubert et al. (BaBar), Phys. Rev. Lett. **103**, 081803 (2009)
25. M. Pospelov, Phys. Rev. D **80**, 095002 (2009)
26. D. Babusci et al. (KLOE), Phys. Lett. B **720**, 336 (2013)
27. H. Czyz, A. Grzelinska, J.H. Kuhn, G. Rodrigo, Eur. Phys. J. C **39**, 411 (2005)
28. G. Amelino-Camelia, F. Archilli, D. Babusci et al., Eur. Phys. J. C **68**, 619 (2010)

**LHCb/LNF 2014**

M. Anelli (Tec.), G. Bencivenni, P. Campana ,
P. Ciambrone, P. De Simone, G. Felici, G. Lanfranchi,
F. Murtas, M. Palutan (Resp.), E. Paoletti (Tec.), L. Pasquali (Tec.), M. Rama,
A. Saputi (Tec.), A. Sarti (Ass.), B.Sciascia,
R. Vazquez Gomez (Bors. PD)

In collaboration with "LNF-SEA"
A. Balla, M. Carletti, G. Corradi, M. Gatta

## 1 Research activity

The $B_s^0 \to \mu^+\mu^-$ decay has been recently observed with a significance of $6.2\sigma$ through the combined analysis of LHCb and CMS data of LHC RUN I. [1)] The measured BR, $2.8^{+0.7}_{-0.6} \times 10^{-9}$, is in agreement with the SM prediction. With the same data, an evidence of the $B^0 \to \mu^+\mu^-$ decay with $3.2\sigma$ significance was observed ($1.8\sigma$ and $2.6\sigma$ from LHCb and CMS data, respectively). The measured BR is in this case $3.9^{+1.6}_{-1.4} \times 10^{-10}$, which is $2.2\sigma$ above the SM prediction. The above result concludes a search that started more than three decades ago, and initiates a phase of precision measurements of the properties of this decay. The LNF team, which represented in 2012 and 2013 the driving force in the LHCb $B_s^0 \to \mu^+\mu^-$ analysis working group, contributed substantially to this achievement, partecipating in all the aspects of the combination.

We remind here that a departure from the SM prediction on the $B_d/B_s$ ratio would falsify the Minimal Flavour Violation (MFV) hypothesis, consisting of identifying the flavour symmetry and symmetry breaking structure of the SM and enforcing it also for physics beyond the SM (BSM). The latter hypothesis is indeed an excellent phenomenological explanation for the lack of BSM physics signals in the flavor physics data so far. For the above reasons, the clarification of the experimental picture on the $B^0 \to \mu^+\mu^-$ decay rate is the challenge for this analysis during LHC RUN II.

In preparation of this, the LNF team devoted a considerable effort during 2014 in the optimization of the sensitivity for the $B^0 \to \mu^+\mu^-$ decay mode. On this respect, the main issue is the optimization of the rejection cuts for both the peaking background and the combinatorial background. Also important, is the control of the systematics in the determination of the peaking background. Our work, consisted of an improved determination of the hadron particle identification (PID) probabilities,

the usage of a new PID selection in the rejection of peaking background, and the introduction of more performant isolation variables in the rejection of the combinatorial background. The results have been presented in plenary LHCb meetings and documented in an internal note. [2)]

Besides the above analysis activity, considerable efforts have been spent by the LNF team on the PID calibration and performance assessment. The high degree of competence reached in this field has been recognized by the LHCb Collaboration, by appointing two members of LNF team, B. Sciascia and R. Vazquez Gomez, to the roles of LHCb PID coordinator and Muon Identification convener, respectively. As PID coordinator, B. Sciascia also acted as one of the editors of the LHCb detector performance paper. [3)]

Even though the physics harvest is now in full flow, and will continue certainly during the forthcoming LHC RUN II, the LHCb Collaboration has been already approved for an upgrade of the experiment, intended to collect $\sim 50$ fb$^{-1}$ starting in 2019, after the long shutdown 2 of LHC. This very large sample should allow to determine several SM variables in the flavor sector to a precision comparable with the ultimate theoretical uncertainty.

The LNF team will guarantee the full operation of the muon system readout in the upgrade conditions. Moreover, the LNF team is now coordinating the production of more than 50 MWPC muon chambers to use as spares in the next LHCb runs. Accepting this challenge was possible thanks to the support of LNF infrastructure, and to the local highly qualified expertise in this field. The material procurement phase is now close to completion, while the production chain has been fully activated at the LNF site.

For the upgrade phase, detailed studies on the detector hardware performances in special high luminosity runs have been carried out, which are the basis of the Particle Identification Upgrade TDR, [4)] endorsed by the CERN Research Board at beginning of 2014. Following these studies, during 2014 we concentrated on the projected performances of the muon identification algorithm at high luminosity, which are being now improved with a better deployment of the muon detector full information.

As demonstrated above, the LHCb LNF group has a leadeship role in many aspects, and this has been fully recognized by appointing Pierluigi Campana as spokeperson of the LHCb collaboration; Pierluigi concluded his three years mandate end of June 2014.

## 2 List of Talks by LNF Authors in Year 2014

1. P. Campana, "Summary Talk", Moriond QCD 2014, La Thuile, Italy, 22 - 29 Mar 2014.

2. P. Campana, "Highlights from LHC", QCD Confinement IX, St.Petersburg, 8-12 Sept 2014.

3. G. Lanfranchi, "Highlights from rare decays at LHCb", Incontri di Fisica delle Alte Energie, Laboratori Nazionali del Gran Sasso, 9-11 Apr 2014.

4. G. Lanfranchi, "The LHCb upgrade: physics perspectives", The Landscape of Flavour Physics in the high intensity era, Pisa, 9-10 Dec 2014.

5. M. Palutan, "Studio di decadimenti rari a LHCb" Congresso SIF 2014, Pisa, 22-26 Sept 2014.

6. B. Sciascia, "Rare B decays at LHC experiments", FPCP 2014, Marseille, 25-30 May 2014.

7. R. Vazquez Gomez,"Searches for exotica at LHCb", International Conference on High Energy Physics, Valencia, 2-9 Jul 2014.

## References


1. The CMS and LHCb Collaborations, "Observation of the rare $B_s^0 \to \mu^+\mu^-$ decay from the combined analysis of CMS and LHCb data", arXiv:1411.4413, accepted by Nature.

2. F. Archilli, M. Palutan, M. Rama, A. Sarti, B. Sciascia, R. Vazquez Gomez, "Background studies for $B^0 \to \mu^+\mu^-$ analysis optimization", LHCb-INT-2014-047.

3. The LHCb Collaboration, "LHCb detector performance", arXiv:1412.6352, published in International Journal of Modern Physics A, Vol. 30, No. 7 (2015).

4. The LHCb Collaboration, "LHCb Particle Identification Upgrade TDR", CERN/LHCC 2013-022, LHCb TDR 14, 28 November 2013.

# LAV Update

## Rapporto attivita lnf 2014

**A. Antonelli (Resp.), F. Gonnella (AR),G. Lamanna,
V.Kozhuharov (associato),G.Mannocchi (associato) M.Moulson, M.Raggi (Art.36,),T.Spadaro
In collaboration with
E. Capitolo, R. Lenci, V. Russo,
S.Valeri, T. Vassilieva
the Servizio di Progettazione Apparati Sperimentali (SPAS)
C. Capoccia, A. Cecchetti
the Servizio di Sviluppo e Costruzione Rivelatori (SSCR)
G. Bisogni, A. Franceschi
the Divisione Acceleratori, Servizio di Vuoto
V. Lollo
and the Servizio di Elettronica
G. Corradi, D. Tagnani.**

## The NA62 Experiment

The branching ratio (BR) for the decay $K^+ \rightarrow \pi^+ \nu\nu$ can be related to the value of the CKM matrix element $V_{td}$ with minimal theoretical uncertainty, providing a sensitive probe of the flavor sector of the Standard Model. The goal of the NA62 experiment at the CERN SPS is to detect ~100 decays decay $K^+ \rightarrow \pi^+ \nu\nu$ with a S/B ratio of 10:1.

The experiment makes use of a 75 GeV unseparated positive secondary beam. The total beam rate is 800 MHz, providing ~50 MHz of $K^+$'s. The decay volume begins 102 m downstream of the production target. 5 MHz of kaon decays are observed in the 65-m long fiducial vacuum decay region. Ring-shaped large-angle photon vetoes (LAVs) are placed at 12 stations along the decay region and provide full coverage for decay photons with 8.5 mrad < θ < 50 mrad. The last 35m of the decay region hosts a dipole spectrometer with four straw-tracker stations operated in vacuum. The NA48 liquid-krypton calorimeter (LKr) is used to veto high-energy photons at small angle. Additional detectors further downstream extend the coverage of the photon veto system (e.g.\ for particles traveling in the beam pipe).

### LNF group activity: Large Angle Veto detector

The principal achievements of the photon-veto working group in 2014 were in the completion of the construction and commissioning of the Large-Angle Veto (LAV) system that is under LNF group responsibility. Particular progress was made in the following areas:

- Construction, testing, and installation of the last LAV station, A12.
- Final cabling and HV tests for all of the LAV stations.
- Commissioning of the front-end and readout electronics for all stations.
- Development of the level-zero trigger firmware for the LAV system.
- Implementation and optimization of the reconstruction code for the LAV system.
- Analysis of 2014 data and measurement of LAV system performance.

The LAV system consists of 12 detector stations arranged at intervals of 6 to 10 m along the vacuum tank along its entire length. The first 11 stations are incorporated into the tank itself and are operated in vacuum; the 12th station is placed immediately downstream of the RICH and is operated in air. The diameter of the stations increases with distance from the target, as does the number of blocks in each, from 160 to 256, for a total of 2496 blocks. Each station consists of four or five rings of blocks, with the blocks staggered in azimuth in successive rings. The total depth of a five-layer station is 27 radiation lengths. This structure guarantees high efficiency, hermeticity, and uniformity of response.

The LAV system will mainly detect photons from kaon decays, as well as muons and pions in the beam halo. For each incoming particle, the veto detectors are expected to provide a time measurement with 1 ns resolution and an energy measurement of moderate precision (of order 10%). The system must be able to operate with thresholds of a few millivolts, well below the signal amplitude for minimum-ionizing particles (MIP) traversing the blocks, and maintain the detection efficiency as high as possible for muons and low energy photons.
Because of the intrinsic time resolution of the lead-glass blocks (<1ns) and the rise time of the Hamamatsu R2238 PMTs (5 ns), the requirements on the precision of the time measurement are not stringent. On the other hand, the amount of energy deposited in the LAV stations from photons from $\pi 0$ decays spans a very wide range, from about 100 MeV up to 30 GeV. Using the measured average photoelectron yield of 0.3 p.e./MeV and a nominal gain of 1 $x10^6$ for the R2238 PMT, one expects a signal charge of 4.5 pC for a MIP, corresponding to a signal amplitude of 20 mV on a 50 load. At the upper end of the photon energy range, signals from 20 GeV showers can reach an amplitude of 10V. The readout chain for the LAV stations consists of two different types of boards, a dedicated frontend board (LAV-FEE) developed for the LAV detector, and a common digital readout board called TEL62, used by most of the NA62 detectors.
The LAV-FEE splits the analogue signal from the PMT into two copies and converts each into a logical LVDS signal, using two comparators with independently adjustable thresholds. The duration of the LVDS pulses is equal to the time during which the analogue signal is above the programmed threshold. The LVDS logic signals are sent o the TEL62 readout board, in which a custom-designed TDC mezzanine converts each signal into digital leading and trailing times. The FPGAs on

board of the TEL62 are used to correct raw hit times for slewing and to produce a level-zero (L0) trigger primitive,which is sent to the L0 trigger processor using a dedicated gigabit Ethernet interface.
The system is designed to sustain hit rates of up to 100 KHz per channel and to be able to transmit a data volume to the L1 PC farm of up to 2.4 Gbit/s for each station.
The basic idea is to exploit the time-over-threshold (ToT) technique to measure the signal charge over a broad interval. A custom 9U board designed by the LNF Servizio di Elettronica converts the analogue signals from the PMTs into logical LVDS signals of equivalent width, as described above.

The first LAV station, A1, was constructed in 2009 and served as a prototype. As of August 2014, all twelve stations have been completed, delivered to CERN and installed on the beam line. During the construction of the LAV detectors, more than 2500 lead-glass blocks from the OPAL electromagnetic barrel calorimeter were processed (structurally reinforced, cleaned, fitted with new HV dividers, tested, and characterized).

After installation was completed, all of the LAV channels were tested in two steps. Signals from each channel were first examined manually with an oscilloscope. All 32 input channels on each front-end board were then simultaneously pulsed, and data from the board were read out with the full NA62 data-acquisition chain. At the start of data taking in October, inoperative channels were approximately 1% of the total.

During the lead-up to the 2014 run, there was significant progress on the implementation of the level-0 trigger for the LAV system. The NA62 level-0 trigger receives inputs, or “primitives”, from each detector system. These are generated by the FPGAs on the TEL62 boards, which examine buffered data during acquisition, and then forwarded to the central L0 trigger processor, which decides whether to initiate readout. The LAV level-0 firmware reconstructs physical hits by searching for matching leading edges on the low- and high-threshold channels of each block within a programmable coincidence window, nominally 6 ns; if a coincidence is found, a slewing correction is applied to obtain the hit time. The hits are sorted and hits within a programmable window up to 25 ns in length are merged. The primitive, if generated, contains the timestamp of the acquisition window to read out; the time resolution is 100 ps.

Primitives are continuously generated with a rate of up to 10 MHz, and during the 2014 run were used as a zero-bias monitor of the activity on LAV12. As illustrated in Fig. LAV-1, the spill structure is evident in the LAV12 primitive rate. During the 2014 run, the level-0 primitives provided the first evidence for the 75-Hz microstructure in the spill seen in the zoom in the bottom panel of the figure.

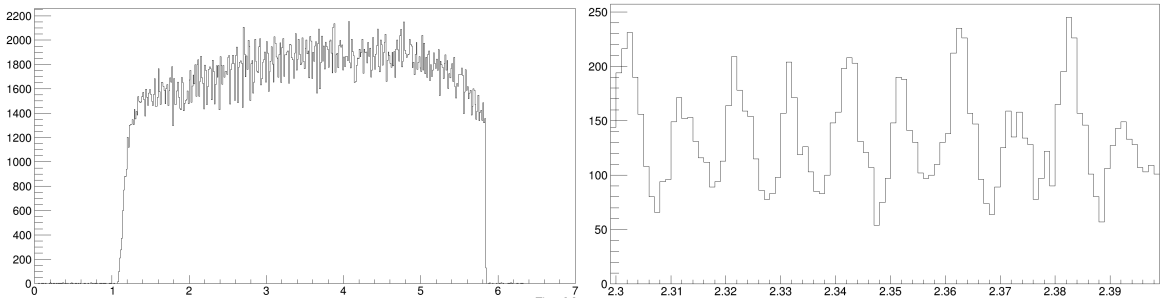


**Figure LAV-1.** Continuous monitoring of LAV12 hits from level-0 trigger primitives, in bins of 0.5 s (left), and zoom in bins of 0.02 s (right), showing evidence of 75-Hz spill structure.

During the 2014 run, the level-0 firmware for the LAV system was used as the basis for the development of the level-0 firmware for other NA62 detectors.

Much progress has been made on the LAV reconstruction code. Reconstructed hits are assembled by time-ordering the edges for the two thresholds on each block, matching leading and trailing edges, and looking for topologies such as a leading edge followed by a trailing edge on the low threshold only, or, for signals exceeding both thresholds, leading edges on the low and high thresholds, respectively, followed by trailing edges on the high and low thresholds, again respectively. Sequences of up to four edges from the same block are thus grouped into a single hit, and the hit time is calculated with channel-by-channel time offsets subtracted and slewing corrected. After hit reconstruction, hits on neighboring blocks are grouped into clusters, starting from a seed hit. Finally, the total charge, energy, time, and position are calculated for each cluster.

We have studied the performance of the LAV system using data collected during the 2014 run. Some preliminary results of these performance studies are presented in Figs. LAV-2 though LAV-4.

In Fig. LAV-2, the difference between reconstructed hit time and the event time from the trigger is plotted as a function of signal rise time, where the rise time is evaluated from the time between which the low and high thresholds are crossed. As noted above, first-order slewing corrections are performed during hit reconstruction. The effectiveness of these corrections is evident from the figure; the residual dependence observed of the hit time on rise time is parameterized from the distribution shown and applied separately as a final correction.

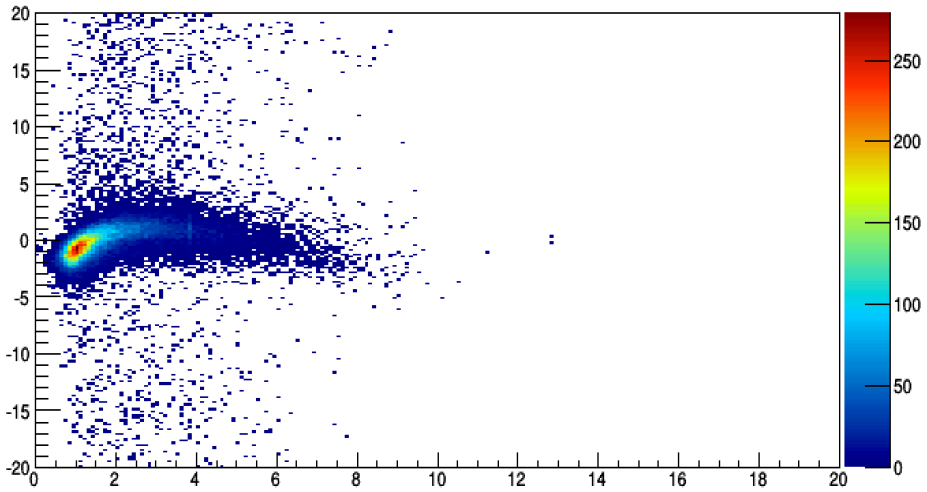


**Figure LAV-2.** Difference between LAV hit time and event time from KTAG (ns) as a function of signal rise time (ns).

The distribution of the difference between LAV hit time and event time from the trigger obtained after applying these residual slewing corrections is shown in Fig. LAV-3. A time resolution of better than 1 ns is obtained.

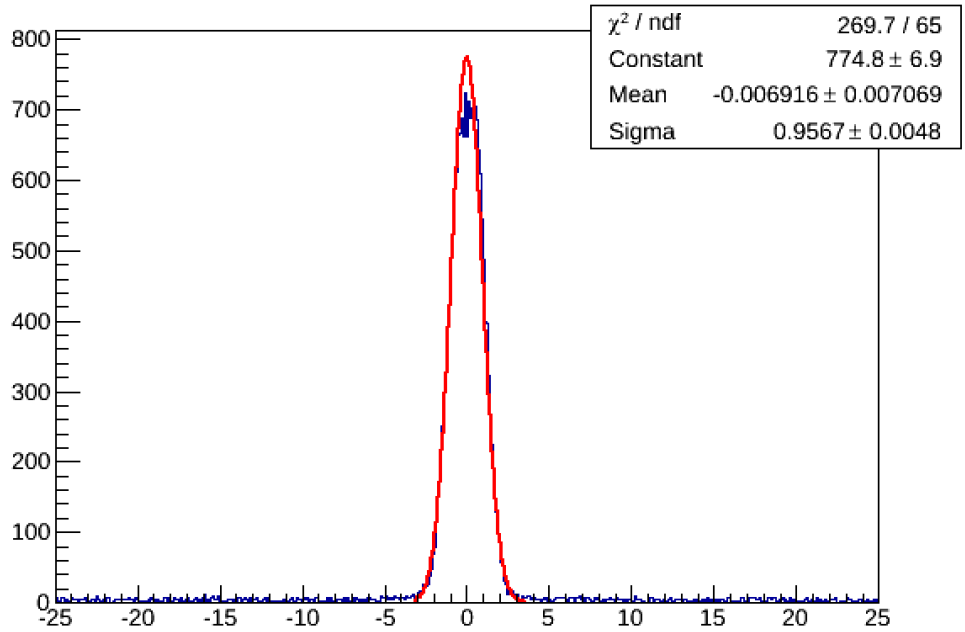


**Figure LAV-3.** Difference between LAV hit time and event time from KTAG (ns)

Two algorithms have been implemented for the collection of hits into clusters: one for photon clusters, which combines hits on adjacent blocks from an electromagnetic-like shower, and one for minimum-ionizing particles (mips), which combines hits passing through different layers, leaving a track-like signature. Figure LAV-4 shows the distribution of the difference in azimuth, $\Delta\phi$, between clusters on different stations vs. the number of stations between the most upstream and downstream clusters. Tracks from halo muons crossing many—even all—LAV stations are clearly observed. This suggests an extension of the mip clustering algorithm to provide for the reconstruction of mip tracks across LAV stations. This work is currently in

progress.

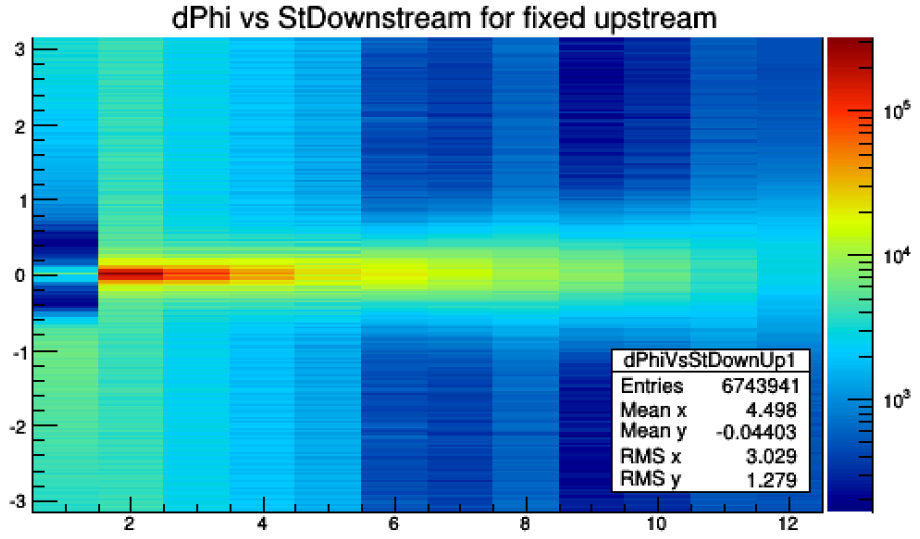


**Figure LAV-4.** Distribution of difference in azimuth, $\Delta\phi$, between clusters on different stations vs. the number of stations between the most upstream and downstream clusters.

By reconstructing hits from the passage of a mip on two appropriately chosen layers of a given station, the mip detection efficiency of the blocks on the remaining layers at the same azimuthal position can be determined. On two occasions in 2014, data with muon beam were taken. During these "muon runs", threshold scans were performed with the LAV detectors and used to study the mip detection efficiency via the method described above. The results are presented in Fig. LAV-5, which summarizes the average efficiency for all 12 LAVs as a function of threshold. The LAVs were operated successfully with thresholds as low as 4.5 mV. For threshold values below about 6 mV, a clear plateau is reached, with all stations reaching 96.5-98% mip efficiency. Recall that a mip passing horizontally through a LAV block leaves a signal of about 12 mV (after 6 meter cables attenuation) , corresponding to about 80 MeV of deposited energy.

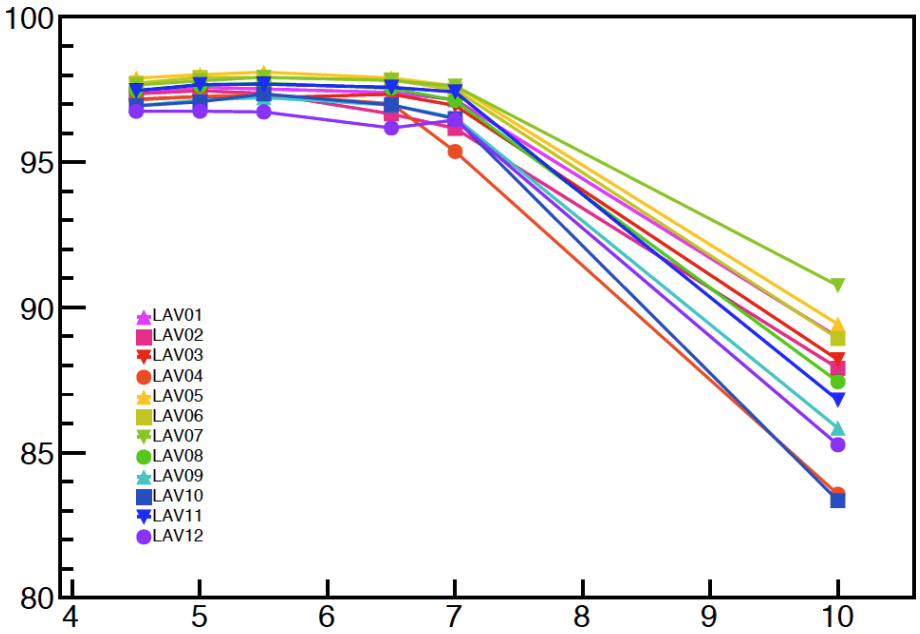


**Figure LAV-5.** Average mip detection efficiency for different stations as a function of threshold.

The photon detection efficiency for the LAV stations can be measured by reconstructing kaon decays for which the kinematics can be completely determined even without detecting a photon in the final state. We have begun to examine the LAV photon detection efficiencies using $K^+ \rightarrow \pi^+\pi^0$ events in the 2014 data. These events can be reconstructed on the basis of the candidate $\pi^+$ track on the spectrometer and a photon cluster from the $\pi^0$ in the LKr calorimeter. Assuming that the $K^+$ follows the nominal beam trajectory and that the secondary track in the spectrometer is a pion, $K^+ \rightarrow \pi^+\pi^0$ events can be cleanly selected by cuts on $M_{\mathrm{miss}}{}^2$ for the $K^+$-$\pi^+$ system and $\Sigma E_{\mathrm{miss}} - \Sigma P_{\mathrm{miss}}$ for the $K^+$-$\pi^+$-$\gamma$ system. The 4-momentum of the unobserved photon can then be obtained from kinematic closure. This analysis is in progress. To illustrate the potential of the method, Fig. LAV-6 shows the difference in azimuth between the expected position of the photon and the hit found in the LAV. Because beam tracking was not available in 2014, this plot was obtained using the nominal beam momentum; in addition, the algorithm used to reconstruct tracks in the spectrometer is preliminary. With information of the beam momentum and direction and the definitive spectrometer tracking, as well as refinements such as kinematic fitting, the angular resolution is expected to improve significantly.

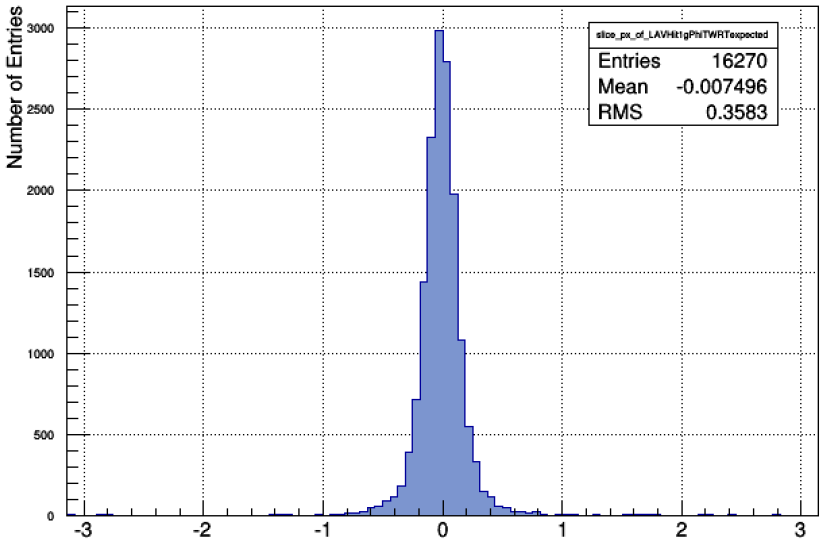


**Figure LAV-6.** Difference in azimuth (rad) between the expected position of the photon in $K^+ \rightarrow \pi^+\pi^0$ events and the hit found in the LAV.

**LNF group activity: SAC and IRC**

The small angle veto detectors covering photon angles down to zero degree with respect o kaon flight direction, SAC and IRC, are shashlyk type electromagnetic calorimeters.

They are exposed to a very high rate of photons from kaon decays and (for the IRC) muons from pion and kaon decays.

During this year the following tasks were accomplished:

- Completion of the IRC design
- Construction, installation, and commissioning of the IRC
- Analysis of 2014 data and evaluation of the SAC and IRC performance

At the start of 2014, the design of the IRC was completely reviewed at INFN Frascati, and the decision was taken to construct the IRC as a monolithic detector, rather than as two separate detectors modules suspended from the beam tube. All of the components were fixed with respect to the downstream flange of the IRC beam tube, and, in addition, the PMT support flange was glued at fixed position.

Special attention was paid to the certification of the IRC beam tube. Due to its thin walls, the IRC tube is one of the most critical elements of the vacuum system of the experiment. Several different stress tests were performed. The deformation with a free-floating upstream edge and evacuated tube was found to be less than 10 μm. The evacuated tube was also exposed to an external overpressure 50% higher than nominal for more than 18 hours; the tube did not develop any significant leakage and the vacuum inside was preserved. In addition, a complete finite element calculation indicates that the external buckling pressure is more than 2 bar. After these tests and calculations, the tube was certified for use in IRC construction.

The scintillating plates for the IRC were delivered by the end of June and the

assembly of the detector took place in July. Based on the results of a simulation using a purely geometrical model for light collection and signal propagation, a decision was taken to use straight fibers cut in front of the detector, rather than curved and threaed back through the holes. The use of cut fibers decreases the signal width from 25 ns to about 15 ns, which is crucial for double-pulse separation. The complete IRC assembly, as seen in Fig. SAV-1, was shipped from Frascati to CERN at the beginning of August.

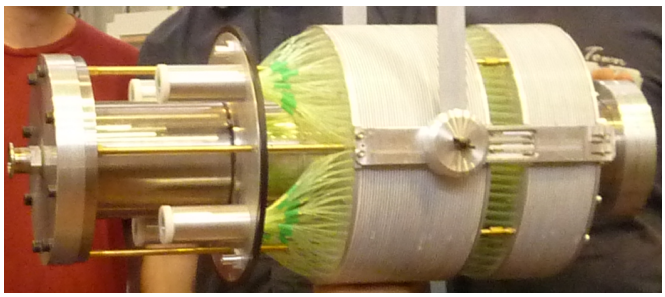

**Figure SAV-1.** The IRC assembly before shipping it to CERN

Both the SAC and the IRC were installed August and September 2014. They were aligned to a precision of better than 1 mm for each of the reference rod holes, since the IRC is the closest downstream detector to the beam axis, and the 23-mrad rotation angle of the SAC is necessary for high efficiency, to eliminate the possibility of photons escaping longitudinally via the through holes for the fibers.

Both the SAC and IRC were operated from the beginning of the run. The signals from both detectors were read out with the standard NA62 readout system, based on the LAV front-end board developed in Frascati and the TDC-TEL62 chain developed in Pisa. In parallel, a GANDALF-based FADC readout was installed. Although the firmware for interfacing the GANDALF system with the central NA62 data-acquisition system is not yet complete, the FADC system was tested during the run.

A simple online monitor for the SAC and IRC was implemented, based only on the total normalized rate, defined as the total number of hits in each detector normalized to the total number of recorded events for each burst, as shown in Figure SAV-2. This allowed monitoring of changes in the trigger definition and beam alignment, in addition to the proper operational status of the detectors.

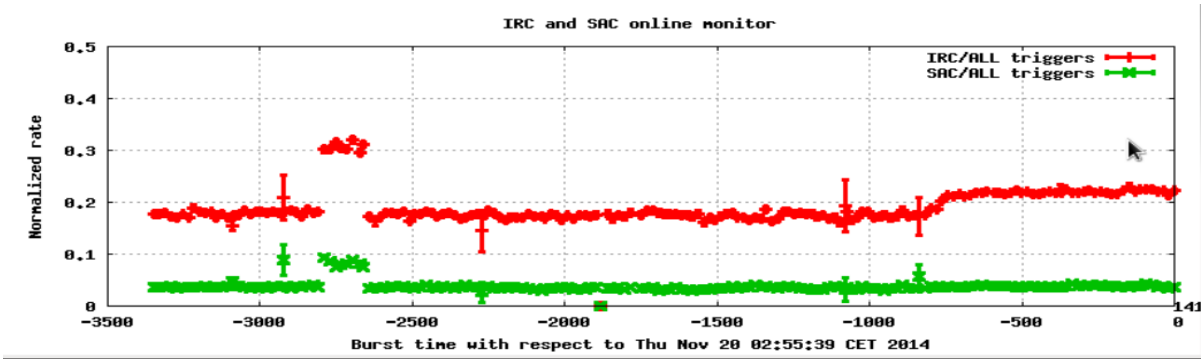

**Figure SAV-2.** The online monitor for the SAC and IRC.

The response of both detectors to minimum-ionizing particles (mips) was studied with data from the muon runs discussed in the previous section. The SAC and IRC event rates for different thresholds were fit with a cumulative Landau distribution function. The most probable value for the mip signal amplitude was found to be around 4 mV, which is consistent with expectation, and stable in both data sets.

Published paper

1)Study of the $K^+ \rightarrow \pi^+ \gamma \gamma$ decay by the NA62 experiment
C.Lazzeroni, et al, NA62 Collaboration, **Physics Letters B 732C (2014)**

Conference talk

**PANIC 14 ,Hamburg, Germany, 25-29 Aug 2014,** Tommaso Spadaro: Precision tests of the Standard Model with kaon decays at CERN

**BEACH 2014 , Birmingham, UK, 21-26 Jul 2014,** Mauro Raggi: QCD tests with kaons

**ICHEP 2014 , Valencia, Spain, 2-9 Jul 2014,** Gianluca Lamanna: Precision tests of the Standard Model with kaon decays at CERN

**QCD@work 2014 , Giovinazzo, Bari, Italy, 16-19 Jun 2014,** Venelin Kozhuharov: The NA62 experiment at CERN

**TIPP 2014 , Amsterdam, Holland, 2-6 Jun 2014,** Francesco Gonnella: The NA62 LAV front-end electronics and the L0 trigger generating firmware

**MESON 2014 , Krakow, Poland, 29 May - 3 Jun 2014,** Francesco Gonnella: ChPT tests at NA48 and NA62

# The MU2E project

M. Anelli, M. Cordelli, G. Corradi, U. Denni, A. Frani, G. Fuga, S. Giovannella, F. Happacher, A. Lucà (Dott.), M. Martini (Ass.), S. Miscetti (Resp.), B. Ponzio, G. Pileggi, R. Rosellini, A. Saputi, I. Sarra, V. Stomaci (Laur.), G. Venanzoni

## 1 Introduction

The Mu2e experiment, proposed at Fermilab, aims to search for the neutrinoless, coherent conversion of a negative muon into an electron in the Coulomb field of a nucleus [1)]. The measurement will be expressed by the ratio of the muon-to-electron conversion rate relative to the ordinary muon capture rate on an aluminum nucleus:

$$R_{\mu e} = \frac{\Gamma(\mu^- + Al \rightarrow e^- + Al)}{\Gamma(\mu^- + Al \rightarrow \nu_\mu + Mg)} \,. \tag{1}$$

The process of muon to electron conversion is an example of Charged Lepton Flavor Violation (CLFV). While it is strongly suppressed in the Standard Model (SM), (BR($\mu \rightarrow e$) $\approx 10^{-54}$), many scenarios of physics beyond the SM, predict enhanced BRs close to the reaches of current or near future experiments. Therefore, any signal is a compelling evidence of New Physics. If no events are seen in the signal window, the experiment is designed to set an upper limit of $R_{\mu e} \leq 6 \times 10^{-17}$ at 90% C.L. in three years of running. This value represents an improvement of four orders of magnitude over the current best experimental limit $R_{\mu e}(Au) < 7 \times 10^{-13}$, from the SINDRUM II experiment [2)]. The conversion of a muon to an electron in the field of a nucleus occurs coherently, resulting in a monoenergetic electron with an energy equal to the muon rest mass, apart from corrections for the nuclear recoil and the K-shell binding energy of the muon ($E_e = 104.97$ MeV). This distinctive signature has several experimental advantages, including the near-absence of background from accidentals and the suppression of background electrons near the conversion energy from muon decays.

The overall design of Mu2e is driven by the need to suppress potential backgrounds and to produce a high intensity, low energy muon beam that should provide around $10^{18}$ stopped muons on target. The desired Mu2e muon beam will be produced using the Fermilab accelerator complex, which will deliver 8 GeV protons into the *Mu2e beamline*. A pulsed structure of beam and a veto gate allow prompt beam background to die down during 750 ns, after which the detector is activated to look for $\mu$-atom decays. The Mu2e beamline consists in an evacuated inner bore (to $10^{-4}$ Torr) of a series of superconducting solenoids which form a graded magnetic field. Pions produced by target interactions and the muons into which they decay are captured. The muon stopping target composed of a set of thin aluminum foils and has a graded magnetic field. The graded field increases the acceptance for conversion electrons and plays a key role in rejecting certain backgrounds. The downstream section of the DS has a nearly uniform field ($< 1\%$ non-uniformity) in the region occupied by the Tracker and the Calorimeter that accurately analyze electrons emerging from the stopping foils.

The LNF group, together with INFN groups of Pisa and Udine is in charge of the construction of the calorimeter.

## 2 Characterization of LYSO crystals

The Mu2e calorimeter is composed by $\sim 2000$ crystals. The choice of the crystal composition is still in progress. Possible alternatives are $BaF_2$, pure CsI and LYSO. Extensive studies has been

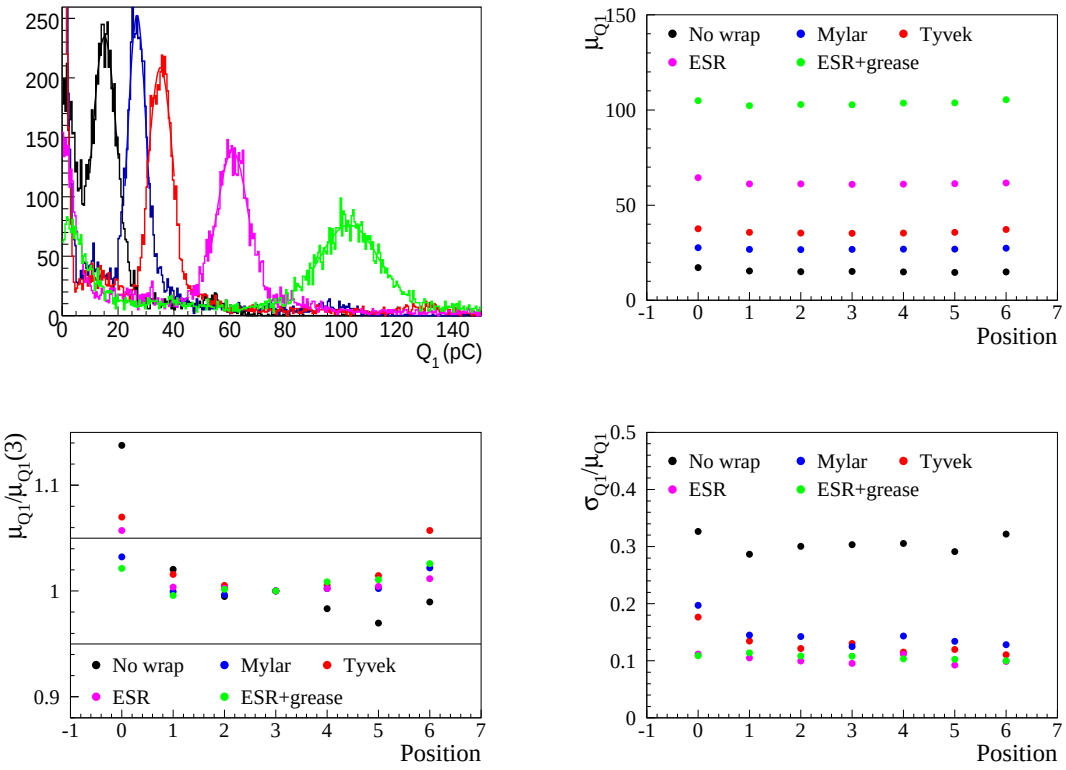


Figure 1: *Top-left: charge spectrum for a LYSO crystal, with $^{22}$Na source placed in the middle of the crystal along the longitudinal position, for different kind of wrapping: without any wrap (black), mylar (blue), tyvek (red) and ESR (magenta). The green distribution is obtained with ESR wrapping and optical grease. Light yield (top-right), linearity (bottom-left) and resolution (bottom-right) obtained from the $^{22}$Na scan of the same crystal along its length, for all configurations.*

done for sixteen $(3 \times 3 \times 13)$ cm$^3$ LYSO crystals. used to build a small calorimeter prototype (Sec. 2.2). For all of them, light yield, longitudinal uniformity, emission spectra and transmission quality have been measured.

### 2.1 Test results with $^{22}$Na source

Light yields and longitudinal uniformity for LYSO crystals have been measured using a collimated $^{22}$Na source that illuminates the crystals in a region of few mm$^2$. One of the two 511 keV photons produced by this source is tagged by means of a small monitor system constituted by a LYSO crystal, $(3\times3\times10)$ mm$^3$, readout by a $(3\times3)$ mm$^2$ MPPC. The second photon is used to calibrate the crystals, that is readout by means of a 1 inch bi-alkali Hamamatsu photomultiplier (PMT). Tag and test signals are both acquired by means of a CAEN DT5751 digitizer system at 1 Gsample.

Crystals have been tested both undressed and fully wrapped with different materials: mylar, tyvek and Enhanced Specular Reflector (ESR) from 3M. In this last configuration the effect of optical grease has also been studied. The longitudinal scan has been done in seven points, with 2

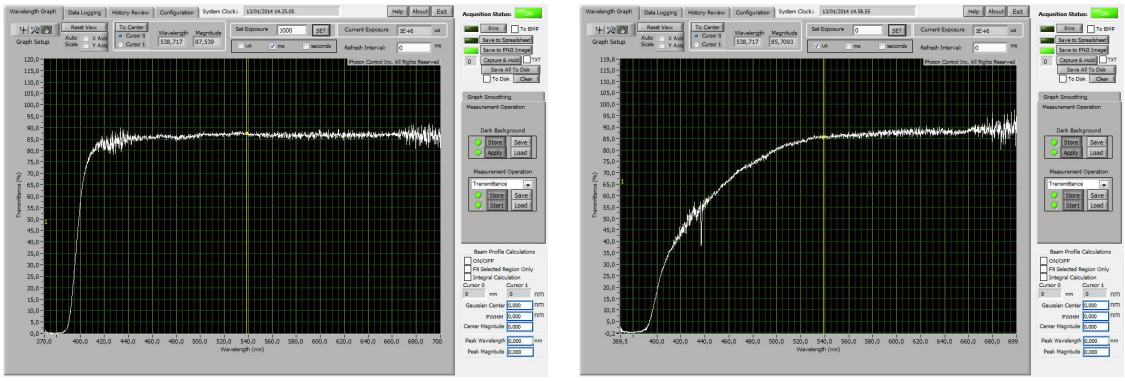

Figure 2: *Longitudinal transmittance (%) as a function of the wavelength in nm for a good (left) and a bad (right) transmitting crystal.*

cm steps, using both crystal orientation. In Fig. 1 light yield, linearity and resolution for one LYSO crystal with different types of wrapping are shown. The best yield is obtained with ESR wrapping, that increase the light output by a factor of 4. With the usage of optical grease a further 1.5 increase is obtained. After wrapping crystals, a resolution below 20% and a response uniformity better than $-1 \div 5\%$ are obtained.

### 2.2 Test results with spectrophotometer

A transmission station, LATTER (Longitudinal and Transverse Transmission Emission Response), has been designed and assembled during 2013 at LNF, tuned in the range 350-900 nm. A light source uniformly illuminates the back of the crystal while a spectrophotometer with a special focusing optics, is able to read light transmitted in a narrow ellipse of 1.5, 2 mm radii. The crystal can be positioned in front of the spectrophotometer by means of a dedicated crystal movement arm and can then be translated longitudinally, adjusted vertically or rotated around its axis by precise step-motors. The whole measurement of transmittance takes 5 sec/point. This setup allows to measure transmission and uniformity in both longitudinal and transverse directions. The emission spectra of the crystal can be also tested by firing a UV Led (350 nm) over its surface. All $(3 \times 3 \times 13)$ cm$^3$ LYSO crystals have been tested and qualified for longitudinal transmission by acquiring 8 points/crystal. Only one crystal was found with a bad longitudinal transmission, while all the others are above 75% at 420 nm and 80% at 440 nm. Examples of an acceptable and a not acceptable spectra are shown in Fig.1.2-left, 1.2-right respectively.

## New Prototype construction

During the year 2013 we have designed and realized a new larger prototype for the crystal calorimeter. This matrix is composed of 5x5 LYSO crystals of $(3 \times 3 \times 13)$ cm$^3$ dimension. Each crystal is read out by a $(10 \times 10)$ mm Hamamatsu APD and the signal is processed through a custom made voltage amplifier. We have also designed a custom board to provide HV to the APD and LV to the buffer/amplifier card. The analog signals are then digitized using VME CAEN V1720 modules. A light distribution system prototype has also been assembled. It consists of a 0.5 microJ/pulse green emitting laser (530 nm) synchronized with an external trigger followed by a 2 inch diffusing sphere from ThorLab and a bundle of 50 LEONI fused silica fibers. The fibers are inserted by means of

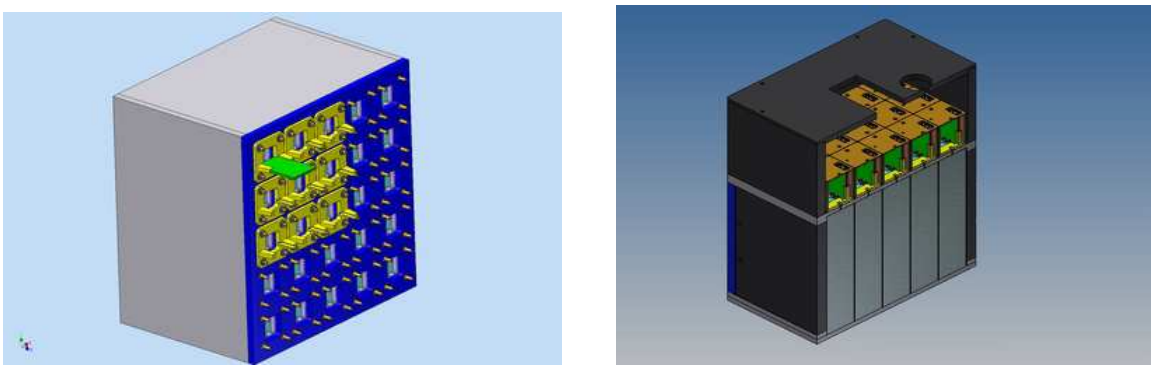

Figure 3: *Drawings of the crystal matrix prototype.*

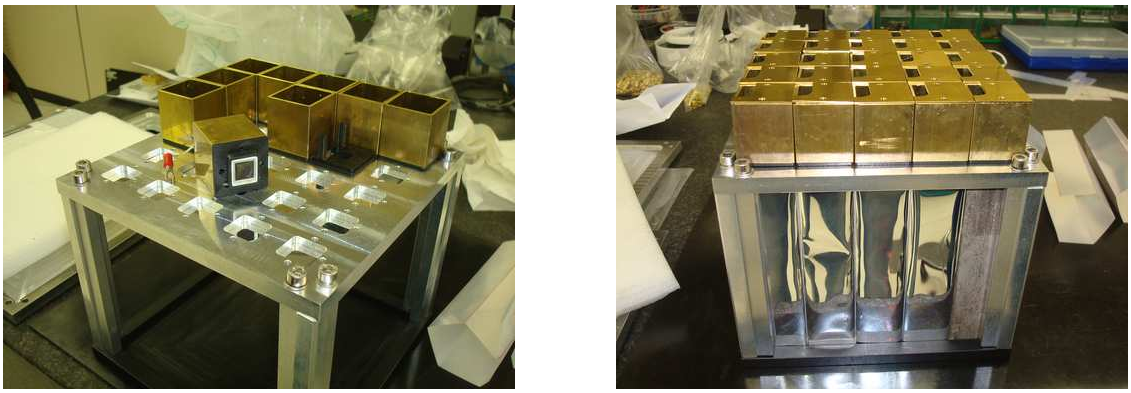

Figure 4: *Realization of the crystal matrix prototype.*

a dedicated connector close to the APD holders thus illuminating the crystal. By reflection and diffusion they allow to calibrate and monitor the APD gains.

In Fig. 3 the CAD drawings of the matrix layout are shown; the APD and the FEE boards are housed in holders that are obtained using PVC 3D printing. All LYSO crystals are wrapped in a 3M ESR film. The APD holders are inserted in a copper case with Faraday cage functionality to avoid noise pick up. The matrix is now fully assembled (see Fig. 4) and we will undertake a test beam campaign at the BTF facility in Frascati and with a tagged photon beam at the Mainz Microtron. For the moment we are calibrating the prototype with cosmic rays and laser pulses.

**Acknowledgments**

The authors are grateful to many people for the successful realization of the matrix. In particular, we thank all the LNF mechanical shop for the realization of the support, especially G. Bisogni, U. Martini and A. De Paolis. We also thank the SEA electronic department for the realization of the preamplifiers and for the design and control of the crystal test station.

## 3 List of Conference Talks by LNF Authors in Year 2013

1. F. Happacher, "A Crystal calorimetert for the Mu2e experiment", CHEF2013 - Calorimetry for High Energy Frontier 20-25 April 2013, Paris, France

## 4 List of Papers/Proceedings

1. G. Pezzullo *et al.*, "Cosmic Background rejection by means of the calorimeter in the Mu2e experiment at Fermilab", proceedings of CLFV-2013, Lecce, to appear on Nuclear Physics B Proceedings Supplement.
2. D. Brown for the Mu2e Collaboration, "Mu2e: A Muon to Electron Conversion Experiment", proceedings of CLFV-2013, Lecce, to appear on Nuclear Physics B Proceedings Supplement.
3. G. Pezzullo *et al.*, "The LYSO crystal calorimeter for the Mu2e experiment", proceedings of IPRD 2013, Siena, to appear on Nuclear Physics B.
4. F. Happacher *et al.*, "A LYSO crystal calorimeter for the Mu2e experiment", proceeding of CHEF 2013, Parigi.

## References


1. The Mu2e Collaboration, R. M. Carey *et al.*, http://mu2e-docdb.fnal.gov, document 388-v1.
2. W. Bertl *et al.*, Eur. Phys. J. C **47**, 337 (2006).

# UA9

S. Dabagov (Resp.)

Not received

# CUORE

M.A. Franceschi (Resp.)

Not received

# ICARUS_DTZ

H. Bilokon (Resp.)

Not received

# JEM-EUSO-RD

A. Franceschi, A. Marini (Assoc.), G. Modestino, T. Napolitano, M. Ricci (Resp. Naz.), F. Ronga (Assoc.)

The JEM-EUSO experiment (Extreme Universe Space Observatory at the Japanese Experiment Module of the International Space Station), is a planned space mission devoted to the observation and study of cosmic rays at the highest energies (UHECRs, UltraHigh Energy Cosmic Rays) above $10^{20}$ eV.
JEM-EUSO is a new type of observatory, based on a large UV telescope, which uses the whole Earth as a detector. It will observe, from an altitude of ~ 400 km, the fluorescence tracks produced at (330÷400) nm by Extensive Air Showers (EAS) originated by UHE primaries which traverse the Earth's atmosphere at ultra-relativistic speed.
The main scientific objectives, the instrument and the observational principle of JEM-EUSO have been described in detail in previous reports. Presently, new, intermediate configurations for a similar instrument to be placed on the Russian segment of the ISS (KLYPVE, K-EUSO) are being studied and in the phase of agreements with the Russian Space Agency Roscosmos.
Two pathfinders have already been developed, the first, EUSO-Balloon – managed by CNES, France - successfully flew on board a stratospheric balloon in August 2014 from Canada; a second, EUSO-TA on ground, is in operation at the Telescope Array site in Utah. A third, Mini-EUSO, approved by Roscosmos and selected by the Italian Space Agency, ASI, will be installed inside the ISS to study and measure the UV background from Earth. More short and long duration balloon flights are envisaged.
The LNF JEM-EUSO group is responsible (in collaboration with the SPCM LNF Service) of the design of the Focal Surface (FS) mechanical structure and of the 137 PDMs (Photo Detector Modules) which cover the entire FS where about 5000 multi anode Photomultipliers Hamamatsu M64 are accommodated.
Engineering studies have been carried out, including 3D CAD design of the structure, finite element model calculations, vibration mode studies related to the launch vehicle parameters. First assembled prototypes of PDMs have been produced for testing and for both pathfinders EUSO-TA and EUSO-Balloon. The mechanic box and the system interfaces of Mini-EUSO are under study, also in view of a possible integration of the whole instrument at LNF.
Members of the LNF group are involved in the JEM-EUSO Editor's Team of the Technical Reports and Design Reviews and in the JEM-EUSO Speaker's Bureau which manages and organizes the activities related to publications and conferences. The group participates and contributes to the definition and assessment of the scientific objectives of the mission. In 2014, the activity has been be mainly dedicated to the continuation and implementation of the engineering project of the FS structure according to different launch vehicle configurations. In the second part of the year, work on the analysis of EUSO-Balloon data has started. Scientific and technical contributions have been presented at the biennial COSPAR Conference, Moscow 2014 and in other Conferences and Workshops.

**Recent publications**

1. "The JEM-EUSO mission"; T. Ebisuzaki, et al (JEM-EUSO Collaboration), Adv. Space Res. **53**, 1499 (2014)
2. "Performance and air-shower reconstruction techniques for the JEM-EUSO mission"; M. Bertaina et al (JEM-EUSO Collaboration), Adv. Space Res. **53**, 1515 (2014)
3. "Calibration for extensive air showers observed during the JEM-EUSO mission"; J. Adams Jr et al. (JEM-EUSO Collaboration), Adv. Space Res. **53**, 1506 (2014)
4. "Observation of extensive air showers in cloudy conditions by the JEM-EUSO Space Mission"; G. Saez-Cano et al. (JEM-EUSO Collaboration), Adv. Space Res. **53**, 1536 (2014)
5. "A balloon-borne prototype for demonstrating the concept of JEM-EUSO"; P. von

Ballmoos, et al (JEM-EUSO Collaboration), Adv. Space Res. **53**, 1544 (2014)
6. "The Infrared Camera Prototype Characterization for the JEM-EUSO Space Mission"; J. A. Morales de los Rios, et al. for the JEM-EUSO Collaboration, NIMA **749,** 74 (2014)
7. "The JEM-EUSO Space mission"; G. Osteria for the JEM-EUSO Collaboration, Proceedings of the 14th ICATPP Conference (2014) p. 90
8. "The Data Processor of the JEM-EUSO pathfinders"; V.Scotti et al. for the JEM-EUSO Collaboration, Proceedings of the 14th ICATPP Conference (2014) p. 120

# KM3

Orlando Ciaffoni(Tec.), Marco Cordelli, Agnese Martini (Resp.), Luciano Trasatti (Ass.), Roberto Habel (Ospite)

The KM3 collaboration, in the framework of the KM3Net initiative, aims at building a km^3 scale Cerenkov neutrino detector in the Mediterranean Sea.
The first four PORFIDO probes were installed on the tower of NEMO Phase II (deployed in april 2013) and worked properly, reading and transmitting Temperature from a depth of 3500m until the tower was turned off in june 2014.
The LNF group has continued the development of the PORFIDO probes adding two 24 bit ADCs with 2 NTC temperature probes read by the WISP and providing two temperature measurements with an accuracy of better than 0.001 °C.
Four of these probe were installed in Optical modules in december 2014 to be mounted in one of the towers that will be deployed at the beginning of 2015. Eight more will be assembled and installed in Optical modules in 2015 as approved by the collaboration.
In addition we have realized a prototype of a salinity monitor connected to the same ADC with a resolution of about 1 ppm
On November 2014 the collaboration has deployed the first KM3Net Tower of the 12 to be deployed in the 2015 and the first Junction Box at the final site, 100 km SE of Capo Passero.

Publications

1. O. Ciaffoni et al.Using Neutrino Astronomy and RFID to Gather Oceanographic Data
Joshua R. Smith Ed. - Wirelessly powered Sensor Networks snd Computational RFID, Springer 2013

2. O. Ciaffoni et al. PORFIDO on the NEMO phase 2 and KM3 phase 1 towers
INFN- 14/12/LNF

**The NESSiE experiment proposal**

A. Longhin, A. Paoloni
in collaboration with
LNF-SPAS (Div. Ric.): A. Cecchetti, D. Orecchini

## 1 NESSiE and sterile neutrinos

A significant effort is ongoing in the neutrino physics community towards either verifying or disproving with sufficient confidence the experimental indications on *sterile* neutrinos. The hints of the existence of one or more extra neutrinos, not coupling via the electro-weak interaction, are: a deficit of $\bar{\nu}_e$ from nuclear reactors measured at distances of $\mathcal{O}$(10-100 m) from the core, a deficit of $\nu_e$ from MCi $^{51}$Cr and $^{37}$Ar calibration sources at $\mathcal{O}$(m) distances (SAGE, GALLEX), an excess of $\nu_e$ and $\bar{\nu}_e$ in artificial $\nu_\mu$ and $\bar{\nu}_\mu$ at distances of $\mathcal{O}$(km) (LSND, MiniBooNE) [1].

The NESSiE (Neutrino Experiment with SpectrometerS in Europe) experiment was first proposed in 2012 to search for sterile neutrinos with a short-baseline neutrino beam. The Collaboration is composed by groups from Zagreb, Moscow, Bari, Bologna, Lecce, LNF, Roma-1 and Padova.

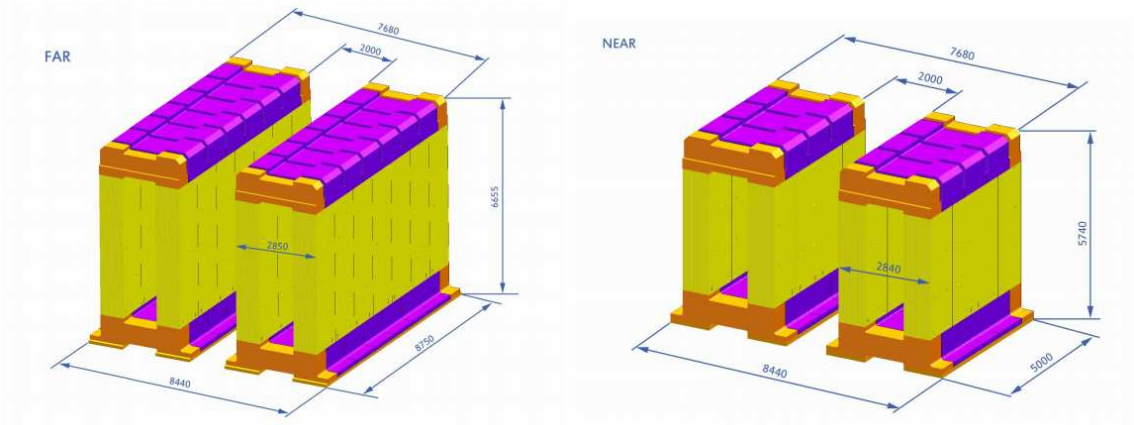


Figure 1: *Mechanical model of the far ICM (left), near ICM (right) from the SPAS.*

The experiment, which was originally conceived to be located at CERN, consisted of two almost identical detectors exposed to a 2 GeV $\nu_\mu/\bar{\nu}_\mu$ beam at two locations 640 and 1600 m away from the source. The existence of extra neutrinos with a squared mass difference with respect to the three known states $\Delta m^2$ of $\mathcal{O}(\mathrm{eV}^2)$ is expected to manifest itself both in terms of an energy-dependent disappearance of the $\nu_\mu$ and an appearance of $\nu_e$ above the intrinsic beam contamination. The NESSiE twin spectrometer would then have measured the charge and momentum of muons from $\nu_\mu^{CC}$ interactions occurring either inside the spectrometer iron or in an upstream LAr-TPC (ICARUS). After the CERN decision of not hosting a neutrino beam the experiment has been redesigned in 2014 to operate as a stand-alone experiment [1] to address the study of $\nu_\mu$ disappearance at the existing Fermilab (FNAL) Booster Neutrino Beam (BNB) [2].

Figure 2: *NESSiE at FNAL. Foreseen locations of the two spectrometers along the BNB beam.*

## 2 Activities of the NESSiE-LNF group

### 2.1 Spectrometer mechanical design

The LNF OPERA group, in synergy with the SPAS service, has been actively involved in the proposal since the beginning of the project and has played a crucial role thanks to the recognized expertise gained during the design and construction of the OPERA iron core magnet (ICM) spectrometers (mechanics and RPC detectors). The project has been naturally connected with the dismantling of the OPERA detector, activity in which the group is also involved. The layout of the ICMs for NESSiE is shown in Fig. 1 (SPAS technical drawings).

### 2.2 Beam simulation and sensitivity assessment for the FNAL option

The proposed double-site installation at FNAL is shown through an aerial view of the near and far sites locations in Fig. 2. The magnetic spectrometers would be hosted in existing infrastructures: the near site inside the SciBooNE experiment pit (100 m from the target) and the far one, on surface, at the NoVA-NDOS building (about 700 m). The LNF group has performed the beam simulation, the evaluation of beam systematics and their dependence from the position of the detectors along the beam. As an example we show in Fig. 3 one of the configurations which has been investigated. The performances have been evaluated considering the stability of the near-to-far ratio as a function of energy with respect to variations in the hadro-production model, using fits based on experimental data (HARP, E910). The study [2)] shows that this scenario could allow extending the exclusion region of $\nu_\mu$ disappearance at short baseline by about one order of magnitude in the mixing angle. The experimental proposal has been developed and submitted to the FERMILAB PAC.

### 2.3 Cosmic-ray tests of the Front-End electronics at LNF

The RPC chambers (about 1000) equipping the OPERA spectrometers are sufficient to instrument both the near and far site spectrometers. The RPC gas system, two power supplies and the refrigerating system for the magnet coils of the OPERA spectrometers can also be recovered.

NESSiE RPCs are foreseen to be operated in streamer mode, similarly to the OPERA system. The read-out chain however has been re-designed, to cope with the higher counting rates. The data acquisition system, is composed of a Front-End Board (FEB), a Controller Board and a Trigger

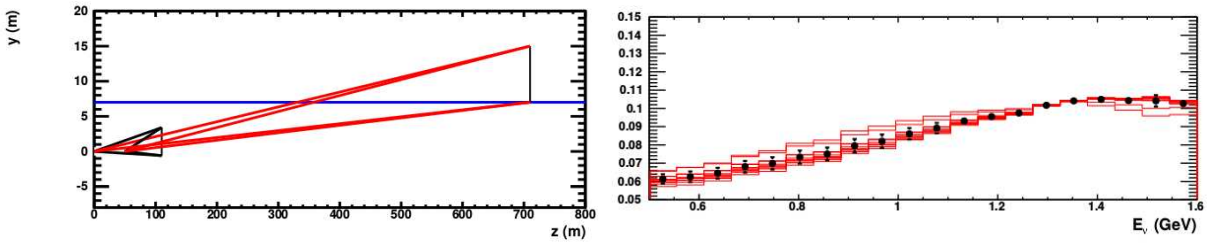


Figure 3: *Left: one of the considered far-near detector layouts. The x-axis is the coordinate along the beam, the y-axis is the vertical coordinate. The detectors are schematized by the black vertical lines. The blue line is the level of ground. Right: variations on the near-to-far ratio as a function of the neutrino energy introduced by hadro-production uncertainties in proton-target interactions. Each read histogram represents a variation of the hadro-production model within uncertainties* [2].

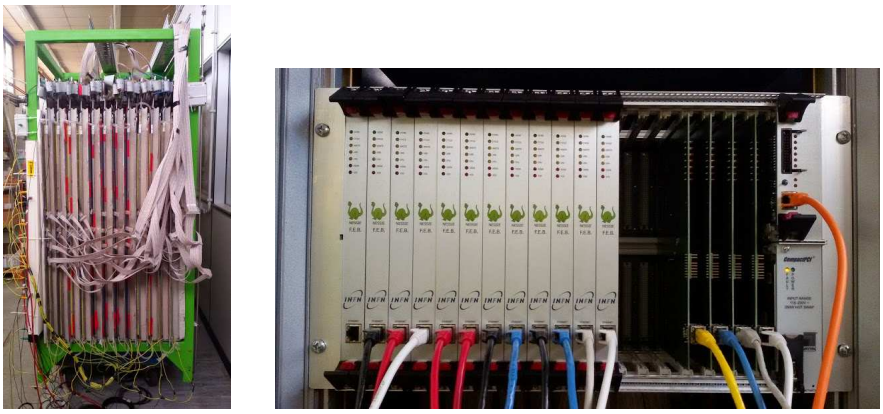

Figure 4: *Left: RPC test-stand at LNF. Right: NESSiE FEB boards under test at LNF.*

Supervisor. All the boards, designed by the INFN Bari electronics workshop, are provided with an Ethernet interface for configuration and data communication.

The full read-out chain has been tested, with the collaboration of the colleagues from NESSiE-Bari, in a dedicated cosmic ray test-stand which has been set-up inside LNF building 29. A batch of chambers belonging to the OPERA production and discarded by the quality control tests [3] has been used for the first measurements. The facility (Fig. 4, left) can house up to 12 RPCs, powered by CAEN SY127 units. The measurement of the current being performed at 50 nA precision level. The read-out of the signals induced by the passage of cosmic rays is performed by means of 3 cm wide read-out copper strips, connected through 6 m long twisted flat cables to the FEBs. The chambers can be flushed both with pure Argon (for resistivity measurements) and with the standard OPERA gas mixture [3]. In Fig. 5, left, the efficiency measured as a function of the operating voltage is shown for an applied signal threshold of 60 mV. The right plot shows instead the dependence on the threshold at a 6.2 kV voltage. High statistics efficiency maps (Fig. 6, top) have also been measured: the 10 cm pace spacer lattice is clearly visible, as well as the four grooves which are present along the upper edge of the chamber. Typical counting rates of 220

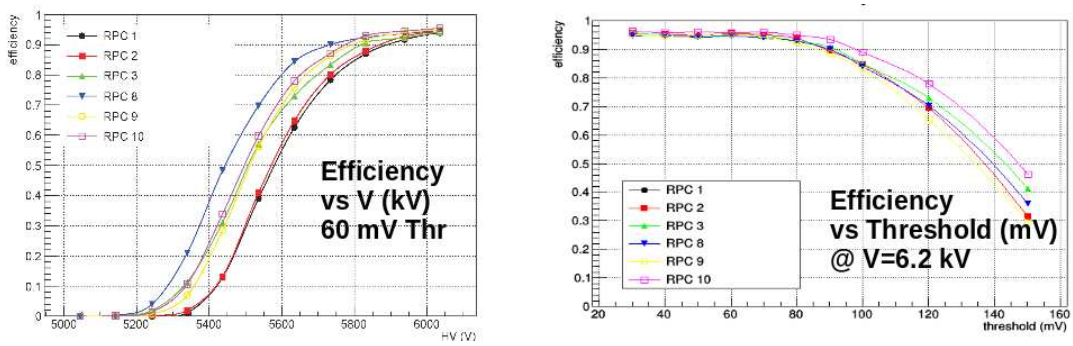


Figure 5: *Left: RPC efficiency as a function of the operating voltage. Right: RPC efficiency as a function of the discrimination threshold at 6.2 kV. Each curve corresponds to a different RPC chamber.*

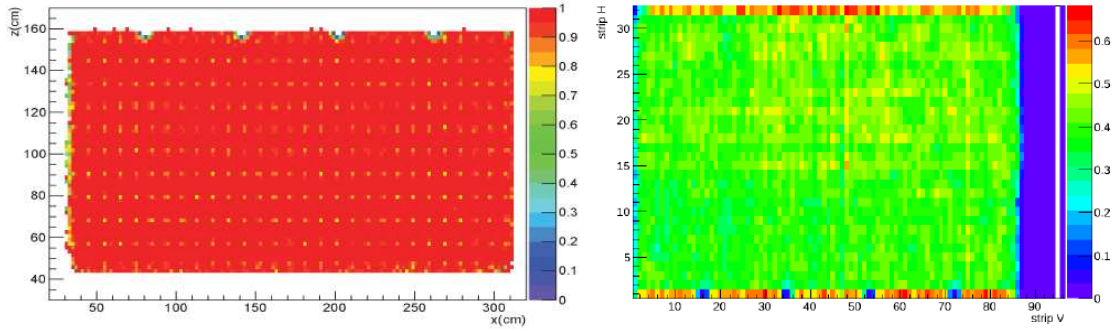


Figure 6: *Efficiency (top) and noise (bottom) map (Hz/9 cm$^2$) of one RPC measured at 6.2 kV with a discrimination threshold of 60 mV. The map has been obtained with a statistics of about one million reconstructed cosmic tracks.*

Hz/m$^2$ and operating currents below 700 nA have been measured. Detailed noise maps have been also produced by self-triggering each single RPC. An example is shown in Fig. 6, bottom.

This facility will be used in the future to characterize the functionality and performance of RPC chambers after nine years of operation, as they will become available during the dismantling of the OPERA spectrometers.

## References


1. L. Stanco *et al.* , *An Appraisal of Muon Neutrino Disappearance at Short Baseline*, Adv. High Energy Phys. 2013 (2013) 948626.

2. A. Anokhina *et al.* (NESSiE Coll.), *The NESSiE way to searches for sterile neutrinos at FNAL*, arXiv:1410.3980.

3. A. Paoloni *et al.*, *Gas mixture studies for streamer operation of RPCs at low rate*, Nucl. Instr. Meth. A **583** (2007) 264. *Tests on OPERA RPCs*, Nucl. Phys. B (Proc. Suppl.) **158** (2006) 93.

# The OPERA experiment

V. Chiarella, N. Intaglietta (Tec., art.15), A. Longhin, A. Mengucci (Tec.), A. Paoloni (Resp.), F. Pupilli, M. Spinetti, F. Terranova, T. Tonto (Tec.), M. Ventura (Tec.), L. Votano

in collaboration with

LNF-SEA: U. Denni, G. Papalino
LNF-SPAS: A. Cecchetti

## 1 The experiment

OPERA [1)] has been designed to provide a direct evidence for $\nu_\mu \rightarrow \nu_\tau$ oscillations in the parameter region indicated by Super-Kamiokande as the explanation of the zenith dependence of the atmospheric neutrino deficit. It is a long baseline experiment located at the Gran Sasso Laboratory (LNGS) and exploiting the CNGS neutrino beam from the CERN SPS. The detector [2)] is based on a massive lead/nuclear emulsion target. The target is made up of emulsion sheets interleaved with 1 mm lead plates and packed into removable "bricks" (56 plates per brick). Each brick is equipped with a detachable emulsion doublet ("Changeable Sheet", CS), which is scanned before the full development of the brick emulsions. The bricks are located in a vertical support structure making up a "wall". These bricks were produced in situ by a "brick assembly machine" (BAM) located near the OPERA experimental Hall; they are inserted into the wall support structure by a dedicated robot (BMS). Nuclear emulsions are used as high resolution tracking devices for the direct observation of the decay of the $\tau$ leptons produced in $\nu_\tau$ charged current interactions. Electronic detectors positioned after each wall locate the events in the emulsions. They are made up of extruded plastic scintillator strips read out by wavelength-shifting fibers coupled with photodetectors at both ends. Magnetized iron spectrometers measure charge and momentum of muons. Each spectrometer consists of a dipole magnet made of two iron walls interleaved with pairs of precision trackers. The particle trajectories are measured by these trackers, consisting of vertical drift tube planes. Resistive Plate Chambers (RPC) with inclined strips, called XPC, are combined with the precision trackers to provide unambiguous track reconstruction in space. Moreover, planes of RPC are inserted between the magnet iron plates. They allow for a coarse tracking inside the magnet to identify muons and ease track matching between the precision trackers. They also provide a measurement of the tail of the hadronic energy leaking from the target and of the range of muons which stop in the iron. A block of 31 walls+scintillator planes, followed by one magnetic spectrometer constitutes a "super-module". OPERA is made up of two super-modules (SM) located in the Hall C of LNGS (see Fig. 1). Since 2008 all bricks have been inserted, for a total of 150036 bricks, corresponding to a target mass of 1.25 kt, now decreased to 1.15 kt after the extraction of the bricks analyzed so far.

OPERA is able to observe the $\nu_\tau$ signal with an impressively low background level. The

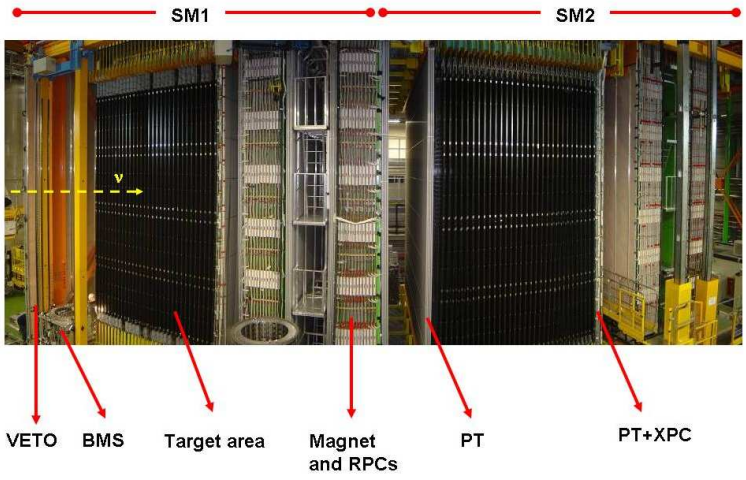


Figure 1: *A fish-eye view of the OPERA experiment. The upper red horizontal lines indicate the position of the two identical super-modules (SM1 and SM2). The "target area" is made up of planes of walls filled with lead-emulsion bricks interleaved with planes of plastic scintillators (TT): the black covers visible in the photograph are the end-caps of the TT. Arrows show also the position of the VETO planes, the drift tubes (PT) followed by the XPC, the magnets and the RPC installed among the magnet slabs. The Brick Manipulator System (BMS) is also visible. The direction of incoming neutrinos from CERN is indicated by the yellow arrow.*

direct and unambiguous observation of $\nu_\mu \rightarrow \nu_\tau$ appearance constitutes a milestone in the study of neutrino oscillations. Moreover, OPERA has some sensitivity to the sub-dominant $\nu_\mu \rightarrow \nu_e$ oscillations [3]. The potential of the experiment for the research of oscillations into sterile neutrinos and non standard interactions has also been investigated [4, 5].

Opera is an international collaboration (Belgium, Croatia, France, Germany, Israel, Italy, Japan, Russia, Switzerland and Turkey) and the INFN groups involved are Bari, Bologna, LNF, LNGS (Gran Sasso), Naples, Padova, Rome and Salerno. The Technical Coordinator (A. Paoloni), its deputy (M. Spinetti) and the Physics Coordinator deputy (A. Longhin) are LNF researchers. A. Longhin is also member of the PTB, Publications and Talks Board.

## 2 Overview of the OPERA activities in 2014

The CNGS complex ended its operation after the 2012 run, collecting, from 2008 to 2012, a total of $17.97 \times 10^{19}$ proton-on-target (about 80% of the statistics considered in the OPERA proposal), corresponding to 19505 events inside the OPERA bricks. To speed up the research of $\nu_\tau$ candidates in the exposed bricks, the collaboration decided to postpone the analysis of those events in which the neutrino vertex is not localized in the first scanned brick and to give priority to events without muons or with muons of momentum lower than 15 GeV. Up to the end of 2014, about 11000 bricks have been scanned and more than 6500 events fully analyzed.

During the last year, the collaboration reported the observation of the fourth $\nu_\tau$ candidate

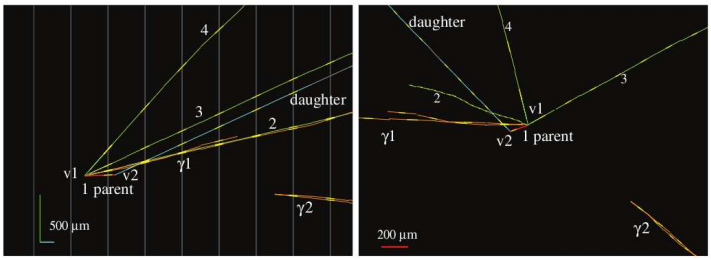


Figure 2: *Event display of the fourth OPERA $\tau$ candidate event in the y-z projection longitudinal to the neutrino beam (left) and in the transverse view (right).*

[6] in the single prong hadron decay channel, whose picture is shown in Fig. 2. The expected number of $\nu_\mu$ into $\nu_\tau$ oscillations is 2.11 (assuming full mixing and $\Delta m^2_{32} = 2.32 \times 10^{-3}\ eV^2$) with 0.22 background events. The non-oscillation hypothesis is therefore excluded at 4.2 $\sigma$.

The analysis of the bricks related to the events not yet located inside the bricks will proceed in parallel with the experiment de-commissioning, which has started in January 2015.

## 3 Activities of the LNF group

The Frascati group has been responsible for the design and the construction of the dipole magnets and the general support structure of the sub-detectors. It shared responsibility with INFN Padova and LNGS for the construction and running of the bakelite RPC planes. Frascati and Naples also designed and prototyped the wall support structures housing the lead/emulsion bricks and LNF was responsible for their production and installation. The Frascati group has been also involved, with the University of Hamburg, in the trigger of the drift tubes, performed by the Resistive Plate Chambers.

On the emulsion side, LNF was highly involved in the construction and operation of the Brick Assembly Machine (BAM) and, since 2008, contributes to the emulsion scanning with one dedicated microscope located in Frascati. Finally, since 2007 LNF follows the brick handling of OPERA, with the management of the X-ray marking facilities.

At present with the help of the SPAS, we are involved in the detector de-commissioning. The group is contributing also to data analysis, with particular interest in the precise background estimation in the $\tau \to \mu$ decay channel and in the sterile neutrino search exploiting the $\nu_\mu \to \nu_\tau$ oscillation channel.

### 3.1 Characterization of backgrounds for the OPERA appearance analysis

Muons originating from $\nu_\mu$ charged-current interactions of CNGS neutrinos can undergo a large-angle scattering in the target materials (lead, emulsion and plastic). This process represents the dominant background for the $\nu_\mu \to \nu_\tau$ search in the $\tau \to \mu$ channel (the remaining part being due to neutrino interactions with production of a charmed hadron decaying into a muon).

The signal region for genuine $\tau \to \mu$ decays was defined already in the OPERA proposal by requiring a kink angle $\theta > 20$ mrad and a transverse momentum $p_T > 250$ MeV/c for muons with

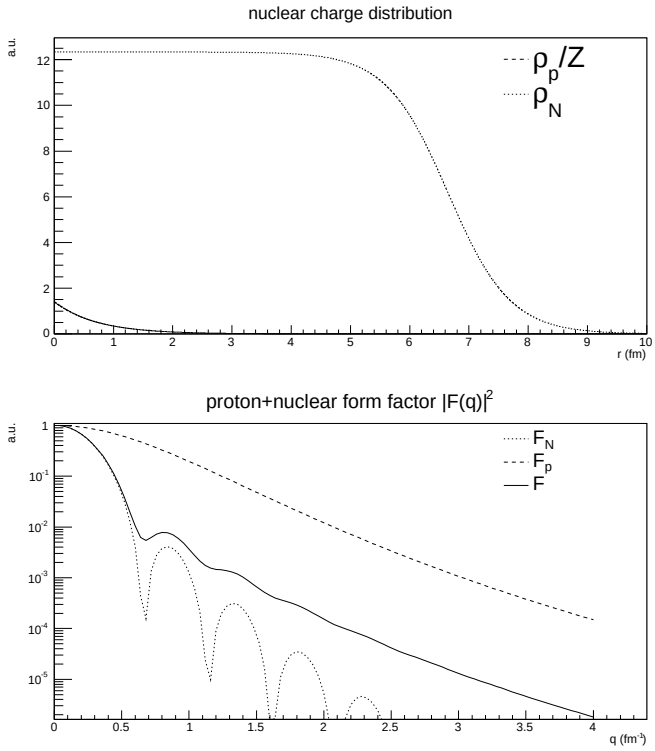


Figure 3: *Top: charge distribution for Lead (dashed) and protons (continuous). Bottom: resulting form factor taking the scattering off protons into account (continuous).*

momenta between 1 and 15 GeV/$c$. In this kinematic regime, the transferred momentum in the scattering is such that the De Broglie wavelength of the probe is smaller than the typical scale of a Lead nucleus. For a correct description of the high-angle tails of the scattering angle distribution it is thus mandatory to precisely take into account the nuclear charge distribution.

We have performed a new estimate of this background contribution using both simulation libraries (GEANT4) and theoretical calculations [7]. The GEANT4 code has been improved by implementing a realistic parametrization of the lead nuclear density based on the Saxon-Wood formula. The form factor for Lead used in the simulation is then the one shown in Fig. 3 (solid curve). The inclusion of scattering off protons (dotted curve) has also been taken into account. A total number of 2.2 billion incident CNGS $\mu^-$ have been simulated applying the sampling based on the form-factor in "single scattering" mode (about 7000 times per mm of Lead). The resulting distribution of the transverse momentum is shown in Fig. 4. The magenta histogram represents events falling in the $\tau \to \mu$ signal region. The background fraction for Lead is only $(5.9 \pm 0.5) \times 10^{-8}$ background events per $\nu_\mu^{CC}$ interaction, a value much smaller than what was previously assumed based on very conservative estimates.

In order to validate this modified simulation we have performed a comparison with previous experimental data from the literature. These data include several target materials (Lead [9], Copper [8]) and thicknesses with muon or electron [10] beams and energies spanning from 0.5 to

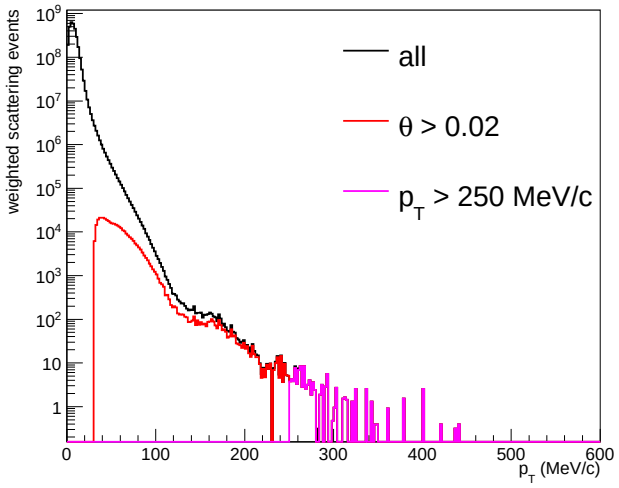


Figure 4: *Simulated distributions of the muon $p_T$ before cuts (black), after the angular cut $\theta > 20$ mrad (red) and after the angular and $p_T > 250$ MeV/c cut (magenta).*

11.7 GeV. The modified simulation is capable of correctly reproducing these measurements.

We have also investigated for the first time possible contributions from the muon photo-nuclear process which might in principle also produce a large angle muon scattering signature in the detector. This study was done using analytic formulas defining the cross section for this process. An upper limit in the OPERA phase space has been derived $< 2.7 \times 10^{-7}$ events/$\nu_\mu^{CC}$.

The new evaluation of the large-angle scattering background makes it a negligible contribution with respect to the charm background. These results are extremely relevant for the OPERA analysis, also in view of the observation of a clear $\tau \rightarrow \mu$ candidate $\nu_\tau$ event in 2013. Writing of a journal paper is in progress.

### 3.2 Sterile neutrino search in $\nu_\tau \rightarrow \nu_\mu$ oscillation channel [11)]

The OPERA experiment has so far detected 4 $\nu_\tau$ candidates, consistent with the number of events expected in the standard three neutrino framework (2.33 events for $\Delta m^2_{32} = 2.32 \times 10^{-3}$ $eV^2$, including 0.22 expected background events). Limits have been derived on the existence of a fourth sterile massive neutrino with mass $m_4$. The oscillation probability is a function of the $4 \times 4$ mixing matrix $U$ and of the squared mass differences. At $L/E$ values of interest for OPERA it can be parametrized as:

$$
\begin{aligned}
P(E) \;=\; & C^2 \sin^2(\Delta_{31}) \;+\; \sin^2(2\theta_{\mu\tau})\ \sin^2(\Delta_{41}) \\
& +\; 0.5\ C\ \sin(2\theta_{\mu\tau})\ \cos(\phi_{\mu\tau})\ \sin(2\Delta_{31})\ \sin(2\Delta_{41}) \\
& -\; C\ \sin(2\theta_{\mu\tau})\ \sin(\phi_{\mu\tau})\ \sin^2(\Delta_{31})\ \sin(2\Delta_{41}) \\
& +\; 2\ C\ \sin(2\theta_{\mu\tau})\ \cos(\phi_{\mu\tau})\ \sin^2(\Delta_{31})\ \sin^2(\Delta_{41}) \\
& +\; C\ \sin(2\theta_{\mu\tau})\ \sin(\phi_{\mu\tau})\ \sin(2\Delta_{31})\ \sin^2(\Delta_{41})
\end{aligned}
\tag{1}
$$

where $C = 2|U_{\mu 3}U^*_{\tau 3}|$, $\phi_{\mu\tau} = Arg(U_{\mu 3}U^*_{\tau 3}U^*_{\mu 4}U_{\tau 4})$, $\sin(2\theta_{\mu\tau}) = 2|U_{\mu 4}U^*_{\tau 4}|$ and $\Delta_{ij} = 1.27\Delta m^2_{ij}L/E$. $\Delta m^2_{31}$ and $\Delta m^2_{41}$ are expressed in eV$^2$, $L$ in km and $E$ in GeV. Given the long baseline and the average CNGS neutrino energy, *P(E)* is independent of $\Delta m^2_{21}$ since $\Delta_{21} \sim 0$. The terms proportional to $\sin(\phi_{\mu\tau})$ are CP-violating, while those proportional to $\sin(2\Delta_{31})$ are sensitive to the mass hierarchy of the three standard neutrinos, normal ($\Delta m^2_{31} > 0$, N.H.) or inverted ($\Delta m^2_{31} < 0$, I.H.). Matter effects have been neglected because the effective potential is identical for $\nu_\mu$ and $\nu_\tau$.

The experiment result likelihood has been defined as

$$
L(\Delta m^2_{41}, \phi_{\mu\tau}, \sin^2(2\theta_{\mu\tau}), C^2) = e^{-\mu}\ \mu^n/n! \tag{2}
$$

where $n = 4$ is the number of $\nu_\tau$ candidate events and $\mu$ is the expected number of events, obtained convoluting the oscillation probability with the neutrino flux, the $\nu_\tau$ charged current cross section and the $\tau$ selection efficiency, and adding the expected background. The value of $|\Delta m^2_{31}|$ has been fixed to $2.32 \times 10^{-3}$ eV$^2$ [12].

The analysis presented here is based on the $\chi^2$ statistics appropriate to small sample sizes:

$$
\chi^2 \;= -2\ \ln(\widetilde{L}(\Delta m^2_{41}, \sin^2(2\theta_{\mu\tau}))/L_0), \tag{3}
$$

where $L_0 = e^{-n}\ n^n/n!$ is a normalization factor and $\widetilde{L}(\Delta m^2_{41}, \sin^2(2\theta_{\mu\tau}))$ is the profile likelihood obtained by maximizing the likelihood over $C^2$ and $\phi_{\mu\tau}$. The likelihood profiling ($\chi^2$ minimization) procedure is performed considering the correlation between $C^2$, $\sin^2(2\theta_{\mu\tau})$ and $\phi_{\mu\tau}$ due to the dependence on the mixing matrix parameters.

In Fig. 5 the 90% Confidence Level (CL) exclusion limits are represented for normal and inverted mass hierarchy in the parameter space $\Delta m^2_{41}$ vs $\sin^2(2\theta_{\mu\tau})$. For simplicity sake, the sign of $\Delta m^2_{41}$ is considered to be positive. In the figure, the limits of direct searches for $\nu_\mu \rightarrow \nu_\tau$ oscillations obtained by NOMAD [13] and CHORUS [14] experiments at short baseline are also shown.

Our analysis extends down to $\Delta m^2_{41} \sim 10^{-2}$ eV$^2$ the limits obtained by the short baseline experiments, for $\sin^2(2\theta_{\mu\tau})$ values above 0.1. An exclusion region at $\Delta m^2_{41} \sim 10^{-3}$ eV$^2$ is also visible in the case of the direct hierarchy of the three standard neutrino masses, as a consequence of the fact that the expected number of $\tau$ events is lower than that expected in the standard three neutrino framework. The exclusion region at $\Delta m^2_{41} \sim 10^{-3}$ eV$^2$ disappears fixing the number of observed events equal to the number of events expected in the three neutrino framework. For negative values of $\Delta m^2_{41}$, similar plots are obtained with the three standard neutrino hierarchies exchanged.

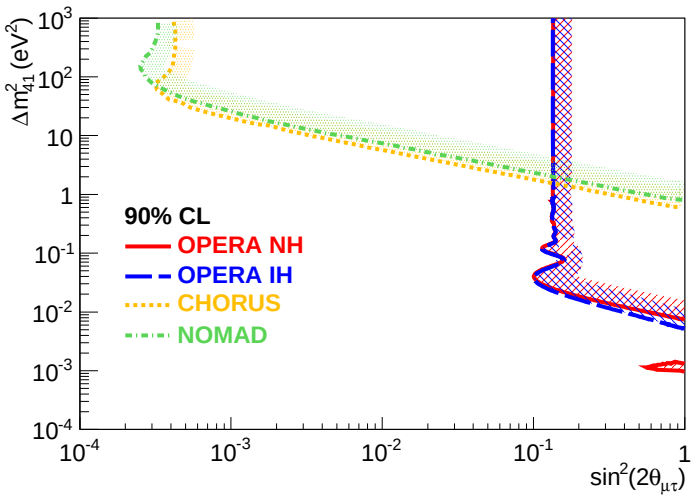


Figure 5: 90% *CL exclusion limits in the* $\Delta m^2_{41}$, $\sin^2(2\theta_{\mu\tau})$ *parameter space for normal (red) and inverted hierarchy (blue). Bands are drawn to indicate the excluded sides.*

### 3.3 Analysis of the OPERA emulsion detectors at the LNF scanning station

The OPERA brick is based on the Emulsion Cloud Chamber (ECC) detector concept, fulfilling the requirements of high granularity and micro-metric resolution necessary to distinguish the $\tau$ decay vertex from the primary $\nu_\tau$ interaction. Each ECC can act as a standalone detector that can be selectively removed from the target, developed and analyzed after the interaction took place.

A detailed description of the automatic microscopes developed for the analysis of OPERA ECCs can be found in Ref. [15]. The ECC (or "brick") dimensions and length are optimized to contain the primary as well the decay vertex and to provide particle identification and kinematical reconstruction. The use of passive material, combined with high accuracy tracking devices, allows for momentum measurement of charged particles via multiple Coulomb scattering (MCS) and for electromagnetic shower identification [16].

The bricks selected by the electronic detectors as containing a neutrino interaction vertex are extracted from the OPERA target and equally shared between Japan and Europe for the scanning. The CS doublet acts as a confirmation of the trigger provided by the Target Tracker: the brick is developed only if the prediction is confirmed, otherwise the CS is replaced and the brick is put back in the target. For events assigned to the European community the CS doublets are analyzed at the LNGS scanning station and the scanning load is shared among a group of specialized shifters. Since 2008 the LNF group contributes to the CS doublets scanning performing shifts at the LNGS station, in addition to the work load at the home scanning laboratory. The LNF scanning station [17] is part of the network of italian scanning groups including Bari, Bologna, LNGS, Napoli, Padova and Roma1 to which the emulsions developed at LNGS are sent for the final analysis.

The LNF emulsion scanning station (Building 29) is hosted in a climatised environment to ensure good conditions for emulsion storage. The station is equipped with a motorized optical

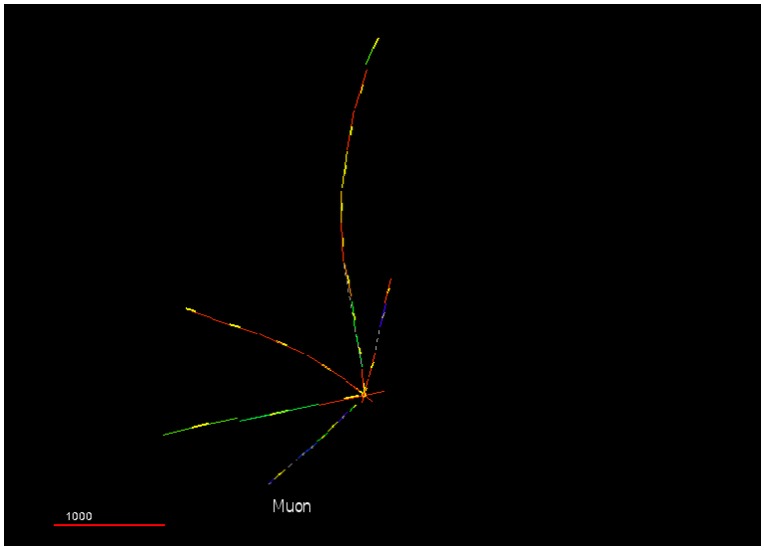


Figure 6: *Beam view of a charged-current neutrino interaction in an OPERA brick found at the LNF scanning station. The primary track matching the electronic detector reconstruction of the muon is also highlighted. The horizontal line defines a scale of 1 mm.*

microscope instrumented with a system for the emulsion plates loading on the microscope stage (Plate Changer). The whole chain for brick scanning at LNF is fully operational since 2008. It consists of three phases: the brick scanning, the event reconstruction and the data publication on the central database.

The 2014 activity of the LNF scanning station was addressed to the completion of the assigned data sample, in order to fit with the dismounting operations and the brick removal from the OPERA target. All the bricks belonging to the second super-module, the first one to be emptied, were fully analyzed, thus avoiding any relevant interference of our data sample analysis with the decommissioning. A small bunch of events recorded in the second super-module, that will be dismounted later next year, will be easily digested during 2015. A total amount of about 35 events was treated during 2014, with an overall location efficiency of $\sim$67%, well compatible with expectations. The emulsion reconstruction of one event located by the LNF facility is shown in Fig. 6.

The Frascati group also contributed to the systematic search of $\nu_e$ interactions with a dedicated analysis of an event sub-sample, selected by the presence of a shower-like topology in the related CS films. By a careful investigation of the emulsion films near to the primary vertex, we were able to explain the generation of the electromagnetic showers by $\gamma$-conversions, thus excluding the presence of $\nu_e$ interactions in the selected sample.

Besides the scanning activity we are also deeply involved in the development of the simulation and the global analysis of the emulsion data in view of upcoming publications.

## 4 List of Conference Talks by LNF Authors in Year 2014

1. A. Paoloni, "The OPERA RPC system", XII Workshop on Resistive Plate Chambers and Related Detectors, Beijing, China, 23-28 February 2014.

2. A. Longhin "Recent results from the OPERA experiment at the CNGS beam", DISCRETE 2014, Fourth Symposium on Prospects in the Physics of Discrete Symmetries, London, GB, 2-6 December 2014.

## 5 Publications

1. N. Agafonova *et al.* [ OPERA Collaboration ], "Evidence for $\nu_\mu \to \nu_\tau$ apperarance in the CNGS neutrino beam with the OPERA experiment", Phys. Rev. D **89**, 051102(R) (2014).

2. N. Agafonova *et al.* [ OPERA Collaboration ], "Measurement of the TeV atmospheric muon charge ratio with the complete OPERA data set", Eur. Phys. J. C 74:2933 (2014).

3. N. Agafonova *et al.* [ OPERA Collaboration ], "Procedure for short-lived particle detection in the OPERA experiment and its application to charm decays", Eur. Phys. J. C 74:2986 (2014).

4. N. Agafonova *et al.* [ OPERA Collaboration ], "Observation of tau neutrino appearance in the CNGS beam with the OPERA experiment", Prog. Theor. Exp. Phys. **101C01** (2014).

5. A. Paoloni, "The OPERA RPC system", JINST vol.9 C10003 (2014).

## References


1. M. Guler *et al.*, OPERA proposal, CERN/SPSC 2000-028, SPSC/P318, LNGS P25/2000.

2. R. Acquafredda *et al.*, JINST **4**, P04018 (2009).

3. M. Komatsu, P. Migliozzi, F. Terranova, J. Phys. **G29**, 443 (2003); P. Migliozzi, F. Terranova, Phys. Lett. **B563**, 73 (2003).

4. A. Donini, M. Maltoni, D. Meloni, P. Migliozzi and F. Terranova, JHEP **0712**, 013 (2007).

5. M. Blennow, D. Meloni, T. Ohlsson, F. Terranova and M. Westerberg, Eur. Phys. J. **C56**, 529 (2008).

6. N. Agafonova *et al.* [ OPERA Collaboration ], Prog. Theor. Exp. Phys. 101C01 (2014).

7. M. A. Meyer, Nucl. Phys. **28** 512 (1961).

8. S.A. Akimenko *et al.*, Nucl. Instr. Meth. **A 243** 518 (1986).

9. Masek *et al.*, Phys. Rev. **122** 937 (1961).

10. Frois *et al.*, Phys. Rev. Lett. **38** 152 (1977).

11. N. Agafonova *et al.* [ OPERA Collaboration ], ArXiv:1503.01876v1, submitted to JHEP.

12. J. Beringer *et al.* [ Particle Data Group Collaboration ], Phys. Rev. **D86** 010001 (2012).

13. P. Astier *et al.* [ NOMAD collaboration ], Nucl. Phys. **B601** 3 (2001).

14. E. Eskut *et al.* [ CHORUS collaboration ], Nucl. Phys. **B793** 326 (2008).

15. N. Armenise *et al.*, Nucl. Instrum. Meth. **A551**, 261 (2005).

16. L. Arrabito *et al.*, JINST **2**, P05004 (2007).

17. LNF scanning station.
`http://www.lnf.infn.it/esperimenti/opera/scanning.html`,
`http://www.lnf.infn.it/esperimenti/opera/scanning/figs/animation_54105.gif`

# ROG

G. Giordano (Resp.)

Not received

# WIZARD/PAMELA

G.Basini, M.Martucci (Dott.), G. Pizzella (Assoc.), M.Ricci (Resp.)

The space mission PAMELA, on board the Russian Satellite Resurs-DK1, is running and taking data since 2006 and will operate until the end of 2015 according to recent agreements between INFN, ASI and the Russian Space Agency Roscosmos. The instrument, the main scientific goals and the results of the experiment have been described in detail in the previous reports.
The LNF WIZARD/PAMELA group has continued in 2014 the regular activity in the analysis, running and quick-look control of the mission. In particular, it is fully involved in the study and analysis of solar events (Solar Flares, Solar Energetic Particles (SEP), Forbush decrease) in collaboration with Universities and Institutions (including NASA) in USA, Germany and South Africa. This work, in particular, is the object of a PhD thesis on the study of low energy protons in the cosmic radiation and the role of the Sun and the Heliosphere in their production and propagation in the Galaxy.
As it is well known, significant results have been obtained and published on the spectrum of positrons, electrons antiprotons, protons and He nuclei. An implementation and update of these results is in progress with the refinement of data reduction algorithms and the extension of the statistics.
The collection of all the results so far obtained by PAMELA has been published in 2014 in a monographic issue of Physics Report Journal (see publications below).
Presentations on the most recent results of the experiment have been given in several Conferences, in particular at the biennial COSPAR 2014 Conference, Moscow.
It is worth to note that, since 2013, under the agreement between INFN, ASI and Telespazio, a dedicated database for PAMELA has been created and developed and is in operation in the ASI Science Data Center (http://www.asdc.asi.it) as a data archive with open access through web interface to the scientific community.

**Recent publications**

1. "The PAMELA Mission: Heralding a new era in precision cosmic ray physics"; O. Adriani et al., Physics Reports, **544**, 323-370 (2014)
2. "Measurement of Boron and Carbon Fluxes in Cosmic Rays with the PAMELA Experiment"; O. Adriani et al., ApJ **791**, 93 (2014)
3. "The PAMELA experiment and antimatter in the universe"; M. Boezio et al. Hyperfine Interactions, **228,** 101, (2014)
4. "A method to detect positron anisotropies with Pamela data"; B. Panico et al., Nucl. Phys, B – Proc. Suppl., **256-257**, 173 (2014)
5. "PAMELA: Mission Status and Future Analysis Development"; E. Mocchiutti et al., Proceedings of the 14th ICATPP Conference (2014) p. 78
6. "Solar modulation of galactic protons and helium with the PAMELA experiment"; V. Formato et al., Proceedings of the 14th ICATPP Conference (2014) p.182

# ALICE

N. Bianchi, L. Calero Diaz (Ass.), P. Di Nezza (Resp. Loc.), A. Fantoni,
P. Gianotti, S.Liuti (Ass.), A. Moregula (Ass.), V. Muccifora, A. Orlandi (Tec.),
A.R. Reolon, F. Ronchetti, S. Sakai, E. Spiriti, A. Viticchié (Tec.)

## 1 Introduction

ALICE is an experiment at CERN which involves about 1600 physicists from more than 150 Institutions from several Countries. Italy participates with 12 groups and about 200 physicists. The Frascati group is deeply involved in the electromagnetic calorimeters (EMCal, DCal), both on the hardware and software side, while for the data analysis the group is focused on the physics of the jets from both light and heavy flavours. The choice of these specific analyses comes from the fact that the calorimeters, in addition to the tracking, enables ALICE, like no other experiment before, to explore the physics of jet quenching, i.e. the interaction of energetic partons with the QCD hot and dense medium, over the large kinematic range provided by the LHC. EMCal and DCal provide both fast triggers (level 0 and 1) for photons, electrons, and jets, and a High Level Trigger (HLT) as well. They also measure the neutral energy component of jets, enabling full jet reconstruction in all collision systems, from proton-proton to Pb–Pb, passing through the p–Pb collisions. The combination of the EMCal+DCal calorimeters, the excellent ALICE charged tracking capabilities, and the modest ALICE magnetic field strength, is a preferred configuration for jet reconstruction in the high background environment of heavy-ion collisions, allowing detailed optimization of background rejection while preserving the crucial jet quenching signals down to very low transverse momenta.

The majority of the INFN groups in ALICE decided to participate to the major upgrade of the spectrometer by constructing a new generation Inner Tracking System (ITS) based on hybrid silicon pixel detectors or Monolithic Active Pixel Sensors (MAPS), with greatly improved features in terms of: determination of the distance of closest approach (DCA) to the primary vertex, standalone tracking efficiency at low $p_T$ , momentum resolution and readout rate capabilities. The new detector will replace the existing ITS and will be installed during the LHC Long Shutdown 2. The Frascati group is involved both in the R&D for the electronic testing station and as the hub for the final assembly and test of the modules (staves) ready to be installed in the ALICE spectrometer. ALICE data open the frontiers to rare events, to very high transverse momentum jets, to flavour jet physics, and give new tools for investigating the QCD and the Quark Gluon Plasma.

## 2 Calorimeters

The DCal expands the physics capabilities of the EMCal by enabling back-to-back correlation measurements, which are impossible with the EMCal alone and are essential to obtain a complete picture of the physics addressed by the EMCal. Together, DCal and EMCal form a two-arm electromagnetic calorimeter. The EMCal subtends 110° and the DCal subtends 60° in the azimuthal angle $\phi$, with both detectors covering a pseudorapidity range $|\eta|$ <0.7, thereby providing good acceptance for di-jets with radii R<0.4.

The LNF group had the responsibility of coordinating the construction and assembly of the detector in the European-Asiatic zone and provided all WLS fibers for 1.5 DCal super-modules and for the 2 reduced length super-modules, for a total of 62000 fibers, grouped in 1700 bundles.

After a full calibration, the DCal installation has been completed on October $28^{th}$ 2014, about two weeks ahead of schedule, the commissioning activities started immediately after.

All Front End Cards have been reprogrammed with the new Board Controller firmware, while work on the readout of both EMCal and DCal has been carried on.

## 3 Post LS1 and RUN2 Readiness contribution

LHC Long Shutdown 1 (LS1) has been a time of intense installation, consolidation and upgrade work also for the ALICE detector. The interventions touched virtually all sub-detectors and online systems of the experiment.

LNF group had the heavy and important responsibility for coordinating the consolidation work and preparation for the data taking 2015.

During the shut-down period many new features have been implemented in the readout/online environment to double the readout rate and improve the efficiency of data taking online. In particular it has been developed a fast Start Of Run / End Of Run DAQ to reduce the time required to stop/start a run in case of hardware failures. Another improvement is given by the PAR (Pause And Recover) which will allow the detectors to reset the hardware with a simple pause of the data taking. A dynamical tune of the different triggers will allow fast coupling with different luminosities. In July a new control room has been put into operation. From July till the end of the year the integration of all detectors in the new framework has been completed and several weeks of cosmics runs for detector calibration/alignment have been taken. LS1 has also seen the design and installation of a new subsystem, the ALICE Diffractive (AD) detector consisting of two double layers of scintillator counters placed rather far from the interaction region, respectively in the ALICE cavern (at z=16 m) and in the LHC tunnel (at z=-19 m).

After the major LS1 detector installations and the massive interventions performed on almost all components of the hardware, electronics, and supporting systems, ALICE has began an early integration campaign at the end of 2014. This has lead to the first data taking during the beam splash events of the transfer line test of the past November.

## 4 The new Inner Tracking System

LNF will be one of the five world laboratories for the assembly of the new ALICE Inner Tracking System (ITS). The decision came in October 2014 and since then activities to prepare a new laboratory and a clean room fully instrumented are intensively carried out. In addition, a strong contribution has been given in an intensive test campaign taken place at the LNF Beam Test Facility in order to characterize the sensors under development for the ITS upgrade. The testing setup previously used for other activities has been upgraded with four planes of M28 sensors (binary output, 20.8 $\mu$m pitch, 50 $\mu$m thickness, 2 x 2 cm$^2$ area) developed for the STAR experiment upgrade (at RHIC BNL) to improve the tracking capabilities implementing a final configuration of six tracking planes including the two 1.6 mm close M18 pixel sensors (analog output, 10 $\mu$m pitch, 50 $\mu$m thickness, 5 x 5 mm$^2$ area) that allow a final single point resolution at the DUT (Device Under Test) of the order of the micrometer. The quoted performance has been validated by a complete GEANT3 simulation of the tracking system to extract the expected contribution to the resolution of the measurement of the multiple scattering that is dominant at the 500 MeV energy of the used beam. To validate the double row readout architecture and the large pixel pitch to be used in the outer layer of the ITS upgrade, for the MISTRAL solution proposed by the Strasbourg group, the measurement of the M2THRb prototype (64x64 pixels matrix, binary output, 22 $\mu$m horizontal pitch, 33 $\mu$m vertical pitch, 50 $\mu$m thickness) has been done with the system previously briefly described in the following. In Fig. 1(left) the table reports the simulated and experimental spatial resolution for the two coordinates for different $\chi^2$ values. To validate the results and to define the proper cuts to be used in the analysis, the simulation has been essential

| | Horizontal coordinate | | | Vertical coordinate | | |
|---|---|---|---|---|---|---|
| Chi2 cut | Exp Resid | Sim. Resid. | Resolution | Exp Resid | Sim. Resid. | Resolution |
| 20 | 6.7 | 5.2 | 4.2 | 8.1 | 5.2 | 6.2 |
| 55 | 7.3 | 6.2 | 3.9 | 8.9 | 6.2 | 6.4 |
| 200 | 8.2 | 6.7 | 4.7 | 9.6 | 6.6 | 7.0 |

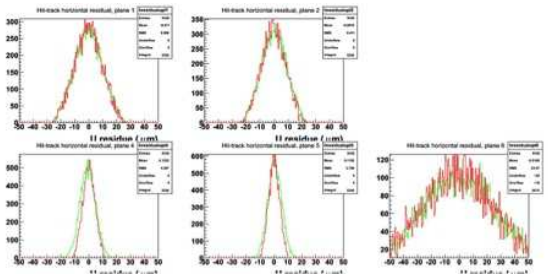

Figure 1: *Left panel: simulated and experimental spatial resolution for the two coordinates and for different $\chi^2$ values. Right panel: simulated and measured horizontal residual in the five tracking planes.*

to prove that we are able to disentangle the multiple scattering main effect. In Fig. 1(right) it is shown the simulated and measured horizontal residual in the five tracking planes (last M28 plane of the tracker was not used due to a temporary malfunction) being in a remarkable agreement.

## 5 Heavy-flavour jet measurement via electrons

Heavy quarks, i.e. charm and beauty, are produced primarily in the initial, hard partonic scatterings in hadron collisions. Their production in *pp* collisions is well described by perturbative QCD. In ultra-relativistic heavy-ion collisions, heavy quarks propagate through and interact with the hot and dense QCD matter, the so-called Quark-Gluon Plasma. Therefore, measurements of heavy-flavour production provide relevant information on the early stage of the collisions and parton-medium interaction. In Pb–Pb collisions, a strong suppression of $D$ mesons and electrons from heavy-flavour decays has been observed. Further information of mechanism of energy loss of heavy-flavours in the QCD matter can be obtained by measuring production of jets which originally comes from heavy flavours. In ALICE, inclusive jets production has been successfully measured at $p_{\rm T}$ >20 GeV/$c$ both in *pp* and Pb–Pb collisions. The idea of the analysis is to use heavy-flavour decay electrons to find heavy-flavour jets. From a Monte Carlo simulation, heavy-flavour decay electrons are well correlated with original heavy quarks in rapidity and azimuthal direction. By electron measurements in the *pp* and Pb–Pb collisions, the fraction of the heavy-flavour hadron decay electrons in measured electron samples with the ALICE detectors is about 50% at $p_{\rm T} \sim 3$ GeV/$c$ and it becomes dominant at high $p_{\rm T}$. Therefore using high $p_{\rm T}$ electrons, it is possible to measure heavy-flavour jets with small background contributions. With data recorded during LHC Run1, we observed the raw spectrum up to around 60 GeV/$c$ in most central Pb–Pb collisions. Currently, the analysis is concentrated on the determination of efficiencies and unfolding. In addition, we measure dijet of heavy-flavour following the same concepts. For the moment, such recoil jets have already been observed on away-side in *pp* collisions at $\sqrt{s} = 8$ TeV.

## 6 HP3: a Di-Jet Electromagnetic Calorimeter for Jet Quenching Study

Part of the activities of the LNF group described in the present activity report, have been performed in HadronPhysics3 in the Seventh Framework European Programme. In particular a Joint Research Activity has been developed in collaboration with the Centre National de la Recherche Scientifique CNRS/IN2P3 and the Universidad de Santiago de Compostela, with the aim to expand the physics capabilities of the ALICE Electromagnetic Calorimeter (EMCal) by enabling back-to-back correlation measurements.

The completion of the installation of DCal supermodules in 2014, allows to start an extensive program of combined inclusive and correlation measurements. To this aim jet trigger development, jet reconstruction and new theoretical formalism have been implemented in the framework of this project.

The electromagnetic calorimeter online jet trigger component has been developed to provide an unbiased jet sample by refining the hardware Level1 (L1) trigger decisions. A more accurate definition of the jet area, than the one provided by the hardware L1 jet patch, is obtained by choosing a jet cone based on the jet direction calculated online. In addition we have found that the use of the HLT jet trigger allows a better characterization of the trigger response as a function of the centrality dependent threshold. This is fundamental in the case of heavy-ion collisions, where an unacceptably high threshold for jet signals should be fixed.

## 7 Polarization studies

Another analysis which sees the group involved starts from the fact that there are still several fundamental questions related to the spin structure of the nucleon which remain unanswered. The $\Lambda^0$ hyperon polarization is a potentially powerful way of probing polarized quark content inside the nucleon. Its decay into a proton and a pion in a parity violating weak decay opens to the determination of the $\Lambda^0$ hyperon polarization by measuring the angular distribution of its decay products. Particularly, the study of the transverse polarization of $\Lambda^0$ and $\bar{\Lambda}^0$ hyperon in ALICE would allow to access the Boer-Mulders distribution that measures the transverse spin asymmetries of quarks inside an unpolarised hadron in a kinematic regime never reached before.

After having reconstructed these particles in events at different collision energies ($\sqrt{s} = 2.76$, 7 and 8 TeV) both a multiplicity and an asymmetry distribution study have been performed. The asymmetry in $\Lambda^0$ ($\bar{\Lambda}^0$) decays, both with respect to the production plane and the thrust vector has been measured as a function of $p_T$ and $\eta$. Promising results show an asymmetry as a function of $\eta$ for the whole $p_T$ spectra of less than per cent. The measured asymmetry has opposite sign for $\Lambda^0$ and $\bar{\Lambda}^0$, increases as a function of $p_T$ and flips the sign when going from positive to negative pseudorapidity region.

## Publications

The ALICE Collaboration has published 22 papers in 2013. The publications are accessible at the link: http://aliceinfo.cern.ch/ArtSubmission/publications

Other papers:


1. N.Branbilla, P.Di Nezza et al., "QCD and strongly coupled gauge theories: challenges and perspectives", Eur. Phys. J. C (2014) 74:2981.


## Talks

1. N.Bianchi, Seminar: *"ALICE results in Pb-Pb collisions at the CERN LHC"*, 18 Feb 2014, USP, Brasil;
2. N.Bianchi, Seminar: *"ALICE results in Pb-Pb collisions at the CERN LHC"*, 21 Feb 2014, UESC, Brasil;
3. P.Di Nezza, Invited talk: *"Highlights from the LHC"*, Nucleon Structure at Large Bjorken x, November 2014, LNF, Italy;

4. P.Di Nezza, Talk: *"Jet Physics at the LHC as probe of the QGP"*, Quark Confinement and the Hadron Spectrum XI, September 2014, St.Petersburg (Russia);

5. V.Muccifora, Talk: *"Hard Nuclear Scattering"*, Gordon Research Conference on Photonuclear Reaction, August 2014, Holderness (NH) USA;

6. S.Sakai, Talk: *"Measurement of heavy-flavour decay leptons with ALICE"*, $3^{rd}$ International Conference on New Frontiers in Physics, August 2014, Kalymbari, Greece.

**Proceeding and Notes**

1. S.Sakai, *Heavy-flavour production in ALICE*, International Conference on the initial Stages in High-Energy Nuclear collisions, Nuclear Physics A, Vol. 926, June 2014, Page 41-48;

2. S.Sakai, ALICE analysis note: *"Measurement of electrons from semi-leptonic heavy-flavour hadron decays in pPb collisions at* $\sqrt{s_{NN}}$ *= 5.02 TeV"*.

**Activity Report 2014 - JLAB12**

M. Aghasyan (Art. 23), G. Angelini (Ass., gratuated La Sapienza Univ.),
A. Courtoy (Ass. from Liege Universite'), S. Anefalos Pereira (Ass. from Sao Paulo University),
E. De Sanctis (Ass.), D. Hasch, V. Lucherini, M. Mirazita (Resp.) ,
R. Montgomery (PostDoc INFN), A. Orlandi (Tech.),
J. Phillips (Ass. from Glasgow University), S. Pisano (Ass.),
P. Rossi, S. Tomassini, A. Viticchié (Tech.)

In Collaboration with LNF-SPAS:
D. Orecchini

## 1 Introduction

The Frascati JLAB12 group participates into the physics program carried on by the CLAS collaboration in the Hall B of the Jefferson Laboratory (JLab). The physics program of the group is focused on the precision study of the three-dimensional structure of the nucleon and its internal dynamics. This is achieved through the determination of three-dimensional parton distribution functions: the Transverse Momentum Dependent parton distribution (TMD) and the Generalized Parton Distribution (GPD) functions. The former describe the quarks and gluons inside the nucleon in the 3D momentum space and are accessible in Semi-Inclusive Deep Inelastic Scattering (SIDIS) measurements. The latter describe longitudinal momentum distributions at a given transverse spatial point and are measured in exclusive reactions. The structure functions containing the TMDs and GPDs enter in the Fourier components of the cross section of the process and they are accessed through the measurement of single or double spin asymmetries.

The operation of the JLab electron accelerator has been shout down in May 2012 to increase the maximum beam energy up to 12 GeV, to upgrade the three exististing experimental halls and to build a fourth new hall. In Hall B, the new CLAS12 spectrometer is now under construction. To improve the particle identification capabilities of this new detector also to the kaons, the Frascati group is involved in the construction of a RICH detector.

In the period covered by this report, two analysis items have been completed and published and others are still going on. For the RICH activity, the $R\&D$ has been mostly completed and the construction of the detector has been started.

## 2 Data analysis activity

### 2.1 GPD measurements

The simplest way to access GPDs is to study the Deeply Virtual Compton Scattering (DVCS) exclusive process, in which a hard photon is produced in the final state. The Fourier coefficients of the cross section can be written in terms of the so-called Compton Form Factors (CFF), particular combinations of GPDs. By measuring cross section asymmetries, it is possible to extract from the data these CFF.

Data have been collected with 5.5 GeV energy polarized electron beam and a longitudinally polarized proton target. This allowed to measure at the same time Single Beam and Target Spin Asymmetries (BSA and TSA) as well as Double Spin Asymmetries (DSA). All the three final state particles of the reaction (the scattered electron, the recoil proton and the hard photon) are clearly identified in CLAS so that the kinematics of the process can be fully reconstructed.

The analysis has been completed and approved by the CLAS Collaboration during 2014 and the results have been published in two papers with members of the LNF-JLAB12 group as first

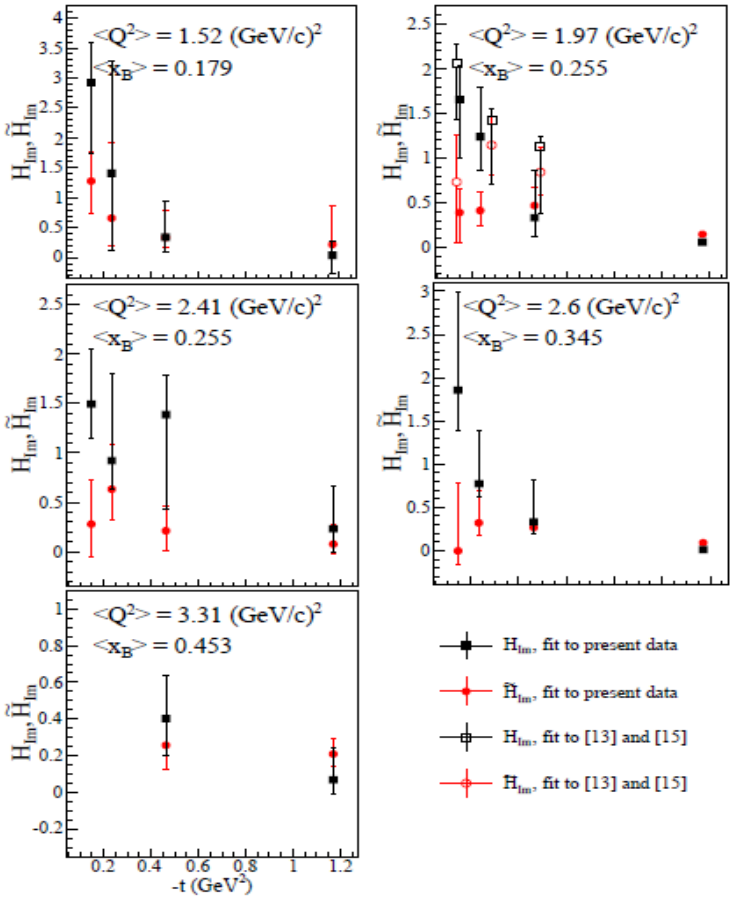


Figure 1: *The t-dependence for each $Q^2$-$x_B$ bin of $H_{Im}$ (black squares) and $\tilde{H}_{Im}$ (red circles). The full points are obtained by the present data (TSA, BSA and DSA), the empty points were obtained by previous data.*

authors (see Publications 1 and 2). As an example of the results, we show in Fig. 1 the $t$, $Q^2$ and $x_B$ dependence of the CFF $H_{Im}$ and $\tilde{H}_{Im}$ (full circles) compared with previous extractions (empty circles). Our new data extend over a much larger kinematic region and improve the precision of previous measurements in the overlap region.

### 2.2 TMD measurements and extraction

The TMDs, 3D extension of the collinear Pardon Distribution Functions (PDFs), are in general measured in SIDIS experiments with a meson (pion or kaon) in the final state. In these processes, the TMDs enter in convolution integrals with the Fragmentation Functions, thus sophisticated algorithms for their extraction are required. In recent years, the calculation of the Bessel-weighted asymmetries has been proposed as a convenient extraction method, because it transform the convolution integrals in the transverse momenta into simple products in the conjugate transverse coordinate space. This approach has been tested with simulated data, using a dedicated Monte Carlo event generator in which the kinematic correlations between the parton and hadron momenta

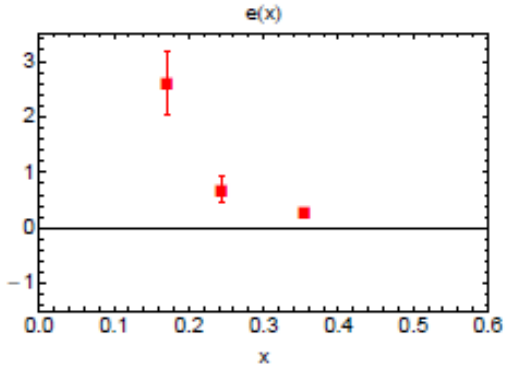


Figure 2: *The extraction of the combination $e^V$ in the WW scenario. The error bars correspond to the propagation of the experimental and DiFF errors.*

have been introduced. Systematics uncertainties in the extraction of the TMDs from the data in this new approach have been evaluated for a number of reference channels. These results have been published (Publication 4).

An alternative way to the TMDs is provided by the DiHadron SIDIS processes (DiSIDIS), in which two mesons (for example two pions) are produced in the final state. In this case, the cross section takes a much simpler form, with TMDs and DiHadron Fragmentation Functions (DiFF) entering as products instead of convolution integrals. In the collinear limit, the DiSIDIS allows the access to the higher-twist PDF $e$, $g_T$ and $h_L$, that, together with the leading twist unpolarized $f_1$, helicity $g_1$ and transversity $h_1$, complete the collinear desctiption of the nucleon structure up to *twist-3*. Measurement of DiSIDIS asymmetries with a charged pion pair has been performed with both unpolarized as well as longitudinally polarized hydrogen target as a function of the relevant kinematic variables. The analysis with unpolarized target has been completed and is now under the Collaboration review, while for the polarized target one the analysis note is in preparation.

From the Beam Spin Asymmetry (BSA) results of the unpolarized data, a preliminary extraction of the PDF $e(x)$ has been attempted. This PDF enters in the expression of the BSA together with a second term, of the same *twist*, containing an unknown DiFF, thus its extraction requires a theoretical assumption to model this unknown term. As an example, we show in Fig. 2 the Bjorken-x dependence of the valence quark combination

$$e_V = \frac{4}{9}e^u - \frac{1}{9}e^d \tag{1}$$

under the so-called Wandzura-Wilczek (WW) approximation. This analysis has been published (Publication 3).

## 3 Proposals of 12 GeV experiments

Two new proposals for measurements to be performed with the 12 GeV beam with CLAS12 have been presented by physicist of the LNF-JLAB12 group and approved in 2014 by the JLab Program Advisory Committee (PAC).

The first one [1)], is devoted to the study of the electroproduction of $\Lambda$ in SIDIS reaction. The goal is the extraction of the Fracture Functions, generalization of the PDFs and Fragmentation

functions that describe the production of a given hadron in the final state when the virtual photon hits a given quark in the target nucleon. These functions are accessible in the Target Fragmentation Region, where the final hadron is produced by the fragmentation of the nucleon quark remnants.

In the second one [2], the goal is the extention, with higher beam energy, larger kinematic coverage and better statistical precision, of the studies already in progress in the di-hadron SIDIS electroproduction. These new measurements will be performed using both hydrogen and deuterium target, so that the valence quark decomposition of the $e(x)$ will be possible.

## 4 The CLAS12 Rich for the Hall B of JLab

The new CLAS12 detector under construction for the Hall B will have unique features (luminosity, resolution and large acceptance) to allow substantial progresses in the nucleon structure studies. In its baseline configuration, CLAS12 allows the identification of particles with the combination of time-of-flight and Cherenkov detectors in six azimuthal independent sectors. While these detectors are adequate for the identification of electrons, pions and protons, they don't allow clean identification of kaons. Nevertheless, SIDIS experiments with kaons in the final state are a key ingredient in the understanding of the nucleon structure.

In order to extend the capabilities of CLAS12 to detect kaons in the momentum range from 3 to 8 GeV/c, the Frascati group proposed in 2010 to replace one of the Cherenkov counters with a Ring Imaging CHerenkov (RICH) detector. This project involves other INFN groups (Fe, Roma1/ISS, Ge, Ba) as well as International institutions: besides JLab, also the University of Glasgow (UK), the Gutenberg Universitat of Mainz (Germany), the UTFSM in Valparaiso (Chile), the Argonne Laboratory and the Universities of Duquesne and of Connecticut (USA) and the Kyungpook National University (Korea). After the final approval of the project obtained in 2013, in 2014 most of the $R\&D$ activities have been completed and the construction of the detector has been started.

The detector is basically made by a large trapezoidal box containing the aerogel radiator, an array of Multi-Anode Photo Multiplier Tubes (MAPMTs) for the detection of the Cherenkov photons and a mirror system that allows the reduction of the area instrumented with photodetectors to about 1 $m^2$. The MAPMTs and the Front-End readout electronics, based on the MAROC3 chip and made by about 25000 channels, are contained in a panel installed in the lower part of the downstream face of the detector.

The main activities pursued in 2014 are:

- the completion of the studies on the Hamammatsu H8500 MAPMTs, with the publication of the results (Publication 5);
- the purchase of the first two squared meters of aerogel;
- the finalization of the design of the mechanical structure of the detector and the beginning of the tender for its construction;
- the definition of the specifications of the mirror system [3];
- the construction of two large-scale prototypes for the study of the cooling system of Front-End electronics and of its assembly.

## 5 List of Conference Talks

1. S. Pereira - "Di-hadron production at the Jefferson Lab." - XXII International Workshop on Deep-Inelastic Scattering and related Subjects (DIS 2014) April 28 May 2 2014, Warsaw (Poland).

2. S. Pisano - The JLAB 3D program at 12 GeV (TMDs + GPDs) - Fourth International Workshop on Transverse Polarisation Phenomena in Hard Processes (TRANSVERSITY 2014) June 9-14 2014, Chia, Cagliari (Italy).

3. S. Pisano - Experimental investigation of the nucleon transverse structure - ELBA XIII Workshop on Electron-Nucleus Scattering June 23-27 2014, Isola dElba (Italy).

4. P. Rossi - SIDIS Asymmetries at JLab - Physics Opportunities at an ElecTron-Ion Collider (POETIC V) - September 22- 26 2014, New Haven (CT-USA)

5. P. Rossi - JLab12: On the path to CD4b - Fourth Joint Meeting of the Nuclear Physics Divisions of the American Physical Society and The Physical Society of Japan - October 7-11 2014, Hawaii (USA)

6. S. Pisano - "3D imaging of the nucleon with JLab experiments" - Fourth Joint Meeting of the Nuclear Physics Divisions of the American Physical Society and The Physical Society of Japan - October 7-11 2014, Hawaii (USA)

7. P. Rossi - Status and Plan of JLab12 - International Conference on Science and Technology for FAIR in Europe 2014 October 13-17 2014, Worms (Germany)

## 6 Publications

1. E. Seder, S. Pisano *et al.*, (CLAS Collaboration), Longitudinal target-spin asymmetries for deeply virtual Compton scattering - Phys. Rev. Lett. **114** (2015) 3, 032001.

2. S. Pisano, M. Mirazita *et al.*, (CLAS Collaboration), Single and double spin asymmetries for deeply virtual Compton scattering measured with CLAS and a longitudinally polarized proton target - arXiv:1501.07052 and Physical Review D, in print.

3. A. Courtoy, Insights into the higher-twist distribution e(x) at CLAS - arXiv:1405:7659 [hep-ph].

4. M. Aghasyan, E. De Sanctis, M. Mirazita, P. Rossi *et al.*, Studies of Transverse Momentum Dependent Parton Distributions and Bessel Weighting JHEP **1503** (2015) 039.

5. V. Lucherini, M. Mirazita, R.A. Montgomery, A. Orlandi, S. Anefalos Pereira, S. Pisano, P. Rossi, A. Viticchie' *et al.*, Investigation of Hamamatsu H8500 phototubes as single photon detectors - arXiv:1409.3622 [physics.ins-det] and N. Instr. and Meth. A, in print.

6. V. Lucherini, M. Mirazita, R. Montgomery, D. Orecchini, S. Anefalos Pereira, J. Phillips, S. Pisano, P. Rossi S. Tomassini (Frascati), A. Viticchie' *et al.*, The large-area hybrid-optics CLAS12 RICH detector: Tests of innovative components - Nucl.Instrum.Meth. **A766** (2014) 22-27.

## References


1. Semi-Inclusive Λ electroproduction in the Target Fragmentation Region - https://www.jlab.org/exp_prog/proposals/14/E12-06-112A_E12-09-008A.pdf

2. Higher-twist collinear structure of the nucleon through di-hadron SIDIS on unpolarized hydrogen and deuterium - https://www.jlab.org/exp_prog/proposals/14/E12-06-112B_E12-09-008B.pdf

3. G. Angelini, Characterization of the Mirror Focusing System for the CLAS12 RICH - Graduation Thesis, University of Rome La Sapienza, A.A. 2013-14.

# KAONNIS

M. Bazzi (Art. 23), C. Berucci (Ric. Str.), M. Bragadireanu (Bors. UE), A. Clozza,
C. Curceanu (Resp. Naz.), A. D'Uffizi (Ass. Ric.),
C. Guaraldo, M. Iliescu (Art. 23), P. Levi Sandri, F. Lucibello (Tecn.),
S. Okada (Art. 23), D. Pietreanu (Bors. UE), K. Piscicchia (Bors.),
M. Poli Lener (Art. 23), E. Sbardella (Bors.),
A. Scordo (Ass. Ric.), H. Shi (Assoc.),
D. Sirghi (Art. 23), F. Sirghi (Bors. UE), I. Tucakovic (Bors.),
O.Vazquez Doce (Bors. UE) J. Zmeskal (Ric. Str.)

## 1 The KAONNIS scientific program

KAONNIS represents an integrated initiative in the field of the low-energy kaon-nucleon/nuclei interaction studies. Under KAONNIS the following activities are performed:

- the study of kaonic atoms by the SIDDHARTA and SIDDHARTA-2 experiments
- the study of kaon-nuclei interaction at low energies in the framework of AMADEUS.

We present in what follows these scientific lines, together with the 2014 activities and the plans for 2015. The KAONNIS scientific program and its realization were partially financed within the FP7 HadronPhysics2 and HadronPhysics3 EU programs.

## 2 The SIDDHARTA and SIDDHARTA-2 experiments

The objective of the SIDDHARTA (Silicon Drift Detector for Hadronic Atom Research by Timing Application) experiment and of its successor, SIDDHARTA-2, is to perform high precision measurements of X-ray transitions in exotic (kaonic) atoms at DAΦNE.

The precise measurement of the shift and width of the $1s$ level, with respect to the purely electromagnetic calculated values, in kaonic hydrogen and kaonic deuterium, induced by the strong interaction, through the measurement of the X-ray transitions to this level, will allow the first precise experimental determination of the isospin dependent antikaon-nucleon scattering lengths, fundamental quantities for the understanding of the low-energy QCD in strangeness sector.

The accurate determination of the scattering lengths will place strong constraints on the low-energy $K^-N$ dynamics, which, in turn, constraints the SU(3) description of chiral symmetry breaking in systems containing the strange quark. The implications go from particle and nuclear physics to astrophysics (the structure of neutron stars).

SIDDHARTA performed the most precise measurement of kaonic hydrogen and the first exploratory one of kaonic deuterium. Moreover, the kaonic helium 4 and 3 transitions to the 2p level were measured, for the first time in gas in He4 and for the first time ever in He3. Presently, a major upgrade of SIDDHARTA, namely SIDDHARTA-2, is under way, with the aim to measure kaonic deuterium and other types of kaonic atoms in the coming years.

### 2.1 The SIDDHARTA setup

SIDDHARTA represented a new phase in the study of kaonic atoms at DAΦNE. The previous DEAR experiment's precision was limited by a signal/background ratio of about 1/70 for the kaonic hydrogen measurement, due to machine background. To significantly improve this ratio, a

breakthrough was necessary. An accurate study of the background sources at DAΦNE was done. The background includes two main sources:

- synchronous background: coming from the $K^-$ interactions in the setup materials and $\phi$-decay processes; it can be defined as *hadronic background*;
- *asynchronous background*: final products of electromagnetic showers in the machine pipe and in the setup materials, originating from particles lost from primary circulating beams either due to the interaction of particles in the same bunch (Touschek effect) or due to the interaction with the residual gas.

Accurate studies showed that the main background source in DAΦNE is of the second type, which points to the way to reduce it. A fast trigger correlated to a kaon entering into the target would cut the main part of the asynchronous background. X rays were detected by DEAR using CCDs (Charge-Coupled Devices), which are excellent X-ray detectors, with very good energy resolution (about 140 eV FWHM at 6 keV), but having the drawback of being non-triggerable devices (since the read-out time per device is at the level of 10 s). A new device, which preserves all good features of CCDs (energy resolution, stability and linearity), but additionally is triggerable - i.e. fast (at the level of 1$\mu$s), was implemented. The new detector was a large area Silicon Drift Detector (SDD), specially designed for SIDDHARTA. The development of the new 1 cm$^2$ SDD device, together with its readout electronics and very stable power supplies, was partially performed under the Joint Research Activity JRA10 of the I3 project"Study of strongly interacting matter (HadronPhysics)" within FP6 of the EU.

The trigger in SIDDHARTA was given by a system of scintillators which recognized a kaon entering the target making use of the back-to-back production mechanism of the charged kaons at DAΦNE from $\phi$ decay:

$$\phi \rightarrow K^+K^-. \tag{1}$$

The SIDDHARTA setup contained 144 SDD chips, 1 cm$^2$ each, placed around a cylindrical target, filled with high density cryogenic gaseous hydrogen (deuterium or helium). The target was made of kapton, 75$\mu$m thick, reinforced with aluminium grid.

The SIDDHARTA setup was installed on DAΦNE in late summer 2008, see Figure 1 - and the period till the end of 2008 was used to debug and optimize the setup performances (degrader optimization included). The kaonic atoms (hydrogen, deuterium, helium4 and 3) measurements were done in 2009 and data analysis followed in the coming years.

### 2.2 SIDDHARTA activities in 2014

SIDDHARTA was in data taking until 9 November 2009. In 2014 the group activity was dedicated to the yield of kaonic helium 3 and 4 atoms analysis, and to the upgrade of the setup, SIDDHARTA-2, to perform in the future the kaonic deuterium and other precision kaonic atoms measurements.

### 2.3 *SIDDHARTA-2*

In 2010 the proposal for the SIDDHARTA upgrade was put forward in 2010. The upgrade of SIDDHARTA to SIDDHARTA-2 is based on five essential modifications:

- *Trigger geometry and target density*: By placing the upper kaon-trigger detector in front of the target entrance window the probability that a triggered kaon really enters the gas and is stopped there is improved. Making the detector smaller than the entry area gives away some signal, but suppresses efficiently the kaonic lines from "wall-stops" (kaons entering the

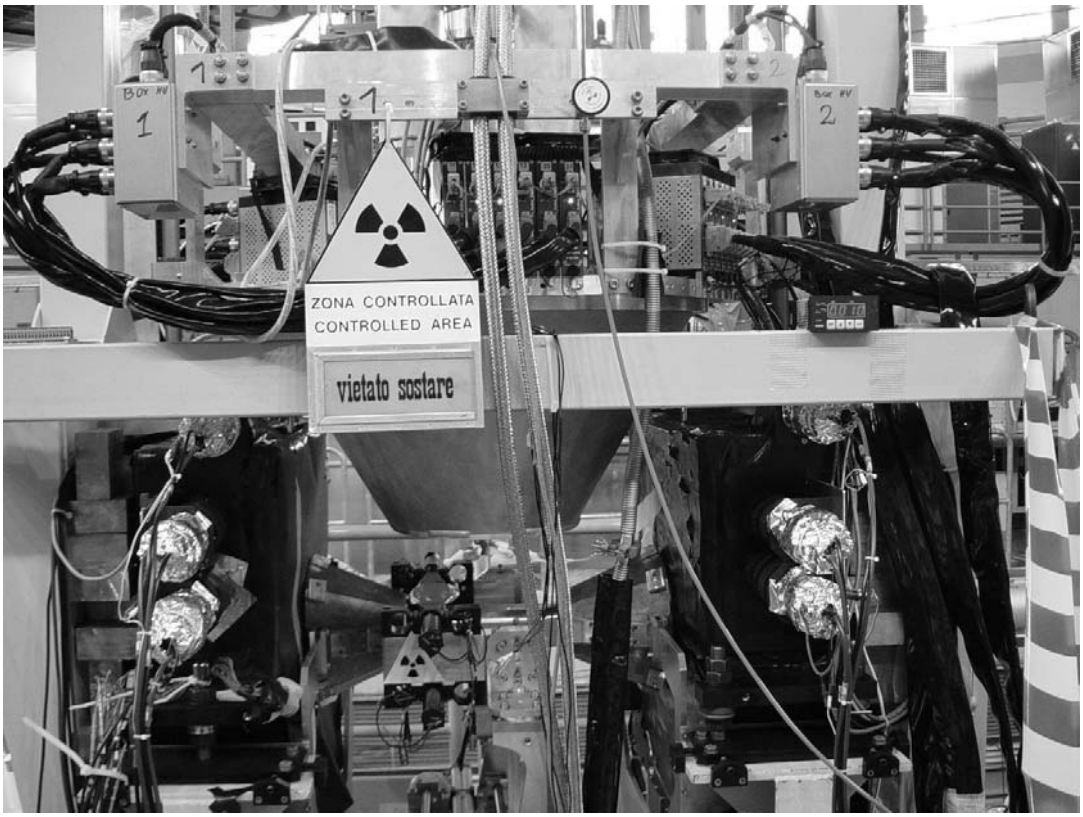


Figure 1: The SIDDHARTA setup installed at DAΦNE

gas volume, but passing from the inside of the target to the cylindrical walls). The number "signal per trigger" goes up, which also reduces the accidental background coming along with every trigger. We plan as well to double the gas density which enhances the gas stops and further reduces the wall-stops.

- $K^+$ *discrimination to suppress kaon decay background*: A "kaon stopper"scintillator is placed directly below the lower kaon trigger scintillator. When a $K^-$is stopped there, only one (large) signal from pileup of stopping and kaon-absorption secondaries is seen, whereas when a $K^+$ is stopped, the kaon-decay particles are seen after the signal from the stopping (mean $K^+$ lifetime 12.8 ns). Using a flash-ADC we will be able to efficiently separate the 2 cases. In addition, we will use scintillators surrounding the target to measure $K^-$ absorption secondaries pions). The time window for gas stops is about 4 ns wide. By this condition we also suppress stops in the entry window.

- *Active shielding*: The scintillators surrounding the target will also be used in prompt anticoincidence if the spatial correlation of SDD and scintillator hits indicates that it originated from a pion ("charged particle veto"). An anticoincidence covering the SDD time window of about 600 ns (with the exception of the 4 ns of the gas stopping time) will reduce the accidental background. Although the scintillators have low efficiency for gammas, the abundance of secondaries from the electromagnetic showers allows a relevant reduction of accidental ("beam") background. The upper trigger scintillator has 2 functions, it is also used as an anticoincidence counter: after the kaon and eventual prompt kaon-absorption secondaries pass, it vetos beam background.

- *Use of new SDD detectors*, produced by FBK, having a much better active/total surface ratio (about 85%, with respect to 40% in SIDDHARTA SDDs).

- *Operating SDDs at a lower temperature*: tests indicate that an improvement of the timing resolution by a factor of 1.5 is feasible by more cooling. The signal enhancement by a factor 2 to 3 is due to moving the target cell closer to the IP, by changing its shape, by a better solid angle of the SDDs and by the higher gas density. In such conditions, with an integrated luminosity of 800 pb$^-$1 a precision of about 70 eV for the shift, and 160 eV for the width are attainable, resulting in a relative precision similar to that obtained for kaonic hydrogen.

A scheme of the SIDDHARTA-2 setup is shown in Figure 2.

In 2014 various tests on SDD prototypes, of the veto and the trigger systems were performed, together with Monte Carlo simulations to optimize the setup.

More details can be found in the various presentations to the LNF International Scientific Committee on the LNF-INFN web-site.

### 2.4 Activities in 2015

The LNF group main activities in SIDDHARTA-2 for 2015 are the following ones:

- Monte Carlo simulations for the SIDDHARTA-2 setup and physics;

- construction and tests of the SIDDHARTA-2 setup components: target, veto counters, new trigger, new cryogenic systems;

- definition of the strategy for SIDDHARTA-2 measurements (including interaction region definition and construction).

The SIDDHARTA scientific program is an important part of the Network LEANNIS (WP9) in the framework of the EU FP7 HadronPhysics3 program.

## 3 The AMADEUS proposal and the 2014 activities

The low-energy kaon-nuclei interaction studies represent the main aim of AMADEUS. In order to do these type of measurement, in a most complete way, by detecting all charged and neutral particles coming from the $K^-$ interactions in various targets with an almost $4\pi$ acceptance, the AMADEUS collaboration plans to implement the existent KLOE detector in the internal region of the Drift Chamber with a dedicated setup (see Figure 3). The dedicated setup contains the target which can be either solid or a gaseous cryogenic one, a trigger (TPC-GEM) and a tracker system (scintillating fibers read by SiPM detectors).

The negatively charged kaons can stop inside the target or interact at low energies, giving birth of a series of processes we plan to study. Among these, a key-role is played by the generation of $\Lambda(1405)$ which can decay into $\Sigma^0\pi^0$, $\Sigma^+\pi^-$ or $\Sigma^-\pi^+$. We plan to study all these three channels in the same data taking. Another important item is represented by the debated case of the "kaonic nuclear clusters", especially the $K^-$pp, and $K^-$ -ppn cases. We can study these channels by measuring their decays to $\Lambda$p and to $\Lambda$d. In the same time, many other kaon-nuclei processes will be investigated, either for the first time, or in order to obtain more accurate results than those actually reported in literature. Cross sections, branching ratios, rare hyperon decay processes will be investigated, taking advantage of the unique kaon-beam quality delivered by DA$\Phi$NE and of the unique characteristics of the KLOE detector implemented with the AMADEUS dedicated setup.

As targets to be employed, we plan to use gaseous ones, like d, $^3$He or $^4$He and solid ones as C, Be or Li. In the summer of 2012 a first dedicated target, half cylinder done in pure carbon

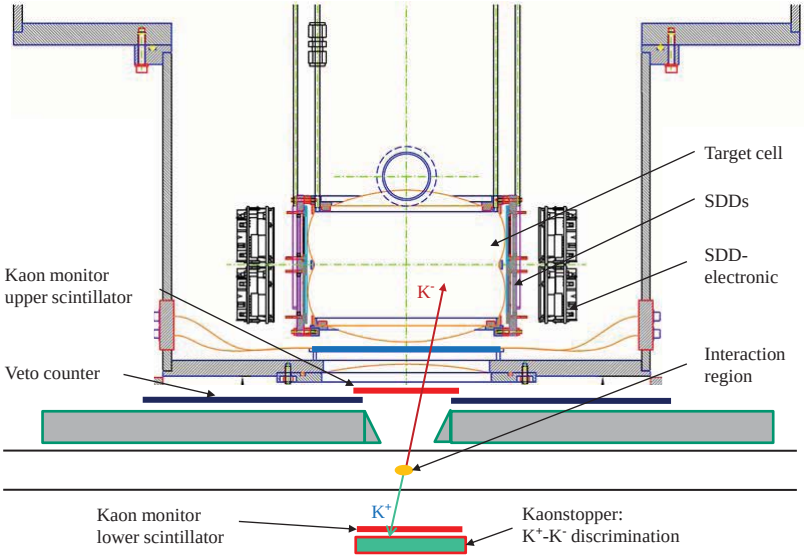


Figure 2: Schematic view of the SIDDHARTA-2 setup

was realized and installed inside the Drift Chamber of KLOE as a first setup towards the realization of AMADEUS (see Figure 4). The target thickness was optimized to have a maximum of stopped kaons (about 24% of the generated ones) without degrading too much the energy of resulting charged particles inside the target material. In the period of data taking a total integrated luminosity of about 80 $pb^{-1}$ was achieved. The analysis of these data will provide new insights in the low-energy interactions of charged kaons in the nuclear matter. For the future, other targets are planned to be used compatible with the beam assignment.

Activities done in 2014:

- analysis of 2002-2005 KLOE data searching for processes generated by negatively cherged kaons interacting at rest or in-flight in the setup materials (wall of the Drift Chamber and gas inside the Drift Chamber);
- analysis of the 2012 Carbon target data;
- R&D for the trigger system: a prototype based on scintillating fibers read by Silicon Photo-Multipliers;
- R&D for the inner tracker - a small TPC-GEM prototype, Fig. 5, for traking performance;
- Monte Carlo dedicated simulations.

### 3.1 AMADEUS activities in 2015

The main activities of AMADEUS in 2015 will be:

- continuation of the R&D for the trigger system: tests of the prototype and readout electronics at BTF-LNF and PSI.

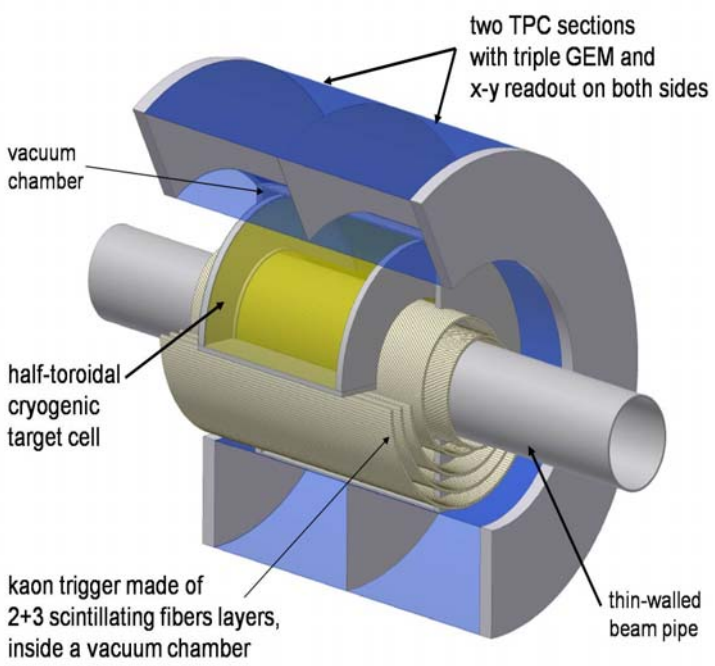


Figure 3: The AMADEUS dedicated setup to be implemented in the Drift Chamber of the KLOE detector. In this situation a cryogenic gaseous target is used.

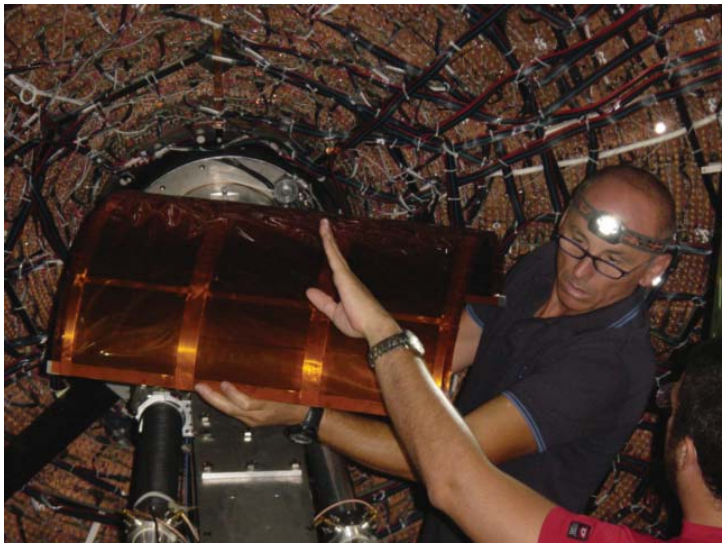

Figure 4: The AMADEUS carbon target (half cylinder) installed inside the Dift Chamber of KLOE detector.

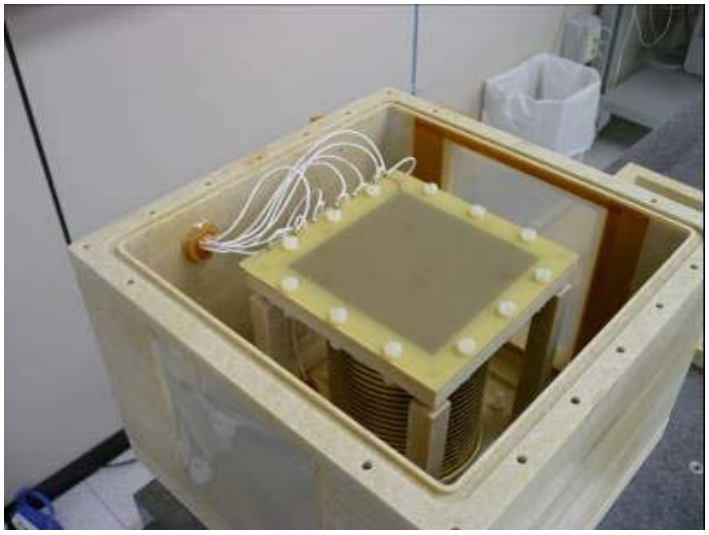

Figure 5: The TPC-GEM prototype

- continuation of the R&D for the inner tracker: tests of the prototype at BTF-LNF and PSI
- Monte Carlo simulations.
- KLOE 2002-2005 data analyses searching for processes generated by kaons interacting in the materials of the KLOE setup.
- continuation of the analyses of data taken with the dedicated carbon target
- definition of the experiment strategy

The AMADEUS activities were supported in the framework of the EU FP7 HadronPhysics3 by WP24 (GEM), WP28 (SiPM) and WP9 (Network on kaon-nuclei interaction studies at low energies) programs.

### 3.2 Workshops organization

In 2014 the following workshops, where the KAONNIS physics was discussed, were organized:

- Investigating Strangeness: from Accelerators to Compact Stellar Object, LNF-INFN, 14 May 2014.
- Achievements and Perspectives in Low-Energy QCD with Strangeness, ECT*, Trento, Italy, 27-31 October 2014.

**Acknowledgements**
The support from HadronPhysics3 FP7 project is acknowledged.

## 4 Publications in 2015

1. C. Curceanu *et al* (AMADEUS Collaboration), Unprecedented studies of the low-energy negatively charged kaons interactions in nuclear matter by AMADEUS, e-Print: arXiv:1501.05781.
2. J. Zmeskal *et al*, Measurement of the strong interaction induced shift and width of the 1s state of kaonic deuterium at J-PARC, e-Print: arXiv:1501.05548.
3. J-PARC E15 Collaboration, Search for the $K^-pp$ bound state via the in-flight $^3He(K^-,n)$ reaction, European Phys. Journal Conf. **81** (2014) 02016.
4. J. Marton *et al*, Kaonic atoms - studies of the strong interaction with strangeness, European Phys. Journal Conf. **81** (2014) 01017.
5. J-PARC E15 Collaboration, Search for the $K^-pp$ bound state via the $^3He(K^-,n)$ reaction at 1 GeV/c, J. Phys. Conf. Ser. **569** (2014) 1, 012080.

6. J-PARC E15 Collaboration, Search for deeply bound Kaonic nuclear states via $^3$He(K$^-$,n) reaction at J-PARC, DOI: 10.1142/9789814618229020.

7. M. Iliescu *et al*, Progress and perspectives in the low-energy kaon-nucleon/nuclei interaction studies at the DA$\Phi$NE collider, J. Phys. Conf. Ser. **556** (2014) 1, 012004.

8. J-PARC E15 Collaboration, Search for the deeply bound $K^-$pp state via the $^3$He(K$^-$,n) reaction at p$_K$=1 GeV/c, e-Print: arXiv:1408.5637 [nucl-ex].

9. A. Scordo, C. Curceanu, K. Piscicchia, I. Tucakovic, O. Vazquez Doce, Study of the $\Lambda$(1405) Resonance Through its Neutral and Charged Decay Channels by AMADEUS at DA$\Phi$NE, Few Body Syst. **55** (2014) 741.

10. M. Cargnelli *et al*, X-ray spectroscopy of kaonic atoms at SIDDHARTA, European Phys. Journal Web Conf. **73** (2014) 05008.

11. M. Bazzi *et al*, L-series X-ray yields of kaonic $^3$He and $^4$He atoms in gaseous targets, European Phys. Journal **A50** (2014) 91.

12. H. Ohnishi *et al*, A Search for $\Phi$ Meson Nucleus Bound State Using Antiproton Annihilation on Nucleus, Acta Phys. Polon. **B45** (2014) 3, 819.

13. T. Ishiwatari *et al*, Kaonic Atoms - Results of the SIDDHARTA Experiment, Acta Phys. Polon. **B45** (2014) 3, 787.

14. J-PARC E15 Collaboration, A Search for Deeply-bound Kaonic Nuclear States by In-flight $^3$He(K$^-$,n) Reaction at J-PARC, Acta Phys.Polon.**B45** (2014) 3, 767.

15. C. Curceanu *et al*, Unprecedented Studies of the Low-energy Negatively Charged Kaons Interactions in Nuclear Matter by AMADEUS, Acta Phys.Polon. **B45** (2014) 3, 753.

16. H. Shi *et al*, The yield of kaonic hydrogen X-rays in the SIDDHARTA experiment, European Phys. Journal Conf. Web Conf. **66** (2014) 09016.

17. J-PARC E15 Collaboration, A search for the K$^-$pp bound state in the $^3$He(K$^-_{in-flight}$,n) reaction at J-PARC, European Phys. Journal Conf. Web Conf **66** (2014) 09008.

18. C. Curceanu *et al*, Unveiling the strangeness secrets: low-energy kaon-nucleon/nuclei interactions studies at DA$\Phi$NE , European Phys. Journal Conf. Web Conf. **66**(2014) 09004.

19. T. Ishiwatari *et al*, New precision era of experiments on strong interaction with strangeness at DA$\Phi$NE /LNF-INFN, European Phys. Journal Conf. Web Conf **66** (2014) 05016.

# MAMBO

P. Levi Sandri (R), D. Pietreanu and A. Saputi.

## 1 Introduction

MAMBO groups together three complementary INFN activities in Germany: the experimental activity with the MAMI-C microtron in Mainz, the development of MRPC counters and the preliminary measurements towards a full proposal to measure the electric dipole moments (EDM) of proton and deuteron, and the new BGO-OD experiment at Bonn-ELSA. LNF are involved in the last two activities.

## 2 BGO-OD experiment

The BGO-OD esperiment is performed in collaboration between INFN sections of Roma2, LNF, Messina, Pavia, ISS-Roma1 and Torino, the University of Bonn, Physikalisches Institut, ELSA department, the University of Bonn, Helmholtz Institut für Strahlen- und Kernphysik, the University of Edinburgh, the National Science Center Kharkov Institute of Physics and Technology, the University of Moscow, Russia, the Petersburg Nuclear Physics Institute (PNPI), Gatchina and the University of Basel. More that 70 physicists participate to this experimental program foreseen to last until 2017 with possible extention.

The INFN contribution consist in the *Rugby Ball* calorimeter and associated detectors previously used at GRAAL, the target system, the cylindrical tracking chambers and the MRPC detector.

## 3 Activity in 2014

The main issue of year 2014 was the optimization of the photon beam by reducing the machine background with appropriate shielding and a better alignment system. A new goniometer was installed that allows the remote choice and the precise alignment of the *Bremsstrahlung* radiator. The experiment is now routinely capable of producing a photon beam of intensity $3 \cdot 10^7 s^{-1}$ very close to the design value of $5 \cdot 10^7 s^{-1}$. The beam can be polarised *via* the technique of the coherent *Bremsstrahlung*. around 1.5 GeV, the region of major interest, a degree of linear polarisation $\sim 0.4$ was obtained (see Fig. 1).

During 2014 the construction and installation of the detectors still missing from the experimental setup was continued. These are the following

- MRPC chambers (Roma2 and LNF) were constructed (80%).
- MWPC cylindrical chambers were debugged. A new electronics was designed to solve the noise problem.
- ARGUS microscope was designed and a prototype was built. It will allow for a very fine tagging binning in the region of the polarisation peak ($\Delta E_\gamma \sim 5 MeV$).

A first 3 weeks run was performed in november-december 2014 and first data, albeit with a reduced and still incomplete detector set, were collected by using Hydrogen, Deuterium anc Carbon targets.

The experiment was presented at various international conferences (Crakow, Gordon).

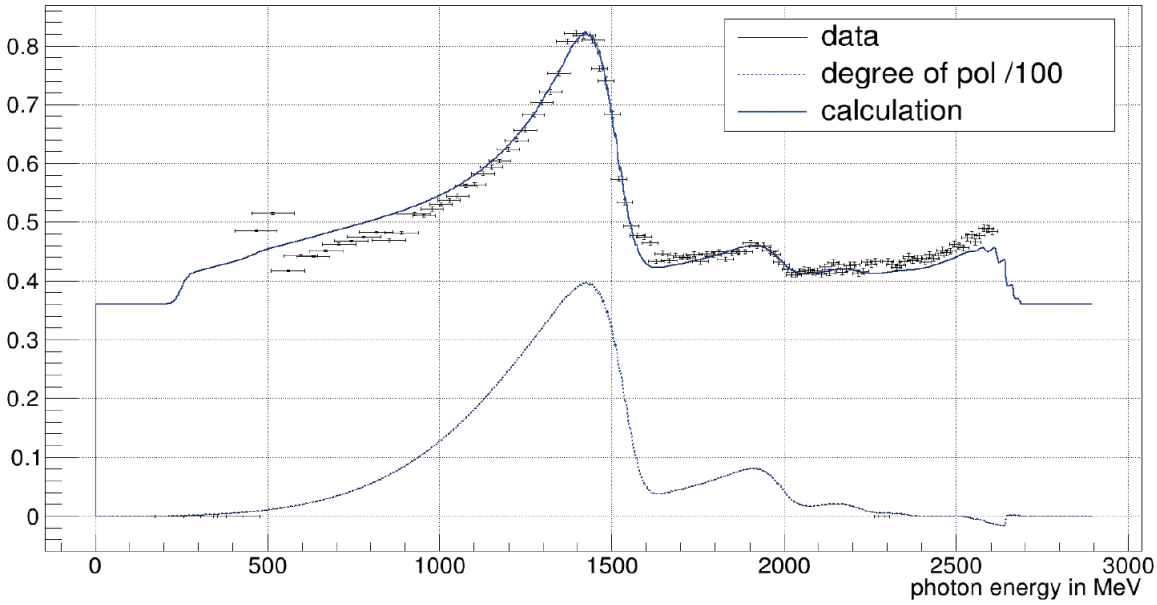


Figure 1: *Photon energy spectrum and degree of linear polarisation*

## 4 Planned activity in 2015

Two detectors must be installed to complete the apparatus. The MRPC chambers are being installed and a test beam is expected in may. The ARGUS microscope will be installed as well and will be available starting june 2015.

The experiment is expected to take data for three months in 2015. These will be sufficient to complete the experimental program as approved by the PAC in 2013.

# $\overline{\text{P}}$ANDA - $\overline{\text{p}}$ Annihilation at Darmstadt

N. Bianchi, A. M. Bragadireanu (Ass.), P. Dorel (Ass.), P. Gianotti (Resp. Naz.),
C. Guaraldo (Ass.), V. Lucherini, E. Pace, D. Pietreanu (Ass.)
In collaboration with LNF SPAS: D. Orecchini (Tec.).
In collaboration with LNF nuclear physics esperiments support:
L. Passamonti (Tec.), D. Piergluigi (Tec.), A. Russo (Tec.)

## 1 Introduction

$\overline{\text{P}}$ANDA is one of the biggest experiments of hadron and nuclear physics that will be carried out at the new Facility for Antiproton and Ion Research (FAIR) at Darmstadt, Germany. It is dedicated to the study of the annihilations of antiprotons on nucleons and nuclei up to a maximum center-of-mass energy in $\overline{\text{p}}$p of 5.5 GeV.

The $\overline{\text{P}}$ANDA collaboration consists of more than 500 physicists from 19 countries spread all over the world. The Italian groups involved are: Torino, University, Politecnico and INFN, Trieste, University and INFN, Genova INFN, Pavia, University and INFN, Ferrara, University and INFN, Legnaro INFN laboratory and Frascati INFN laboratory. The LNF group is involved in the design and construction of the central straw tube tracker of the $\overline{\text{P}}$ANDA detector.

## 2 $\overline{\text{P}}$ANDA experiment

The construction in Germany of the new FAIR accelerator complex started in January 2013. It consists of a major upgrade of the presently running GSI accelerator complex of Darmstadt [?]. Figure **??** shows a view of the construction site. The actual schedule of the project foresees the

Figure 1: *Aerial view of the FAIR construction site.*

first beams in year 2020.

An intense, high momentum resolution antiproton beam, with momenta between 1.5 and 15 GeV/$c$, will be available at the High Energy Storage Ring (HESR), and the experimental activity will be carried out using a general purpose detector $\overline{\text{P}}$ANDA that will be build surrounding an internal target station installed in one of the two straight sections of the storage ring. Figure **??** shows a schematic drawing of the $\overline{\text{P}}$ANDA apparatus. It is designed as a large acceptance

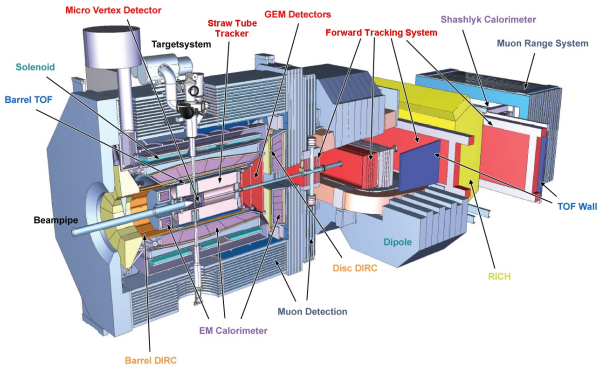


Figure 2: *A schematic view of the $\overline{P}ANDA$ apparatus.*

multi-purpose detector consisting of two distinct parts: a solenoidal spectrometer, surrounding the interaction target region, and a forward spectrometer to cover the solid angle between 5 and 22 degrees. It will allow the detection and the identification of either the neutral and the charge particles emitted following $\bar{p}$ annihilation.

## 3 The $\overline{P}$ANDA Central Tracker

For tracking charge particles in the target spectrometer, $\overline{P}$ANDA will use different detectors: a silicon Micro Vertex Detector (MVD) a Straw Tube Tracker (STT) and a set of forward GEM chambers [**?**]. Figure **??** shows the layout of the Target Spectrometer tracking system.

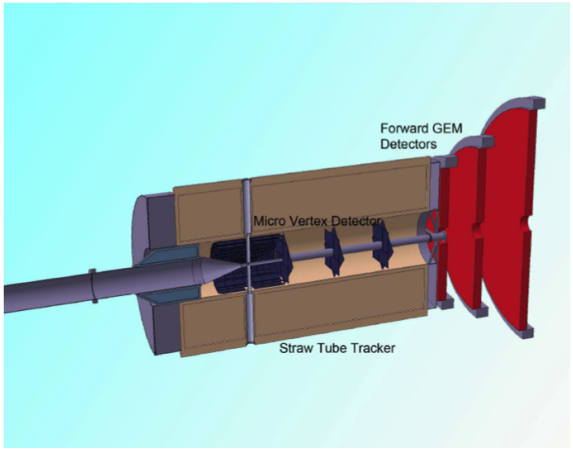


Figure 3: *The $\overline{P}ANDA$ tracking system of the Target Spectrometer. It consists of three detectors: Micro Vertex Detector, Straw Tube Tracker, Forward GEM.*

The requirements for this system are:

- almost full solid angle coverage;

- momentum resolution $\delta p/p \sim 1.5\%$;
- low material budget $X/X_0 \sim$ few %;
- good spatial resolution $\sigma_{r,\phi} = 150$, $\mu$m, $\sigma_z =$ few mm.

The Technical Design Report (TDR) of the STT has been approved in 2013 and the construction of the straw tubes started in 2014.

The LNF $\overline{\text{P}}$ANDA group is deeply involved in the STT realization and has the responsibility of the mechanics of the whole tracking system.

### 3.1 Layout of the straw tube detector

The $\overline{\text{P}}$ANDA STT will consist of two identical chambers separated by the beam-target cross-pipe that is cutting the $x, y$ plane in two halves (see fig. **??**). Each chamber is made of aluminized mylar straw tubes, diameter 10 mm, length 1500 mm, thickness 30 $\mu$m, arranged in planar double layers.

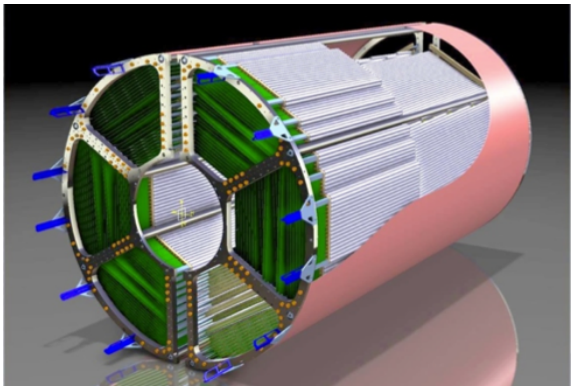

Figure 4: *CAD drawing of the $\overline{P}$ANDA Straw Tube Tracker*

Inside a double layer the tubes are glued together and operated with an Ar+$CO_2$ (90+10) gas mixture with an over-pressure of 1 bar. This solution has been chosen to avoid strong support structures and to keep the detector design modular and simple. To measure also particle $z$ coordinate, some layers will be mounted with a skew angle $\pm 3^o$ with respect to the beam axis.

## 4 Activity of the LNF $\overline{\text{P}}$ANDA group

The STT mechanical structure has to support also the beam-target cross-pipe and the MVD. This frame, has to be extremely light and has to allow the movements of the whole block of detectors during the installation or the maintenance operations. It has been designed by LNF SPAS and it realization is foreseen for 2015, provided that INFN approve the Italian participation to the project. In fact up to now only R&D fund have been given to the Italian collaboration.

The activity of the LNF $\overline{\text{P}}$ANDA group during 2014 has been devoted to the following tasks:

- design of the service system support structure;
- participation to the test beams at Juelich to determine the performance of different electronic setups for the STT.

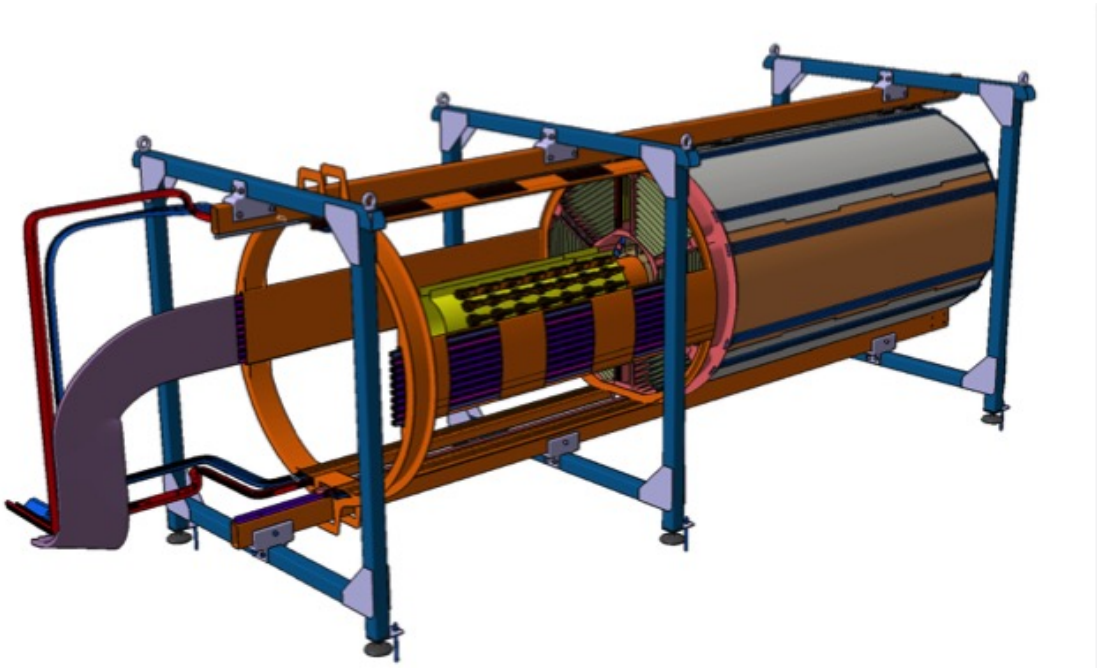

Figure 5: *The Layout of the Central Tracker holded by the insertion support frame. The cable and services routing system is also shown.*

## 5 List of Conference Talks presented by LNF group members in Year 2013

1. P. Gianotti, "The hadron spectroscopy progam at $\overline{\text{P}}$ANDA", invited talk at the *Lattice QCD and hadron physics Conference*, Trento, Italy, 14-16 January 2014.
2. P. Gianotti, "Experimental techniques in hadron spectroscopy", invited talk at the *3rd International Conference on New Frontiers in Physics*, Kolymbari, Grece, 28 July 4 Agust 2014.
3. P. Gianotti, "Physics prospects for first experiments at $\overline{\text{P}}$ANDA", relazione su invito al *International Conference on Science and Technology for FAIR in Europe 2014*, Worms, Germany, 13-17 October 2014.

## 6 Publications

1. M. Bragadireanu *et al.* "Tracking with Straw Tubes in the PANDA Experiment ", EPJ Web Conf. 66 (2014) 11007.

## References


1. `http://www.fair-center.com/`.
2. `http://www-panda.gsi.de/`.

# VIP

S. Bartalucci, M. Bazzi (Art. 23), A. Clozza, C. Curceanu (Resp. Naz.),
C. Guaraldo, M. Iliescu (Art. 23), F. Lucibello (Tecn.), J. Marton (Ric. Str.), A. Pichler (Ric. Str.),
D. Pietreanu (Bors. UE), K. Piscicchia (Ass.), A. Scordo (Ass. Ric.), H. Shi (Ric. Str.),
D. Sirghi (Art. 23), F. Sirghi (Bors. UE), L. Sperandio (Ric. Str.), O. Vazquez Doce (Bors. UE)

## 1 The VIP scientific case and the experimental method

The Pauli Exclusion Principle (PEP), which is a consequence of the spin-statistics connection, plays a fundamental role in our understanding of many physical and chemical phenomena, from the periodic table of elements, to the electric conductivity in metals and to the degeneracy pressure which makes white dwarfs and neutron stars stable. Although the principle has been spectacularly confirmed by the huge number and accuracy of its predictions, its foundation lies deep in the structure of quantum field theory and has defied all attempts to produce a simple proof. Given its basic standing in quantum theory, it is appropriate to carry out precise tests of the PEP validity and, indeed, mainly in the last 20 years, several experiments have been performed to search for possible small violations. Many (if not all) of these experiments are using methods which are not obeying to the so-called Messiah-Greenberg superselection rule. Moreover, the indistinguishability and the symmetrization (or antisymmetrization) of the wave-function should be checked independently for each particle, and accurate tests were and are being done.

The VIP (VIolation of the Pauli Exclusion Principle) experiment, an international Collaboration among 9 Institutions of 6 countries, has the goal to either dramatically improve the previous limit on the probability of the violation of the PEP for electrons, ($P < 1.7 \times 10^{-26}$ established by Ramberg and Snow: *Experimental limit on a small violation of the Pauli principle*, Phys. Lett. **B 238** (1990) 438) or to find signals from PEP violation, by exploring a region where new theories could allow for the PEP violation.

The experimental method consists in the introduction of electrons into a copper strip, by circulating a current, and in the search for X-rays resulting from the forbidden radiative transition that occurs if some of the new electrons are captured by copper atoms and cascade down to the 1s state already filled by two electrons with opposite spins. The energy of $2p \rightarrow 1s$ transition would differ from the normal $K_\alpha$ transition by about 300 eV (7.729 keV instead of 8.040 keV) providing an unambiguous signal of the PEP violation. The measurement alternates periods without current in the copper strip, in order to evaluate the X-ray background in conditions where no PEP violating transitions are expected to occur, with periods in which current flows in the conductor, thus providing "new" electrons, which might violate PEP. The rather straightforward analysis consists in the evaluation of the statistical significance of the normalized subtraction of the two spectra in the region of interest (if no signal is seen).

The experiment is being performed at the LNGS underground Laboratories, where the X-ray background, generated by cosmic rays, is reduced.

Presently, the group is considering as well the extension of its scientific program to the study of the collapse models, by the measurements of the spontaneous radiation (X rays), predicted by these models. Very encouraging preliminary results were obtained.

## 2 The VIP experimental apparata

The first VIP setup was realized in 2005, starting from the DEAR setup, reutilizing the CCD (Charge Coupled Devices) as X-ray detectors, and consisted of a copper cylinder, were current was circulated, 4.5 cm in radius, 50 $\mu$m thick, 8.8 cm high, surrounded by 16 equally spaced CCDs of type 55.

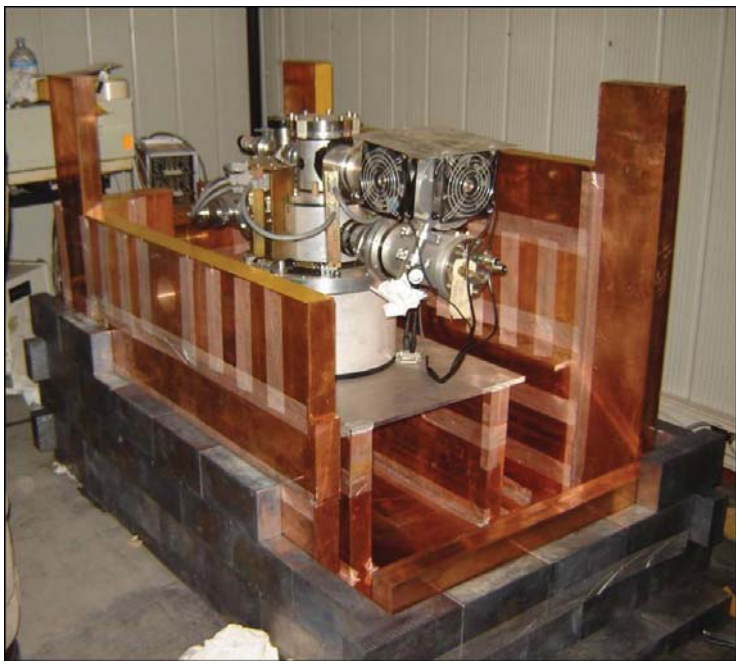

Figure 1: The VIP setup at the LNGS laboratory during installation.

The CCDs were placed at a distance of 2.3 cm from the copper cylinder, grouped in units of two chips vertically positioned. The setup was enclosed in a vacuum chamber, and the CCDs cooled to 165 K by the use of a cryogenic system. The setup was surrounded by layers of copper and lead to shield the setup against the residual background present inside the LNGS laboratory, see Fig. 1.

The DAQ alternated periods in which a 40 A current was circulated inside the copper target with periods without current, referred as background.

VIP was installed at the LNGS Laboratory in Spring 2006 and was taking data in this configuration until Summer 2010. In 2011 we started to prepare a new version of the setup, VIP2, with which we will gain a factor about 100 in the probability of PEP violation in the coming years.

## 3 Activities in 2014

### 3.1 Present VIP limit on PEP violation

Until summer 2010 the VIP experiment was in data taking, alternating periods of "signal" (I=40 A) with periods without signal (I=0 A). Data analyses were performed (energy calibration, sum of spectra, subtraction of background) and the probability of violation of PEP for electrons obtained after a new re-analysis in 2014, where CCD charge transport corrections were optimized, is:

$$\frac{\beta^2}{2} < 3 \times 10^{-29} \tag{1}$$

We are attempting an interpretation of our results in the framework of quon-theory, which turned out to be a consistent theory of *small* violations of PEP. The basic idea of quon theory is

that (anti)commutators, are replaced by weighted sums

$$\frac{1-q}{2}\left[a_i, a_j^+\right]_+ + \frac{1+q}{2}\left[a_i, a_j^+\right]_- = a_i a_j^+ - q a_j^+ a_i = \delta_{i,j} \tag{2}$$

where $q = -1$ ($q = 1$) gives back the usual fermion (boson) commutators. The statistical mixture in equation (2) also shows that the PEP violation probability is just $(1+q)/2$ and thus our best experimental bound on $q$ is

$$\frac{1+q}{2} < 3 \times 10^{-29} \tag{3}$$

We are in close contact with theoreticians and philosophers, looking for implications of the possible small violation of PEP in physics, cosmology and philosophy.

### 3.2 VIP2 - a new high sensitivity experiment

In order to achieve a signal/background increase which will allow a gain of two orders of magnitude for the probability of PEP violation for electrons, we built a new setup with a new target, a new cryogenic system and using new detectors with timing capability and an active veto system. As X-ray detectors we use Silicon Drift Detectors (SDDs) which were employed in the SIDDHARTA experiment measuring kaonic atoms at the DAΦNE electron-positron collider of Laboratori Nazionali di Frascati. SDDs have an even better energy resolution than CCDs and provide as well timing capability which allow to use anti-coincidence operation with scintillators and therefore an active shielding. The VIP2 system will provide:

1. signal increase with a more compact system with higher acceptance and higher current flow in the new copper strip target;

2. background reduction by decreasing the X-ray detector surface, more compact shielding (active veto system and passive), nitrogen filled box for radon radiation reduction.

In the table 1 the numerical values for the improvements in VIP2 are given which will lead to an expected overall improvement of a factor about 100.

Figures 2 shows a picture of the VIP2 setup under test in laboratory in 2014. The copper strip target is 30 mm long, 10 mm wide and is about 40$\mu$m thick, and is installed in the center of the setup. The copper strip is cooled at ∼90K by the use of an external cryogenic system using liquid argon as the cooling medium. The current connection lines made of copper wires with a cross-section area of 1.5 cm$^2$, allow a current flow of (at least) 100 A.

The current lines exhibit a temperature gradient from inside the vacuum chamber to the outside connectors of about 180 K. Monte Carlo simulations were performed to study the effect of the active shielding in various configurations of the setup and models of the background radiation. The background profiles measured at LNGS were used as input parameters in the simulations. As the veto counters, 2 pieces of 10 cm thick plastic scintillators are found to be optimal. During 2014 the setup was assembled and tested at LNF-INFN and SMI-Vienna.

We are, as well, extending the scientific program towards studies of limits on the parameters of the collapse model (as a solution of the measurement problem, put initially forward by Ghirardi, Rimini and Weber) by measurements of the X rays spontaneously emitted and which are predicted by the continuous spontaneous localization (CSL).

Our preliminary results are very encouraging and shows that this method is the most powerful one, presently, in setting limits on the collapse models (see Publications list).

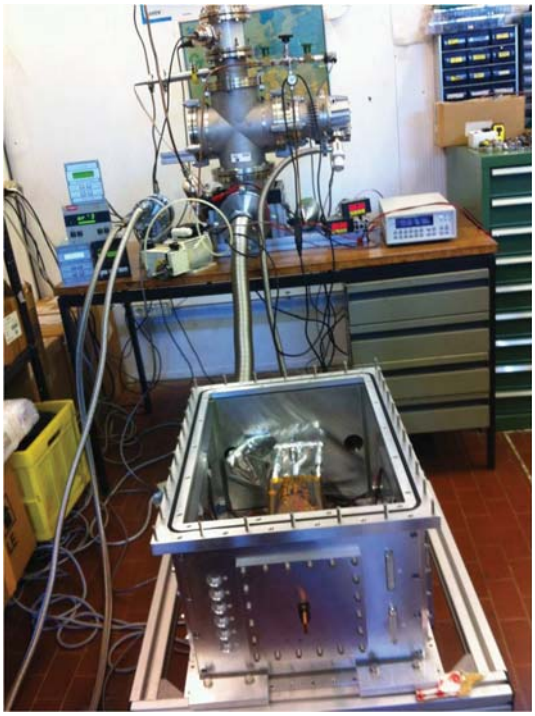

Figure 2: The VIP2 setup using SDD detectors and an external veto-system under test in LNF-INFN laboratory.

Table 1: List of expected gain factors of VIP2 in comparison to VIP (given in the brackets).

| Changes in VIP2 | value VIP2(VIP) | expected gain |
|---|---|---|
| acceptance | 12% | 12 |
| increase current | 100A (50A) | 2 |
| reduced length | 3 cm (8.8 cm) | 1/3 |
| total linear factor | | 8 |
| energy resolution | 170 eV(340 eV) | 4 |
| reduced active area | 6 $cm^2$(114 $cm^2$) | 20 |
| better shielding and veto | | 5-10 |
| higher SDD efficiency | | 1/2 |
| background reduction | | 200-400 |
| **overall gain** | | **∼120** |

### 3.3 Workshops organization

In 2014 the following workshops related to the physics of VIP, and, more generally, to quantum mechanics, were organized at LNF-INFN:

1. "Quantum theory and Gravity: which way?", LNF- INFN, December 18-19, 2014.
2. "Is quantum theory exact? The endeavor for the theory beyond standard quantum mechanics - FQT2014", LNF-INFN, April 28-30 2014.

The results and the future plans for VIP2 were discussed, together with new directions which might be of interest for the Collaboration.

## 4 Activities in 2015

In 2015 we plan to transport, install, debug and test VIP2 setup at LNGS and start the data taking. We are, as well, going to continue the studies on the collapse model (as a solution of the measurement problem, put initially forward by Ghirardi, Rimini and Weber) by measurements of X rays spontaneously emitted in the continuous spontaneous localization (CSL) model.

**Acknowledgements**

The VIP Collaboration wishes to thank all the LNGS laboratory staff for the precious help and assistance during all phases of preparation, installation and data taking. The supports from Museo Storico della Fisica e Centro Studi e Ricerche Enrico Fermi, Roma, the HadronPhysics FP6, HadronPhysics2 and HadronPhysics3 FP7 and from the EU COST 1006 Action projects are acknowledged.

## 5 Publications in 2014

1. C. Curceanu *et al.*, Quantum explorations from the waltz of the Pauli exclusion Principle to the rock of the spontaneous collapse, Phys. Scr. **90** (2014) 028003 - this paper was selected as the "paper of the week".
2. C. Curceanu *et al.*, X-rays help to unfuzzy the concept of measurement, to appear in Journal of Advanced Physics.
3. K. Piscicchia *et al.*, Beyond quantum mechanics? Hunting the "impossible " atoms (Pauli Exclusion Principle violation and spontaneous collapse of the wave function at test), Acta Physics Polonica, **B46** (2015) 147.
4. C. Curceanu *et al.*, Experimental Tests of Quantum Mechanics: Pauli Exclusion Principle and Spontaneous Collapse Models, Springer Proc. Phys. **145** (2014) 181.
5. H. Shi *et al.*, Testing the Pauli Exclusion Principle for electrons at LNGS, e-Print: arXiv:1405.1634.

# FTECP

M. P. Lombardo (Resp.)

Not received

# GSS: Gauge and String Theories

S. Bellucci (Resp.), S. Ferrara (Ass.), S. Krivonos (Osp.), A. Sutulin (Bors. PD), B.N. Tiwari (Ospite), A. Yeranyan (Bors. Fermi Institute)

**Research Activity**

S. Ferrara investigated different aspects of black-hole physics, which include a classification of charge-orbits for extremal single-center black holes and first-order flows of extremal black holes with different BPS properties. He also investigated some aspects of multi-center black holes and, in particular, the classification of two-center orbits and first order flows for multi-center composites.

He studied several aspects of supersymmetry breaking. Applications to Particle Physics or to inflation rest on N=1 spontaneously broken supergravity where some multiplets mediate
supersymmetry breaking while others accommodate the inflaton.
The supersymmetric extension of the Starobinsky model depends on the off-shell formulation of the local supersymmetry algebra. This allows one to show the equivalence of this higher curvature theory to a standard Einstein supergravity. Depending on the chosen formulation the model corresponds to supergravity coupled either to two massive chiral multiplets, one of which is the goldstino multiplet, or to a massive vector multiplet. He also introduced a set of minimal models, where the inflaton sector is described by a single scalar field (with D term and Fayet-Iliopoulos term
generating potential), unlike in models based on chiral multiplets based on an F-term potential. In minimal models the scalaron is dual to the inflaton, and being the member of a massive vector multiplet, it is the superpartner of the Stueckelberg field.
Subsequently, replacing the Goldstino multiplet with its non-linear realization via a nilpotent superfield, he arrived at a new universal Volkov-Akulov-Starobinsky Supergravity. Using this technique new inflationary models were recently constructed by a number of authors. This modification simplifies significantly a broad class of models, the simplest one of which is chaotic inflation, and serves as an uplifting tool in the KKLT-type string theory landscape.
Ferrara proposed a novel type of multi-field supersymmetric Born-Infeld theories, which reduce to the supersymmetric Born-Infeld action in the case of a single vector multiplet. These multi-field extensions, unlike previous proposals, possess a second non-linearly realized supersymmetry, and in fact can be obtained starting from standard N=2 supersymmetric field theories with N=1 vacua. Their classification rests on deep results in Algebraic Geometry.

In the preprint
Comments on N= 2 Born-Infeld Attractors
S. Bellucci, S Krivonos, A Sutulin
arXiv preprint arXiv:1411.5592

Bellucci, Sutulin et al. considered the N=2 supersymmetric Born-Infeld action and discussed some of the peculiar characteristics of the new approach by Ferrara to multi-field supersymmetric Born-Infeld theories.

In the papers:
Wightman function and the Casimir effect for a Robin sphere in a constant curvature space, S. Bellucci,

AA Saharian, NA Saharyan
The European Physical Journal C 74 (9), 1-19 (2014)

Casimir densities from coexisting vacua
S. Bellucci, AA Saharian, AH Yeranyan
Physical Review D 89 (10), 105006 (2014)

Finite temperature fermionic condensate and currents in topologically nontrivial spaces
S. Bellucci, ERB de Mello, AA Saharian
Physical Review D 89 (8), 085002 (2014)

Fermionic vacuum polarization in compactified cosmic string spacetime
S. Bellucci, ERB de Mello, A de Padua, AA Saharian
Eur. Phys. J. C 74, 2688 (2014)

S. Bellucci and coworkers considered field theory in curved space and cosmological implications.

In the paper
Partial breaking of global supersymmetry and super particle actions
S. Bellucci, N Kozyrev, S Krivonos, A Sutulin
Journal of High Energy Physics 2014 (1), 1-16

Bellucci, Sutulin et al. showed, based on the finding that the component on-shell actions for the theories with one half spontaneous breaking of global supersymmetries have an extremely simple form, being written in terms of proper physical components, that on-shell component super particle actions have a universal form, in which the physical fermions enter the action through the ein-bein and the space-time derivatives of the matter fields, only. Bellucci presented the talk "Coset approach to supersymmetric component actions", as an Invited Presentation at the EU-Russia-JINR@Dubna Round Table What next?: Theoretical and Experimental Physics after the discovery of the Brout-Englert-Higgs boson, March 3 – 5, 2014. Bellucci presented the talk "Nonlinear realizations and supersymmetric component action approach", as an Invited Presentation at the XXIInd International Conference on Integrable Systems and quantum symmetries (Prague, June 23–29, 2014). Bellucci presented the talk "Partial breaking of global supersymmetry within the coset approach", as an Invited Presentation at the 5th International Workshop "Supersymmetry in Integrable Systems" held at the Bogoliubov Laboratory of Theoretical Physics of the Joint Institute for Nuclear Research from September 11 to September 13 of 2014.

Bellucci organized the Workshop "Breaking of Supersymmetry and Ultraviolet Divergences in Extended Supergravity" (INFN-LNF, March 25 - 29, 2013), where he presented the talk "Partial Breaking of Global Supersymmetry in d=1". Bellucci published the volume "Black Objects in Supergravity", Springer Proceedings in Physics, vol. 144, pp. 1-358 (2013), ISSN 0930-8989 ISSN 1867-4941 (electronic), ISBN 978-3-319-00214-9 ISBN 978-3-319-00215-6 (eBook), DOI 10.1007/978-3-319-00215-6, Springer Cham Heidelberg New York Dordrecht London. Bellucci published the volume "Supersymmetric Gravity and Black Holes", Springer Proceedings in Physics Volume 142, 2013, S. Bellucci ed.,
Bellucci published the volume "Breaking of Supersymmetry and Ultraviolet Divergences in Extended Supergravity", Springer Proceedings in Physics Volume 153, 2014, DOI 10.1007/978-3-319-03774-5.

Another member of the group at LNF-INFN, Armen Yeranyan, worked on black holes and Born-Infeld theory.

The problems posed in this project are a natural continuation of our previous results obtained in recent years also within the framework of the ERC grant "SUPERFIELDS"(N.226455, 2009-2014) and in collaboration with groups from Torino University, Padua University, JINR-Dubna, Yerevan State University and CERN.

**List of Conference Talks**

S. Bellucci, Coset approach to supersymmetric component actions, Invited Presentation at the EU-Russia-JINR@Dubna Round Table What next?: Theoretical and Experimental Physics after the discovery of the Brout-Englert-Higgs boson, March 3 – 5, 2014.

S. Bellucci, Nonlinear realizations and supersymmetric component action approach, XXIInd International Conference on Integrable Systems and quantum symmetries (Prague, June 23–29, 2014),

S. Bellucci, Partial breaking of global supersymmetry within the coset approach, Invited Presentation at the 5th International Workshop "Supersymmetry in Integrable Systems" held at the Bogoliubov Laboratory of Theoretical Physics of the Joint Institute for Nuclear Research from September 11 to September 13 of 2014.

## Publications by LNF Authors in the Year 2014


[1] Partial breaking of global supersymmetry and super particle actions, S. Bellucci, N Kozyrev, S Krivonos, A Sutulin, arXiv preprint arXiv:1309.3902, published in Journal of High Energy Physics 2014 (1), 1-16

[2] Wightman function and the Casimir effect for a Robin sphere in a constant curvature space, S. Bellucci, AA Saharian, NA Saharyan, The European Physical Journal C 74 (9), 1-19 (2014)

[3] Casimir densities from coexisting vacua, S. Bellucci, AA Saharian, AH Yeranyan, Physical Review D 89 (10), 105006 (2014)

[4] Finite temperature fermionic condensate and currents in topologically nontrivial spaces, S. Bellucci, ERB de Mello, AA Saharian, Physical Review D 89 (8), 085002 (2014)

[5] Fermionic vacuum polarization in compactified cosmic string spacetime, S. Bellucci, ERB de Mello, A de Padua, AA Saharian, Eur. Phys. J. C 74, 2688 (2014)

[6] State-Space Geometry, Statistical Fluctuations, and Black Holes in String Theory, S. Bellucci, BN Tiwari, Advances in High Energy Physics vol. 2014, Hindawi Publishing Corporation, (2014)

[7] Component on-shell actions of supersymmetric 3-branes II. 3-brane in D= 8, S. Bellucci, N Kozyrev, S Krivonos, A Sutulin, arXiv preprint arXiv:1411.7550 [hep-th].

[8] Comments on N= 2 Born-Infeld Attractors, S. Bellucci, S Krivonos, A Sutulin arXiv preprint arXiv:1411.5592 [hep-th].

[9] Component on shell actions of supersymmetric 3-brane I. 3-brane in D= 6, S. Bellucci, N Kozyrev, S Krivonos, A Sutulin, arXiv preprint arXiv:1409.0641, to appear in Class. Quantum Grav.

[10] Supermembrane in D= 5: component action, S. Bellucci, N Kozyrev, S Krivonos, A Yeranyan, Journal of High Energy Physics 2014 (5), 1-18

[11] Partial breaking of global supersymmetry and super particle actions, S. Bellucci, N Kozyrev, S Krivonos, A Sutulin, Journal of High Energy Physics 2014 (1), 1-16

[12] Coset approach to the partial breaking of global supersymmetry, S. Bellucci, S Krivonos, A Sutulin, Breaking of Supersymmetry and Ultraviolet Divergences in Extended Supergravity, Pages 205-248, Springer International Publishing Editor (2014).
[13] Supersymmetry breaking by higher dimension operators, Fotis Farakos, Sergio Ferrara , Alex Kehagias , Massimo Porrati, Nuclear Physics B Vol. 879 Elsevier Netherlands 01/02/2014 348-369
[14] On the topology of the inflaton field in minimal supergravity models, Sergio Ferrara, Pietro Fré , Alexander S. Sorin, Journal of High Energy Physics Vol. 2014/Issue 4 Springer Verlag Germany 01/04/2014 095
[15] Free boundary conditions and the AdS3/CFT2 correspondence, Luis Apolo, Massimo Porrati, Journal of High Energy Physics Vol. 2014/Issue 3 Springer Verlag Germany 01/03/2014 116
[16] On the gauged Kaehler isometry in minimal supergravity models of inflation, S. Ferrara , P. Fré , A.S. Sorin, Fortschritte der Physik Vol. 62/Issue 4, Wiley-VCH Verlag Germany 01/04/2014 277-349
[17] Iwasawa nilpotency degree of non compact symmetric cosets in N-extended supergravity, S.L. Cacciatori , B.L. Cerchiai , S. Ferrara , A. Marrani, Fortschritte der Physik Vol. 62/Issue 4 Wiley-VCH Verlag Germany 01/04/2014 350-386
[18] The Volkov-Akulov-Starobinsky supergravity, I. Antoniadis, E. Dudas, S. Ferrara, A. Sagnotti, Physics Letters, Section B: Nuclear, Elementary Particle and High-Energy Physics 733 Elsevier 15/04/2014
[19] The imaginary Starobinsky model, S. Ferrara, A. Kehagias , A. Riotto, Fortschritte der Physik Vol. 62/Issue 7 Wiley-VCH Verlag Germany 01/07/2014 573-583 Yes
[20] A search for an N =2 inflaton potential, A. Ceresole, G. Dall'Agata, S. Ferrara, M. Trigiante, A. Van Proeyen, Fortschritte der Physik Vol. 62/Issue 7 Wiley-VCH Verlag Germany 01/07/2014 584-606
[21] Minimal R + R^2 supergravity models of inflation coupled to matter, Sergio Ferrara, Massimo Porrati, Physics Letters, Section B: Nuclear, Elementary Particle and High-Energy Physics, Vol. 737 Elsevier Netherlands 01/10/2014 135-138
[22] Cosmology with nilpotent superfields, Sergio Ferrara, Renata Kallosh , Andrei Linde, Journal of High Energy Physics Vol. 2014/ Issue 10 Springer Verlag Germany 01/10/2014 143
[23] N = 2 Born-Infeld attractors, S. Ferrara , M. Porrati , A. Sagnotti, Journal of High Energy Physics Vol. 2014/Issue 12 Springer Verlag Germany 01/12/2014 065
[24] Black holes in the Superworld, L. Andrianopoli, R. D'Auria, S. Ferrara, Erice 2012. International School of Subnuclear Physics World Scientific Singapore 04/04/2014

# PHENOLNF

G. Isidori (Resp.)

Not received

# SEMS: Spectroscopies, Electron correlations, Modeling-Simulations and low-dimensional systems

S. Bellucci (Resp. Naz.), M. Benfatto, S.Bistarelli (Dott.), M. Bozzi (Ass.), A. Cataldo (Bors.), M. Cini (Ass.), G. Giannini (Osp.), K. Hatada (Borsista PD), K. Hayakawa (Borsista PD), D. Mencarelli (Ass.), F. Micciulla (A.R..), C. Natoli (Ass.), F. Palumbo (Ass.), L. Pierantoni (Ass.), G. Stefanucci (Ass.)

**External collaborating Institutions:**

IHEP-Protvino, Russia
Belarus State Univ. Minsk,
Department of Physics, Yerevan State University, Armenia
Department of Physics, Univ. Roma Tor Vergata, Italy
Institute of Solid State Physics, University of Latvia, Kengaraga Str. 8, 1063 Riga, Latvia
Instituto de Ciencia de Materiales de Aragon, CSIC-Universidad de Zaragoza, 50009 Zaragoza, Spain.
ICB, UMR 5209 Universite' de Bourgogne - CNRS, BP 47870, F-21078 Dijon, France
Institut de Physique de Rennes, UMR UR1-CNRS 6251, Campus de Beaulieu, Universite' de Rennes, 35042 Rennes-cedex, France

**Research Activity**

Our theoretical study in collaboration focused on:

- Electron spectroscopy of magnetic systems,
- The fundamental properties of carbon nanotubes and graphene interconnects
- Energy functional of ensemble density functional theory (DFT) in systems with attractive interactions
- Scissors modes in crystals.
- Multiple scattering expansions.
- Magnetic properties of quantum rings

**List of Conference Talks**

S. Bellucci, Research highlights in Nano Science and Technology at Frascati Laboratories, National Institute of Material Physics, Magurele, Bucharest, Romania, 16 October 2014.

S. Bellucci, Graphene as a Tunable Resistor, Semiconductor Conference (CAS), 2014 International, Sinaia (Romania) 13 - 15 October 2014.

S. Bellucci, Memory nanodevices based on carbon nanotube-Fe-Pt interconnects: electromagnetic simulations and magnetically stimulated nanotube growth, Nanostructures and Nanomaterials Self Assembly International Conference (NANOSEA) 2014, 7 – 11 July 2014.

S. Bellucci, Research highlights in Nano Science and Technology at Frascati Laboratories, 2nd International Symposium on Optics and its Applications (OPTICS-2014), 1 - 5 September 2014,

Yerevan - Ashtarak, ARMENIA

S. Bellucci, Transport mechanisms and dielectric relaxations of epoxy nanocomposites from DC to microwave range, Workshop on Nanoelectromagnetics of advanced materials for microwave-to-THz applications, European Microwave Week (EuMW 2014), Roma, 5 October 2014.

S. Bellucci, Le nanotecnologie per la riduzione della dipendenza energetica, Ricerca Scientifica e diffusione dell'informazione, CNR Roma 20 May 2014.

S. Bellucci, Research highlights in Nano Science and Technology at Frascati Laboratories, FM&NT-2014 | Functional Materials and Nanotechnologies, Riga (Latvia), 29 September-2 October 2014

S. Bellucci, I nanomateriali: cosa sono, dove si trovano, CORSO NAZIONALE I nanomateriali e la gestione dei rischi nei luoghi di lavoro, INFN-LNF Frascati, 10 Dicembre 2014

S. Bellucci, Microscopia Elettronica, Stage Estivi Residenziali 2014, 20 – 21 May 2014, Istituto Nazionale di Fisica Nucleare – Laboratori Nazionali di Frascati

S. Bellucci, Microwave response properties of epoxy resin composites filled with graphitic fillers, Numerical Electromagnetic Modeling and Optimization for RF, Microwave, and Terahertz Applications (NEMO), 2014 International Conference on, Pavia (Italy), 14 – 16 May 2014.

A. Cataldo, Structural investigation and mechanical properties of epoxy resins nanocomposites through solid state NMR and nanoindentation, Conference on nanoscience and nanotechnology n&n2014, 6 – 7 October 2014, INFN-LNF Frascati.

G. Stefanucci, Introduction to nonequilibrium Green's functions, Conference on nanoscience and nanotechnology n&n2014, 6 – 7 October 2014, INFN-LNF Frascati.

M. Cini, Production, measurement and storage of spin currents in quantum circuitsConference on nanoscience and nanotechnology n&n2014, 6 – 7 October 2014, INFN-LNF Frascati.

L. Pierantoni, Radio-Frequency Nanoelectronics – Bridging the Gap between Nanotechnology and R.F. Engineering Applications, Conference on nanoscience and nanotechnology n&n2014, 6 – 7 October 2014, INFN-LNF Frascati.

D. Mencarelli, Modeling and simulation of carbon nano transistors, Conference on nanoscience and nanotechnology n&n2014, 6 – 7 October 2014, INFN-LNF Frascati.

## Publications by LNF Authors in the Year 2014

[1] Nanocomposites of epoxy resin with graphene nanoplates and exfoliated graphite: Synthesis and electrical properties, A Dabrowska, S Bellucci, A Cataldo, F Micciulla, A Huczko, physica status solidi (b) 251 (12), 2599-2602, 2014

[2] Heat-resistant unfired phosphate ceramics with carbon nanotubes for electromagnetic application A Plyushch, D Bychanok, P Kuzhir, S Maksimenko, K Lapko, A Sokol, J. Macutkevic, J. Banys, F. Micciulla, A. Cataldo, S. Bellucci, physica status solidi (a) 211 (11), 2580-2585, 2014
[3] Multi-walled Carbon Nanotubes/Unsaturated Polyester Composites: Mechanical and Thermal Properties Study, MSI Makki, MY Abdelaal, S Bellucci, M Abdel Salam, Fullerenes, Nanotubes and Carbon Nanostructures 22 (9), 820-833, 2014
[4] Graphene as a tunable resistor, S Bellucci, M Bozzi, A Cataldo, R Moro, D Mencarelli, L Pierantoni, Semiconductor Conference (CAS), 2014 International, 17-20, 2014
[5] Full-wave techniques for the electromagnetic-quantum transport modeling in nano-devices, L Pierantoni, D Mencarelli, M Bozzi, R Moro, A Sindona, L Spurio, S Bellucci, Semiconductor Conference (CAS), 2014 International, 11-16, 2014
[6] Microwave applications of graphene for tunable devices, L Pierantoni, D Mencarelli, M Bozzi, R Moro, S Bellucci, European Microwave Integrated Circuit Conference (EuMIC), 2014 9th, 512-515, 2014
[7] Advanced techniques for the band structure-quantum transport modeling in graphene and 2D-materials beyond graphene, L Pierantoni, D Mencarelli, A Sindona, M Gravina, M Pisarra, L Spurio, S Bellucci, Nanotechnology (IEEE-NANO), 2014 IEEE 14th International Conference on, 624-627, 2014
[8] Differences in Cytotoxic, Genotoxic, and Inflammatory Response of Bronchial and Alveolar Human Lung Epithelial Cells to Pristine and COOH-Functionalized Multiwalled Carbon Nanotubes CL Ursini, D Cavallo, AM Fresegna, A Ciervo, R Maiello, G Buresti, S Casciardi, S Bellucci, S Iavicoli, BioMed research international 2014 Article ID 359506, 14 pages, http://dx.doi.org/10.1155/2014/359506, 2014
[9] Epoxy Nanocomposite Based on Carbon Nanotubes for Electromagnetic Interface Shielding, S Bellucci, F Micciulla, Advanced Nanomaterials for Aerospace Applications, 267, 2014.
[10 Brief Introduction to Nanocomposites for Electromagnetic Shielding, S Bellucci, F Micciulla Advanced Nanomaterials for Aerospace Applications, 227, 2014
[11] Dielectric properties of graphite-based epoxy composites, I Kranauskaite, J Macutkevic, P Kuzhir, N Volynets, A Paddubskaya, D Bychanok, S Maksimenko, J Banys, R Juskenas, S Bistarelli, A Cataldo, F Micciulla, S Bellucci, V Fierro, A Celzard, physica status solidi (a) 211 (7), 1623-1633, 2014.
[12] Graphene-based electronically tunable microstrip attenuator, L Pierantoni, D Mencarelli, M Bozzi, R Moro, S Bellucci, Microwave Symposium (IMS), 2014 IEEE MTT-S International, 1-3, 2014
[13] Microwave response properties of epoxy resin composites filled with graphitic fillers S Bellucci, S Bistarelli, A Cataldo, F Micciulla, J Macutkevic, I Kranauskaite, J Banys, P Kuzhir, N Volynets, A Paddubskaya, D Bychanok, S Maksimenko, V Fierro, A Celzard, Numerical Electromagnetic Modeling and Optimization for RF, Microwave, and Terahertz Applications (NEMO), 2014 International Conference on, Pages 1-4, IEEE Editor, 2014
[14] On the use of electrostatically doped graphene: Analysis of microwave attenuators, L Pierantoni, M Bozzi, R Moro, D Mencarelli, S Bellucci, Numerical Electromagnetic Modeling and Optimization for RF, Microwave, and Optimization for RF, Microwave, and Terahertz Applications (NEMO), 2014 International Conference on, Pages 1-4, IEEE Editor, 2014
[15] Growth inhibition, cell-cycle alteration and apoptosis in stimulated human peripheral blood lymphocytes by multiwalled carbon nanotube buckypaper, O Zeni, A Sannino, S Romeo, F Micciulla, S Bellucci, MR Scarfi, Nanomedicine, 1-10, 2014
[16] Magnetization transfer by a quantum ring device, M Cini, S Bellucci, The European Physical Journal B 87 (5), 1-7 , 2014
[17] Quantum rings in magnetic fields and spin current generation, M Cini, S Bellucci, Journal of Physics: Condensed Matter 26 (14), 145301, 2014

[18] Deflection of a 100-MeV positron beam by repeated reflections in thin crystals, S Bellucci, YA Chesnokov, PN Chirkov, M Ćosić, G Giannini, VA Maisheev, S Petrović, IA Yazynin, JETP letters 98 (11), 649-651, 2014
[19] Magnetization non-rational quasi-plateau and spatially modulated spin order in the model of the single-chain magnet,[{(CuL) 2Dy}{Mo (CN) 8}]· 2CH3CN· H2O, S Bellucci, V Ohanyan, O Rojas, EPL (Europhysics Letters) 105 (4), 47012, 2014
[20] Targeted Nanodrugs for Cancer Therapy: Prospects and Challenges, M Bottini, C Sacchetti, A Pietroiusti, S Bellucci, A Magrini, N Rosato, N Bottini, J. Nanosci. Nanotechnol 14, 1-17, 2014
[21] Targeted nanodrugs for cancer therapy: Prospects and challenges, M Bottini, C Sacchetti, A Pietroiusti, S Bellucci, A Magrini, N Rosato, N Bottini, Journal of nanoscience and nanotechnology 14 (1), 98-114, 2014
[22] Time-resolved charge fractionalization in inhomogeneous Luttinger liquids, E Perfetto, G Stefanucci, H Kamata, T Fujisawa, Physical Review B 89 (20), 201413, 2014
[23] Time-dependent Landauer-Büttiker formula: Application to transient dynamics in graphene, nanoribbons, R Tuovinen, E Perfetto, G Stefanucci, R van Leeuwen, Physical Review B 89 (8), 085131, 2014
[24] Charge dynamics in molecular junctions: Nonequilibrium Green's function approach made fast, S Latini, E Perfetto, AM Uimonen, R van Leeuwen, G Stefanucci, Physical Review B 89 (7), 075306, 2014.
[25] Diagrammatic expansion for positive spectral functions beyond G W: Application to vertex corrections in the electron gas, G Stefanucci, Y Pavlyukh, AM Uimonen, R van Leeuwen, Physical Review B 90 (11), 115134, 2014.
[26] Ultra-nonlocality in density functional theory for photo-emission spectroscopy, AM Uimonen, G Stefanucci, R van Leeuwen, The Journal of chemical physics 140 (18), 18A526, 2014
[27] Time-dependent Landauer-Büttiker formula: Application to transient dynamics in graphene nanoribbons, R Tuovinen, E Perfetto, G Stefanucci, R van Leeuwen, Physical Review B 89 (8), 085131, 2014.
[28] Nonadiabatic Van der Pol oscillations in molecular transport, A Kartsev, C Verdozzi, G Stefanucci The European Physical Journal B 87 (1), 1-12, 2014.
[29] A two rotor model with spin for magnetic nanoparticles, K Hatada, K Hayakawa, A Marcelli, F Palumbo, Physical Chemistry Chemical Physics 16 (43), 24055-24062, 2014.
[30] Probing the electronic and geometric structure of ferric and ferrous myoglobins in physiological solutions by Fe K-edge absorption spectroscopy, Frederico A. Lima, Thomas J. Penfold, Renske M. van der Veen, Marco Reinhard, Rafael Abela, Ivano Tavernelli, Ursula Rothlisberger, Maurizio Benfatto, Christopher J. Milnea and Majed Chergui, Phys. Chem. Chem. Phys., 2014,16, 1617-1631, DOI: 10.1039/C3CP53683A

**TAsP: Theoretical Astroparticle Physics**

S. Boucenna (Ass.), A. Meroni (Ass.), M. Krauss (Ass.), E. Nardi (Resp.), E. Peinado (Bors.)

**Description of the main scientific achievements during the year 2014**

**Leptogenesis:** The general theory of leptogenesis, with special attention to its most striking phenomenological consequences, and including all the most recent refinements, was one of the main research topic of the group during the past few years. During 2014 we have proposed a leptogenesis inspired scenario, in which the cosmological matter-antimatter asymmetry can arise from the baryon number conserving CP asymmetry in two body decays of heavy particles, when the two final states carry equal and opposite baryon number, and one couples directly or indirectly to electroweak sphalerons so that its baryon asymmetry gets partly reprocessed into a lepton asymmetry, while the other remains chemically decoupled from the thermal bath with its baryon content frozen [1]. After sphaleron switch-off the decay of the decoupled particles inject in the thermal plasma an unbalanced baryon asymmetry, giving rise to baryogenesis.

**Neutrinoless double beta decay and neutrino physics:** Neutrinoless double beta decay is another topic in which the group has developed a good expertise. Predictions for this process in some scenarios with admixture of pseudo-Dirac and Majorana neutrinos in the 3 and 3+1 neutrino frameworks have been studied in [2]. The complementarity between cosmological constraints and the future sensitivity for the next generations of the neutrinoless double beta decay searches has been also exploited in the same study.

The recent results of the Planck experiment put a stringent constraint on the sum of the light neutrino masses, $m1 + m2 + m3 < 0.23\,\text{eV}$ (95 % CL). On the other hand, two-zero Majorana mass matrix textures predict strong correlations among the atmospheric angle and the sum of the masses. The Planck result has been used to show that, for the normal hierarchy case, the texture with vanishing (2,2) and (3,3) elements is ruled out at a high confidence level [3]. The implication of the above mentioned correlations for neutrinoless double beta-decay have been also discussed, for both normal and inverted orderings.

**Discrete family symmetries:** Discrete family symmetries, as a tool to explain the observed neutrino mass and mixing pattern, has been another important research topic for the group. The interplay of generalized CP transformations and the non-Abelian discrete group $T'$ as family symmetry acting in the lepton sector was analyzed in [4]. The family symmetry was shown to be spontaneously broken in a geometrical manner. In the resulting flavour model, naturally small Majorana neutrino masses for the light active neutrinos are obtained through the type I see-saw mechanism. The known masses of the charged leptons, lepton mixing angles and the two neutrino mass squared differences are reproduced by the model with a good accuracy. The model allows for two neutrino mass spectra with normal ordering and one with inverted ordering. Predictions for the sum of the neutrino masses, for the Majorana CPV phases and for the effective Majorana mass in neutrinoless double beta decay have been also presented.

Another model, where Majorana neutrino mass terms are forbidden by the flavor symmetry group $\Delta(27)$, was discussed in [5]. Neutrinos are Dirac fermions and their masses arise in the same way as that of the charged fermions, due to very small Yukawa couplings. The model fits current neutrino oscillation data and correlates the octant of the atmospheric angle with the magnitude of the lightest neutrino mass, with maximal mixing excluded for any neutrino mass.

**Dark matter:** The nature of dark matter (DM), and in which way DM particles could interact with ordinary matter, is one of the most compelling questions in particle physics, and is an active

topic of research in our group. Ref. [6] discusses higher dimensional effective operators describing interactions between fermionic dark matter and Standard Model particles. The ultraviolet completions of the effective operators, which we systematically study, require new particles. These particles can potentially have masses at the TeV scale and can therefore be phenomenologically interesting for LHC physics.

**Spontaneous breaking of the $SU(3)^3$ quark flavour symmetry:** A major achievement of a line of researches that we started a couple of years ago has been the paper [7] in which we prove that the complete pattern of quark Yukawa couplings (quark masses, CKM mixing angles, and the CKM CP violating phase) can be obtained as a consequence breaking spontaneously the $SU(3)^3$ quark-flavour symmetry, with no need to introduce hierarchical parameters, since all hierarchies are generated dynamically.

**Publications**


1 Cloistered Baryogenesis
Diego Aristizabal Sierra (Liege U.), Chee Sheng Fong, Enrico Nardi, Eduardo Peinado (LNF).
Published in JCAP 1402 (2014) 013

2 The quest for neutrinoless double beta decay: Pseudo-Dirac, Majorana and sterile neutrinos
A. Meroni (Rome III U. & LNF), E. Peinado (LNF).
Published in Phys.Rev. D90 (2014) 5, 053002

3 Two-zero Majorana textures in the light of the Planck results
D. Meloni (Rome III & INFN, Rome3), A. Meroni (Rome III & LNF), E. Peinado (LNF).
Published in Phys.Rev. D89 (2014) 5, 053009

4 Generalised geometrical CP violation in a T' lepton flavour model
Ivan Girardi (SISSA, Trieste), Aurora Meroni (SISSA, Trieste & Rome III & LNF), S.T. Petcov (SISSA, Trieste & INFN, Trieste & Tokyo U., IPMU), Martin Spinrath (SISSA, Trieste & INFN, Trieste & Karlsruhe U., TTP).
Published in JHEP 1402 (2014) 050

5 Dirac neutrinos from flavor symmetry
Alfredo Aranda (Colima U.), Cesar Bonilla (Valencia U., IFIC), S. Morisi (Wurzburg U.), E. Peinado (LNF), J.W.F. Valle (Valencia U., IFIC).
Published in Phys.Rev. D89 (2014) 3, 033001

6 Higher Dimensional Effective Operators for Direct Dark Matter Detection
Martin B. Krauss (LNF), Stefano Morisi, Werner Porod, Walter Winter (Wurzburg U.).
Published in JHEP 1402 (2014) 056

7 Quark masses, mixings, and CP violation from spontaneous breaking of flavor $SU(3)^3$
Chee Sheng Fong, Enrico Nardi (LNF).
Published in Phys.Rev. D89 (2014) 3, 036008

8 *Proceedings:* Testing Models with Higher Dimensional Effective Interactions at the LHC and Dark Matter Experiments
M.B. Krauss (LNF).
Published in Frascati Phys.Ser. 59 (2014) 37-42

**Talks**

1 The Majorana nature of massive neutrinos as a possible hint for new physics
A. Meroni, *Astroparticle Physics 2014,* Amsterdam, NL 23 - 28 June 2014

2 Flavoured Dark Matter,
E. Peinado, *4th Workshop on Flavor Symmetries and Consequences in Accelerators and Cosmology (FLASY14)*, University of Sussex, Brighton,UK 17 - 21 June 2014.

3 Quark Yukawa pattern from spontaneous breaking of flavour $SU(3)^3$
E. Nardi, *4th Workshop on Flavor Symmetries and Consequences in Accelerators and Cosmology (FLASY14)*, University of Sussex, Brighton, UK 17 - 21 June 2014.

4 The Majorana nature of massive neutrinos as a possible hint for new physics
A. Meroni, *17th International Conference From the Planck Scale to the Electroweak Scale, (PLANCK 2014)* Paris, France, 26 - 30 May 2014.

5 Testing Effective Interactions of Dark Matter at Colliders and Direct Detection Experiments
M. B. Krauss *DESY Theory Workshop: Particle Cosmology after Planck* Desy, Hamburg, Germany, 23 - 26 September 2014.

6 Quark Yukawa pattern from spontaneous breaking of flavour $SU(3)^3$
E. Nardi, *10th Simposio Latinoamericano de Fsica de Altas Energas (X SILAFAE)*, Ruta N, Medellin, CO, 24 - 28 November 2014.

**Editorial Work**

1 Proceedings: *4th Young Researchers Workshop: Physics Challenges in the LHC Era*,
Frascati, Rome, Italy, May 12-15, 2014.
Editor: Enrico Nardi
Published in Frascati Phys.Ser. 59 (2014) pp.1-60

# !CHAOS Annual Report 2014

S. Angius (Tecn.), C. Bisegni (Tecn.), P. Ciuffetti (Tecn.), G. Di Pirro, L. G. Foggetta (Art. 23), F. Galletti (Tecn.), R. Gargana (Art. 23), E. Gioscio (Ass. Ric.), D. Maselli (Tecn.), G. Mazzitelli (Resp.), A. Michelotti (Art. 23), R. Orrù (Ass. Ric.), M. Pistoni (Tecn.), F. Spagnoli (Ass. Ric.), D. Spigone (Tecn.), A. Stecchi, T. Tonto (Tecn.), M. A Tota (Ass. Ric.)

In collaboration with
L. Catani, C. Di Giulio, G. Salina
*INFN-TV (Sezione di Tor Vergata)*
P. Buzzi, B. Checcucci, P. Lubrano, M. Piccini
*INFN-PG (Sezione di Perugia)*
E. Fattibene
*INFN-CNAF (Centro Nazionale Tecnologie Informatiche)*
M. Michelotto
*INFN-PD (Padova)*
S. R. Cavallaro, B. F. Diana, E. Furia, S. Pulvirenti,
*INFN-LNS (Laboratori Nazionali di Catania)*

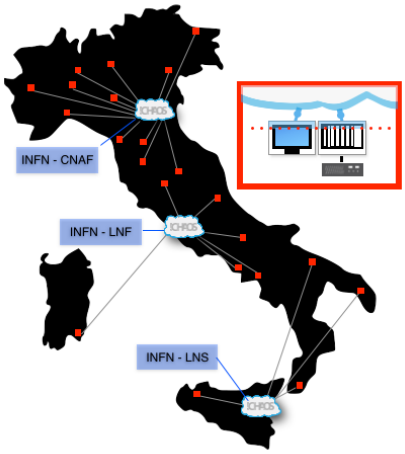


In 2014 the !CHAOS project, previously funded through Cabibbo Lab/SuperB and CSN5 financing, started to be supported by MIUR trough the premiale 2013 [1]. Actually, the project approved in October 2013, received INFN budget approval only in June 2014 and, because of various delays, is still waiting to hire the latest four positions: 2 fellows at LNF, 1 fellow at LNS, 1 technical position at CNAF foreseen for the beginning of March 2015.
Moreover, on the 9th of April 2014, the project started and it was organized the collaboration Kick Off meeting in order to plan the activities and resources.

"!CHAOS: a cloud of controls" is an open source project aimed to develop a national infrastructure prototype to deploy high performing services devoted to devices and polyfunctional sensors distributed on LAN and WAN. The project evolved from a candidate of Distributed Control Systems (DCS) & Data Acquisition (DAQ) for the SuperB HEP collider to a prototype of a national cloud infrastructure that offers monitoring and control services also to society and to industries. To achieve these objectives, the project consists of 4 major activities (WP2-5) and a coordination, communication and documentation activity (WP1).

- (WP2) Framework development: it consists in the development of C++ routines of the common architecture aimed to ensure the communication of data among the five nodes of the system: data acquisition (CU – Control Unit), presentation (UI – User Interface), proxies/indexing/storage (CDS - CHAOS Data Service), data handling (EU – Execution Unit) and system state information (MDS - Metadata Service).

- (WP3) Drivers' and CU development and integration: it consists in the development of C++ routines devoted to the drivers' implementation and CU development and their integration and deployment for the use cases; framework tests and debugs.
- (WP4) Use cases implementation: it consists in software and hardware implementation devoted to the specific CU, EU and UI for the three main use cases: BTF DAQ and accelerator devices and diagnostic controls; LNS beam source control; Touschek auditorium environmental control.
- (WP5) IT infrastructure development and implementation: it consists in the analysis and implementation of the cloud infrastructure and services to offer the !CHAOS framework as a service (CDS, MDS) to our HEP community and external users.

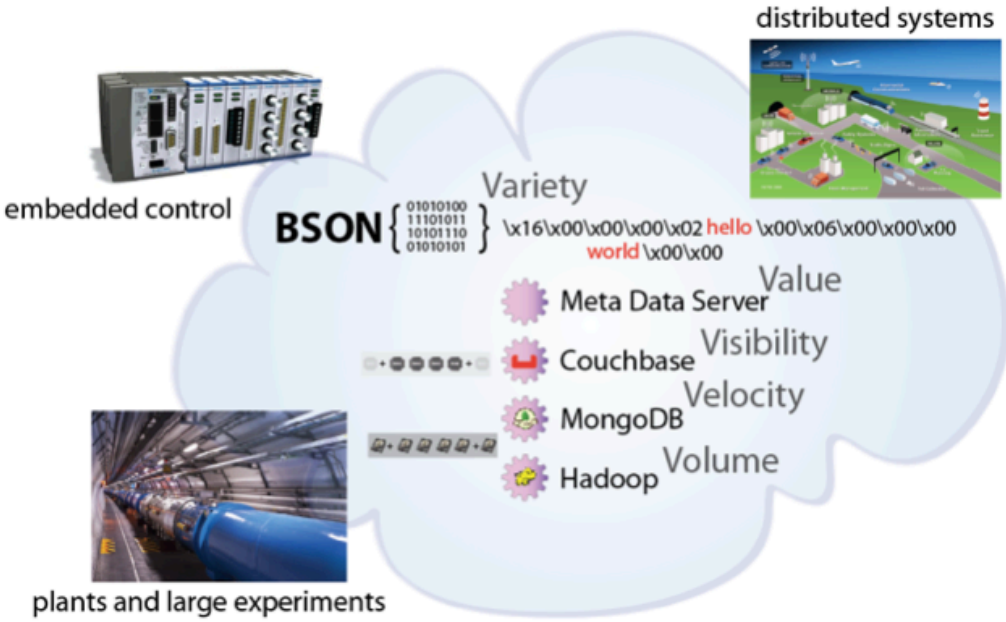


**Figure 1 - !CHAOS architecture exploits the new high performance web technologies that strongly increase control systems performances and services, preserving scalability, redundancy and reliability. It embeds by design the DAQ topology and object data concepts which make the project able to handle Big Analog Data and their Variety, Volume, Velocity, Value and Visibility**

The WP2 (LNF) was well head in the analysis of the !CHAOS framework and started to provide its implementation and adaptation to the cloud infrastructure service, in particular the activities done were centered on: the implementation of direct I/O communication channels among system nodes for large data throughput; implementation of CDS alpha version, implementation MDS java prototype, CU beta release.
The WP3 (LNF) focused it's action on the implementation of the software for the use cases: CU for generic MODBUS, OCEM, FEMTO ampere-meters, Java script client GUI; developing tools for compile, test and deployment for the various supported architectures (I386, X86_64, ARMHF); MDS Graphical Interface and save/restore/configuration datasets functionalities; framework test and debug.
During the summer, it has been hosted a young Summer Student – Pierandrea Conti - from the University of Oxford who developed the API to interface of !CHAOS through MATHLAB.

The WP4 (LNF/LNS/ROMA2/INFN-PE) is mainly not belonging to Frascati staff, anyhow centered the work on the analysis of the use cases for Touschek auditorium and LNS beam source.
Moreover, the Frascati Staff, during 2014, organised two tests at the BTF to monitor and control accelerator devices and diagnostics. The first test was done in March to debug the framework and attempt to controls BTF line magnet controlled trough MOXA serial interface and CU completely running on virtual machine. During the second run, it has been implemented a mixed infrastructure based on beagle bone, equipped with a 485 serial drivers developed by the DAFNE control Team and virtual machine interface with several MOXA serial devices, successfully controlling the beam and it's parameters [2]. Moreover, for the same test, we developed a LabView GUI and Java script GUI for magnets.
The WP5 (LNF/CNAF/INFN-PA) started to analyze the project requirements and the best choice needed to offer !CHAOS as a service: documentation is currently under publication. In the meanwhile, two static infrastructures accessible via VPN based on !CHAOS services on virtual machine infrastructure (one for tests, one for development) where deployed and are available for accounted users.

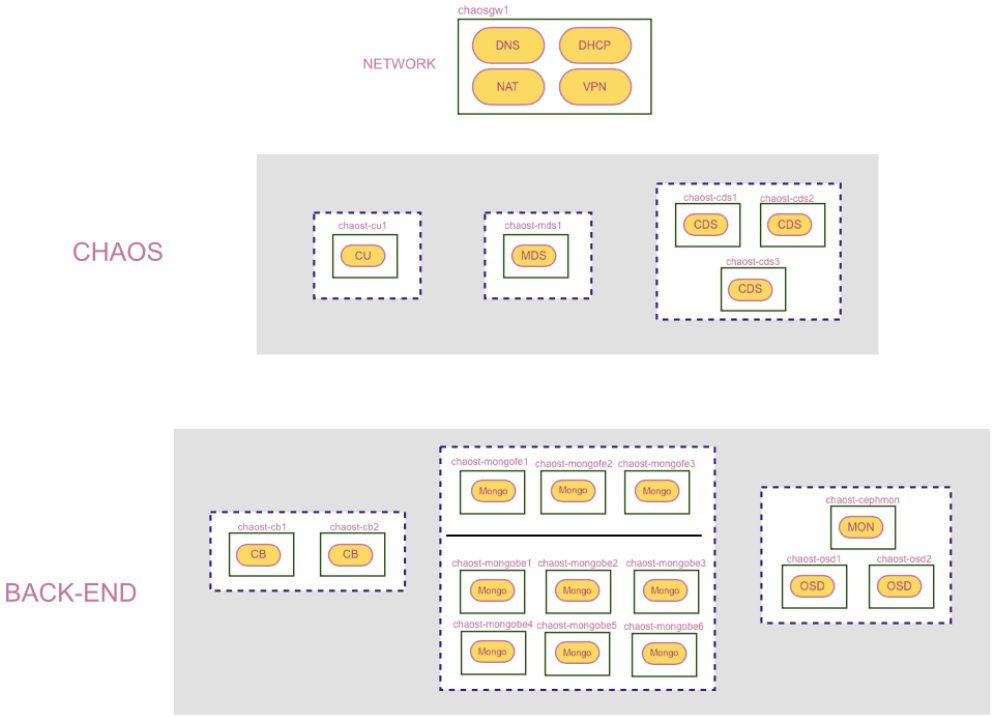


**Figure 2 - !CHAOS static infrastructure layout**

An LNF installation of an open-stack platform (open source software for creating private and public clouds) has been realized, implementing the CDS (based on remote NoSQL Couchbase and mongoDB databases and local POSIX file systems) and an MDS java prototype. Moreover, the Frascati group also worked on the generalization of the Java Script GUI interface and to the analysis of the Atlassian suite (a collaborating tool to plan, code, and service software projects). The Frascati team also provided the local installation at Frascati of the Atlassian suite and suddenly its migration and installation as national service for INFN at CNAF.
The Frascati group (WP1) is in charge of the coordination, communication and dissemination of the project: to maintain the national web site

http://chaos.infn.it; document the whole project https://opensource-confluence.infn.it/; organize regular meetings[1] for monitoring and coordinating the technical development. In December 2014 a two days training school has been organized with 12 attendants.

**Presentation**

G. Mazzitelli - CSN5 meeting - Ferrara, 29 September 2014, Italy
L. Catani - 10th International Workshop on Personal Computers and Particle Accelerator Controls, 14th - 17th October 2014, Karlsruhe, DE
A. Michelotti - NI Week - Big Physics Symposium (Austin-TX) - August 2014, USA
G. Mazzitelli - CCR Workshop, 27-30 May, 2014 Catania, Italy
G. Mazzitelli - ANSA Scienza LAB gNE2014 – 30 May Campus X Tor Vergata, Italy
A. Stecchi - 1st Synergy LNF-OAR Workshop, 16-17 April, 2014 Frascati, Italy

**Publications**

[1] !CHAOS: a cloud of controls - MIUR project proposal, INFN-14-15/LNF, 19 November 2014
[2] First operational experience with the !CHAOS framework, PCaPAC 2014, Karlsruhe (DE), 14 - 17 October

[1] https://agenda.infn.it/categoryDisplay.py?categId=673

# 3L_2D
# (Time Resolved e+/e- Light in 2-Dimension)


*Scientific Staff*

A.Drago (Resp.), A.Marcelli, M.Cestelli Guidi, E.Pace (Ass.).

*Technical Staff*

R.Sorchetti (Acc.Div., Vacuum Serv.), D.Pellegrini, U.Frasacco, E.Gaspari (Acc.Div., SELCED), A.Grilli, A.Raco (Res.Div., DAΦNE Light).


The 3L_2D experiment, funded by the 5-th National Scientific Commission of INFN for the years 2013-2014, has been proposed and approved to study multiple scientific cases: to experiment with special IR detectors (uncooled, multi-pixel, time resolved) for beam diagnostics, to investigate on the behavior of the parasitic e-cloud in storage rings, to develop innovative bunch-by-bunch diagnostic tools, to help to increase the luminosity in DAΦNE by studying the beam dynamics.

In the first part of the activity the team has designed a new device to study the transverse instabilities by using the mid-infrared light emitted by synchrotron acceleration from a bending magnet in DAΦNE. Main focus of the experiment is to collect bunch-by-bunch and turn-by-turn transverse data from beams in storage rings to study the behavior induced by parasitic e-cloud or by other instabilities, mostly evaluating the bunch enlargement effects in the vertical plane. Two experimental array detectors working in mid-infrared (~10 micron) and fabricated by the VIGO System S.A. company are the base of the experiment. The arrays are semiconductors made by HgCdTe layer grown on GaAs substrate. The first one consists of 2x32 pixels operating at room temperature having each element with a size of ~50x50 micron^2 and a signal rise time <1 ns. The second array, just made by the VIGO farm, has 100x100 micron^2 pixels in two lines of 16 elements each. The arrays can monitor each DAΦNE bunch (2.7 ns) in longitudinal and in transverse dimensions. The second array should produce four time more powerful signals than the first one. In Fig.1 and Fig.2 there are photos of the new 2x16 pixel array. It is important to note that the second array has been designed and built by VIGO in base of the detailed requirements of the authors.

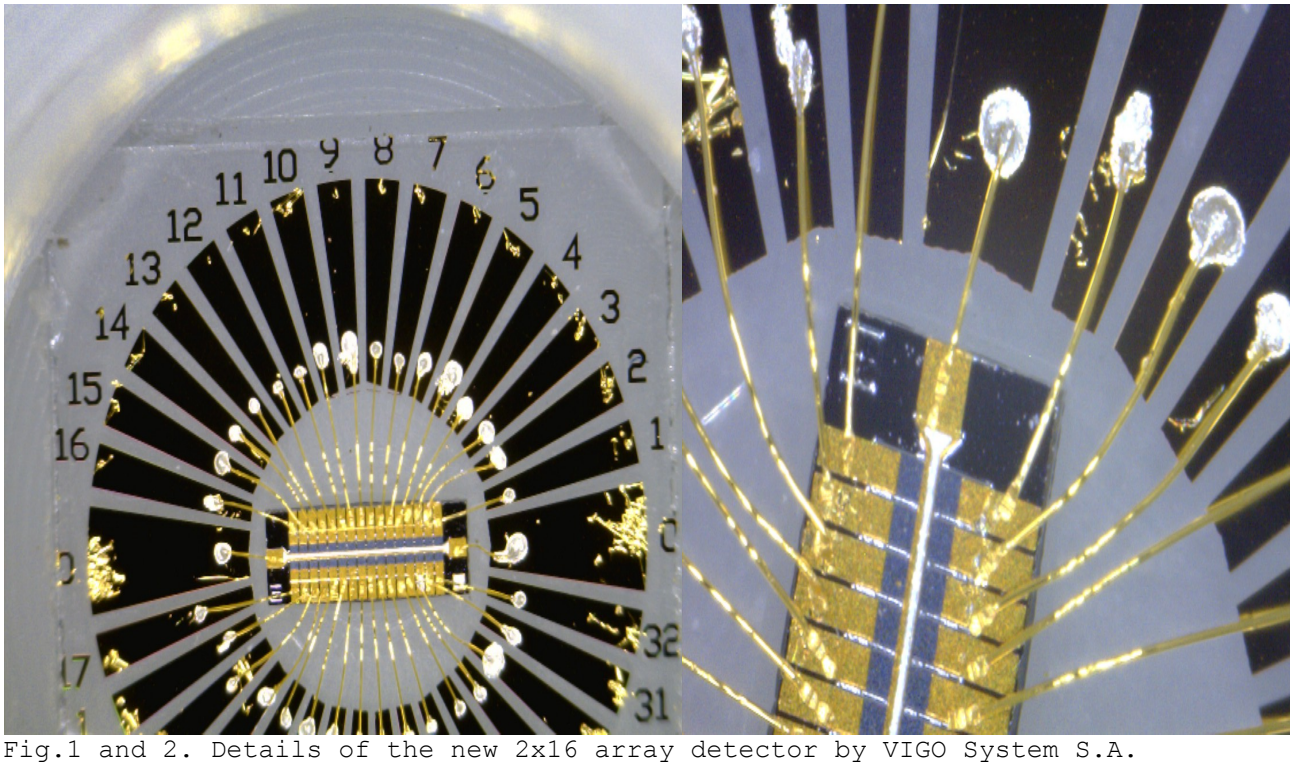


Fig.1 and 2. Details of the new 2x16 array detector by VIGO System S.A.

**Design and electronics**

The HgCdTe semiconductor array need to be interfaced to collect transverse beam data and this is not a simple task. To do this, a dedicated multi-channel apparatus with three-stage amplification and large frequency range has been designed and built. The multi-pixel array is illuminated by infrared SR coming out from 3+L beamline located in the e+ ring of DAΦNE and it is able to produce signals of the order of few tens of μV. The array is placed on a printed circuit board as shown in Fig. 3. To acquire the transverse beam shape, a dedicated compact camera with 16 channels and 3-stage amplification has been designed. The analog modules are shown in Fig. 4 and are placed inside an aluminum alloy made camera box. The amplification give a gain of about 40 dB for each signal. The amplified analog signals are then connected to a FPGA based systems with 14 bits ADC. The number of conversion bits is important to have a very good dynamic range in the conversion to digital maintaining a good signal bandwidth.

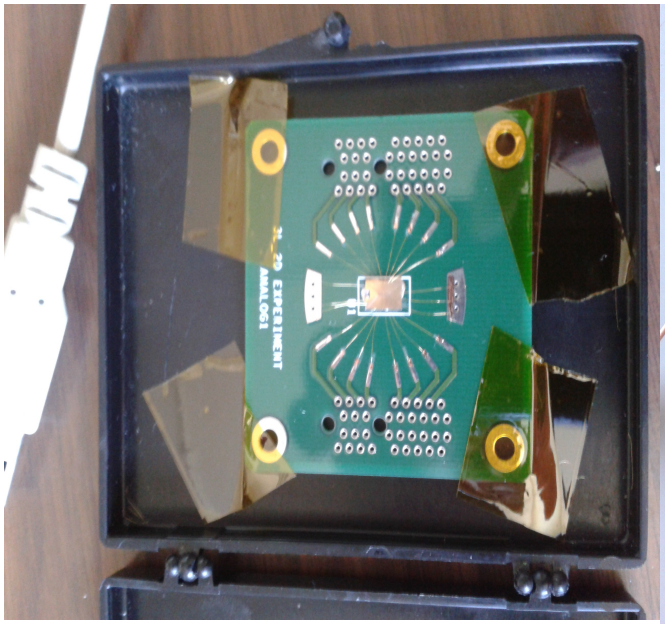

Fig.3 The array detector placed on PCB.

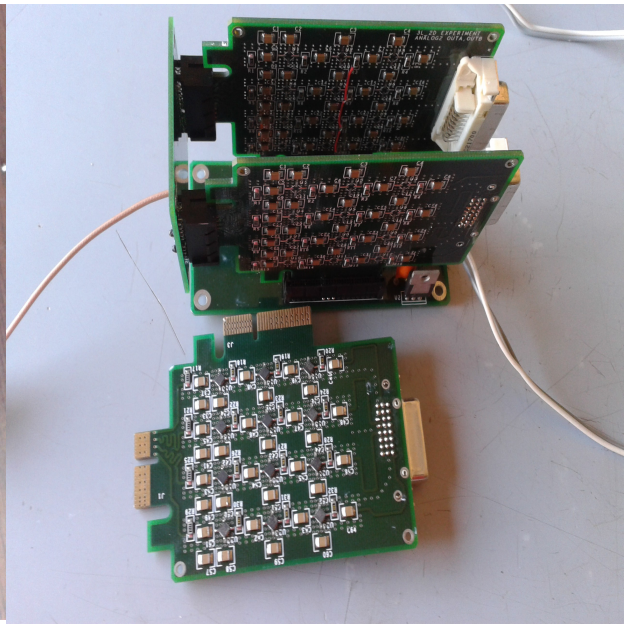

Fig.4 The analog modules of the camera.

Fig.5 Timing module with Arduino

Fig.6 FPGA and ADC modules (8 channels)

To acquire correctly the signals from each individual pixel a programmable modular timing board has been designed (shown in Fig. 5). The module in the picture can serve 8 acquisition channels, with 1-2ps of rms jitter and from 10ps to 10.23ns of programmable steps. The LVPECL logic levels has be chosen to be easily converted to the LVDS standard as the clock input level used in the FPGA modules. The delay for each pixel is downloaded by an Arduino Due board interfacing a PC through USB. All the timing data are stored on the flash memory inside Arduino (see Fig.5, pcb in blue). The timing module is also able to fan out 8+8 lines for trigger 1 and 2. The bunch-by-bunch and turn-by-turn data acquisition can load up to 1 mega contiguous values at 14 bits that are stored in real time on each FPGA. This means that the data acquisition system can store 16 M words for each beam tracks, that produces up to 133 thousands turn-by-turn data for each bunch. The FPGA is a Virtex-6 allocated on the XILINX-ML605 board shown in the lower side of Fig. 6. To complete the process flow, the data are sent to a server through a private LAN working at 1 Gbps. Given that the ML605 board does not have the ADC feature to acquire the input signals, this task is done by the custom AD-DA board that is loaded on the ML605, as shown in the top part of Fig. 6.

Fig.7 3L_2D rack at the e+ ring.

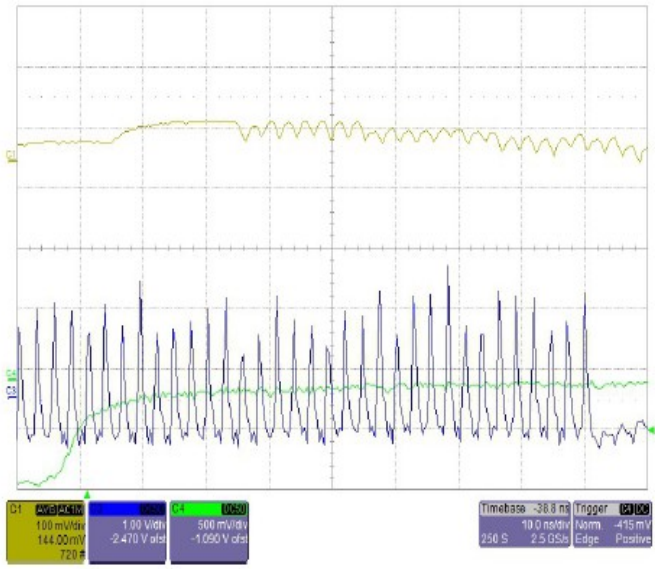

Fig.8 e- beam data taking (SINBAD, 13/6/2014)

**Measurements and Conclusion**

The frequent periods of DAΦNE shutdown have strongly limited the tests on real beam signals. Preliminary electron beam data of DAΦNE collected at SINBAD in June 13th, 2014 are presented in Fig. 8. The horizontal scale is 10ns for square. The green trace of this figure plots the machine revolution trigger. The beam signal is acquired from an electromagnetic pickup (in blue with a scale of 1V/div) and from a single 100x100 micron^2 pixel HgCdTe VIGO detector amplified by 40 dB (in yellow with a scale of 100 m/div). The blue signal from the standard pickup shows the last bunches before the gap, while the yellow signal from the IR detector shows the first part of the bunch train. This is prove of principle that the method is able to take bunch-by-bunch data.

## Reference


[1] A.Drago, "Beam Diagnostics by Infrared Time Resolved Detectors". Invited talk to the 20th IMEKO TC4 International Symposium, Benevento, Italy, Sept.15-17, 2014.

[2] A.Drago, M.Cestelli Guidi, A.De Sio, A.Marcelli, E.Pace, "Beam Diagnostics by Infrared Time Resolved Detectors". Proc of 20th IMEKO TC4 International Symposium, Benevento, Italy, Sept.15-17, 2014.

[3] A.Drago, A.Bocci, M.Cestelli Guidi, A.De Sio, A.Marcelli, E.Pace, "Bunch-by-bunch profile diagnostics in storage rings by infrared array detection". In publication, submitted on 15/11/2014.

# BEAM4FUSION

F. Murtas (Resp.)

Not received

# CHNET

A. Esposito (Resp.)

Not received

# ETRUSCO-GMES and MoonLIGHT-2

G. Bellettini (Ass.), G. Bianco (Ass.), A. Boni (AR), C. Cantone (Art. 36),E. Ciocci (PhD), S. Dell'Agnello, G.O. Delle Monache, N. Intaglietta (Tecn.),C. Lops (AR), M. Maiello (Ass.), R. March (Ass.), M. Martini (PhD), C. Mondaini (Bors.),G. Patrizi (AR), L. Porcelli (AR), L. Salvatori (Tecn.), R. Tauraso (Ass.), M. Tibuzzi (Tecn.), P. Tuscano (Tecn.), R. Vittori (Ass.)

## 1 Introduction

The SCF_Lab (Satellite/lunar/GNSS laser ranging/altimetry and Cube/microsat Characterization Facilities Laboratory) is a specialized infrastructure, unique worldwide, dedicated to design, characterization and modeling of the space segment of Satellite Laser Ranging (SLR), Lunar Laser Ranging (LLR) and Planetary Laser Ranging and Altimetry (PLRA) for industrial and scientific applications. We developed advanced laser retroreflectors for solar system exploration, geodesy and for precision tests of General Relativity (GR) and new gravitational physics. Our key experimental innovation is the concurrent measurement and modeling of the optical Far Field Diffraction Pattern (FFDP) and the temperature distribution of the SLR/LLR payload of retroreflectors under thermal conditions produced with a close-match solar simulator. The primary goal of these innovative tools is to provide critical design and diagnostic capabilities for SLR to Galileo and other GNSS (Global Navigation Satellite System) constellations. The implementation of new retroreflectors designs being studied will be helpful to improve GNSS orbits, increasing, this way, accuracy, stability, and distribution of the International Terrestrial Reference Frame (ITRF), in order to provide a better definition of the geocenter (origin) and the scale (length unit). The SCF is also actively used to develop, validate and optimize 2nd generation LLR arrays for precision tests of GR with the MoonLIGHT-2 (Moon Laser Instrumentation for General relativity High-accuracy Tests Phase 2) project. Laser ranging and laser reflectors throughout the solar system are also used to develop new fundamental gravity physics models and study the experimental constraints to these models. Starting from 2004 INFN invested resources and manpower to build and operate the SCF_Lab in Frascati, near Rome, dedicated to the characterization of the thermal properties and the laser ranging response of laser retroreflector arrays (LRAs) of CCRs (Cube Corner Retroreflectors) in space conditions accurately simulated in the laboratory (SCF-Test). The SCF_Lab consists of two OGSE (Optical Ground Support Equipment) called SCF (property of INFN) and SCF-G (which doubles our metrology capabilities for applications to GNSS, property of INFN and ASI). A schematic view of the cryostats is shown in Fig.:1. We have tested a large variety of CCRs, from LAGEOS (Laser GEOdynamics Satellite) to Apollo and GNSS LRAs.

## 2 APPLICATIONS TO GALILEO AND OTHER GNSS

With SCF-Testing of old-generation, Al back-coated retroreflectors, deployed on satellites of GPS, GIOVE and GLONASS (prior to GLONASS-115) we have de-qualified the use of Al back-coating for GNSS. From 2010 to 2014 INFN performed an extensive SCF-Test campaign under ESA contract, on Galileo IOV retroreflectors. These are fused silica uncoated CCRs, arranged in planar arrays of 84 units on four Galileo IOV (In Orbit Validation) satellites.

Measurements on the Galileo IOV retroreflector prototype during the simulated orbit (Fig.:2) have demonstrated that the choice of uncoated retroreflectors has improved significantly the optical response of GNSS LRAs. These results will be published soon, after having been authorized by ESA and Galileo (in progress). With the ETRUSCO and the ETRUSCO-2 (Extra Terrestrial Ranging to Unified Satellite COnstellations) RD programof INFN and ASI, we designed and characterized a full size GNSS Retroreflector Array (GRA), with application to Galileo and future GNSS.The GRA is a planar array with CCRs mounted on an aluminum base. On the array there are 55

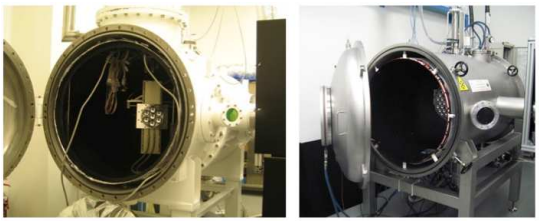

Figure 1: *SCF and SCF-G cryostats with GNSS LRAs inside.*

CCRs; each one of them is a solid uncoated retroreflector, made of Suprasil 1, with a circular front face of 33 mm diameter. The analysis of thermal and optical simulations are fundamental to test the designed prototype in conditions impossible to realize in laboratory. We realized a finite element and thermal model of the CCR based on the characteristics of the GRA retroreflector. The excellent and unsurpassed GRA optical performance measured inside the SCF_Lab is shown in Fig.:3 and Fig.:4 shows the results of ourthermal modeling of the measurement along the GCO orbit reported in Fig.:3.

### 2.1 Earth Observation

We are developing a midsize LRA suited for LEO and EO constellations like ESA Sentinels and, in general, for the space segment of Copernicus (European Flagship space program, also part of HORIZON2020). One model is shown in Fig.:5, which is one co-developed and co-studied by INFN and the Italian Ministry of Defense and the Italian Ministry of Foreign Affairs and International Cooperation (high-relevance Italy-USA bilateral project AUGUSTUS-2014, Absolute crust, Glacier and iceberg Georeferencing with Unified Sar, optical, gnss laser observations by Italy and USa-2014). CORA and/or its appropriately adapted versions are suited for deployment as Phobos AND Deimos laser Retroreflector Arrays (PANDORAs).

## 3 TESTS OF GENERAL RELATIVITY WITH LLR

LLR provides accurate measurements of the lunar orbit through a high-precision measurement of ranges between a laser station on the Earth and the Apollo CCRs on the lunar surface. For decades LLR has provided the best tests to validate Einsteins theory of General Relativity with measurements of the weak and strong equivalence principle, the Parameterized Post Newtonian (PPN) Parameter $\beta$, the time change of the Gravitational Constant, the Geodetic Precession ($K_{GP}$) and $\frac{1}{r^2}$ deviations. Over the years, LLR has benefited from improvements in both observing technology and data modeling, which led to the current 2cm precision. Unfortunately, the current geometry of the CCR array deployed on the Moon significantly limits further improvements. The main problem that affects the Apollo CCR array is caused by the lunar librations in longitude that result from the eccentricity of the Moons orbit around the Earth. Because of this phenomenon, one corner of the Apollo arrays is more distant from the Earth than the opposite corner by several centimeters, broadening the pulse coming back to the Earth. Together with University of Maryland (PI of Apollo LRAs), we developed a new CCR design which is not affected by lunar librations or regolith motion as indicated by Fig.:7. Figure 6 shows GR tests from (column 3, cm accuracy); best-case expected improvements for several MoonLIGHTs of 1mm and 0.1mm accuracy deployed on best locations (poles/limbs), observed by stations with ideal performance and orbit software capable of reaching 0.1mm, that is, capable of exploiting the ultimate improved accuracy provided

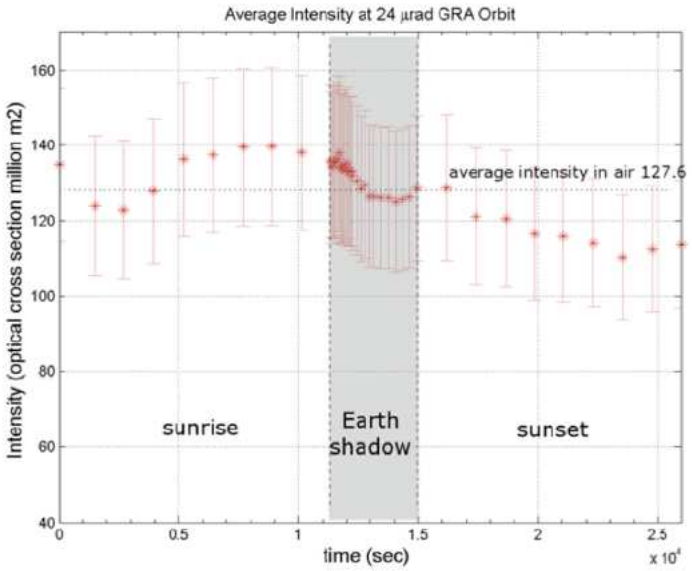


Figure 2: *FFDP intensity of GRA during GCO test compared with the nominal performance in air and isothermal conditions: the GRA developed by INFN and ASI shows, on average, no performance degradation under GCO SCF-Test.*

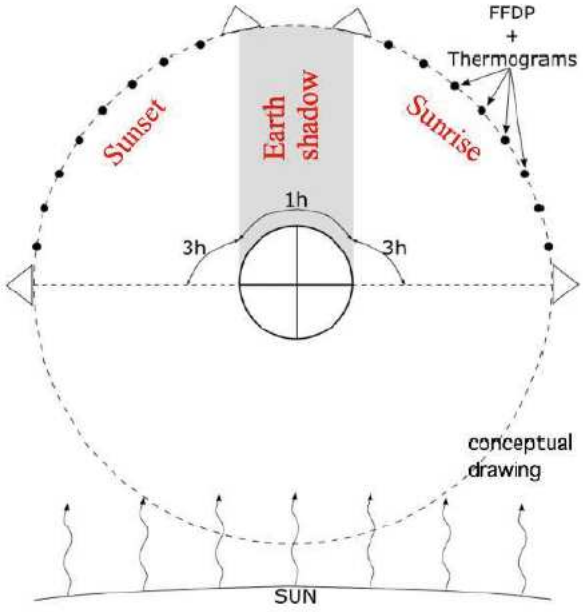


Figure 3: *The GCO, GNSS Critical Orbit, for Galileo.*

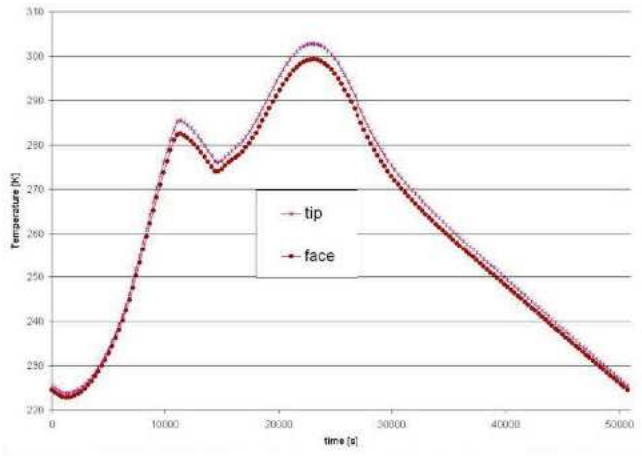


Figure 4: *Temperature trend of CCR's front face and tip along the orbit, showing that the axial thermal gradient of the GRA CCR is very small, thus it ensures negligible FFDP perturbations.*

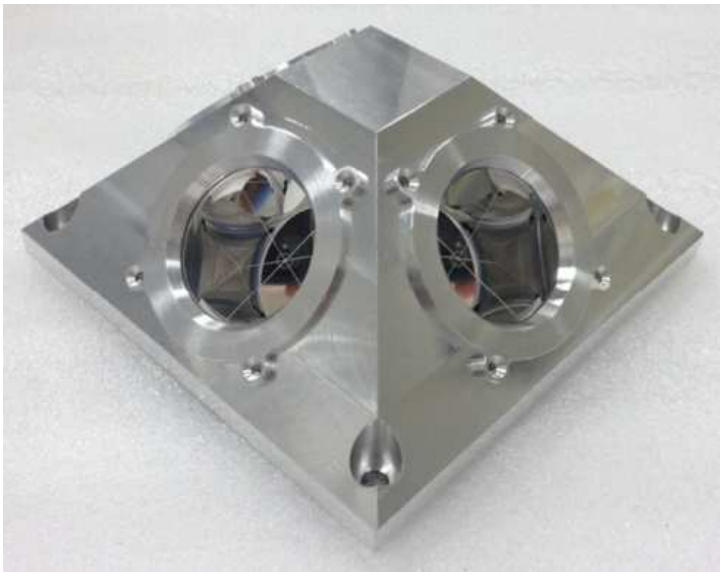

Figure 5: *Model of CORA, COpernicus laser Retroreflector Array.*

| Gravity Science Measurement | Timescale | LLR Measurement Accuracy | | |
|---|---|---|---|---|
| | | Current (cm) | 1 mm | 0.1 mm |
| Weak Equivalence Principle (WEP) | Few years | $\lvert\Delta a/a\rvert<1.3\times10^{-13}$ | $10^{-14}$ | $10^{-15}$ |
| Strong Equivalence Principle (SEP) | Few years | $\lvert\eta\rvert<4.4\times10^{-4}$ | $3\times10^{-5}$ | $3\times10^{-6}$ |
| Time Variation of Gravitational Constant | ~5 years | $\lvert\dot{G}/G\rvert<9\times10^{-13}\text{yr}^{-1}$ | $5\times10^{-14}$ | $5\times10^{-15}$ |
| Inverse Square Law (ISL) | ~10 years | $\lvert\alpha\rvert<3\times10^{-11}$ | $10^{-12}$ | $10^{-13}$ |
| Parameterized Post-Newtonian (PPN) β | Few years | $\lvert\beta-1\rvert<1.1\times10^{-4}$ | $10^{-5}$ | $10^{-6}$ |

Figure 6: *The expected improvements on the GR measurements with MoonLIGHT are shown in table, together with their measurement time scale.*

by the new MoonLIGHT CCRs. The parameter under estimation is shown in the first column; the timescale indicates the approximate data campaign length for achieving the scientific goal and in the last two columns are shown the estimation of the parameters using the accuracy of 1 mm and 0.1 mm. In order to test GR with LLR, we use the Planetary Ephemeris Program (PEP) developed by the Center for Astrophysics (CfA) during $1960_s$. This software is designed not only to generate ephemerides of planets and Moon, but also to compare models with observations. One of the first applications of the PEP software was the first measurement of the geodetic precession of the Moon. We have performed a preliminary analysis of real LLR data from station and dummy observations using MoonLIGHTtype $CCR_s$. The parameters considered are the variation of the gravitational constant G, the Nordtvedt parameter $\eta$, the geodetic precession KGP and the PPN parameter $\beta$. The original design of MoonLIGHT-2 had a sunshade (Fig.:8) that was designed to block the direct sun into the CCR for most of the lunar day. It also reduced the exposure to dust that could accumulate on the front surface of the CCR, over the very-long term, reducing the return signal.

## 4 GR Test results from LLR

During 2014-2015, the SCF_Lab in collaboration with the CfA (Center for Astrophysics) runned a number of numerical simulations using PEP (Planetary Ephemeris Program) to develop and optimize the MoonLIGHT-2 design in time for its launch and deployment. PEP is a FORTRAN software package, developed by I. Shapiro at CfA since 1970 and includes a detailed mathematical model of the solar system, with the masses of all solar system bodies and a large number of adjustable parameters. With PEP we can also include the position of different Earth laser stations like APOLLO (Apache Point Observatory Lunar Laser-ranging Operation, USA) or CERGA (Centre d'Etudes et de Recherches Géodynamiques et Astronomiques, France) useful for simulations. The main GR tests which are now being done in collaboration with CfA are the KGP, $\beta$, $\eta$ and $\frac{\dot{G}}{G}$ and for these simulations we used both real and dummy data from the real Apollo CCR in addition with the dummy data from MoonLIGHT-2. We run two different GR simulations using the Apollo CCR array and MoonLIGHT-2 CCR. Simulation n.1: In the first simulation, we used dummy data for MoonLIGHT-2 from the APOLLO ground Station and real data from the Apollo CCR computing the values of KGP, $\beta$ and $\frac{\dot{G}}{G}$. We use two different Moon site for MoonLIGHT-2, first simulating only one MoonLIGHT-2 on one of the two sites separately and then simulating two MoonLIGHT-2 simultaneously. With this simulation we studied if the GR measurements with

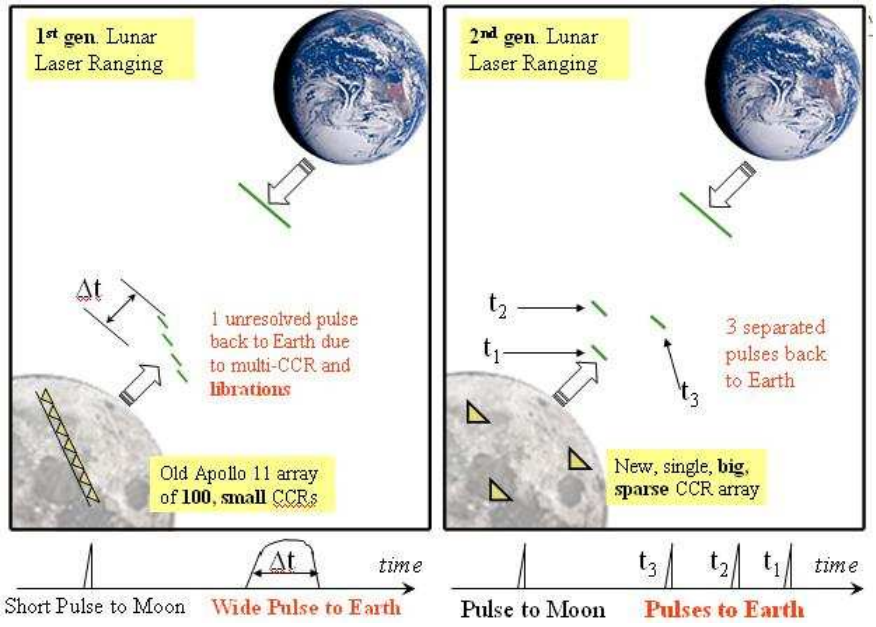


Figure 7: *Concept of the 2nd generation of Lunar Laser Ranging*

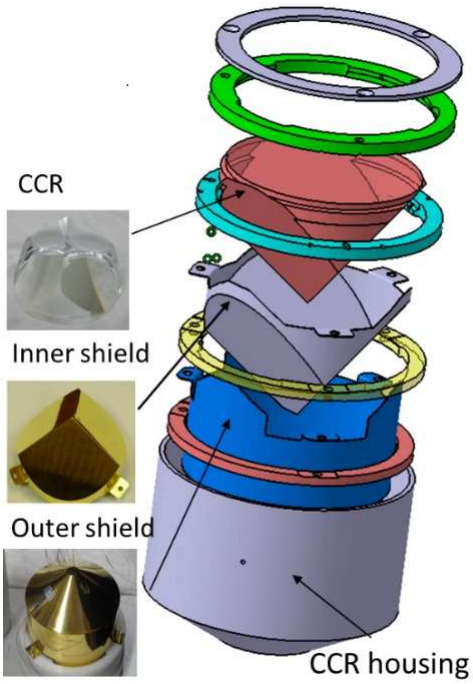


Figure 8: *Design concept.*

MoonLIGHT-2 will be depended from the lunar position, and if we can determine an optimal deployment site. We refer to Table 9 for details about simulation parameters used. The results of the

| SIMULATION #1: DEPLOYMENT SITE | | | | | |
|---|---|---|---|---|---|
| **CCR Array** | **Data Type** | **Time Span** | **Sites** | **Stations** | **Accuracy** |
| **Apollo** | Real | 2002 2012 | 11-14-15 | - | - |
| **MoonLIGHT** | Dummy | | $65^0$N, $40^0$W | APOLLO | 2.5cm |
| | | | $87^0$N, $40^0$W | | |

Figure 9: *Details about the best deployment site simulation with PEP.*

Simulation n.1: Deployment site are presented in Table 10. The data using only one MoonLIGHT-2 (the third column) gives similar results for both the Moon site showing that the GR simulations with MoonLIGHT-2 are poorly dependent from the Moon site position. The worst positions for this kind of simulation, where we use only few spot for MoonLIGHT-2 with few data collected, are at the poles since the array will not be always visible from Ground Station because of the Moon libration. In addition, the current PEP version does not allow us to considerate automatically the libration. The fourth column shows that in the case of low precision in the assessment of the geometry of the CCR array (for this simulation we use a precision of 2.5mm for the dummy data), we do not have any improvement in the GRs test even when adding additional CCR array to the Apollo CCR. It is important to underline that in this simulation the Apollo data became predominant respect to MoonLIGHT-2 because the low MoonLIGHT-2 precision data and the few spot used for MoonLIGHT-2. For this reason, we obtain that MoonLIGHT-2 is spot independent. In order to better understand the MoonLIGHT-2 performance we make another set of simulations, Simulation n.2. Simulation n.2: In the second simulation, we used only dummy data from the Apollo and the

| | **Only Apollo** | **Apollo + 1 MoonLIGHT-2** | **Apollo + 2 MoonLIGHT-2** |
|---|---|---|---|
| $\boldsymbol{\beta}$ | $2{,}0 \cdot 10^{-4}$ | $2{,}0 \cdot 10^{-4}$ | $2{,}0 \cdot 10^{-4}$ |
| $\boldsymbol{KGP}$ | $-8.6 \cdot 10^{-3}$ | $-6.7 \cdot 10^{-4}$ | $-2.0 \cdot 10^{-4}$ |
| $\boldsymbol{\dot{G}/G}$ | $9.2 \cdot 10^{-14}$ | $3.6 \cdot 10^{-14}$ | $3.1 \cdot 10^{-14}$ |

Figure 10: *Results of Simulation n.1: MoonLIGHT-2 best deployment site. All the results are expressed in terms of variation from constant value.*

MoonLIGHT-2 CCR for four different ground stations: APOLLO, CERGA, MLRS (McDonald Laser Ranging Station, USA) and MLRO (Matera Laser Ranging Observatory, Italy). For the MoonLIGHT-2 sites, we chose realistic deployment sites, the ones for the mission MoonExpress, Astrobotic and Israel. We simulated data until 2030 and use two types of MoonLIGHT-2 design, with and without sunshade. In design with a sunshade the MoonLIGHT-2 reflectors were shielded and therefore available whenever conditions were suitable at the observation site. In the case without sunshade, the MoonLIGHT-2 reflectors were unavailable when illuminated, reducing the amount of collectable data. Also for this simulation, we computed the values of KGP, $\beta$, $\eta$ and

$\frac{\dot{G}}{G}$. We refer to Table 11 for parameters used. The results of Simulation n.2: Optimal design and

| SIMULATION #2: OPTIMAL DESIGN AND GR EXPECTED IMPROVEMENT | | | | | |
|---|---|---|---|---|---|
| **CCR Array** | **Data Type** | **Time Span** | **Sites** | **Stations** | **Accuracy** |
| **Apollo** | Dummy | 2013<br>2030 | 11-14-15 | APOLLO | 0.1cm |
| | | | | CERGA | 0.2cm |
| | | | | MLRS | |
| | | | | MLRO | |
| **MoonLIGHT-2** | Dummy | 2016<br>2030 | $65^0$N, $40^0$W<br>*(MoonExpress)* | APOLLO | 0.5cm |
| | | | | CERGA | 1.0 cm |
| | | | $50^0$S, $35^0$E<br>*(Astrobotic)* | MLRS | |

Figure 11: *Details about the optimal design and GR expected improvement simulation with PEP.*

GR expected improvement are presented in Table 12. The GR tests with the sunshade show a slightly better accuracy compared to the case without the sunshade. The improvement is due to the longer data acquisition interval available for the design with sunshade. We think that this improvement doesnt affect significantly the GR results and the minor decrease in performance in the absence of a sunshade is compensated by the optimization of the MoonLIGHT-2 weight for its deployment. Comparing the expected GR results at 2030 in Table 12 with the actual best accuracy in GR test we can see the expected improvement in GR test accuracy using the new generation lunar retroreflector MoonLIGHT-2 CCR with the Apollo CCR.
Figure 13, Figure 14 and Figure 15 show the accuracy improvement until 2030 of $\beta$, $\frac{\dot{G}}{G}$ and KGP. For these simulations, the accuracy improvement in the GR tests using the new generation lunar retroreflectors is about one/half order of magnitude. All the results of this simulation show an accuracy improvement in the GR simulation results using MoonLIGHT-2 together with Apollo. However, results GR test accuracy shown in Table 12 is still lesser to the expected improvement predicted. However for a better data analysis we must considerate few points:

- The simulations use only a minimal number of MoonLIGHTs deployed in non-optimal locations (neither the poles, nor the limbs). In addition we use the current and non-upgraded laser station hardware neither the improvements in their data taking. Many of this improvements are already planned (like for LLR stations at ASI-Matera).

- We do not consider none of the new LLR stations that will be operative in the next few years (like the one in South Africa).

- The simulations does not include the updates, optimizations and improvements of any current orbit software (PEP) with which the current version supports a total LLR error budget on the order of a few cm. The updates will have to be implemented, and that will be possible to implement, as the LLR instrumental accuracy will improve thanks to the progressive deployment of MoonLIGHT CCRs on the Moon and thanks to the progressive upgrades of the LLR ground stations and/or additions of new LLR ground stations. Future software updates will allow us also a better estimation of libration. Summarazing the expected results shows the best improvement case while the simulation results in Table 12 we carried out shows the pessimistic case.

| | 2013 | 2016 | 2018 | 2020 | 2022 | 2025 | 2030 | Sunshade |
|---|---|---|---|---|---|---|---|---|
| $\dot{G}/G$ | $1.6 \cdot 10^{-14}$ | $7.7 \cdot 10^{-15}$ | $5.4 \cdot 10^{-15}$ | $3.8 \cdot 10^{-15}$ | $2.7 \cdot 10^{-15}$ | $1.7 \cdot 10^{-15}$ | $1.1 \cdot 10^{-15}$ | with |
| | - | $7.6 \cdot 10^{-15}$ | $5.2 \cdot 10^{-15}$ | $3.6 \cdot 10^{-15}$ | $2.6 \cdot 10^{-15}$ | $1.6 \cdot 10^{-15}$ | $1.0 \cdot 10^{-15}$ | without |
| $\eta$ | $2.6 \cdot 10^{-3}$ | $1.6 \cdot 10^{-3}$ | $1.1 \cdot 10^{-3}$ | $8.2 \cdot 10^{-4}$ | $7.4 \cdot 10^{-4}$ | $5.9 \cdot 10^{-4}$ | $4.9 \cdot 10^{-4}$ | with |
| | - | $1.5 \cdot 10^{-3}$ | $9.8 \cdot 10^{-4}$ | $7.2 \cdot 10^{-4}$ | $6.3 \cdot 10^{-4}$ | $4.9 \cdot 10^{-4}$ | $4.2 \cdot 10^{-4}$ | without |
| $KGP$ | $3.4 \cdot 10^{-4}$ | $2.0 \cdot 10^{-4}$ | $1.5 \cdot 10^{-4}$ | $1.1 \cdot 10^{-4}$ | $1.0 \cdot 10^{-4}$ | $7.8 \cdot 10^{-5}$ | $6.3 \cdot 10^{-5}$ | with |
| | - | $1.9 \cdot 10^{-4}$ | $1.3 \cdot 10^{-4}$ | $9.5 \cdot 10^{-5}$ | $8.0 \cdot 10^{-5}$ | $6.5 \cdot 10^{-5}$ | $5.3 \cdot 10^{-5}$ | without |
| $\beta$ | $6.4 \cdot 10^{-4}$ | $4.2 \cdot 10^{-4}$ | $2.7 \cdot 10^{-4}$ | $2.1 \cdot 10^{-4}$ | $1.9 \cdot 10^{-4}$ | $1.5 \cdot 10^{-4}$ | $1.2 \cdot 10^{-4}$ | with |
| | - | $3.9 \cdot 10^{-4}$ | $2.4 \cdot 10^{-4}$ | $1.9 \cdot 10^{-4}$ | $1.6 \cdot 10^{-4}$ | $1.3 \cdot 10^{-4}$ | $1.0 \cdot 10^{-4}$ | without |

Figure 12: *Results of Simulation n.2: Optimal design and GR expected improvement. Be careful, all the results are expressed in terms of variation from constant value.*

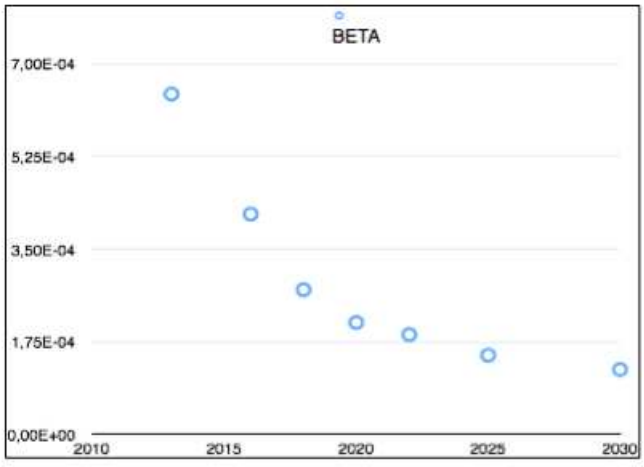


Figure 13: *$\beta$ improvement during a long time simulation using MoonLIGHT-2 with Apollo CCR.*

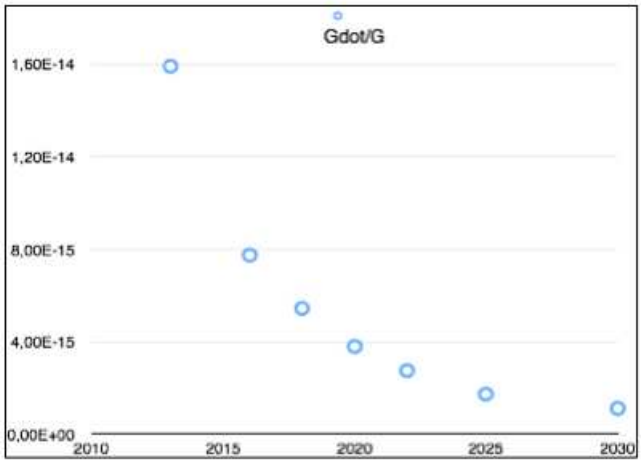


Figure 14: $\frac{\dot{G}}{G}$ *improvement during a long time simulation using MoonLIGHT-2 with Apollo CCR.*

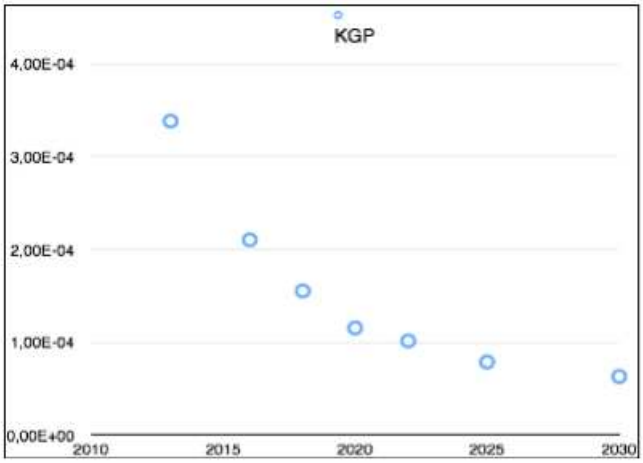


Figure 15: *KGP improvement during a long time simulation using MoonLIGHT-2 with Apollo CCR.*

## 5 Conclusion

Although Apollo retroreflectors will continue to operate and provide new science results, their geometry is now limiting the precision of the single photoelectron returns. The next generation retroreflector, MoonLIGHT-2, will support improvements in ranging precision, by one order of magnitude, depending on the method of deployment. With the preliminary simulations described in this work we show that:

- The GR tests with MoonLIGHT-2 will be not dependent from the MoonLIGHT-2 deployment site with the exceptions of the poles (because of the lunar libration, the array is not always visible from Earth).
- There are not great differences in the GR tests using a MoonLIGHT-2 design with or without Sunshade. So we choose the design without the sunshade that will provide an important weight optimization (about 1kg) with similar results in GR tests.
- The expected improvement in the GR with MoonLIGHT-2 is about one/half order of magnitude during the 10 years of analysis for most GR tests. The improvements shown in the simulations represent the most pessimist case where we do not considerate the LLR station upgrade or any software update and only few MoonLIGHT deployed in non-optimal locations.

In addition we are working at the thermal and mechanical design of MoonLIGHT-2 package, conducting a number of experimental tests in the SCF_Lab and simulations in order to define and optimize the CCR optical and thermal behavior on the Moon. The results of the tests, although are only preliminary, has provided us useful data for the characterization. Other experimental tests will be conducted in the SCF_Lab as other GR simulations. All of this will allow us to fulfill the ultimate scientific objective of MoonLIGHT-2: provide constraints on the theories that are proposed to determine the properties of Dark Matter and Dark Energy, and other gravitational theories. The improved precision that MoonLIGHT-2 will provide us once it will be deployed (in adequate number) on the Moon will be useful to identify the theoretical directions that will further the development of an understanding of these mysterious phenomena.

## References


1. DellAgnello, S., et al, *"Creation of the new industry-standard space test of laser retroreflectors for the GNSS and LAGEOS"*, Adv. in Space Res. 47,822-842, http://dx.doi.org/10.1016/j.asr.2010.10.022.
2. DellAgnello, S., et al. (2011) ETRUSCO-2, an ASI-INFN Project for the Development and SCF-Test of GNSS *Laser Retroreflector Arrays. ESA Proc. of 3rd International Colloquium- Scientific and Fundamental Aspects of the Galileo Programme, Copenhagen*, http://ilrs.gsfc.nasa.gov/missions/satellite_missions/current_missions/ga01_reflector.html.
3. Murphy T., Battat J., et al., *"The Apache Point Observatory Lunar Laser-Ranging Operation (APOLLO): two years of Millimeter-Precision Measurements of the Earth-Moon Range"*, PASP 121, 29 (2009).
4. D.G.Currie, S. Dell'Agnello, *"A Lunar Laser Ranging Retroreflector Array for the 21st Century"*, AMOS 2009.
5. J.G.Williams, S.G.Turyshev, D.H.Boggs, *"Progress in Lunar Laser Ranging Test of Relativistic Gravity"*, Phys.Rev.Lett.93:261101,2004.

6. Bender P. L., et al, *"The Lunar Laser Ranging Experiment"*, Science, Volume 182, Issue 4109, pp. 229-238, 1973.

7. Williams J. G., Turyshev S. G., Boggs D. H., Ratcliff J. T., *"Lunar Laser Ranging Science: Gravitational Physics and Lunar Interior and Geodesy"*, 35th COSPAR Scientific Assembly, July 18-24, 2004.

8. Williams J. G., Boggs D. H., Ratcliff J. T., *"A larger lunar core?"*, 40th Lunar and Planetary Science Conference, March 23-27, 2009.

9. Williams J. G., Turyshev S. G., Boggs D. H., *"Lunar Laser Ranging Test of the Equivalence Principle with the Earth and Moon"*, International Journal of Modern Physics D, Volume 18, 1129-1175, 2009.

10. Rambaux N., Williams J. G., Boggs D. H., *"A Dynamically Active Moon-Lunar Free Librations and Excitation Mechanisms"*, 39th Lunar and Planetary Science Conference, March 10-14, 2008.

11. Williams J. G., Boggs D. H., Ratcliff J. T., *"Lunar Tides, Fluid Core and Core/Mantle Boundary"*, 39th Lunar and Planetary Science Conference, March 10-14, 2008.

12. Nordtvedt K., *"Lunar Laser Ranging: a comprehensive probe of post-Newtonian gravity"*, Gravitation: from the Hubble length to the Planck length, edited by Ciufolini I., Coccia E., Gorini V., Peron R., Vittorio N., ISBN 07503 0948, published by Institute of Physics Publishing, the Institute of Physics, London, 2005, p.97.

13. Murphy T. W., Adelberger E. G., Strasburg J. D., Stubbs C. W., Nordtvedt K., *"Testing Gravity via Next Generation Lunar Laser-Ranging"*, Nuclear Physics B Proceedings Supplements, Volume 134, 155-162.

14. Nordtvedt K., *"Testing the Equivalence Principle with laser ranging to the Moon"*, Adv. in Space Research, Volume 32, Issue 7, 1311-1320.

15. Dvali G., Gruzinov A., Zaldarriaga M., *"The Accelerated Universe and the Moon"*, Physical Review D, Vol. 68, Issue 2, id. 024012.

16. Currie D. G., et al., *"A Lunar Laser Ranging Retro-Reflector Array for NASA's Manned Landings, the International Lunar Network, and the Proposed ASI Lunar Mission MAGIA"*, 16th International Workshop on Laser Ranging Instrumentation, October 13-17, 2008.

17. Prete F., *"Contact structural analysis of the MoonLIGHT Laser Retro-reflector Assembly with ANSYS"*, Bachelor thesis (unpublished), Dipartimento di Meccanica e Aeronautica, University of Rome "La Sapienza".

18. Minghiglioni A., *"Modal analysis of the MoonLIGHT Laser Retro-reflector Assembly with ANSYS"*, Bachelor thesis (unpublished), Dipartimento di Meccanica e Aeronautica, University of Rome "La Sapienza".

19. `http://ilrs.nasa.gov/docs/retroreflectorspecification070416.pdf`

20. Pearlman M. R., Degnan J. J., Bosworth J. M., *"The International Laser Ranging Service"*, Adv. in Space Research, Vol. 30, No. 2, 135-143, 2002.

21. Urschl C., Beutler G., Gutner W., Hugentobler U., Schaer S., *"Contribution of SLR tracking data to GNSS orbit determination"*, Adv. in Space Research, 39(10), 1515-1523, 2007.

22. Urschl C., Beutler G., Gutner W., Hugentobler U., Ploner M., *"Orbit determination for GIOVE-A using SLR tracking data"*, ILRS Workshop, 2006.

23. `http://ilrs.nasa.gov/docs/ILRSRetroreflectorStandards200812.pdf`

24. Neubert R., Neubert J., Munder J., Grunwaldt L., *"Proposed Single Open Reflector for the GALILEO Mission"*, International Technical Laser Workshop on SLR Tracking of GNSS Constellations, 2009.

# FAEMCAR: FUNDAMENTAL AND APPLIED ELECTROMAGNETICS OF NANOCARBON

S. Bellucci (Resp. INFN), R. Baldini (Tecn.), S.Bistarelli (Dott.), M. Mastrucci (Laur.), A. Cataldo (Dott..), G. Giannini (Osp.), F. Micciulla (Ass. Ric)

External collaborating Institutions:
- Laboratory for solid state physics (LPS) of the Department of Physics of matter and radiations. at the University of Namur (FUNDP), Belgium,
- Laboratory of Electrodynamics of Inhomogeneous Media at the Institute of Nuclear Problems of Belarusian State University,
- Nanostructures Department at Research Institute for Technical Physics and Materials Science, Budapest, Hungary,
- Department of Radiophysics of Faculty of Physics Vilnius University, Lithuania,
Research Institute for Technical Physics and Materials Science,
- Department of New Methods of Biochemical Physics and Materials Science Emanuel Institute of Biochemical Physics of The Russian Academy of Sciences, Moscow,
- Institute for Physics of National Academy of Sciences, Kyiv, Ukraine.

We participate as a partner (the INFN unit) to the PEOPLE MARIE CURIE ACTIONS International Research Staff Exchange SchemeCall: FP7-PEOPLE-2012-IRSES. FAEMCAR has a duration of 48 months and started its activities on 3rd January 2013. The consortium binds together three Universities and four Research Organizations.

## Mid Term Report 2014:

WP1: Synthesis and functionalization of multi-walled CNTs and fabrication of composite materials on the basis of different forms of nanocarbon, both laboratory made and commercially available.
We have synthesized several nanocarbon based composites to carry out different characterization (electromagnetic shielding, electrical, mechanical and thermal characterizations).
Independently from the type of fillers, nanocarbon-based composite samples, using a Epikote 828 epoxy resin, a curing agent called A1 (i.e., a modified Tetraethylenepentamine (TEPA)) (at 0.25, 0.5, 1.0, 1.5 and 2.0 wt. % of carbon fillers typical concentrations) were fabricated as follows: the resin was degassed under vacuum (1–3 mbar) for 12–14 h, then it was put into an oven at 65°C. In the meantime, the carbon was dispersed in propanol through ultrasonic bath for 1.5 h. Afterwards the solution of alcohol and carbon fillers was mixed with the resin. The obtained mixture was inserted inside the oven at 130–150°C for the evaporation of alcohol. The curing agent (A1) was added to the mixture of resin and filler through slow manual mixing for about 7min. The mix was then poured into 1cm x 1cm x 7cm molds, and left as such for 20 h for the curing process at room temperature and then 4 h in oven at 80°C. When the process was completed, the samples were removed from the molds. The uniformity of distribution of the carbon fillers in the polymer samples was studied by scanning electron microscopy; all fabricated composites demonstrated good homogeneity, carbon inclusions were reasonably well dispersed.
Nanocomposites based on few layer graphene flakes (FLG) - or equivalently called graphene nanoplatelets(GNP)-, Carbon NanoTubes (CNT), Carbon Black (CB), and Exfoliated Graphite (EG) were investigated.
The adopted GNP were obtained by means of an innovative technique introduced recently at the

Istituto Nazionale di Fisica Nucleare (INFN), Frascati (Rome), Italy, within the NEXT nanotechnology group. Expandable graphite produced and commercialized by Asbury is used as a source to obtain graphene nanoplatelets. This kind of expandable graphite is intercalated with chemical substances, normally sulfates and nitrates, inserted between the graphene planes of the graphite. As the material undergoes a sudden thermal shock, the intercalating substances vaporize: hence the gas exerts a pressure between neighboring planes, which then separates them, thus exfoliating the material. The fabrication method used by the INFN NEXT nanotechnology group is a variant of the customary thermal expansion obtained in a more conventional oven: normally treatments of such a kind are carried out in ovens where the temperature is kept about 1000°C.

The procedure realized at the INFN Frascati nanotechnology laboratories is rather based upon the use of a normal household microwave (MW) oven: the MW irradiation of the sample produces a sudden heating of the graphite and the vaporization of the intercalating substances, which, in turn, modify the air dielectric properties, thus causing a series of sparks that self-feed the process. During the latter, the temperature grows above 1000°C. The procedure based on MW irradiation yields several advantages, with respect to the customary heating in a conventional oven, namely it is:

cheap and "green" (just about 10 sec of MW irradiation vs. the amount of energy needed in order to heat up the normal oven and maintain its temperature at a constantly high value); very fast; very safe, as the operator does not need introducing the intercalated, expandable graphite in a high temperature environment (e.g. as in a conventional oven); eco-friendly (as it is solvent-free).

After the MW irradiation-induced thermal expansion, the samples appear to have the following morphological and structural characteristics: Worm like structure; Very large particle area; Thickness: 5±3 planes. To be specific, after the expansion of the intercalated graphite, the obtained samples, in the form of worm like structures show how the intercalated multilayer graphite turns out to have undergone an expansion process. By means of a short treatment with ultrasounds in isopropylic alcohol, the graphene nanoplatelets can be freed from the worm like overall structure, thus forming particles with the two dimensional lateral sides having sizes about tens micrometers and a thickness less than 5 nm (i.e. several layers).

Studies on CNT-Epoxy composites dealt with modeling of composites by both simulation of equivalent electric circuit and broad band analysis.

Equivalent electric circuits allowing the simulation of the behavior of nanocomposites based on thermosetting resin and nanocarbon filler are modeled. The electric circuits are derived by a simple multistep procedure. Two main circuital models are achieved for for the two CNT (single and multi walled) nanocomposites with CNT concentration close to the percolation threshold. Since the reproducibility of measured results was high, one can use the obtained equivalent circuits technique to simulate the behavior of another composite made with the same recipe. The obtained equivalent circuits may be employed for the interpretation of the physical mechanisms which are responsible of their EM behavior. In particular, an indication of the thickness of the insulating layer responsible for the tunneling resistance between CNTs aggregates can be achieved. In addition, the networks can be applied in circuit simulators for preliminary design of EM devices where such composites are used.

The dielectric analysis of the MWCNT/epoxy resin reveals a huge influence of the polymer matrix on the temperature dependence of composite dielectric properties. Far below percolation threshold (0.25 wt% MWCNT) the dielectric properties of the composite are mostly determined by the pure matrix, except for the slightly increasing of the complex dielectric permittivity. Close to percolation threshold the composite shows the negative temperature coefficient (NTC) effect in the temperature region, where the pure polymer matrix becomes conductive. The activation energy increases with the MWCNT concentration below percolation threshold and decreases close to it. The effect is connected with MWCNT-polymer and MWCNT-MWCNT electrical contacts properties.

About CB-Epoxy composites, broadband electric/dielectric characterization in a wide temperature

range (25–500 K) was carried out.
At higher temperatures (above 400 K), the electrical conductivity of composites is governed by electrical transport in polymer matrix and current carriers tunneling from carbon black clusters to polymer matrix. The activation energy of such processes decreases when the carrier concentration increases, i.e., with the increase of carbon black concentration. At lower temperatures, the electrical conductivity is governed by electron tunneling and hopping. The electrical conductivity and dielectric permittivity of composites strongly decrease after annealing composites at high temperatures (500 K); at the same time potential barrier for carriers tunneling strongly increases.
Then, we have carried out comparative studies among different filler-epoxy composites.
First of all, we investigated similarities and contrasts between three families of filler particles (CB, MWCNT, and SWCNT) and provide added insight into their ac electric response, progressing toward identifying the models that describe charge transport and polarization mechanisms in these heterostructures. Significantly, all the key spectral features of our frequency-dependent permittivity results can be quantitatively described by Jonscher's model. We suggest that the likely transport mechanisms responsible for the dielectric relaxation in these samples can be modelled by the dipolar relaxation and anomalous LFD below and above percolation, respectively These findings sharpen several earlier reports dealing with ac electrical properties of insulatorconductor composites in a broad frequency range.
After, a comprehensive analysis of electrical, electromagnetic (EM), mechanical, and thermal properties of epoxy resin composites filled with 0.25–2.0wt. % of carbon additives characterized by high surface area, both nano-sized, like carbon nanotubes (CNTs) and carbon black (CBH), and micro-sized exfoliated graphite (EG), was performed. We found that the physical properties of both CNTs- and CBH-based epoxy resin composites increased all together with filler content and even more clearly for CBH than for CNTs. In the case of EG-based composites, good correlation between properties and filler amount was observed for concentrations below 1.5 wt. %.
The cluster architecture of nanocarbon in polymer nanocomposites and the microstructural, elastic and electromagnetic properties of epoxy/graphite composites, were investigated also by means of acoustic microscope techniques, as a guide towards optimization of nanocomposite preparation schemes, in close collaboration with the Laboratory of Acoustic Microscopy, Institute of Biochemical Physics, RAS, Moscow, Russia.

## Publications by LNF Authors in the Year 2014

Epoxy Nanocomposite Based on Carbon Nanotubes for Electromagnetic Interface Shielding, S Bellucci, F Micciulla, Advanced Nanomaterials for Aerospace Applications, 267, 2014.
Brief Introduction to Nanocomposites for Electromagnetic Shielding, S Bellucci, F Micciulla Advanced Nanomaterials for Aerospace Applications, 227, 2014

Nanocomposites of epoxy resin with graphene nanoplates and exfoliated graphite: Synthesis and electrical properties, A Dabrowska, S Bellucci, A Cataldo, F Micciulla, A Huczko, physica status solidi (b) 251 (12), 2599-2602, 2014

Heat-resistant unfired phosphate ceramics with carbon nanotubes for electromagnetic application A Plyushch, D Bychanok, P Kuzhir, S Maksimenko, K Lapko, A Sokol, J. Macutkevic, J. Banys, F. Micciulla, A. Cataldo, S. Bellucci, physica status solidi (a) 211 (11), 2580-2585, 2014

## List of Conference Talks by LNF Authors in the Year 2014

S. Bellucci, Transport mechanisms and dielectric relaxations of epoxy nanocomposites from DC to microwave range, Workshop on Nanoelectromagnetics of advanced materials for microwave-to-THz applications, European Microwave Week (EuMW 2014), Roma, 5 October 2014.

A. Cataldo, "Structural investigation and mechanical properties of epoxy resins nanocomposites through solid state NMR and nanoindentation, Conference on nanoscience and nanotechnology n&n2014, 6 – 7 October 2014, INFN-LNF Frascati.

# Activity Report 2014 – GARFIELD

Alessandra Di Gaspare (resp), Roberto Cimino, Giovanni Bencivenni, Rosanna Larciprete (ass), Guglielmo Fortunato (ass), Andrea Notargiacomo (ass)

The project GARFIELD (Graphene Active FIlms for Electronic devices and radiation Detection) is one of the three grant for young researchers funded in 2013 by the National Scientific Committee 5 (CSN5), the national committee of the INFN which is devoted to technological research. The project, started on January 2014, is aiming at the development of a technological platform to realize graphene-based detectors of interest to the INFN. The unique physical properties, like high carrier mobility, electrical and chemical stability, make graphene of potential use for several forefront applications in detector R&D. With the aim to explore the graphene integrability into the detectors technology of interest, the addressed applications are: (i) detection of low-flux/high energy radiation and (ii) radiation hardness.
The experiment is hosted by the Material and Surface Science Lab of DAFNE-L at Laboratori Nazionali di Frascati, where the available facilities for the spectroscopic investigation of graphene have been expanded with the acquisition of a furnace for synthesis of graphene on large area. We have also benefited from both internal and external scientific expertise in material and surface science, microfabrication and microelectronics, and from the experimental facilities available in the Rome area at the ISC, IFN and IMM institutes of Consiglio Nazionale delle Ricerche (CNR).
The first scientific objective of GARFIELD is the development of an experimental setup able to synthetize monolayer graphene, and the optimization of the graphene quality, via systematic spectroscopic analysis. Therefore, the main activity of the project during the 2014 was finalized to the implementation of a growth facility within the lab hosting the project. The addressed technique for the graphene synthesis was Chemical Vapor Deposition (CVD) on Copper (Cu) foils. We have designed and acquired one atmospheric pressure CVD system based on a quartz-tube furnace capable to reach the temperature needed for the synthesis (T of the order of 1000 °C). The CVD furnace has then been equipped with a gas distribution circuit for Hydrogen, Methane and Argon, designed and realized in full agreement with the Italian laws on safety and environmental subjects. A high-accuracy pressure and flows controller system for the injection of precursor agents in the reaction chamber has been also installed. In Fig.1 it is reported a schematic layout of the CVD system, and in Fig. 2 it is reported a picture of the system once installed and tested.

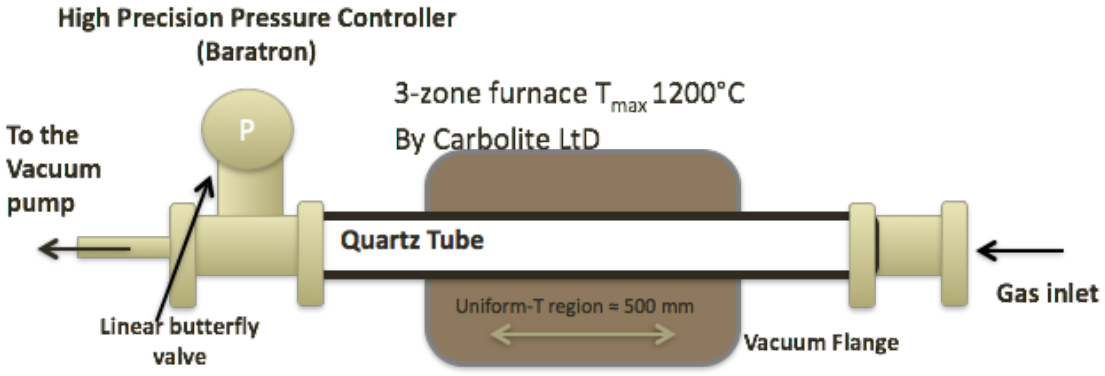


Figure 1: Schematic layout of the CVD system with tube chamber

Figure 2: Picture of the CVD furnace. The main features of the system are: 3-zone temperature controller reaching 1200 °C; 3-inches quartz worktube connected to the gas distribution panel containing 3 gas flow controllers at one end, and to a rotary pump and to high-precision absolute-pressure reader at the other end.

The optimization of the growth of single layer graphene requires a quantitative study of the film quality as a function of growth parameters (temperature, pressure, time, gases composition and substrate surface conditioning). MicroRaman spectroscopy is the tool used to assess the quality of the grown films in terms of density of defects, homogeneity, coverage and number of graphene layers composing the sample. By using this technique, we have conducted a first survey on two of the most critical growth parameters, i. e. the growth temperature and the partial pressure ratio between the precursor gases $CH_4$ and $H_2$, that allowed us to find the conditions most suitable for the synthesis of single-layer graphene with moderate density of defects and good coverage. However, as far as the Raman analysis is performed directly on the growth Cu-substrate, a fully quantitative characterization is quite difficult to obtain. Indeed, due to the coupling existing between the graphene and the metal substrate and the high signal background arising from it, the very strong Raman spectral features of pristine graphene are masked. Hence, we have developed “in-house” the well-known “PMMA-method” to transfer graphene from the CVD substrate to arbitrary substrates (semiconductor or insulating), chosen to be suited for the Raman spectroscopic qualification and, more importantly, for the device applications. This methods is as following: a) spin coating of a PMMA layer on the graphene-on-Cu sample; b) removal of the Cu substrate by using selective wet chemical etching; c) the transfer of the PMMA-on-graphene carrier on the desired substrate; d) the final removal of PMMA, to have graphene-on-substrate at the end of the process. From the first tests on the graphene transfer, conducted in collaboration with the CNR facilities involved in the experiment on our samples and on commercial samples (by GRAPHENEA), we could obtain single layer graphene “pieces” of few $mm^2$ area on Si-subtrastes. These results indicate that we didn’t have a full coverage of the substrate, probably as a consequence of a not well prepared substrate surface before the growth. These results are summarized in Fig.3, where are reported the graphene Raman spectra measured on the as-grown substrate and after the transfer for a commercial single layer graphene (fig. 3a-b) and for two samples grown in our system at different temperatures (fig. 3c-f).

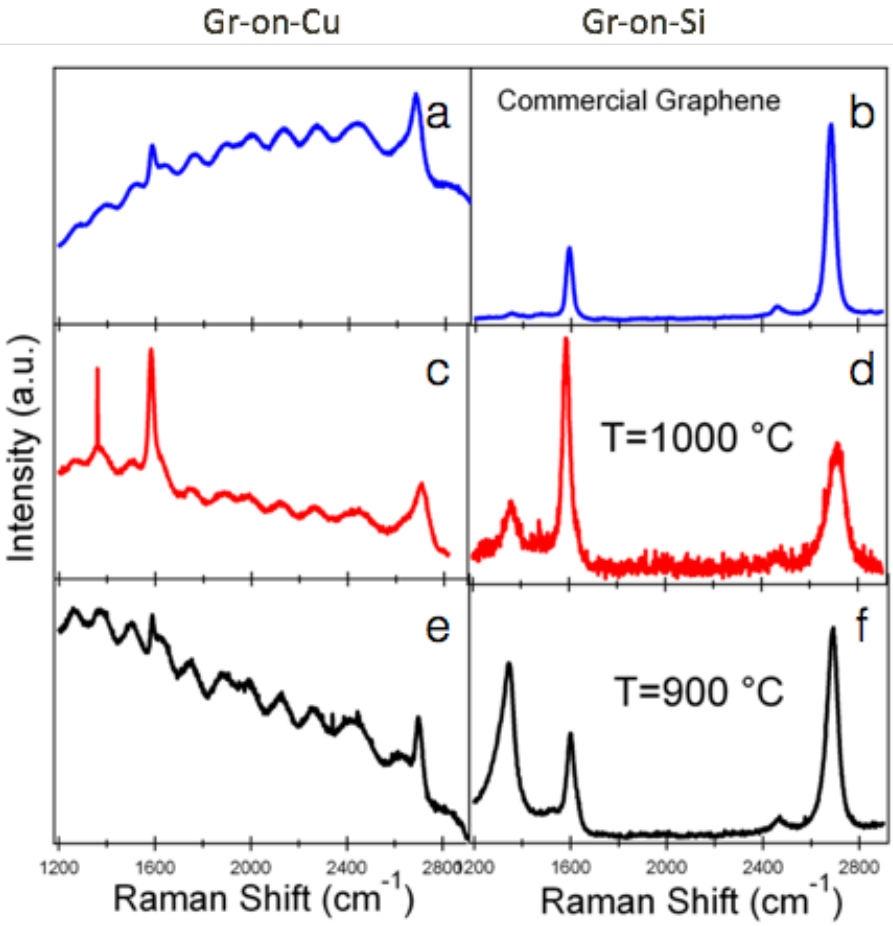


Figure 3: Raman spectra measured before (a,c,e on the left) and after (b, d, f on the right) the transfer of the film from the Cu-substrate used during the CVD growth to a silicon substrate, on a commercial single-layer graphene (a,b), and on two graphene films grown in our CVD at 1000 °C (c,d) and 900 °C (e,f).

Future work will be on the optimization of the surface of the Cu foils by employing chemical cleaning, and the development of more robust transfer methods for $cm^2$-area samples, by introducing different kind of carrier polymer alternative to the PMMA.
The second objective of the GARFIELD experiment, that will be pursued in the 2nd year of the project, will be the development of graphene-based devices to be used as detectors in the form of experimental proof-of-principle prototypes, rather than ready-to-use demonstrators. Therefore, besides the work on material synthesis, during the last part of 2014 we have started a theoretical study on the detector architectures to be developed. The first class of devices addressed will be based on the field-effect transistor (FET) architecture, where the type of semiconducting substrate will be chosen depending on the detector use. With the help of T-CAD software, as a starting point we have simulated a graphene-FET realized on silicon substrate, having one micrometric strip of monolayer graphene as a gate electrode. The graphene gate acts as field sensing electrode, able to detect any change in the field distribution occurring in the silicon substrate upon irradiation. The structure of the simulated device is reported in Fig.4. The evaluation of the performances and the optimization of the structure are still ongoing. The first results revealed that the transient electric field produced by the e-h couple formation upon illumination could enable the field sensing on the graphene gate by properly choosing the geometric parameters of the

device (e.g. oxide thickness, substrate doping, etc), so to produce a significant change in its conductivity. Once the optimized parameters will be established, we will proceed with the fabrication of the first prototypes by using micro-fabrication techniques made available within the collaboration with the CNR [1,2]. The peculiar electro-dynamic properties of the 2-dimensional electron system (2DES) of graphene, as well as of other 2DES, are potentially usable in several forefront photonics applications, like e.g. the development of novel devices with terahertz functionalities. Besides the main goals of the project indicated above, the expertise in 2D materials science and technology gained within the GARFIELD experiment has been used also within scientific collaborations with Sapienza University of Rome and CNR institutes, and has been fruitful in a number of pubblications [2-5] of particular interest in the perspective of novel materials for detectors development. In particular, the spectroscopic studies on the hydrodynamic response of a 2D electronic plasma confined in the transistor micrometric channel have demonstrated that 2D-based FETs can be used to realize a frequency-tunable THz detectors based on plasmonic micro-cavities.

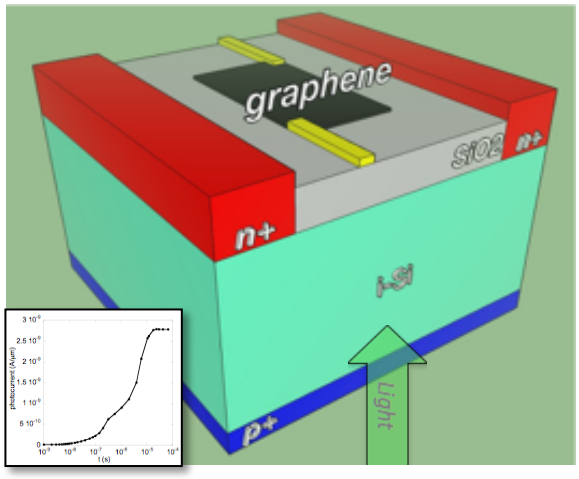


Figure 4: Schematics of the graphene-FET under study; the graphene gate acts as electric field sensor of any transient change produced into the substrate upon irradiation. Inset: photocurrent calculated from the electric field distribution on the graphene micrometric strip after illumination.

## Publications


[1] A. Di Gaspare, "The GARFIELD Project: Activity Status Report", convened talk given to the CSN5, February 2015.

[2] A. Di Gaspare et al, "Graphene-based Field Effect Transistors as Radiation Sensors", submitted to 13th Pisa Meeting on Advanced Detectors on the topic "Frontier Detectors For Frontier Physiscs".

[3] Giliberti, V. ; Ortolani, M. ; Giovine, E.; Di Gaspare, A.; Biasiol, G.; Sorba, L.; Evangelisti, F., "Terahertz plasmon cavity modes in a heterostructure transistor", Proc. Of IRMMW-THz, 2014

[4] V. Giliberti, A. Di Gaspare, E. Giovine, M. Ortolani, L. Sorba, G. Biasiol, V. V. Popov, D. V. Fateev, and F. Evangelisti, "Down conversion of terahertz radiation due to intrinsic hydrodynamic nonlinearity of a two-dimensional electron plasma", submitted to Phys. Rev. B

[5] A. Di Gaspare, "Therahertz plasmon cavity modes in a heterostructure transistor", Oral Presentation to the Workshop Plasmonica 2014

# GILDA - GENERAL PURPOSE ITALIAN BEAMLINE FOR DIFFRACTION AND ABSORPTION - AT ESRF.

A. Balerna, A. Grilli (Tecn.), S. Mobilio (Resp.), A. Raco (Tecn.),
V. Sciarra (Tecn.), V. Tullio (Tecn.)

## 1 Introduction

After 20 years of operations at the end of 2014 the Italian CRG beamline at the ESRF GILDA, financed by CNR and INFN stops its activity. The beamline will undergo a deep refurbishment process leading to a new instrument fully dedicated to X-ray Absorption Spectroscopy and related techniques with the financial support of the CNR only.

## 2 Main activities in 2014

In this last year of activity GILDA has delivered 369 shifts in user mode: 258 for the ESRF beamtime quota and 111 for the CRG beamtime for a total of 24 experiments. Some experiments were carried out using the new instrumentation developed last year (namely XEOL, cryostat for liquid samples and acquisition under excitation).
The scientific beamline activity was severely affected by the breakdown of two ball bearings of the complex monochromator mechanics, stopping the operation during two full months until the intervention of an external company.
Regarding the instrumentation, in 2014 a new differential data acquisition system was implemented, with the aim to reveal by EXAFS studies small structural changes induced by external excitations; this system was used for pump-and-probe experiments on light-responsive compounds and in case of materials sensitive to magnetic fields, changes of temperature in which structural differences between the ground-state and excited system are close to the technique limits. In order to obtain XAS spectra in differential mode between two states of the sample (excited and not-excited) specific acquisition software has been now made available on GILDA. The sequence of operations is as follows: first of all the program selects a specific energy; then data are collected without any sample excitation and stored in a file; successively the program switches on the excitation (optical excitation, electric field, ) and data are collected again and stored in a different file. The differential signal calculated subtracting the unexcited spectrum from the excited one.

## 3 Scientific activity

In 2014 , 27 scientific papers were published on International journals regarding experiments performed on the beamline in the following fields:

- Material Science
- Catalysis
- Environment
- Cultural Heritage
- Life Science and Health

## 4 List of Publications

1) Battocchio C., Fratoddi I., Fontana L., Bodo E., Porcaro F., Meneghini C., Pis I., Nappini S., Mobilio S., Russo M.V., Polzonetti G., Silver nanoparticles linked by a Pt-containing organometallic dithiol bridge: Study of local structure, Physical Chemistry - Chemical Physics 16 11719-11728 2014
2) Bonadiman C., Nazzareni S., Coltorti M., Comodi P., Giuli G., Faccini B., Crystal chemistry of amphiboles: Implications for oxygen fugacity and water activity in lithospheric, Contributions to Mineralogy and Petrology 167 984-1-984-17 2014
3) Cesca T., Maurizio C., Kalinic B., Scian C., Trave E., Battaglin G., Mazzoldi P., Mattei G., Luminescent ultra-small gold nanoparticles obtained by ion implantation in silica, Nuclear Instruments and Methods in Physics Research B 326 7-10 2014
4) Costanzo T., Benzi F., Ghigna P., Pin S., Spinolo G., d'Acapito F., Studying the surface reaction between NiO and Al2O3 via total reflection EXAFS (ReflEXAFS), Journal of Synchrotron Radiation 21 395-400 2014
5) d'Acapito F., Blanc W., Dussardier B., Different Er3+ environments in Mg-based nanoparticle-doped optical fibre preforms, Journal of Non-Crystalline Solids 401 50-53 2014
6) d'Acapito F., Mazziotti Tagliani S., Di Benedetto F., Gianfagna A., Local order and valence state of Fe in urban suspended particulate matter, Atmospheric Environment 99 582-586 2014
7) Di Benedetto F., Capacci F., Fornaciai G., Innocenti M., Montegrossi G., Oberhauser W., Pardi L.A., Romanelli M., Variability of the health effects of crystalline silica: Fe speciation in industrial quartz reagents, Physics and Chemistry of Minerals 41 215-225 2014
8) Fortes L.M., Gonalves M.C., Pereira J.C., d'Acapito F., EXAFS study of Er,Yb doped hollow and dense SiO2 microspheres, Journal of Non-Crystalline Solids 402 244-251 2014
9) Fumagalli P., Poli S., Fischer J., Merlini M., Gemmi M., The high-pressure stability of chlorite and other hydrates in subduction melanges, Contributions to Mineralogy and Petrology 167 979-1-979-16 2014
10) Giustetto R., Seenivasan K., Belluso E., Asbestiform sepiolite coated by aliphatic hydrocarbons from Perletoa, Aosta Valley Region, Western A Mineralogical Magazine 78 919-940 2014
11) Kang M., Bardelli F., Charlet L., Ghin A., Shchukarev A., Chen F., Morel M.C., Ma B., Liu C., Redox reaction of aqueous selenite with As-rich pyrite from Jiguanshan ore mine (China), Applied Geochemistry 47 130-140 2014
12) Krause B., Miljevic B., Aschenbrenner T., Piskorska-Hommel E., Tessarek C., Barchuk M., Buth G., Donfeu Tchana R., Figge S., Gutowski J., Hnschke D., Kalden J., Laurus T., Lazarev S., Magalhes-Paniago R., Sebald K., Wolska A., Hommel D., Influence of a low-temperature capping on the crystalline structure and morphology of InGaN quantum dots, Journal of Alloys and Compounds 585 572-579 2014
13) Laureti S., Brombacher C., Makarov D., Albrecht M., Peddis D., Varvaro G., d'Acapito F., EXAFS investigation of the role of Cu on the chemical order and lattice distortion in L10Fe-Pt-Cu, Journal of Applied Crystallography 47 1722-1728 2014
14) Massaccesi L., Meneghini C., Comaschi T., D'Amato R., Onofri A., Businelli D., Ligands involved in Pb immobilization and transport in lettuce, radish, tomato and Italian ryegrass, Journal of Plant Nutrition and Soil Science 177 766-774 2014
15) Maurizio C., Cesca T., Trapananti A., Kalinic B., Scian C., Mazzoldi P., Battaglin G., Mattei G., Effect of ultrasmall Au-Ag aggregates formed by ion implantation in Er-implanted silica on the 1.54 $\mu$m range, Nuclear Instruments and Methods in Physics Research B 326 11-14 2014
16) Medas D., De Giudici G., Podda F., Meneghini C., Lattanzi P., Apparent energy of hydrated biomineral surface and apparent solubility constant: An X-ray absorption study, Geochimica et Co-smochimica Acta 140 349-364 2014
17) Medas D., Lattanzi P., Podda F., Meneghini C., Trapananti A., Sprocati A., Casu M. A., Mu-

su E., Giudici G., The amorphous Zn biomineralization at Naracauli stream, Sardinia: Electron microscopy and X-ray absorption, Environmental Science and Pollution Research 21 6775-6782 2014
18) Minguzzi A., Lugaresi O., Achilli E., Locatelli C., Ghigna P., Rondinini S., Observing the oxidation state turnover in heterogeneous iridium-based water oxidation catalysts, Chemical Science 5 3591-3597 2014
19) Mohiddon M.A., Naidu K.L., Krishna M.G., Dalba G., Ahmed S.I., Rocca F., Chromium oxide as a metal diffusion barrier layer: An x-ray absorption fine structure spectroscopy, Journal of Applied Physics 115 044315 2014
20) Niu G., Schubert M.A., d'Acapito F., Zoellner M.H., Schroeder T., Boscherini F., On the local electronic and atomic structure of Ce1-xPrxO2-d epitaxial films on Si, Journal of Applied Physics 116 123515 2014
21) Pirola C., Scavini M., Galli F., Vitali S., Comazzi A., Manenti F., Ghigna P., Fischer-Tropsch synthesis: EXAFS study of Ru and Pt bimetallic Co based catalysts, Fuel 132 62-70 2014
22) Portale G., Sciortino L., Albonetti C., Giannici F., Martorana A., Bras W., Biscarini F., Longo A., Influence of metal-support interaction on the surface structure of gold nanoclusters deposited on naphtalene, Physical Chemistry - Chemical Physics 16 6649-6656 2014.
23) Ramamoorthy R.K., Bhatnagar A.K., Invariant bandwidth of erbium in ZnO-PbO-tellurite glasses: Local probe/model, AIP Conference Proceedings 1591 822-824 2014
24) Ramamoorthy R.K., Bhatnagar A.K., Rocca F., Dalba G., Mattarelli M., Montagna M., Er3+ local structure and its optical properties in ZnO-PbO tellurite glasses, Journal of Non-Crystalline Solids 383 153-156 2014
25) Rossi F., Ristori S., Marchettini N., Pantani O.L., Functionalized clay micro-particles as catalysts for chemical oscillators, Journal of Physical Chemistry C 118 24389-24396 2014
26) Taglieri G., Mondelli C., Daniele V., Pusceddu E., Scoccia G., Synthesis, textural and structural properties of calcium hydroxide nano-particles in hydro-alcoholic, Advances in Materials Physics and Chemistry 04 50-59 2014
27) d'Acapito F.; Trapananti A.; Torrengo S.; Mobilio S.; X-ray absorption spectroscoy: the italian beamline GILDA at ESRF, Notiziario Neutroni e Luce Sincrotrone 2014, 19, 14-23.

# GRAPHENE: Graphene-Based Revolutions in ICT And Beyond

S. Bellucci (in charge of scientific and technical/technological aspects), R. Baldini (Tecn.), S.Bistarelli (Dott.), M. Mastrucci (Laur.), A. Cataldo (Dott.), G. Giannini (Osp.), F. Micciulla (Ass. Ric.)

We participate to the project Graphene-Based Revolutions in ICT And Beyond, GRAPHENE, Grant agreement number 604391CP-CSA, one of the most important initiatives in the European research. Among participants there are 23 Italian partners including research institutes, universities and enterprises, with 16 new partners including Istituto Nazionale di Fisica Nucleare represented by the NEXT group at LNF, led by Stefano Bellucci. Owing to the new partnerships the consortium binds together more than 140 organizations from 23 Countries, with the common aim of transfering graphene and related composite materials from academic laboratories to everyday applications.

The Graphene Flagship Project rapresents a European investment of 1 billion euro for the next decade and is part of the Flaghship Initiatives for future emerging technologies (TEF) announced by the European Commission in January 2013. Italy is already a leader in the development of important areas of the Graphene Flagship Project, including research in composite materials and energy applications, and it is involved in technology transfer and dissemination, as well. The participation of INFN is focused on the realization of multi-layered sandwich graphene devices, within the workpackage of high frequency applications.

## Project objectives:

The main objective of the project is to investigate, both theoretically and experimentally, the shielding properties of artificial graphene-based 3D materials in the form of sandwiches alternating polymer films and graphene layers. The polymer thickness could vary between 100 nm to a few microns and the graphene can be composed of one to a few atomic planes. The sandwich can be both on substrate and free standing (and therefore flexible).
The electromagnetic properties of these sandwiches will be studied, not only in the radio-frequency (RF) domain, but also in the optical domain. For RF electromagnetic waves, the sandwich should roughly be equivalent to an effective polymer – graphite-like bilayer, where each layer has a thickness equal to the sum of the thicknesses that the same materials have in the sandwich. However, the electronic properties of the graphite-like effective medium will differ from that of bulk graphite. In the ultimate case where, in the sandwich, one-atom thick graphene is intercalated between polymer films, there will be no van der Waals coupling between the band structures of the individual graphene planes, due to their large separation distance, and the graphite-like effective medium will behave like 2D graphene, with however a thickness in the nanometer range. The same holds true if two or three graphene atomic planes are intercalated between the polymers films, except that the graphite-like effective medium will have the properties of a two- or three-plane graphite.
The possibility to tune graphene layers absorption-transmission characteristics by applying of electric fields, mechanical tension and acoustic waves for realization of switching shielding will be studied theoretically.
The temperature dependence of all EM material parameters (dielectric permittivity, AC conductivity at high frequencies – from MW to THz) for all produced GLM (graphene like materials) and graphene-based composites will be studied theoretically and experimentally.
Using self-consisted field equations describing the interaction of EM field with graphene electron system we will estimate an optimal number of graphene layers at which EM absorption will be

maximal for every MW and THz frequency range. The EM behavior of composites filled with GNP and other GLM will be modeled in microwave and THz ranges using "multi-physics" approach (together with LNF INFN), and nanoelectromagnetics combining classical electromagnetics and quantum properties of graphene nanomaterials.
Fundamental properties of graphene will be also studied as an added value: using THz/MW data on transmission/reflection through the graphene monolayers we can find such a fundamental characteristic of graphene as free path of $\pi$ electrons.

## Objectives of the workpackage High-Frequency Electronics

This workpackage is devoted towards the long term perspective of establishing graphene based high-frequency electronics technologies, which are capable of significantly outperforming state-of-the-art technologies. Therefore the key objectives of this WP are:

- Optimize process technologies critical towards meeting the requirements of specific applications, including work on contact resistance, gate stack, passivation, band gap engineering and integration of different 2D materials.
- Identify further key technological bottlenecks for realizing graphene based high frequency integrated circuits and develop solutions for solving them.
- Develop novel concepts for realizing graphene-based high-frequency devices including ballistic devices.
- Design and realization of graphene-based integrated circuits capable of fully utilizing the unique electronic properties of graphene.
- Develop new concepts for next generation radio-frequency micro-electro-mechanical systems (RF-MEMS) powered by graphene including novel bulk- and surface acoustic wave devices for wireless communications.
- Exploit the remarkable conducting properties of graphene to taylor efficient shielding coating layers that are compatible with the future HF electronics and may protect nanodevices against electromagnetic perturbations.
- Assess the developed technologies towards the current state-of-the-art and define target parameters

## Technical progress in 2014

Graphene-based heterostructures were produced having tunable shielding properties against microwave radiations, for the realization of RF-shielding layers. Power attenuation of 10 dB at 30 GHz for ultra-thin (1 μm) heterostructures was obtained, as targeted. Experiments include sample preparation, mechanical characterization, electromagnetic reflection-transmission measurements. Theoretical efforts was put on the electrodynamics of layered graphene/polymer composites that incorporates the quantum response of the graphene sheets to mechanical strain, on electromagnetic and mechanical modeling of the device characteristics able to identify the most relevant parameters. Along with microwave measurements, THz to IR (1-10 THz) transmission-reflection experiments have been conducted to retrieve the Drude parameters of the dielectric function of graphene versus temperature.

## List of Conference Talks by LNF Authors in the Year 2014

S. Bellucci, Research highlights in Nano Science and Technology at Frascati Laboratories, FM&NT-2014 | Functional Materials and Nanotechnologies, Riga (Latvia), 29 September-2 October 2014

S. Bellucci, Graphene as a Tunable Resistor, Semiconductor Conference (CAS), 2014 International, Sinaia (Romania) 13 - 15 October 2014.

S. Bellucci, Research highlights in Nano Science and Technology at Frascati Laboratories, National Institute of Material Physics, Magurele, Bucharest, Romania, 16 October 2014.

S. Bellucci, Research highlights in Nano Science and Technology at Frascati Laboratories, 2nd International Symposium on Optics and its Applications (OPTICS-2014), 1 - 5 September 2014, Yerevan - Ashtarak, ARMENIA

**NTA - IMCA (Innovative Materials and Coatings for Accelerator).**

A.Balerna, M. Biagini, R.Cimino (Resp.), L.Gonzales (Ass), S. Guiducci,
R. Larciprete (Ass.), M. Zobov (LNF-INFN).

The IMCA experiment was started in 2010 in order to develop new materials and coatings with stable and low enough SEY (Secondary Electron Yield) to guarantee full operation of present and future accelerator machines. This issue, in fact, is crucial in controlling Electron Cloud formation and in reducing its effects, that are well known to be a potential bottle-neck to the performances obtainable from particles accelerators. Frascati has a long-standing experience in qualifying materials in terms of surface parameters of interest to e-cloud issues. We are routinely measuring SEY, its dependence from electron energy, temperature and scrubbing dose. We are now able to characterize "in situ" the surface chemical composition and eventual modifications occurring during electron or photon irradiation by using XPS with a conventional X-ray source. Our experimental measurements of the relevant parameters can be also confidently compared to simulations, performed by running EC codes, in order to elucidate the final consequences on machine performances. Such a combined characterization effort is also suggesting ways to produce low SEY materials coatings. This issue is particularly important in view of the foreseen LHC luminosity upgrades, the ongoing research on Future Circolar Collider (FCC) and ILC- Damping ring studies, where e-cloud issues are expected to be present.

We have two running setups: both are now routinely working, operating in UHV conditions being steadily in a vacuum better than $1 \times 10^{-10}$ Torr after bake-out. The two set-ups are based on a UHV $\mu$-metal chamber, with less than 5 mG residual magnetic field at the sample position. Both are equipped with an Omicron LEED; an electron gun to measure SEY; a Faraday cup to characterize beam currents and beam profiles and both can produce samples with different growing technique inserting them in the measuring system without breaking the vacuum. One system, built in collaboration with CNR, is designed to deposit thin films and analyze their SEY in connection with XPS at room or higher temperature. This is done by using an Omicron electron analyzer and an X-Ray and a UV Lamps to acquire photoemission spectra and to obtain chemical information on the studied surface. The other system is optimized to perform SEY experiment at cryogenic temperature (down to 8 K) and in connection to angle resolved VUV photoemission studies. For this reason has been equipped over the years with an OMICRON AR65 angle resolving analyzer and a monochromatic VUV source.

In 2014 we have addressed a series of issues studying different materials and material properties. Such activity not only is promoting our Material Science Laboratory in Frascati as one of the most advanced Laboratories in this field, but also provided a quite comprehensive understanding on the physical phenomena governing the SEY and its variations during the various surface modifications. This understanding has found its natural context in a published detailed review paper on "electron cloud in accelerators" [1]. In more details, in collaboration with the group of Salerno, (formed by S. Petracca, V. Pierro, A. Stabile and F. Velotti), we performed an experimental study on open-cell metal foams. Such materials have been analytically studied and proposed [2] as high synchrotron radiation particle accelerator beam liners for their estimated low gas desorption, their mechanical-structural properties, their expected capability to resist to eddy-current induced stresses,in case of superconducting magnets' failure, their low impedance and possibly low SEY. Experimental validation of all such very promising properties is under way and preliminary SEY experiments have been presented at IPAC14 and published [3].

A second long lasting activity which has been only recently finalized regards the detailed study on the Low Energy (LE) part of a SEY curve. In response to some debate in recent literature on

the capability to correctly measure such (LE)-SEY as first reported in [4], we solved this apparent controversy showing and confirming that the LNF SEY set-ups can correctly measure SEY down to very low energy above the sample work function $W_s$. This work, of interest to a larger community of scientists interested in such material properties, like the spacecraft community, was presented in a invited seminar at PPPL in Princeton, and, as invited contribution, in SCTC2014. The work has been published as conference proceedings and will appear in IEEE Transactions on Plasma Science on Spacecraft Charging Technology [5]. The notion that our set-ups are unique and capable to measure LE-SEY, has been also used to understand the importance of using realistic and experimentally derived LE-SEY value and not the "usual" parametrization in $e^-$cloud simulations. This work, done in collaboration with CERN, has been presented and published, in short form, as proceedings of IPAC2014 [6] and its complete description is object of a contribution recently submitted to Physical Review ST-AB [7]. In Fig. 1 we report SEY and LE-SEY curves as measured on two as-received Oxygen-Free High thermal Conductivity (OFHC) Cu samples of different origin before and after cleaning them by ion sputtering. Here it is only worth noticing that by "as received" we can not identify a specific surface composition and this obviously reflects in some differences in the detailed structure and shape of SEY. The noticed differences between clean metal and "as received" surfaces are significant and reproducible. While the LE-SEY of the clean Cu goes and stays close to zero showing no electron reflectivity up to $\sim 1$ eV from $W_{Cu}$, our data on "as received" Cu surfaces confirm the ability of contaminated surfaces to reflect electrons at very low landing energies and that their $\delta$ stay above 0.5 - 0.7 eV for the entire LE-SEY energy region. Those data shows that our technique is clearly able to measure SEY at $E_p$ just above the different $W_s$, with the exception of a "blind region" smaller than 1 eV and that is discussed in [5, 6, 7] . Those experiments clarifies the apparent discrepancy of literature data which can be simply ascribed to the different samples cleanliness, and actual composition and metallicity of the outermost layers, which significantly alter the reflectivity $R_{el}$ at zero landing energies. We show here that SEY and, in particular, its LE part is very surface sensitive and it is strongly affected by the presence of a non metallic over layer onto a metal surface.

In collaboration with F. Schäfers, head of the optics group in HZB BESSY-II, Berlin, we continue approaching with the best "state of the art" tools available, the study of Reflectivity and Photoelectron Yield of technical materials [8]. This study is of extreme relevance not only since it gives important input parameters to track the seedings of electrons in $e^-$ cloud simulations, but, even more importantly in machines where single bunch instabilities are expected as induced by the mere presence of a high density of electrons in the beam pipe [1]. We show that the use of the high performance equipment developed to perform in details X-ray metrology at wavelength (i.e. by using monochromatic light) on optical elements is one of the only viable technique to experimentally measure the required technical surface properties.

Our group is also facing the importance of understanding in details the subtle physical mechanisms governing SEY and its variations (as recently done when studying the chemical origin and the energy dependence of the "scrubbing" process, at the base of the reduction and control of SEY in case of the LHC [9]) and we start a long term study on how basic surface properties may affect SEY. Different studies done are now mature for publication. We first study the relation between the atomic hybridization and the SEY in carbon materials during the thermal graphitization of thin amorphous carbon layers deposited by magnetron sputtering on Cu substrates. This work has been published [10]. We also are investigating on the effects on the SEY of Graphite induced by surface defects [11]. This research line shows how a multi-technique approach to study surface science basic properties can help in understanding the process we need to follow and it represents an extremely powerful tool to study mitigation mechanisms of relevance in applications, and will be continued in the following years. For this purose we dote the laboratory with an in air scanning

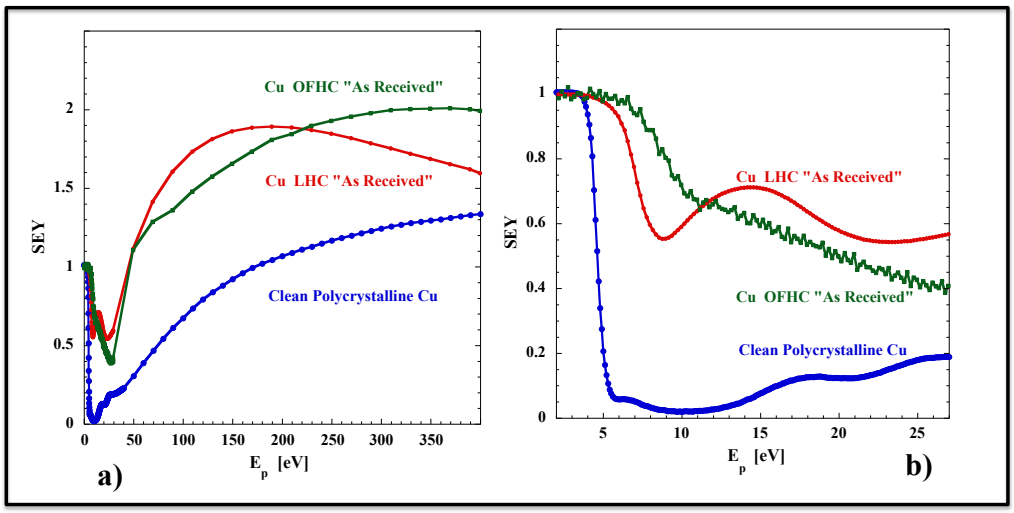


Figure 1: Experimental SEY curves of an OFHC "as received" Cu; a LHC "as received" Cu and, for comparison, of a clean polycrystalline Cu as a function of $E_p$ above $E_F$. a) In the 0-400 energy window b) zooming in the LE-SEY [6, 7].

tunneling microscope (STM), which, in 2014, has been upgraded to be used at variable temperature and in UHV, incrementing the analysis capabilities for such studies.

The collaboration has, in the last years, included researchers of other sections with recognized international experience in the study of impedance and related effects on machine performance. In fact, the challenges offered by the new high intensity machines show a clear link between e-cloud and wake-fields issues. Within our project, the group of Rome 1 ( Mauro Migliorati, Giorgia Favia, Andrea Mostacci, Luigi Palumbo, Letizia Ventura) is extremely active in calculating impedance issues of key interest in many and different machines aspects. In parallel, the group of Napoli (formed by R. Fedele, F. Galluccio, M.R. Masullo and V. Vaccaro), is developing, within the collaboration, a new laboratory method to measure the coupling impedance of high-Q insertion devices below the beam pipe cut-off frequency, when the classical wire method is not reliable. This method should allow a quick and very accurate evaluation of the impedance budget of various insertion structures. The method has been tested on a pill-box cavity and the first results are in good agreement with simulation methods and classical theory and the collaboration is now performing more realistic tests on UA9 and LHC collimator prototypes.

### Conference Talks

- R. Cimino: "Electron cloud mitigation via new materials and material coating", CLIC workshop 2014, CERN, 6-2-2014.
- R. Cimino: "Detailed Investigation of the Low Energy Secondary Electron Yield (LE-SEY) of clean polycrystalline Cu and of its technical counterpart", SCST2014, 23-27/6/2014 Pasadena (USA) .
- R. Cimino: "Material Science for next generation Accelerator systems", PPPL, Princeton (USA) 3-7-2014.

- R. Cimino: "Low Energy-SEY: a Mature technique", e-cloud meeting CERN, 23-7-2014.
- R. Cimino: "Unconventional Vacuum Metrology Issues for Next Generation Accelerator Systems", 20th IMEKO TC4 International Symposium Benevento (Italy), 15-9-2014.
- L. Gonzalez: "On the capability of measuring the very Low Energy Range of Secondary Electron Yield", MULCOPIM14: 2014 September 17 - 19, Valencia (Spain).
- R. Cimino: "Material Science for next-generation accelerator Vacuum systems", 100 Congresso Nazionale della Societa' Italiana di Fisica, Pisa, 22-26 Settembre 2014.
- Rosanna Larciprete: "Physisorption and chemisorption on carbon surfaces", VCS- CERN Invited Seminar, 24-10-2014.

**References**


1. Roberto Cimino and Theo Demma: "Electron Cloud in Accelerators" International Journal of Modern Physics A,Vol. 29, (2014), 1430023 (65 pages) .
2. S. Petracca, and A. Stabile; "Open cell conducting foams for high synchrotron radiation accelerators", Phys. Rev. ST Accel. Beams, 17 (2014) 083503.
3. R. Cimino et al., "Search for New e-cloud Mitigator Materials for High Intensity Particle Accelerators " Proceedings of IPAC14 Dresden (2014).
4. R. Cimino et al., "Can Low-Energy Electrons Affect High-Energy Physics Accelerators?" Phys. Rev. Lett. 93, 14801 (2004).
5. R. Cimino et al. : "Detailed Investigation of the Low Energy Secondary Electron Yield (LESEY) of clean polycrystalline Cu and of its technical counterpart. " SCTC2014 conference proceeding (2014) and accepted for publication on: IEEE Transactions on Plasma Science on Spacecraft Charging Technology, in print (2015)
6. R. Cimino et al., "Detailed Investigation of the Low Energy Secondary Electron Yield of Technical Cu and its Relevance for LHC" Proceedings of IPAC14 Dresden (2014).
7. R. Cimino et al., "Detailed Investigation of the Low Energy Secondary Electron Yield of Technical Cu and its Relevance for LHC" submitted to Phys. Rev. ST Accel. Beams (2015).
8. R. Cimino and F. Schäfers , "Soft X Ray Reflectivity and Photoelectron Yield of technical materials: Experimental input for Instability Simulations in High Intensity Accelerators." Proceedings of IPAC14 Dresden (2014).
9. R. Cimino et al., "Nature of the Decrease of the Secondary-Electron Yield by Electron Bombardment and its Energy Dependence" Phys. Rev. Lett. 109 (2012) 064801.
10. Rosanna Larciprete, Davide Remo Grosso, Antonio Di Trolio and Roberto Cimino: "Evolution of the secondary electron emission during the graphitization of thin C films", Applied Surface Science, Volume 328 (2015) 356 360.
11. Rosanna Larciprete, L. A. Gonzalez, A. Di Gaspare, and Roberto Cimino: "Experimental study of the effects on the Secondary Electron Yield of Graphite induced by surface defects" in preparation (2015).

# MAE-INDIA 2014

A. Marcelli (Coordinatore Italiano), D. Di Gioacchino (Ricerc.),
G. Della Ventura (Assoc.), F. Gozzi (Assoc.), F. Palumbo (Assoc.),
D. Hampai (Ricerc.), K. Hatayama (Ricerc.), K. Hatada (Assoc.), N.L. Saini (Assoc.)

This bilateral project is focused on the synthesis and characterization of magnetic nanoparticles. It has been funded in the framework of the executive programme for scientific and technological cooperation between the Italian republic and the republic of India for the years 2012 – 2014 and then extended for one year until the end of 2015. The agreement recognizes the growing importance of science and technology with the respect to the economical, social and cultural relations of the two countries and the need to develop and to promote bilateral cooperations in the field of science and technology. In particular, this project belongs to a limited number of projects of "particular relevance" funded by the Italian Minister of Foreign Affairs and by the government of India.
The properties of nanosystems are intermediate between the bulk counterpart and isolated atoms but sometime they exhibit enhanced properties that can be optimized if local structural, electronic and magnetic properties are well characterized. Magnetic nanosystems are particularly interesting because of their high saturation magnetization, low coercivity, high permeability and high Curie temperature and already now used in many applications. In particular, magnetic nanoparticles have applications ranging from biomedicine, e.g., drug delivery, tumor treatment; to high density magnetic recording media, solar energy transformers, ferrofluids, etc..

On September 12, 2014, we organized the third Italy-India bilateral project meeting while during the entire year activities proceed with both experimental and theoretical exchanges. The experimental and theoretical activities can be summarized as:

1. Synthesis of nanoparticles. The research group of the Indian Institute for Plasma Research has made available additional sets of both iron and cobalt nanoparticles, even in large amount (~1 kg) to start a new series of experimental tests for applications of industrial interest;
2. Characterization of nanoparticles. In collaboration, the two teams performed experiments of x-ray absorption spectroscopy and x-ray diffraction at the synchrotron radiation facility of ESRF in Grenoble in October (1-6/10/2014) and at the Elettra facility in Trieste in March and September (20-23/3/2014 & 24-27/9/2014). Also experiments of *ac susceptibility* were carried out as a function of temperature at Frascati while a Mössbauer characterization has been performed in collaboration with researchers at the Krakow University;
3. Combined spectroscopical methods with multi-harmonic magnetic susceptibility data to exploit a new route to characterize nanosystems. Indeed, the study of the non-linear electron dynamic transport processes and the spectroscopic analysis represents a new strategic approach fundamental to get information for many possible applications;
4. Development of new theoretical models to treat collective excitations in magnetic materials.

In 2014 we started also to consider the possibility to enhance properties of the concrete, a material of fundamental importance for the contemporary building systems.
The Indian researchers made available ~ 1 kg of nanoparticles an amount sufficient to perform the test planned and also those foreseen in the next months. Other researches of industrial interests have been considered, in particular, for technological applications associated to the future accelerators. Tests started at the end of the year but results are still too preliminary to confirm the feasibility of these activities.
During the year we also started collaborating to the proposal of the researchers of the Facilitation Centre for Industrial Plasma Technologies for the design and the construction of a x-ray beamline at the Indian synchrotron radiation facility INDUS-2 at Indore, an apparatus that will particularly devoted to x-ray spectroscopic and diffraction experiments on nanoparticles and materials to be uses in plasma physics applications.

This project has been made possible with the support of the *Ministero degli Affari Esteri e della Cooperazione Internazionale, Direzione Generale per la Promozione del Sistema Paese*. More information on this bilateral project are available at the URL: http://www.lnf.infn.it/divric/Italy-India/.

References

1) K. Hatada, K. Hayakawa, A. Marcelli and F. Palumbo, *A Two Rotor Model with spin for magnetic nanoparticles,* Phys. Chem. Chem. Phys. 16 (2014) 24055-24062;

2) C. Balasubramanian, B. Joseph, P. Gupta, N.L. Saini, S. Mukherjee, D. Di Gioacchino and A. Marcelli, *X-ray absorption spectroscopy characterization of iron-oxide nanoparticles synthesized by high temperature plasma processing*, J. Elect. Spectr. Rel. Phenom. 196 (2014) 125-129;

3) C. Balasubramanian, B. Joseph, P. Gupta, N.L. Saini, S. Mukherjee, K. Dziedzic-Kocurek, D. Di Gioacchino and A. Marcelli, *Magnetic phases in iron-oxide defective nanoparticles synthesized by high temperature plasma processing*, subm. for publ. (2014)

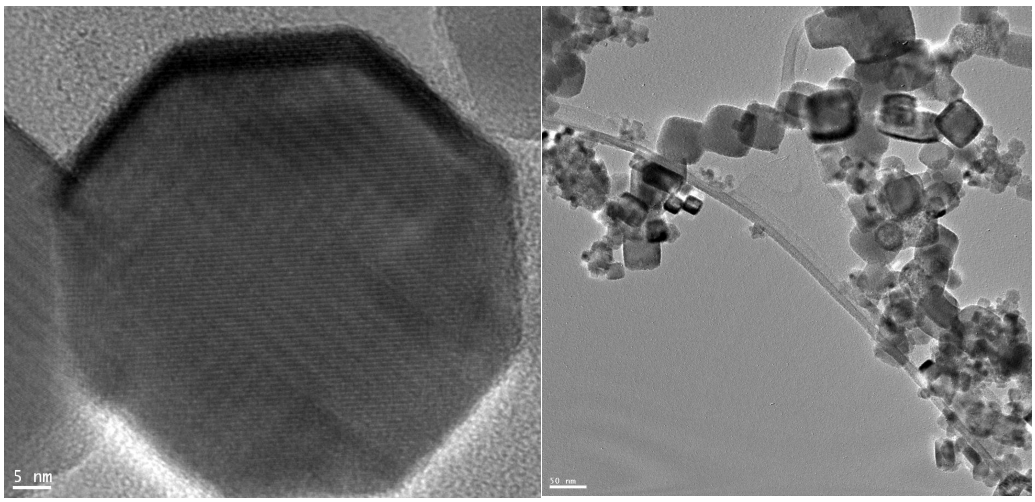


Fig.1 TEM images of nanoparticle samples synthesized by the Indian team for the collaboration; (*left*) a magnified view of an iron nanostructure with a clear octagonal shape; (*right*) a different, larger image, where several cobalt nanostructures of cubic shape ranging from 20 to 50 nm synthesized with a 50 A plasma current can be clearly recognized.

## NAmiceMC: Nano-thin and micro-sized carbons: Toward electromagnetic compatibility application

S. Bellucci (Resp. INFN), R. Baldini (Tecn.), S.Bistarelli (Dott.), M. Mastrucci (Laur.), A. Cataldo (Dott.), G. Giannini (Osp.), F. Micciulla (Osp.)

External collaborating Institutions:
- University of Lorraine, France,
- Laboratory of Electrodynamics of Inhomogeneous Media at the Institute of Nuclear Problems of Belarusian State University,

We participate as a partner (the INFN unit) to the PEOPLE MARIE CURIE ACTIONS International Research Staff Exchange Scheme Call: FP7-PEOPLE-2013-IRSES. FAEMCAR has a duration of 48 months and started its activities in the fall 2013, PIRSES-GA-2013-610875. The consortium binds together two Universities and one Research Organization.

## Project objectives:

The main aim of the project is to provide comparative study of EM shielding effectiveness of carbon foams, carbon ultra-thin films and epoxy/carbon composites with low filler concentration in microwave frequency range and to support the experimental data with an adequate theoretical model of materials' electromagnetics. On the basis of our theoretical simulations and experimental database collected within the project implementation, we intend to contribute to solving one of the most challenging problem in material science: developing EM coating through design-oriented-approach. In the GHz range, due to increasing utilization in EM materials of novel nanostructures, the classical electromagnetic compatibility (EMC) faces new problems, while traditional electromagnetic methods gain new life in their application to new objects. The first aim of the project is to reach a high enough mitigation of the microwave radiation with as small as possible concentration of carbon additives in order not to destroy well-known properties, mechanical and thermal, of polymer used for composites fabrication. Our philosophy is to provide, through a joint synergetic work of participants experienced in condensed-matter physics, chemistry, micro- and nano-carbon synthesis, electromagnetic theory / modeling and functional characterization, not only a detailed experimental analysis for many different densities, and different thicknesses of the samples, but also to provide a consistent theory which will model electromagnetics of these highly non-regular structures, where the typical sizes could be compatible with the wavelength in the material.

## Publications by LNF Authors in the Year 2014

Dielectric properties of graphite-based epoxy composites, I Kranauskaite, J Macutkevic, P Kuzhir, N Volynets, A Paddubskaya, D Bychanok, S Maksimenko, J Banys, R Juskenas, S Bistarelli, A Cataldo, F Micciulla, S Bellucci, V Fierro, A Celzard, physica status solidi (a) 211 (7), 1623-1633, 2014.

Microwave response properties of epoxy resin composites filled with graphitic fillers
S Bellucci, S Bistarelli, A Cataldo, F Micciulla, J Macutkevic, I Kranauskaite, J Banys, P Kuzhir, N Volynets, A Paddubskaya, D Bychanok, S Maksimenko, V Fierro, A Celzard, Numerical Electromagnetic Modeling and Optimization for RF, Microwave, and Terahertz Applications (NEMO),

2014 International Conference on, Pages 1-4, IEEE Editor, 2014

## List of Conference Talks by LNF Authors in the Year 2014

S. Bellucci, Microwave response properties of epoxy resin composites filled with graphitic fillers, Numerical Electromagnetic Modeling and Optimization for RF, Microwave, and Terahertz Applications (NEMO), 2014 International Conference on, Pavia (Italy), 14 – 16 May 2014.

S. Bellucci, Research highlights in Nano Science and Technology at Frascati Laboratories, FM&NT-2014 | Functional Materials and Nanotechnologies, Riga (Latvia), 29 September-2 October 2014

# NATO: Development of Biosensors using Carbon Nanotubes

S. Bellucci (Project Director), R. Baldini (Tecn.), S.Bistarelli (Dott.), M. Mastrucci (Bors. Tecn.), A. Cataldo (Dott..), G. Giannini (Osp.), F. Micciulla (Ass. Ric.)
External collaborating Institutions:
- Yerevan State Univ., Armenia

We direct the project Development of Biosensors using Carbon Nanotubes within the NATO Emerging Security Challenges Division, Science for Peace and Security Programme. The project has a duration of 36 months and started its activities on 1sr October 2013. The consortium binds together a University and a Research Organization.

## Project objectives:

The main direction of the antiterrorist defence is the prevention and/or the early exposure of terroristic attacks. In case of using the biological warfare such as living agents or toxins DNA – biosensors yield one of the most effective tools for early diagnostics. The main goal of the Project is creation of a reliable, sensitive, selective and noise protected prototype of a DNA biosensor. The main objectives of the project are:

i) To create a prototype of one of the technologically state-of-the-art and most effective electrochemical DNA – biosensors.

ii) To investigate and to compare thermodynamics and kinetics of DNA and RNA hybridization both in the bulk and when immobilized on the surface of a substrate, e.g. an electrode

iii) To synthesize polymer – CNT nanocomposites as suitable candidates for biosensor electrodes.

iv) To investigate sensitivity, selectivity and "noise immunity" of DNA-sensors, using a polymer – CNT substrate and agents for the registration of hybridization

v) To develop measuring methods for the registration of the changes in biosensors properties stimulated by DNA hybridization or other processes.

## Technical progress in 2014

1. experimental work about DNA,RNA-ligand interactions (Yerevan State University)

The higher affinity of the certain porphyrins to the double – stranded regions of Nucleic Acids (NA) in comparison to single – stranded is important for the hybridization thermodynamics and kinetics. According to the Project schedule thermostability of the double – stranded NAs (dsNA) in the bulk should be experimentally investigated during the 1st year of the project.

UV-VIS spectrophotometry and circular dichroism (CD) methods were applied to study the binding of meso-tetra 4N-oxyethylpyridyl (TOEPyP4) porphyrin with B-DNA and A-DNA. The binding constant Kb and stoichiometry n were determined from absorbance spectra for each DNA-porphyrin complex. The free energy, enthalpy and entropy of binding also were calculated using the

values of Kb. Obtained results show that this porphyrin interact with B-DNA by intercalation while with A-DNA via outside binding mode.

2. theoretical work, concerning ssRNA folding and hybridization (Yerevan State University)

The event of single – stranded nucleic acids hybridization is a key – point of any DNA or RNA – sensor activity. According to the Project schedule thermodynamics and kinetics of hybridization in the bulk should be investigated theoretically during the 1st year of the project. We proposed the coarse – grained model of a long single – stranded Nucleic Acid (ssNA) folding and hybridization. It is assumed that the characteristic time of the secondary structure rearrangement is much longer than that for the formation of the tertiary structure.

3. description of the polymer - CNT composites, synthesized by the NEXT group at LNF, INFN

The composite with CNT was prepared in this way: to start with, the CNTs were weighed and required wt% of the CNT is mixed in Isopropylic acid and ultrasonicated for 30 min. Then this solution is mixed with known quantity (weight) of resin and heated in an
oven for 2 hr at 80°C. The alcohol evaporates off and the resin with CNT is again sonicated for 15 min. Immediately after this the hardener is mixed and the mixture is applied on the surface of the electrical circuit and allowed to set.

The wide spectrum of polymer – CNT composites was prepared for the subsequent measurements:

- epoxy resins, containing 0.25, 0.5, 0.75 and 1.0 % of the MWCNTs 20 – 30 and 30 – 50
- epoxy resins, containing 0.25 and 0.5 % of the COOH functionalized MWCNTs
- pure epoxy resins

In order to add functional groups on the surface of CNT, we have carried out treatment of oxidation on samples of CNT (outer diameter=8-15 nm). Nitric acid solution (65% vol) and Piranha mixture (ratio sulfuric acid 96%/hydrogen peroxide 30% in volume 7:3 respectively) have been used as oxidant media. Furthermore, both media was used in two different experimental condition: reflux condition and sonication condition.
In reflux condition, we have put 0.15 g of CNT in a round bottom flask with 25mL of media (HNO3 or Piranha mixture). Mixture was heated to obtain reflux condition and maintain it for 4 h.

In sonication condition, we have put 0.15 g CNT in a becker with 25 mL of media (HNO3 or Piranha mixture) and have put in a ultrasonic bath. We have maintained dispersion in sonication for 4 h.

After oxidant treatment, we have filtered and washed with distillated water. We have dried samples in air at room temperature.

The samples were analyzed with At-IR spectroscopy. We can conclude that we add in CNT hydro and carbonyl groups. Different approaches of oxidation lead to the same result. Further experiments will be carried out to improve type and number of functionalized groups on the CNT surface and consequentially to study a reaction to link DNA at CNT.

## List of Conference Talks by LNF Authors in the Year 2014

S. Bellucci, Research highlights in Nano Science and Technology at Frascati Laboratories, FM&NT-2014 | Functional Materials and Nanotechnologies, Riga (Latvia), 29 September-2 October 2014

S. Bellucci, Research highlights in Nano Science and Technology at Frascati Laboratories, National Institute of Material Physics, Magurele, Bucharest, Romania, 16 October 2014.

S. Bellucci, Research highlights in Nano Science and Technology at Frascati Laboratories, 2nd International Symposium on Optics and its Applications (OPTICS-2014), 1 - 5 September 2014, Yerevan - Ashtarak, ARMENIA

**NEURAPID**

**NEutron RAPId Diagnostics**

**2014 Activity Report**

R. Bedogni, D. Sacco (Ass.), J.M. Gomez-Ros (Ass.), B. Buonomo, A. Esposito
INFN- LNF
In collaboration with LNF-FISMEL: A. Gentile

A. Pola (Ass.), D. Bortot (Ass.), M. Lorenzoli (Ass.), M.V. Introini (Ass.)
INFN-Milano / Politecnico di Milano

**Index**



See website **https://sites.google.com/site/csn5neurapid/** for more details

## 1. Project introduction

NEURAPID has the objective of developing instruments to measure neutron spectra in "emerging" fields, i.e. those fields where the neutron detection is made especially difficult due to the following aspects

- **Very low fluence fields**: fields with very low fluence rate such as the neutron component of the cosmic rays at ground level. Cosmic ray field at ground level is characterized by:
  - a continuous spectrum ranging from thermal up to GeV neutrons (12 orders of magnitude in energy)
  - a very low fluence rate, in the order of $10^{-2}$ $cm^{-2}$ $s^{-1}$ (integrated on the whole energy interval). This constraint opens serious problems of detector efficiency, especially when a complete spectrum measurement is expected to be performed in minutes. This is the case of the GLE (Ground Level Enhancement) detection. Real-time detection of GLE with ground-based instruments has substantial impact on aircrew radiation protection and prevention of failures in electronic equipments of aircrafts.

- **SPF (Single Pulse Fields):** fields with "extreme" pulsed structure, such a single pulses with femtosecond duration. Examples are the neutron fields produced by bombarding suitable gaseous or solid targets with ultra-intense (TW-PW) / ultrashort (fs) lasers
  SPF environments present:
  - more than 10 order of magnitudes in neutron energy.
  - An expected spectrum-integrated fluence per pulse in the order of $10^{2}$-$10^{5}$ $cm^{-2}$/shot. In this case a major measurement problem is the very shot pulse duration (fs), likely to cause serious pile-up problems in any combination of active detector + analog electronics.

**Major scientific challenges of NERAPID are:**

***Challenge 1.***

Measuring a neutron spectrum over more than ten order of magnitudes in energy (from thermal up to GeV). This problem is in common to cosmic ray and SPF environments, and a validated solution consists in the spectrometer geometries CYSP and $SP^2$ developed and tested already in the NESCOFI@BTF project (2011-2013).

***Challenge 2.***

Measure thermal neutrons with the highest possible efficiency. This is needed to
- speed up measurements in very low intensity fields

- collect the maximum possible amout of information about a "single pulse" of neutrons With respect to the one-$cm^2$ thermal neutron detectors established within NESCOFI, a major technology challenge is to increase the thermal neutron efficiency, of more than a factor of ten.

***Challenge 3.***

Developing efficient thermal neutron counting system for pulses of $10^2$-$10^5$ $cm^{-2}$/shot, which would cause serious pile-up problems in any combination of active detector + analog electronics. After thermalization in the polyethylene, an ultra-short pulse of neutrons will be spread over tens of microseconds (dye-away time). However, even if the detector pulses are shaped to fractions of microsecond, there is still a serious risk of pile-up for the stated values of fluence per pulse. Two counting alternatives are foreseen:

FAST ELECTRONICS

Acquisition with **large-area semiconductors** covered with $^6$Li compounds, connected to a fast electronics: the NEURAPID group has experience in designing multi-detector analog boards for nuclear spectroscopy, including for every detector (one channel) a bias regulator, a charge pre-amplifier chosen according to the electric characteristics of the detector, and Gaussian-shaper amplifier. Dedicated multi-detector boards will be developed using short shaping times (100 ns or lower), and the analog signal will be digitally filtered and sampled with high-speed digitizers (50 MS/s or more).

BETA RADIATORS

Using conventional electronics (shaping time in the order of 1-2 microseconds and low-speed digitizers, such as 2 MS/s) coupled with new types of thermal neutrons detectors INTRINSICALLY able to dilute in time the pulsed information. To achieve this objective, **large-area semiconductors will be covered with** beta-emitting radiators with large thermal neutron capture cross-section. The betas from the radiator, emitted with decay times in the order of seconds (ore more), will be efficiently detected from the large area detector without causing no pile-up. In and Dy radiators will be tested (See Table 1)

Table 1. Beta radiators to be coupled with LATND

| Parent | Abundance | Daughter | Capture Xs (barn) | $T_{1/2}$ | Max. beta energy (MeV) |
|---|---|---|---|---|---|
| $^{115}$In | 95.7% | $^{116}$In | 202 | 14 s | 3.3 |
| $^{164}$Dy | 28.2% | $^{165}$Dy | 2640 | 78 s | 0.9 -1.0 |

In both FAST ELECTRONICS and BETA RADIATORS approaches, large area silicon diodes will be used.

**A thermal neutron field with uniform flux profile over a large area (as large as several tens of $cm^2$) is needed for testing and calibration purposes.**

**Being the efficiency of the large area thermal neutron detector a key-issue, this should be measured**

**as accurately as possible. Therefore this thermal neutron field should have metrological quality.**
With this philosophy, the development of a large-area and highly uniform thermal neutron fields was included among project's activities: **ETHERNES (Extended THERmal Neutron Source)**

## 2. Prototypes to be developed

a. Large area thermal neutron detectors (LATND)
b. Extended Thermal neutron source (ETHERNES)
c. CYSP-C (Cosmic) (*)
d. CYSP-P (Pulse) (*)
e. SPEEDY

*(*) CYSP means a cylindrical moderating structure embedding up to ten thermal neutron detectors and showing spectrometric capability along a specific direction, identified by a collimator. A CYSP prototype equipped with one-cm$^2$ Silicon diodes covered with $^6$LiF was successfully tested during NESCOFI).*

For cosmic rays application:
**CYSP-C** will be able to accumulate sufficient information to compute a whole neutron spectrum (eV-to-GeV) in approx. one hour of acquisition at flux in the order of 0.01 cm-2 s-1.

For single-pulse neutron fields (such as lasers):
**CYSP-P** will perfom neutron spectrometry in specific direction of interest
**SPEEDY** will perform area monitor measurements with isotropic response. It will be a spherical device and will contain thermal neutron detectors symmetrically arranged along the three axes.

CYSP-C, CYSP-P and SPEEDY will take advantage of moderating geometries developed in NESCOFI. However, for the three of them new thermal neutron detectors with large area (LATND) need to be developed in the framework of NEURAPID.

## 3. 2014 Activities

The 2014 activities were focused on achieving two milestones, namely:

| | |
|---|---|
| Establishing the ETHERNES facility | 31-10-2014 |
| Calculation of the response matrix of CYSP-C and CYSP-P | 31-12-2014 |

In addition, studies on LATND were undertaken.

### *3.1 ETHERNES design*

**Notes:**

*- The executive design of ETHERNES is not published here because under evaluation for patent/s (in collaboration with Technology Transfer Office of INFN-LNF)*

*- For more details about ETHERNES, see presentations BEDO NEURAPID RB 8-7-14.pdf and BEDOGNI NEURAPID RB 4-12-14x.pdf at 8 July 2014 and 4 December 2014 NEURAPID meetings, available on project website.*

Table 2. List of existing (or recently decommissioned) source-based thermal facilities with open space field in Europe

| Facility and Institution | Moderator | Useful flux ($cm^{-2}$ $s^{-1}$) | Am-Be ( Ci ) | Field Uniformity and size (cm) | Thermal fraction | Performance ratio $cm^{-2}$ $s^{-1}$ $Ci^{-1}$ |
|---|---|---|---|---|---|---|
| SIGMA (CEA) France | 8 $m^3$ graphite | 1500 | ≈ 100 | 10% in 30x30 | 88% | 15 |
| PTB Germany | 4 $m^3$ graphite | 80 | 27 | 10% in 20x20 | 99% | 3 |
| ENEA Italy | 1 $m^3$ HDPE | 500 | 15 | 5% in 10x10 | 60% | 33 |

Thermal neutron fields in the range of $10^2$-$10^3$ of $cm^{-2}s^{-1}$ are easily achieved in small cavities (few cm) within moderating assemblies embedding radionuclide neutron sources. This is normally suited for irradiating small samples like activation foils and TLDs. Small cavities are not suited to test complex detecting systems, including multiple-sensors, large 2D screens, cables and phantoms. For these purposes, thermal fields in **open large spaces** are preferred, with the following characteristics:

- uniform field over large sizes (tens of cm in side)
- Gamma background as low as possible
- Low fast neutron contribution

Thermal fields in open large spaces have been achieved in the past by allocating large neutron sources (typ. several tens of Ci of Am-Be) in the geometrical centre of big moderating blocks (several $m^3$ of graphite or polyethylene).

The leakage field was used for testing and calibration purposes. To achieve a satisfactory level of thermalisation, the field must be highly attenuated, thus requiring very big sources (tens of Ci of Am-Be) to get thermal fluence rates in the orde of tens of hundreds of $cm^{-2}s^{-1}$.

Due to the increased difficulties in getting large neutron sources (cost 10-20 k€/Ci (!!), commercial availability, authorizations), the development of new thermal facilities should include new design concepts,

able to maximize the ratio between useful thermal flux and Am-Be activity (performance ratio).

Targets for ETHERNES designs were:

- Achieve flux in the range of $10^2$ -$10^3$ $cm^{-2}s^{-1}$ (design goal about 600)
- Availability of a single 2.6 Ci source of Am-Be
- 30 cm x30 cm homogeneity area in open-space

Available material: one cubic meter of polyethylene in sheets 1 m x 1 m x 10 cm

The idea was to produce thermal neutrons by multiple scattering rather than transmission in a moderating block, thus the polyethylene sheets were used to build a large cavity rather than a "traditional" moderating block. ETHERNES was designed after an extensive calculation campaign with MCNP. See Figgs 1 and 2.

Figure 1. Lateral view of ETHERNES.

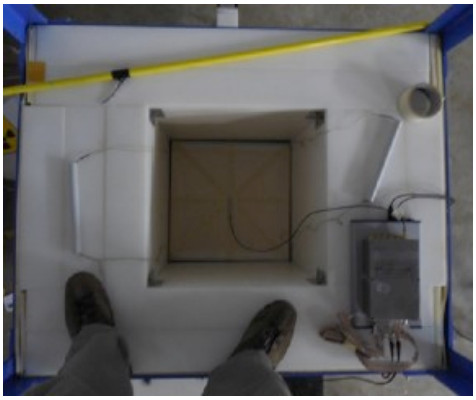

Figure 2. ETHERNES irradiation cavity (45 x 45 x h=63 $cm^3$), from top.

In Fig. 3 the neutron spectrum, at height 15 cm from the cavity bottom, is shown. The thermal fraction is in 74%.

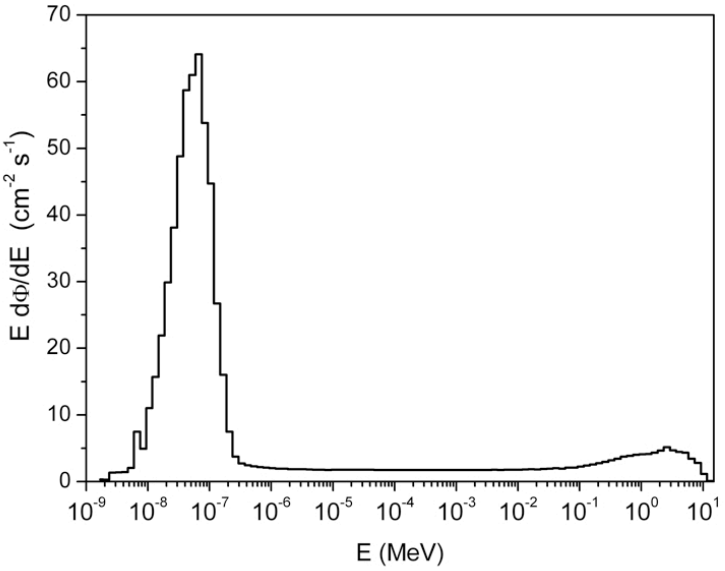


Fig. 3. Neutron spectrum in ETHERNES (MCNP simulation).

According to the simulations, the thermal flux linearly decreases with height in the irradiation cavity, with gradient -2% cm$^{-1}$.

**The field uniformity improves as the height from the cavity bottom increases, see Fig. 4. At 5 cm from cavity bottom the thermal flux variation over 30 cm x 30 cm is ±2.5%, whilst at 15 cm (reference height) is ±0.25% only.**

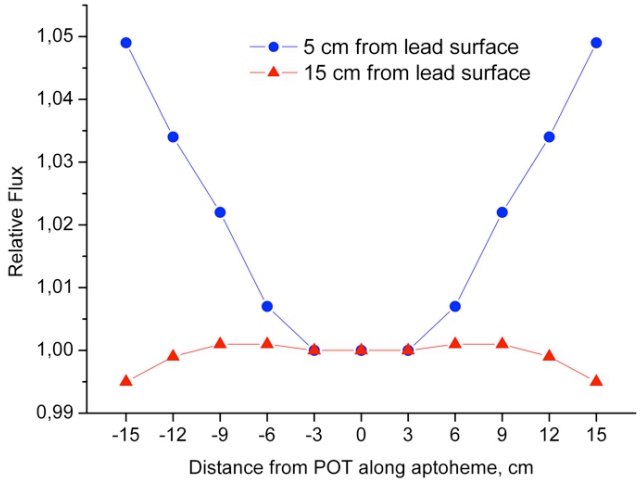


Fig. 4. Thermal field uniformity, with respect to the centre of the irradiation plane, when moving along the apotheme of the irradiation plane. POT = point of test. Results from MCNP.

The gamma component at the reference height (15 cm from cavity bottom) is lower than 3 uSv/h (MCNP simulation) and the expected spectrum is that of Fig. 5.

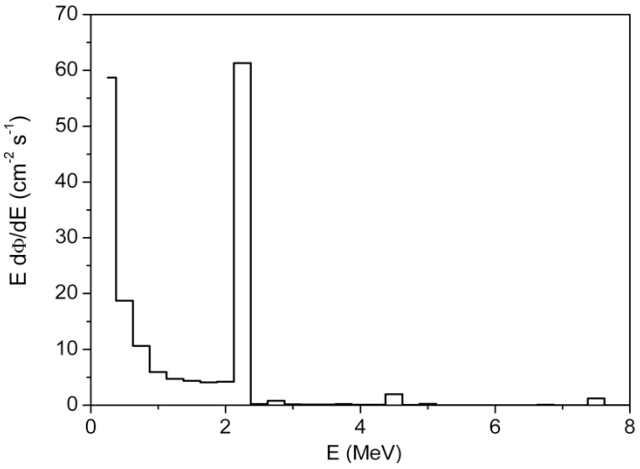


Fig. 5. Gamma spectrum at the reference height (15 cm from cavity bottom). The field is dominated by the 2.2 MeV component, coming from the thermal neutron capture in Hydrogen.

**To conclude, the following design goals were achieved:**

- **Very high performance ratio, about 230 cm$^{-2}$ s$^{-1}$ Ci$^{-1}$** (more than a factor of seven higher than "leakage"-based facilities, see Table 2).
- **Very large homogeneity area (±0.25% flux variation over 30 cm x 30 cm at ref. height)**
- **Reduced gamma background**
- **High thermal fraction (74%)**

### *3.2 ETHERNES experimental validation*

The homogeneity area at ref. height was experimentally verified using a one-cm$^2$ Si-diode covered with 30 μm of $^6$LiF, finding satisfactory agreement with the simulation, See Figg. 6 and 7.

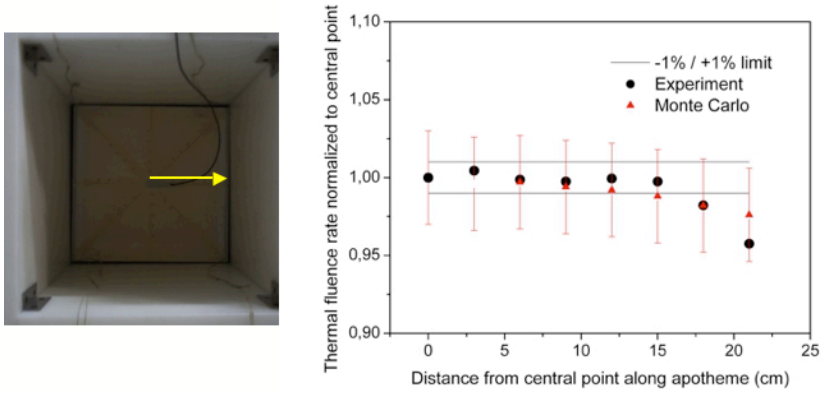


Fig. 6. Verifying the thermal field homogeneity area at ref. height, along the apothem of the irradiation

plane.

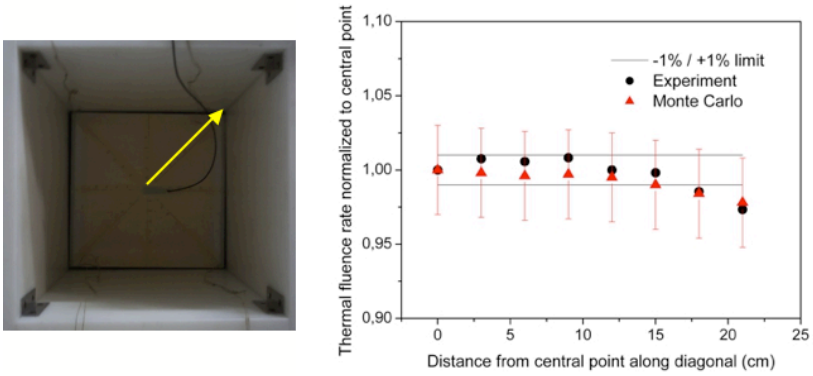


Fig. 7. Verifying the thermal field homogeneity area at ref. height, along the diagonal of the irradiation plane.

**Thermal neutron images from the ETHERNES cavity were acquired** to map the field uniformity across the whole irradiation plane at 15 cm height.

This was done using Gafchromic self-developing films (XRQA2 type) coupled with a 1 mm thick Cd radiator, according to the scheme of Fig. 8.

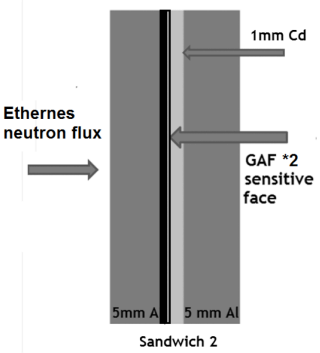


Figure 8. Measurement sandwich developed for measurements in ETHERNES. The radio-chromic film is back-irradiated by the Cd radiator.

The measurement sandwich was preliminarily tests at the ENEA-Triga (Casaccia) ex-core thermal channel, obtaining the images shown in Fig. 9 with different values of thermal fluence.

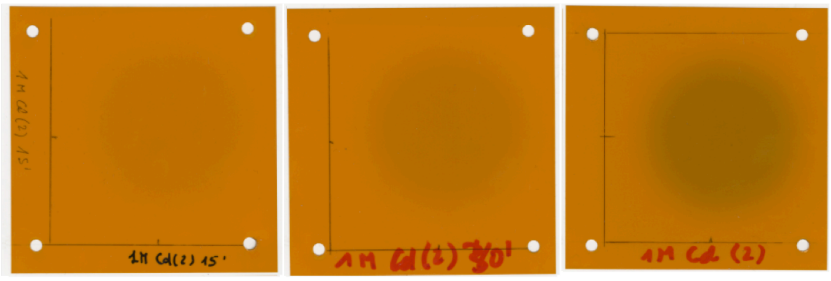

Fig. 9. Radiochromic films exposed in the ENEA TRIGA ex-core thermal channel.

The related calibration curve is shown in Figure 10.

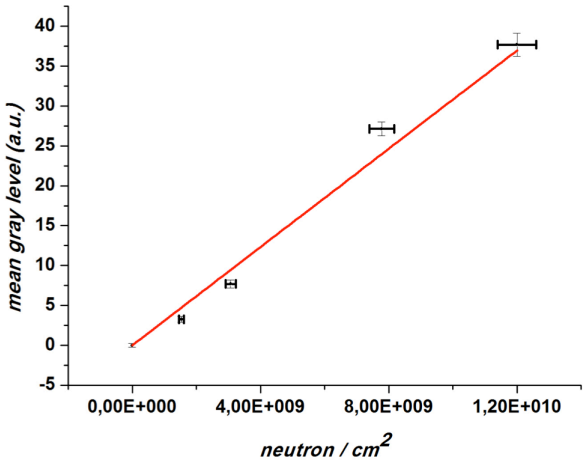


Figure 10. Thermal fluence vs. grey level calibration curve for radio-chromic films.

After a two months exposure in ETHERNES at the reference height (15 from cavity bottom), the grey profiles and false color images of Figg. 11 and 12 were obtained.

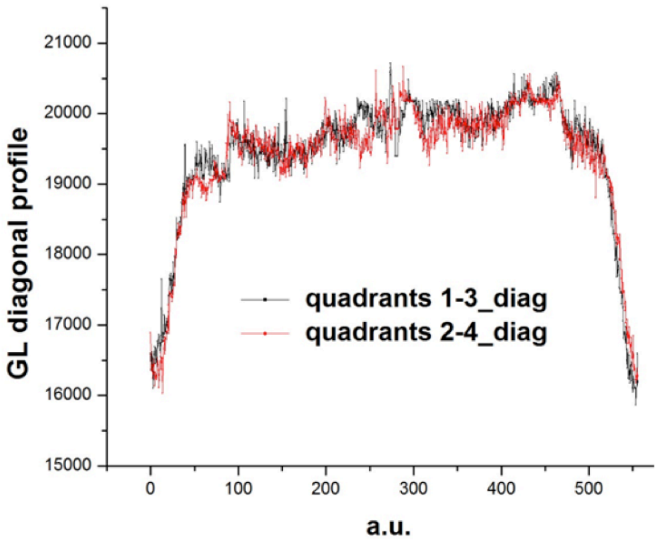


Figure 11. Grey profile of the ETHERNES irradiation plane at reference height. Variability in the plateau region is 0.3% only, fully in agreement with the 0.25% figure obtained from the simulations.

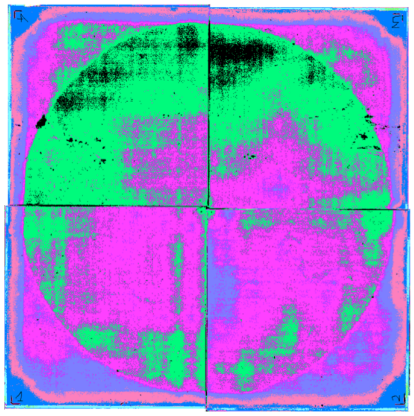

Figure 12. False color image of the ETHERNES irradiation plane at reference height.

**The thermal neutron fluence rate at the centre of the irradiation plane was measured with the gold-foils technique (with and without Cd cover), using very thin foils (0.01 mm x 15 mm diam) counted in a HPGe detector**.

According to the formalism developed in NPL Report DQL RN008 (2005), a sub-Cd flux of 589±12 $cm^{-2}$ $s^{-1}$ was achieved.

A comparison with NPL (Teddington, UK) to inter-compare this value is under conclusion.

In addition, a complete spectrum measurement was performed at the reference point using a Bonner spheres spectrometer operated by the Universitat Autonome de Barcelona. The BSS data were unfolded using the FRUIT code [1,2]. According to the adopted unfolding model, slightly different results can be obtained, but the overall agreement with simulations is always highly satisfactory, see Fig. 13.

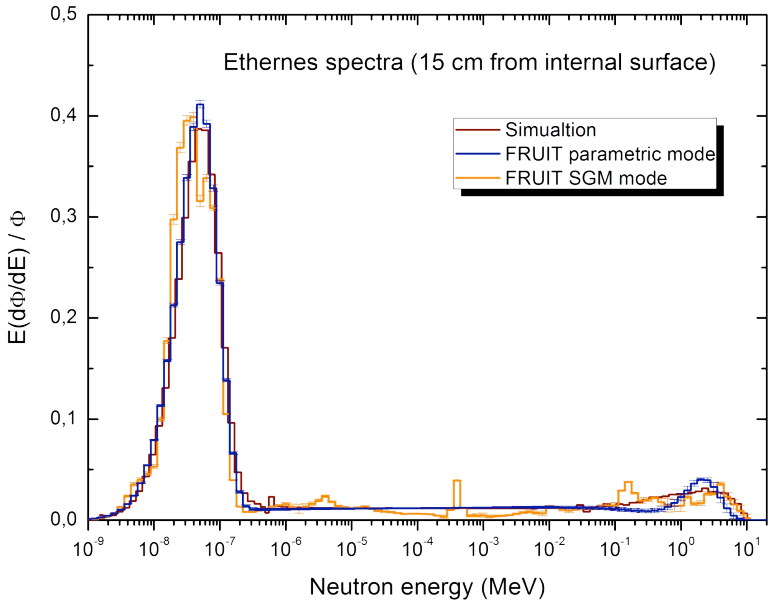


Fig. 13. Neutron spectrum at the ref. point of ETHERNES (centre of the plane located at reference height 15 cm), simulated with MCNP and measured with Bonner spheres. Data were unfolded using either a physical parameterized model (parametric) or a pure numerical convergence algorithm (SGM, special gradient method). Although slightly different results can be obtained from different unfolding approaches, the agreement with the simulated spectrum is highly satisfactory.

### *3.3 Determining the response matrix of CYSP-C and CYSP-C*

The design of the cylindrical spectrometer CYSP was adapted to allocate large area thermal neutron detectors LATNDs. On the basis of the current status of the studies to define the final structure of the LATND, we assumed a 3 cm x 3 cm silicon-based sensitive area covered with a prompt (6LiF) or delayed (beta emitting activation foils) radiator, corresponding to the largest format for commercially available windowless p-i-n diodes. The final objective is to arrange two 3x3 Silicon detectors in a sandwich structure, with the radiator in the middle. See Section 3.4 for characterization of these configurations.

To date, there are no reasons to differentiate the structure of the CYSP-C from that of CYSP-P, because in both cases one or two 3x3 Silicon detectors will be used to register the particles from a radiator. Whilst the CYSP-C will certainly adopt a prompt $^{6}$LiF radiator, the CYSP-P will possibly adopt an In or Dy delayed radiator. Because both radiators approximately show 1/E cross-section dependence, a single response matrix is enough for design evaluation purposes. When the final detector for the cosmic or pulsed version of CYSP will be reached, the response matrix will be specialized for those configurations and this will be

experimentally verified using a real prototype. At this stage the important question to solve is the amount of perturbation (self absorption) generated by large detecting structures in the detector cavities.

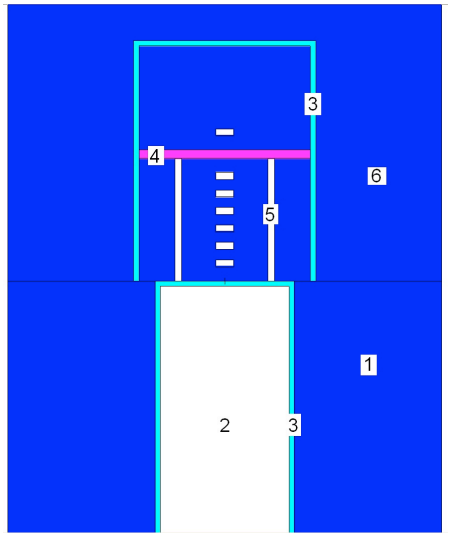


Fig. 14. CYSP general design.

CYSP is a HDPE cylinder with overall diameter 50 cm and total length 65 cm. The dimensions of the cylinder as well as the location of detectors have been chosen to maximize the "spectrometric capability" of the device, i.e. the degree of differentiation between the response functions associated to different detector positions. The collimator (label 1) is 30 cm in length and its collimating hole (label 2), 16 cm in diameter, is covered by 5 mm of borated plastic SWX-238 (label 3, www.shieldwerx.com). The seven thermal neutron detectors, located along the cylindrical axis, are contained in a HDPE capsule (20 cm in diameter, 30 cm in length). An external shield made of 5 mm of SWX-238 (label 3) plus 15 cm of HDPE (label 6) protects the sensitive capsule from lateral contributions over a broad energy range. A one cm thick, 20 cm in diameter, lead disk (label 4), has been inserted between $6^{th}$ and $7^{th}$ positions to increase the response to high-energy neutrons. The distance between two adjacent detector cavities is 2 cm (centre to centre). The seven detectors are located at depths 4, 6, 8, 10, 12, 14 and 21 cm from the end of the collimator. The latter is located under the one-cm lead filter.

Label 5 symbolizes eight cylindrical air cavities, one cm in diameter, designed to enhance neutron streaming towards the deeper detectors.

The HDPE capsule was dimensioned to allocate LATNDs made of a single or double 3 cm x 3 cm silicon diode coupled with a thermal neutron radiator.

An extensive simulation campaign was performed to derive the response matrix of the CYSP with large area detectors and to compare it with the low-sensitivity version, equipped with one-$cm^2$ diodes. See Figures 15 and 16. As expected, the 9 $cm^2$ to 1 $cm^2$ response ratio slightly depends on detector position and on neutron energy.

**In general, a roughly constant ratio of seven can be considered, in the hypothesis that only one silicon diode is used per position. If two 9 cm$^2$ diodes are coupled to the same radiator, this ratio is expected to reach fourteen.**

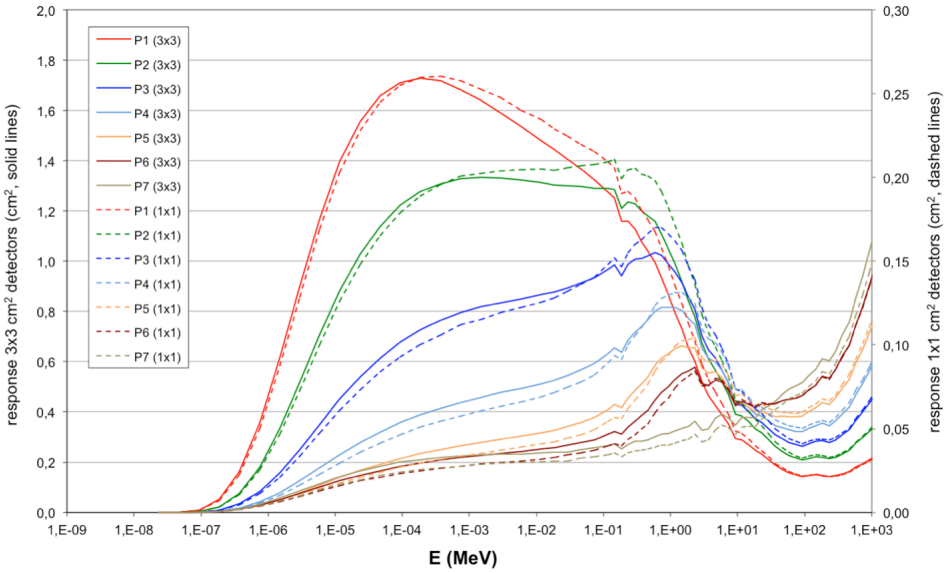


Figure 15. Response matrix of the CYSP-C / -P with 9 cm$^2$ silicon diodes compared with the one-cm$^2$ diode based response matrix of the CYSP.

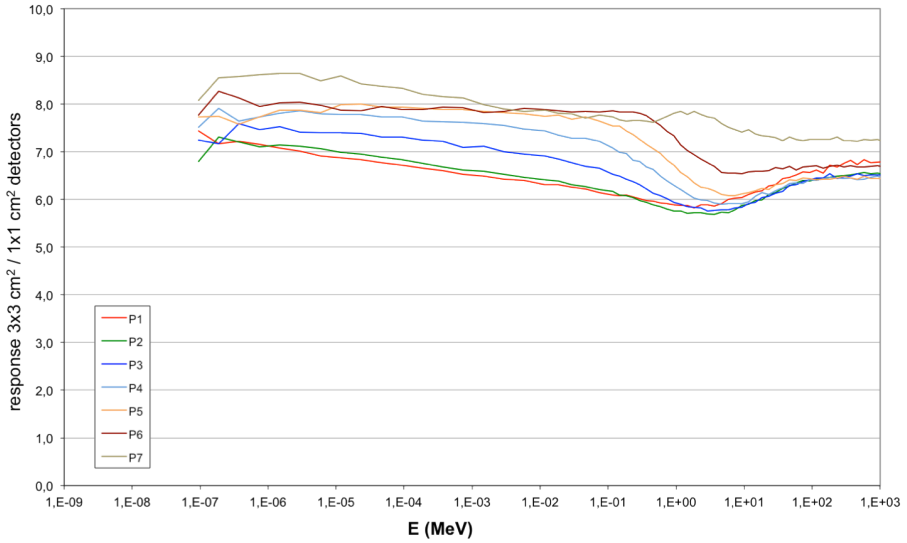


Figure 16. Ratio between the response matrix of the CYSP-C / -P with 9 cm$^2$ silicon diodes and the one-cm$^2$ diode based response matrix of the CYSP.

### *3.4 State of art of large area thermal neutron detectors, LATND*

From the initial single one-cm$^2$ diodes covered with 6LiF, as adopted in previous project NESCOFI, an evolution towards larger area diodes was undertaken as follows:

1. single 1 cm$^2$ (1 cm x 1 cm) diode covered with 6LiF
2. Single 3.24 cm$^2$ (nearly 1.8 cm x 1.8 cm) diode covered with 6LiF
3. Single 7.84 cm$^2$ (nearly 2.8 cm x 2.8 cm) diode covered with 6LiF
4. Double 7.84 cm$^2$ (nearly 2.8 cm x 2.8 cm) diode covered with 6LiF, total sensitive area 15.6 cm$^2$

The deposited layer is always around 30 microns, corresponding to the maximum detection efficiency [3,4]. As low as possible bias voltage was chosen to achieve a good photon-to-neutron discrimination capability but, at the same time, to preserve the maximum efficiency. Signal processing was performed using specially manufactured boards, including for every detector a bias regulator, a charge pre-amplifier and a Gaussian-shaper amplifier (2 μs time constant). The data were acquired on a PC through a commercial 2 MS/s digitizer.

The spectra acquired in the four cases, positioning the detector at the reference position in ETHERNES (centre of irradiation plane at reference height 15 cm from cavity bottom), are reported in Fig. 17

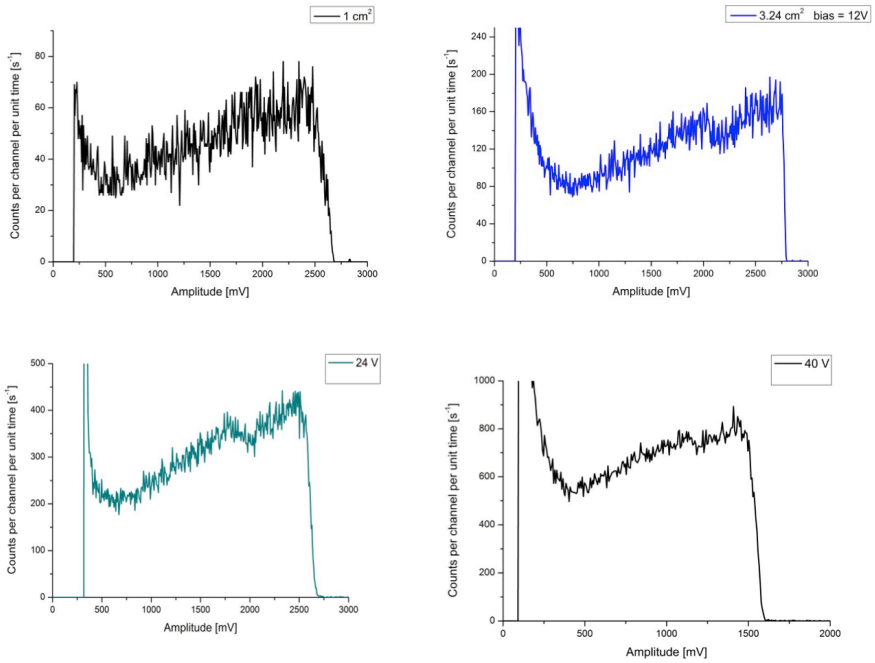


Fig. 17. Spectra acquired in the four detecting configurations, positioning the detector at the reference position in ETHERNES. From top-left: single 1 cm$^2$, single 3.24 cm$^2$, single 7.84 cm$^2$ and double 7.84 cm$^2$.

As expected, the count rate associated with the thermal neutrons (Region of Interest above 0.6 V) linearly increases with the sensitive area, see Fig. 18.

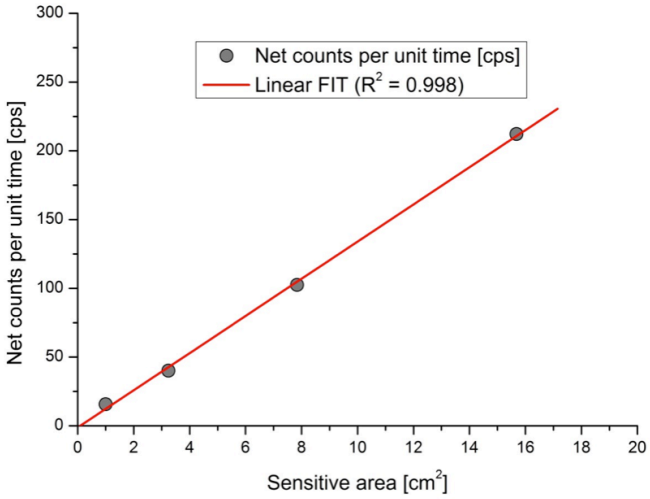


Fig. 18. Response of the four detecting configurations, covered with 6LiF, as a function of the sensitive area

### *3.5 Preparing cosmic measurements*

To start understanding the problems connected with long-term acquisitions, as will be the case of cosmic neutron measurements with CYSP-C, a test was performed with the current CYSP (equipped with 1 $cm^2$ LiF covered single diodes) exposed at the SVIRCO cosmic-ray measurement station of Roma 3 University, see Fig. 19.


Fig. 19. The CYSP exposed to the vertical component of the cosmic-ray-induced neutron field at SVIRCO, Roma 3.

The acquisition took place from December 2014 to February 2015, data under elaboration.
The following interventions were developed to ensure reliable long-terms acquisitions:

- very stable DC supply for electronics,
- additional energy generators,
- remote control of equipments, vis TeamViever.

Using CYSP-C, equipped with LATNDs (total sensitive area per position 15.6 $cm^2$) the time needed for a complete spectrum acquisition will be considerably reduced.

### *3.6 Collaborations*

- CIEMAT Madrid: 35,000 equiv-hours CPU time on EULER cluster for response matrix calculations
- Roma3 University, support for CYSP cosmic measurement test.
- Politecnico di Milano: support for electronics design and testing
- Azienda Ospedaliera San Camillo-Forianini (Roma) and Ospedale Santa Maria delle Croci (Ravenna): usage of 15 MV electron LINACs for testing Silicon detectors under very intense high-Energy gamma field.
- LNF support: 2 man*month at mechanical workshop, experiments performed at FISMEL laboratories.
- UAB Barcellona: donating the HDPE for building ETHERNES, spectrum measurement in ETHERNES with Bonner spheres.

### **3.7. *Project meetings***

(See website for downloading presentations)
- NESCOFI@BTF closure & NEURAPID start up meetings, INFN-LNF, 26 February 2014
- NEURAPID 2014 Midyear meeting, INFN-LNF, 8-7-14
- NEURAPID 2014 end of year meeting, INFN-LNF, 4-12-2014

### **3.8 *International Review Panel***

The panel produced a mid-year report during the 8th July meeting, see enclosed text.
Prof. Carles Domingo, Profesor Titular Universitat Autonoma de Barcelona, carles.domingo@uab.cat
Dr. D.J. Thomas, Head of Neutron Metrology Group of NPL (UK)

**Reviewer's report on NEURAPID review meeting**
**8th July 2014**

We were impressed with the activities of the NEURAPID group. It was good to see a group of people working in a planned and coordinated way on a topic area (neutron detection) where little work is presently being undertaken. It was also good to see that the group were being innovative and not following the route which many labs are going down of simply copying work which has been done in the past, e.g. the development of Bonner spheres based on the designs developed in the 1980s and 1990s by PTB, GSF, NPL and others.

The presentations by the various speakers were logically laid out and outlined the goals and achievements of the project in a clear and understandable way. The project appears to be on track in terms of achieving its objectives with the milestones fulfilled in advance in many cases.

The introduction by Bedogni presented the aims in the areas of pulsed field measurement and very low intensity field measurements, and fully justified these as areas of importance.

Bortot then described the quality control issues for the TNDS detectors which are a very useful addition to the range of detectors available for detecting thermal neutrons with options for different areas and hence sensitivities.

The ETHERNES facility, presented by Bedogni, makes use of multiple scatter approach to thermal neutron production rather than the more conventional approach of moderation and appears to produce excellent results. Further measurements are planned to validate the extensive simulation calculations with MCNP.

The ETHERNES imaging system, described by Sacco, presented a novel technique for using a photon sensitive Gafchromic to detect thermal neutron by using a cadmium sheet to produce gamma rays. Despite its very low sensitivity it should provide a very useful visual measure of the uniformity of the field within the ETHERNES facility.

Gomez Ros described calculations of the response expected for the CYSP detector with new larger area detectors. They raised some interesting questions and further work is planned. Fabrication of the larger area detectors is being approach cautiously as the large silicon diodes are expensive.

The activities of NEURAPID-Milan were outlined by Pola. This group have been concentrating on the electronics aspects of the project and have produced novel electronic devices which will probably have applications outside the project.

The reviewers felt that the goals of the project were fully justified and that progress on the project was well on track which was to be applauded for such a complex multidisciplinary venture.

Frascati, 8-7-2014

D. J. Thomas.....

C. Domingo.....

## 3.9 *Website*

**https://sites.google.com/site/csn5neurapid/**

## 3.10 *2014 Publications*

Radiat. Prot. Dosimetry 161 (2014) 37-40.

Radiat. Prot. Dosimetry 161 (2014) 229-232

Radiat. Prot. Dosimetry 161 (2014) 241-244

Radiat. Prot. Dosimetry 161 (2014) 45-62

Nucl. Instr. and Meth. 746 (2014) 59-63

Nucl. Instr. and Meth. 763 (2014) 547-552

Nucl. Instr. and Meth. 767 (2014) 159-162

Medical Physics 41 (2014) 112105.

European Physical Journal C 74 (2014)

Proceed. INPC 2013 Vol 2 Book Series EPJ Web of conferences (66), article. n. 11032 (2014).

NEURAPID activity was also presented Workshop on accelerator based neutron production (14-15 April 2014, INFN-LNL)

## 4. Bibliography


[1] Bedogni, R., Domingo, C., Esposito, A., Fernandez, F., 2007. FRUIT: an operational tool for multisphere neutron spectrometry in workplaces. Nucl. Instr. Meth. A 580, 1301 1309.

[2] Bedogni, R., Pelliccioni, M., Esposito, A., 2010. A parametric model to describe neutron spectra around high-energy electron accelerators and its application in neutron spectrometry with Bonner Spheres. Nucl. Instr. Meth. A 615, 78-82.

[3] A. Pola, D. Bortot, M.V. Introini, R. Bedogni, A. Gentile, A. Esposito, J. M. Gomez-Ros, E. Passoth, A. Prokofiev. Compact thermal neutron sensors for moderator-based neutron spectrometers. Radiation Protection Dosimetry (2014). doi:10.1093/rpd/nct298.

[4] R. Bedogni, D. Bortot, A. Pola, M.V. Introini, M. Lorenzoli, J.M. Gómez-Ros, D. Sacco, A. Esposito, A. Gentile, B. Buonomo, M. Palomba, A. Grossi. Experimental characterization of semiconductor-based thermal neutron detectors. Nucl. Instr. Meth. A 780 (2015) 51.

# NEXTARCH

M.A. Iliescu (Resp.)

Not received

# 2014 NORCIA GROUP ACTIVITY REPORT

D. Di Gioacchino (Ric.), G. Gatti (Ric.) (Resp.), R. Gunnella (Ass.), A. Marcelli (P.R.), B. Spataro (Ass.)
[*http://www.lnf.infn.it/gr5/website_norcia/home.html*]

*Aim of the experiment*

An extensive experimental and theoretical program to determine reliable ultra-high gradient operations of future linear accelerators is under way in many laboratories. Technological advancements are strongly required to fulfil demands of new accelerators devices with highest accelerating gradients and reliability for future colliders[1,2]. In addition to the highly demanding high-energy applications, X-band accelerators are also considered for compact or portable devices for radiotherapy, mobile cargo inspections, biology, energy and environment, security, etc..

Following the international trend, the NORCIA research activity is dedicated to design studies and to the construction of standing wave (SW) linear accelerating structures working at 11.424 GH with a modern approach in order to maximize the radio-frequency (RF) performance.

In the framework of a large collaboration among SLAC (USA), KEK (Japan), UCLA (Los Angeles) and INFN-LNF laboratories, many researchers are involved in the design, manufacture and test of compact high power SW sections. The activity is mainly devoted to the research and development of key components for existing accelerators and studies of test structures for the next generation. Systematic studies on the 11.424 GHz frequency accelerator structures, R&D on new materials and the associated microwave technology to achieve accelerating gradients well above 120 MeV/m are in progress. Actually, to increase performances of X band linacs many resources have been and are devoted to achieve higher accelerating gradients with extremely low probability of RF breakdown and, at the same time, to operate accelerators with the highest possible reliability. Indeed, the breakdown phenomenon remains a challenging open problem and a dedicated R&D in this field is on going in the large linear-collider community.

In order to improve the higher power performance of X-band structures in terms of the accelerating gradient, the use of materials with a high tolerance to surface fatigue due to the pulsed heating effects, e.g., materials with a higher fusion point, and to avoid the fabrication of soft devices as done in conventional brazing, is also required[2-6]. The effort dedicated to X-band high gradient researches and related accelerator technologies will allow to further advance the X-band technologies and many different accelerator related projects in the world will benefit.

*Electroformed Au-Ni structures - RF low-power tests*

Among the different manufacturing procedures, the electroforming is a very attractive technique to realize compact structures, avoiding the soft brazing but still preserving the mechanical properties and fulfilling high vacuum requirements. To contribute to determine the maximum sustainable gradients in normal conducting RF powered particle beam accelerators operating at X band with extremely low probability of RF breakdown, we fabricated and characterized electroformed SW structures at 11.424 GHz, coated with Au-Ni and with different roughness.[7] In 2014 in particular, we characterized a hard high gradient RF accelerating structure at 11.424 GHz. Low-level RF measurements and high power RF tests were carried out at the SLAC National Accelerator Laboratory on such prototype. Based on the same electroforming process we realized also an alternative original layout where a water-cooling of the irises has been implemented for the first time.

The main cell dimensions and the mechanical drawings of the SW structures we manufactured are reported in Ref.s[2,3,6,8]. These SW devices contain three cells fed by a circular waveguide. The central cell has a gradient twice higher than the adjacent ones used to match the RF power from the input circular waveguide. The mode excited to test the structure is the π-mode. With this layout, breakdowns occur predominantly in the central cell with the highest gradient cell while the two side cells show surface conditions unperturbed by breakdowns[2-4]. Table I reports the main RF parameters measured at SLAC at room temperature for this Au-Ni electroformed structure. Figures 1 show the electroformed structure manufactured with a roughness of ~70 nm. By looking at the Table 1 related to the low power RF tests, we may obtain the longitudinal field profiles of the π, π /2 and 0 mode characterizations showed in Fig. 2. For each mode a good agreement among theoretical values of operating frequencies and the measured longitudinal field profiles on axis is obtained. Moreover, the working π mode is about 3.9 MHz off, a value that can be considered acceptable considering that measurements have been carried out with an un-tuned device. The electric field profile on axis shows also a good matching at the nominal RF frequency of ~11.424 GHz with twice the maximum field intensity in the central cell with respect to the side ones. For sake of completeness, the structure working on the π mode gave a resistivity ~2 times higher than the Cu one because the corresponding quality factor $Q_0$ of the mode is lower than expected. Additional studies are in progress by changing the shape of each cell, reduce the deposited film's porosity, etc. trying in particular, to maximize the conductivity of the Au film. Elliptical-like cells are also good candidates to improve the deposition quality. Similar results have been obtained for a second electroformed structure manufactured with a surface roughness of ~10 nm.

TABLE I. *RF parameters at room temperature of the Au-Ni electroformed structure.*

| Mode | π | π/2 | 0 |
|---|---|---|---|
| $F(GHz)_{measured}$ | 11.4200 | 11.3241 | 11.27088 |
| $F(GHz)_{calculated}$ | 11.42388 | 11.33004 | 11.27766 |
| $Q_0$ | 5130 | 6467 | 5981 |
| $Q_{0\ calculated}$ | 9178 | 9388 | 9110 |
| $Q_{loaded}$ | 3077 | 1874 | 1938 |
| $Q_{ext\ measured}$ | 7315 | 2351 | 2867 |
| $\beta_{measured}$ | 0.726 | 2.75 | 2.08 |

The electroforming process is also attractive to exploit its natural tendency to leave an open channel in a high aspect ratio component. As showed in Figure 3, this natural mechanism offers the possibility to have "open channels" to cool the device. Areas of high current density and faster growth can be naturally obtained at the entrance of the high aspect ratio grooves in the mandrel while forming the irises. Actually, it is the electro deposited material during the electroforming process that closes the grooves (see the right panel in Fig. 3) creating the "channels". In 2014 we completed the first experimental evaluation of a device where this process has been used to obtain cooling channels built-in around the irises. The manufacture of other dedicated single cell prototypes is on going to investigate the change of the resistivity as a function of the gold film obtained with an e-beam with the PVD (Physical Vapour Deposition) procedure. Compared to the galvanic process this method could improve the film deposition, in particular its purity.

*Electroformed Au-Ni structures - RF high-power tests*

As underlined before, one of the main aims of the NORCIA experiments and its collaborations is the characterization of RF breakdowns properties in structures manufactured with procedures alternative to the brazing technique. Actually, the RF breakdown phenomenon in high vacuum accelerator structures does not have a well-defined threshold with respect to the operating parameters such as the peak accelerating field or the input power. However, its statistical behavior can be consistently characterized. Using X band Au-Ni standing wave structures manufactured with the electroforming process to avoid the large heat treatment of the metal, we performed at SLAC also high power RF tests. Breakdown rates were obtained as a function of the accelerating gradient in addition to the peak pulse surface heating in the cavity for different pulse length of the accelerating structures. The RF pulse we used has a charging time of ~170 ns followed by a flat part ranging from 100 to 600 ns. We run with RF pulses with a flat shaped part, whose length was 150, 200 and 400 ns to study the dependence with the pulse length. The first set of experiments with a pulse with a flat shaped part ~150 ns long, was aimed at verifying the reproducibility of the behavior comparing similar structures. During the initial process the electroformed structure run similarly to electroplated Cu or soft Cu structures of the same geometry. As a result, we may claim that the structure performances improve with the accumulated breakdowns and may be additionally improved after several processes[2,7]. In soft Cu SW structures with a disk-loaded type, the breakdown rate is also highly correlated with the peak pulse heating[2]. Moreover, in these geometries the electric and magnetic RF parameters are also well correlated[2]. Figures 4 shows breakdown data of electroformed structures for pulses with a shaped flat part of 150 ns, 200 ns and 400 ns. Actually, data analysis does not show a correlation either with RF fields or with the pulse heating for the same breakdown probability. We consider that this anomalous behavior can be associated to the non-uniform gold coating in the high magnetic areas or to a diffusion of Ni inside the gold plating. Improving the quality of the gold coating, the behavior of such structures will be probably better than Cu-based structures. In addition, the pulse heating damage on the gold coating is also lacking. This latter behavior may be due to the removal of the gold coating by breakdowns (see conclusions). In such a case, the remaining exposed nickel surface exhibits a higher resistance to breakdown. In Figures 5 e 6 we compare breakdown data between a structure made with soft copper and a second one obtained with the electroforming process tested with the same pulse with a flat shaped structure of 150 ns and 200 ns. The RF losses in the electroformed structure are ~60 % higher than in the soft copper structure of the same type. In pite of the higher RF losses and the slow initial conditioning of the gradient, the breakdown rate is similar to soft copper structures with a 200 ns long flat shaped pulse and ~20 % lower with a 150 ns long flat shaped pulse.

*Molybdenum coatings*

To increase the accelerating gradient of RF cavities working at high frequencies we also considered the use of new materials including molybdenum sputtered on copper, the realization of single and multi-layer surfaces with precision-controlled properties, different copper alloys, etc. Actually, an extensive R&D activity concerning molybdenum coatings has been also performed. Copper coated by molybdenum via sputtering under vacuum is indeed promising approach to increase the accelerating gradient of RF cavities working at high frequencies. Dedicated RF devices with

Mo coatings have been already manufactured but still a lot of work is necessary to achieve the performances required at high power.
At Frascati we are studying Mo films grown by RF magnetron sputtering technique on glass and sapphire substrates at room temperature. The sputtering parameters were optimized specifically addressing the growth of oxygen free Mo layers. In cooperation with Roma *Sapienza* and Roma Tre we combined FIB imaging, to visualize at high spatial resolution the morphology of Mo films and to accurately measure their thickness, with transport experiments to measure the resistivity. The characterization of the chemical properties of the coated films has been carried out also at the Diamond Light Source (UK) with the XANES (X-ray Absorption Near Edge Structure) and the XRD (X-Ray Diffraction) techniques, i.e., to evaluate the degree of crystallinity, identify different ordered phases and probe local structure and electronic properties.
The characterization of Mo coatings obtained via the sputtering method has been then performed on coatings annealed up to 600 ºC.[9-12] The latter are multiphase metallic films with negligible contributions of disordered oxide phases. Experiments have shown that in these relatively thick films structural and electronics changes are associated to changes of the resistivity. Indeed, while the starting values of the resistivity are higher or comparable to molybdenum oxides, those measured after annealing are much lower than the best conductive $MoO_2$. These coatings exhibit a resistivity less than one order of magnitude higher than the Mo bulk and comparable with that of bi-layer $MoO_x$ films ($\sim 10^{-5}$ Ωcm) growth with different crystalline phases. Actually, results show that the combination of magnetron sputtering and post-deposition annealing is a powerful method to grow homogenous Mo coatings suitable to increase performances of RF cavities working at high frequencies. However, although conductivity values appear promising and dedicated RF devices with Mo coatings have been manufactured, a lot of R&D is still necessary to achieve the performance required by operations at high power. Further enhancements of the conductivity of Mo coatings are probably achievable tuning growth parameters and post treatment processes optimized to improve these multiphase films characterized by percolative phenomena, critical processes for which the dimensionality is a relevant parameter.

*Conclusions and future activity*

Two electroformed (or hard) SW accelerating structures have been realized with the electroforming processes and tested at room temperature. The experimental results of both structures are in agreement with the design parameters. High power tests of some structures have been carried out at SLAC. In the meantime studies on the deposition of multilayers are also in progress. In addition, a couple of dedicated prototypes (single cell) have been fabricated to investigate how to reduce the resistivity of the gold deposition. A full characterization of conductivity properties of Au coatings achieved with new manufacturing methods are strongly required to identify reliable procedures for such demanding films.
An extensive and accurate characterization of the conductivity properties of optimized Mo coatings is also in progress to identify reliable procedures capable to produce highly demanding films. Existing results are promising and further enhancements of the conductivity are probably achievable tuning the synthesis and post treatment processes of Mo coatings.
Additional work in cooperation with SLAC is on going to understand the damage induced by breakdowns after operation at high gradient. Images in Fig. 7 clearly show that gold coating is removed in the regions of the high-electric field while no obvious pulse heating damage occurs on the plating. The result is very surprising after the observation of the massive pulse heating damage of the copper coating. To clarify this issue, we started to investigate the possibility to apply modern x-ray imaging techniques to obtain full 3D images of RF devices or section of these devices at high spatial resolution to better monitor the induced damage and to understand the occurring breakdown phenomena.

*References*


[1] A. Grudiev, S. Calatroni and W. Wuensch, PRST-AB 12, 102001 (2009)
[2] V. Dolgashev *et al.*, Proceedings of IPAC 2010, Kyoto, Japan, 2010, pp. 3810-3812
[3] V. Dolgashev seminar held at LNF (September 2010)
[4] V. Dolgashev and S.G. Tantawi, private commun.
[5] V. Dolgashev *et al.*, Applied Physics Letters 97, 171501 (2010)
[6] B. Spataro *et al.*, NIM A 657 (2011) 114-121
[7] G. Valsecchi - www.media-lario.com
[8] B. Spataro *et al.*, NIM A 657 (2011) 88-93
[9] S. Bini *et al.*, Chin. Phys. C **37** (2013) 097905-07
[10] P. Chimenti, C. Caliendo and B. Spataro, SPARC-RF-12/ 004, June 8, 2012
[11] Y. Xu *et al.*, J. Physics: Conference Series **430** (2013) 012091
[12] A. Marcelli *et al.*, Surface & Coatings Technology (2015) in press

*Figure captions*

Figure 1. a) Final X band structure and its cross section after removal of mandrel; b) open channel in the irises visible in a sectioned structure

Figure 2. a) Au-Ni electroformed structure; b) $\pi$ - mode, on axis field profile; c) $\pi/2$ mode, on axis field profile and d) 0 mode, on axis field profile

Figure 3. Open channels in the irises visible in a sectioned structure prototype and, on the right panel, the layout of the mechanism that allows the electroforming process to close the grooves.

Figure 4 Breakdown data of electroformed structures for pulses with a shaped flat part 150 ns, 200 ns and 400 ns long.

Figure 5. Comparison of breakdown data of two soft copper electroformed structures of the same shape driven with a RF pulse with a shaped flat part 150 ns long

Figure 6. Comparison of breakdown data of two soft copper electroformed structures of the same shape driven with a RF pulse with a shaped flat part 200 ns long.

Figure 7. Images of the autopsy of an electroformed three cells Au structure. On the left an image of the high gradient side of the center cell while on the right the image of the high gradient side of the end cell. The removal of Au from the surface as induced by multiple breakdowns is evident in the high-electric field area.

Figure 1

a) Final X-band structure (left picture) and its cross section (right picture) after removal of mandrel

Figure 2

a) Au-Ni electroformed structure

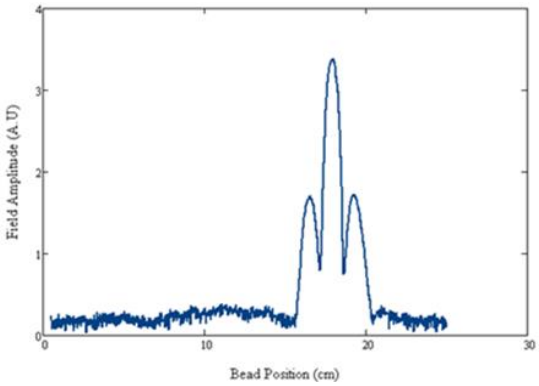


b) π - mode, on axis field profile

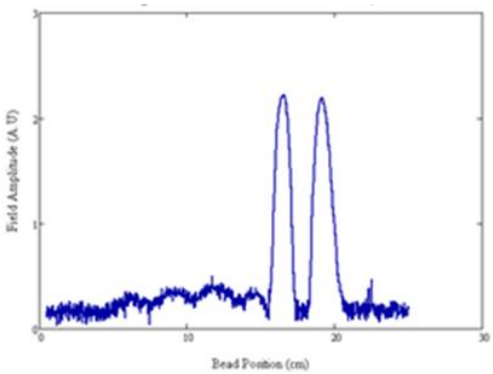


c) π/2 mode, on axis field profile

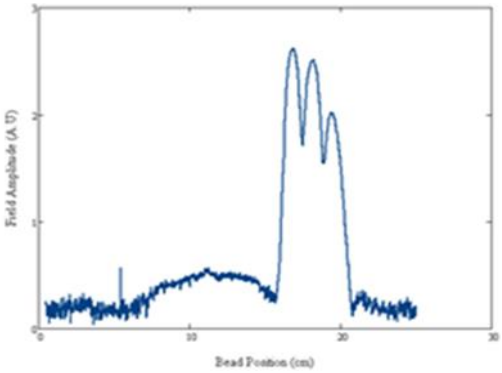


d) Mode 0, on-axis field profile

Figure 3

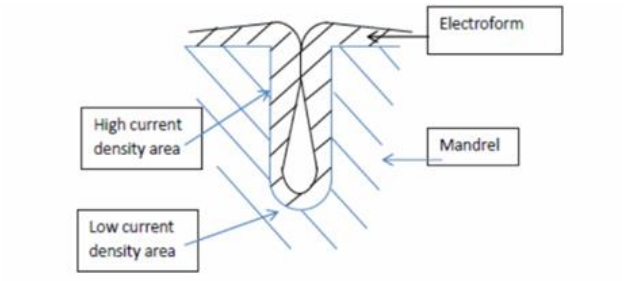


Open channels in the irises visible in a sectioned structure prototype and, on the right panel, the layout of the mechanism that allows the electroforming process to close the grooves.

Figure 4

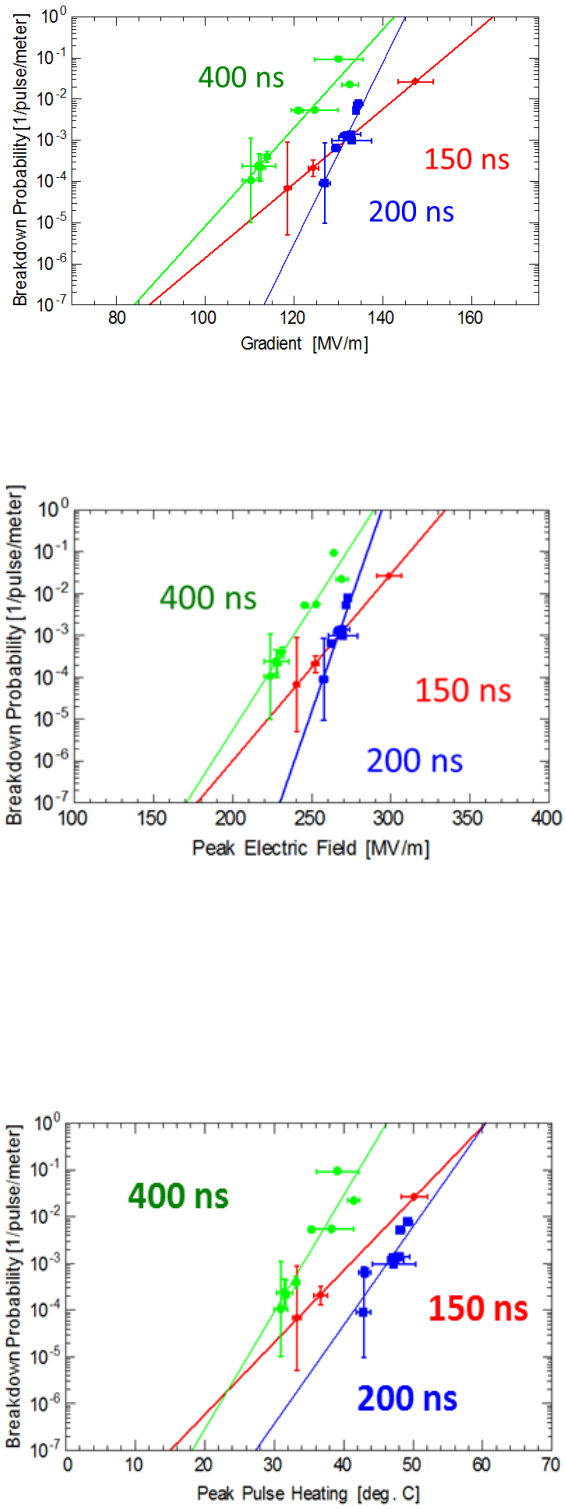


Comparison of breakdown as a function of the RF pulses with a shaped flat part 150 ns (red), 200 ns (blue) and 400 ns (green) long.

Figure 5

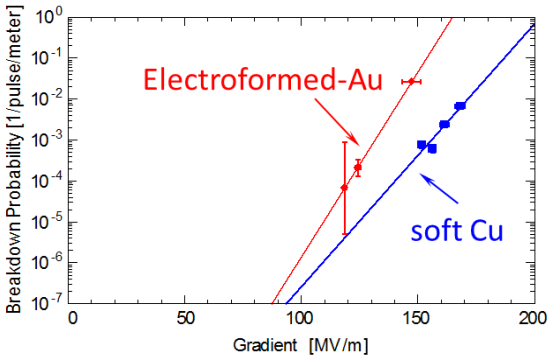


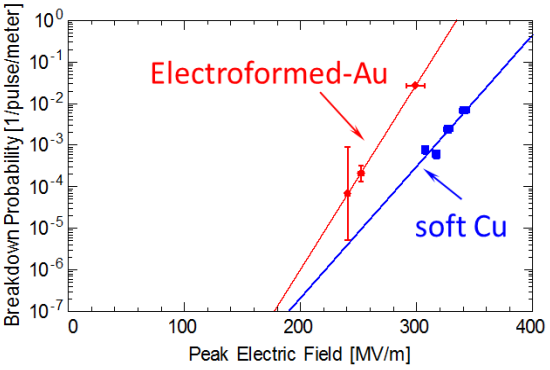


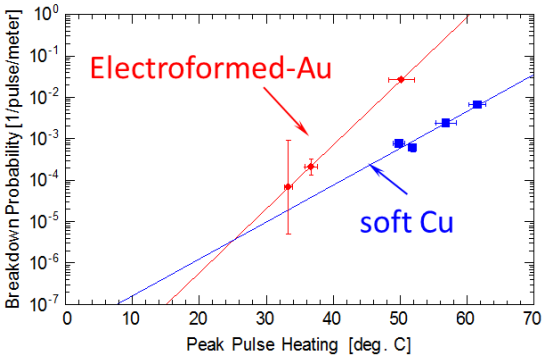


Comparison of breakdown data of two soft copper electroformed structures of the same shape driven with a RF pulse with a shaped flat part 150 ns long

Figure 6

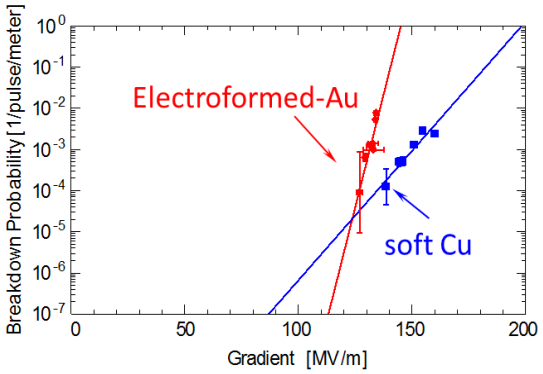


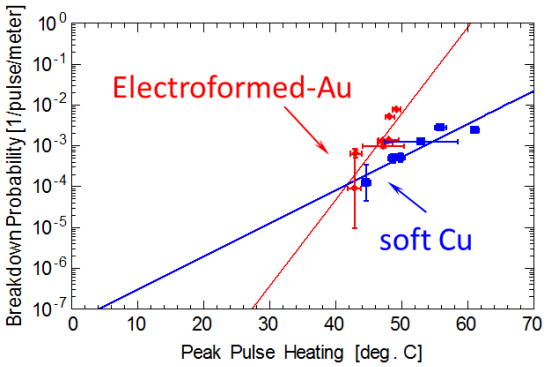


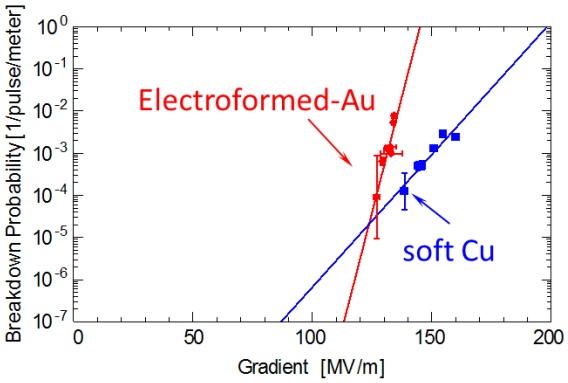


Comparison of breakdown data of two soft copper electroformed structures of the same shape driven with a RF pulse with a shaped flat part 200 ns long.

Figure 7

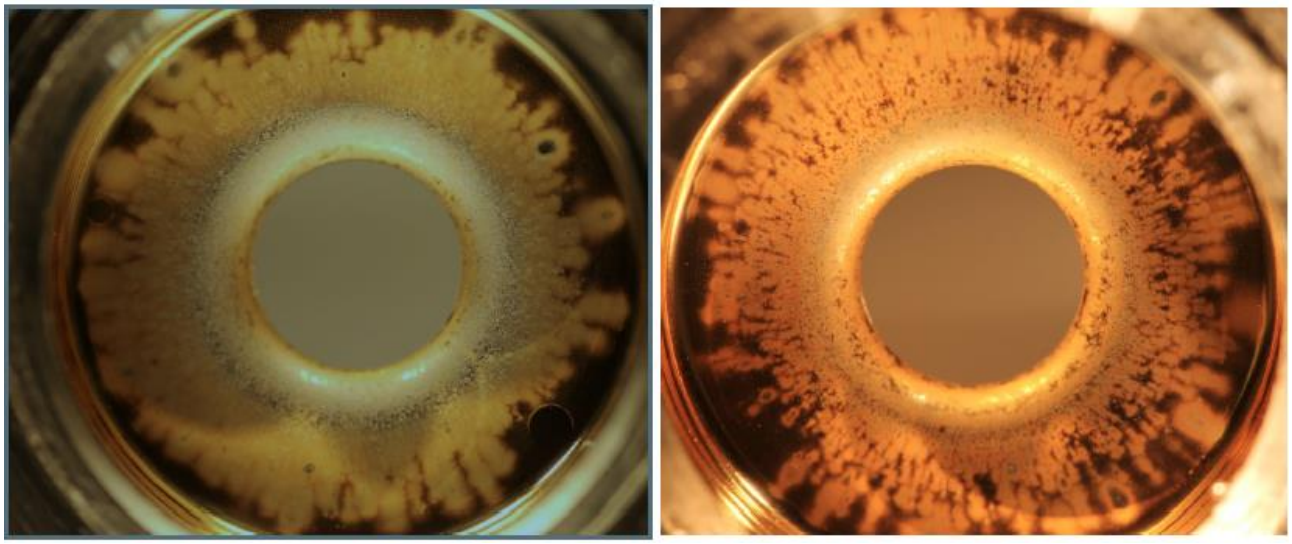

Images of the autopsy of an electroformed three cells Au structure. On the left an image of the high gradient side of the center cell while on the right the image of the high gradient side of the end cell. The removal of Au from the surface as induced by multiple breakdowns is evident in the high-electric field area.

# NTA-SL-POSSO

S. Dabagov (Resp.)

Not received

## The Sparc_Lab Thomson Source commissioning

C. Vaccarezza (Resp. Naz.), M.P. Anania (Ass. Ric.), M. Bellaveglia (Art. 23), E. Chiadroni, A. Cianchi (Ass.), M. Cestelli Guidi (Art. 23) , D. Di Giovenale (Art. 23), G. Di Pirro, A. Drago, M. Ferrario, F. Filippi (Ass), A. Gallo, G. Gatti, A. Ghigo, A. Giribono (Ass.), A. Marcelli, A. Mostacci (Ass.), L. Palumbo (Ass.), R. pompili (Art. 23), S. Romeo (Ass.), F. Villa (Ass. Ric.).

Participant institutions: other INFN sections (Mi, RM1, RM2, Ba, Ca, Pi, Ts, Fe, Le, Fi, Na, LNS), ENEA-Frascati

On February 2014 the first part of the SL-Thomson source commissioning took place resulting in the first signature of Compton X-rays production at SPARC_LAB where a 50 MeV electron beam has been put in collision with a 1J laser pulse coming from the Flame system producing backscattered photons around 60 keV.

Briefly the SPARC_LAB Frascati Thomson couples the SPARC High Brightness photoinjector with the 250 TW FLAME laser system [1] to provide X-ray photons in the range of 20-500 keV; a 20 m double dogleg carries the electron beam output from the photoinjector down to the Thomson Interaction Point where the FLAME laser pulse is brought by a 20 m in vacuum optical transfer line, see Fig. 1. The parameters of the electron and laser beams, reported in Table 1, are presently optimized in view of the first planned experiment of X-ray imaging of mammographic phantoms with phase contrast technique [2], requiring high flux of photons and moderate monochromaticity.

Table 1: Thomson Source Design Parameters

| | | | |
|---|---|---|---|
| X-ray Beam | Photon energy | (keV) | 20-500 |
| | Photon number per shot | | $10^9$ |
| | Source rms radius | (μm) | 10 |
| | Bandwidth | (%) | 10 |
| Laser Beam | Wavelength | (nm) | 800 |
| | Pulse energy | (J) | 1÷5 |
| | Pulse length | (ps) | 6 |
| | Spot size | (μm) | 10 |
| | Rep. rate | (Hz) | 10 |
| Electron Beam | Energy | (MeV) | 30÷150 |
| | Energy spread | (%) | <0.1 |
| | Charge | (pC) | 100-800 |
| | Emittance | (mm mrad) | 1÷3 |
| | Spot size | (μm) | 10÷20 |

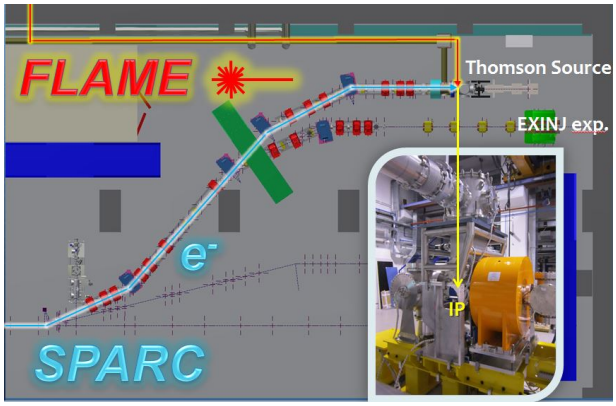


Fig. 1 SPARC_LAB Thomson source schematic layout

### The electron beam

The electron beam is provided by the SPARC photoinjector and is brought to the Thomson Interaction Point (IP) through the 25° double dogleg. For this commissioning phase a low charge working point has been set up with

Q= 200  pC beam and energy E= 50 MeV; the phases of the accelerating sections have been chosen as follows: $\Phi_{S1}$=-26.2°, $\Phi_{S2}$= +78.5, $\Phi_{S3}$= -111° from crest, in order to minimize the effects of the power amplitude jitter from the feeding Klystrons.

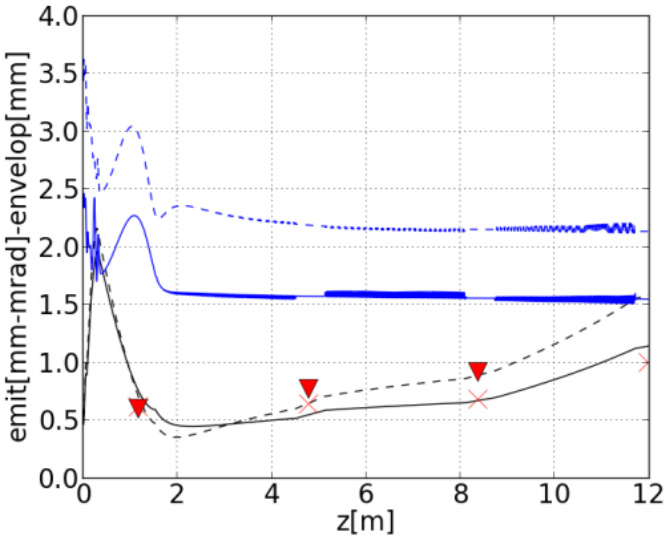


Figure 2: Electron beam emittance (blue curves) and envelope evolution (black curves) from the photocathode to the linac exit calculated with the Astra code. The dots represent the beam spot measurements taken in this configuration at screen locations along the linac.

The beam emittance and envelope evolution through the photoinjector has been simulated with the ASTRA code [3] and 50k particles; the results are shown in Fig. 2 together with the beam spot measurements taken at the screen locations along the linac.
Downstream the photoinjector exit the 25° double dogleg ends with a two branch interaction zone devoted to Thomson and External Injection in plasma experiment, see Fig. 1. The dogleg $R_{56}$ parameter can be set in the range of ± 50 mm, closing the horizontal dispersion at the end of the last dipole (Fig. 3). For the commissioning phase the dispersion is closed at the end of each dipole pair

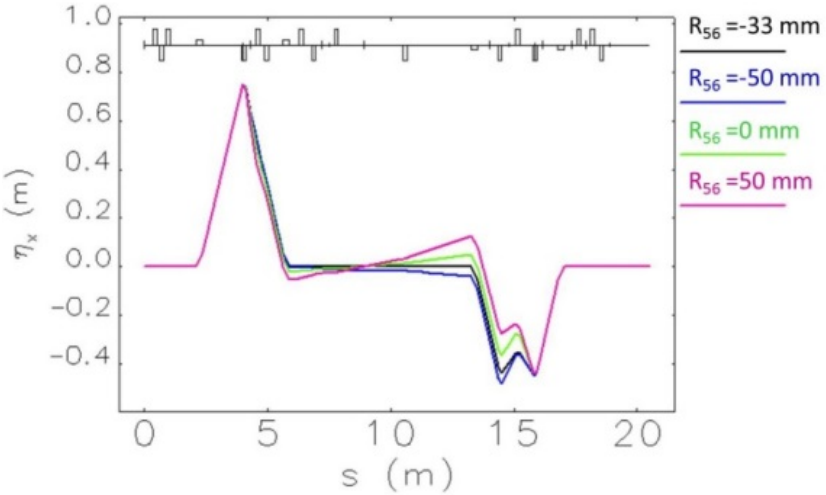


Figure 3: Double dogleg $R_{56}$ tunability and relative horizontal dispersion plot.

and the emittance evolution measurement is performed with the quadrupole scan technique in each straight section downstream the dipole pairs.

From the transverse emittance measurement performed at the linac exit the Twiss parameters are obtained to match the beam to the dogleg entrance for the transport and focusing at the Thomson Interaction Point. The space charge effects are included in the TRACE3D code [4] used for the beam matching. For the commissioning working point with Q=200 pC the energy E=50 MeV has been chosen and the calculated Twiss parameters evolution from the Linac exit up to the Thomson Interaction Point is shown in Fig. 4.

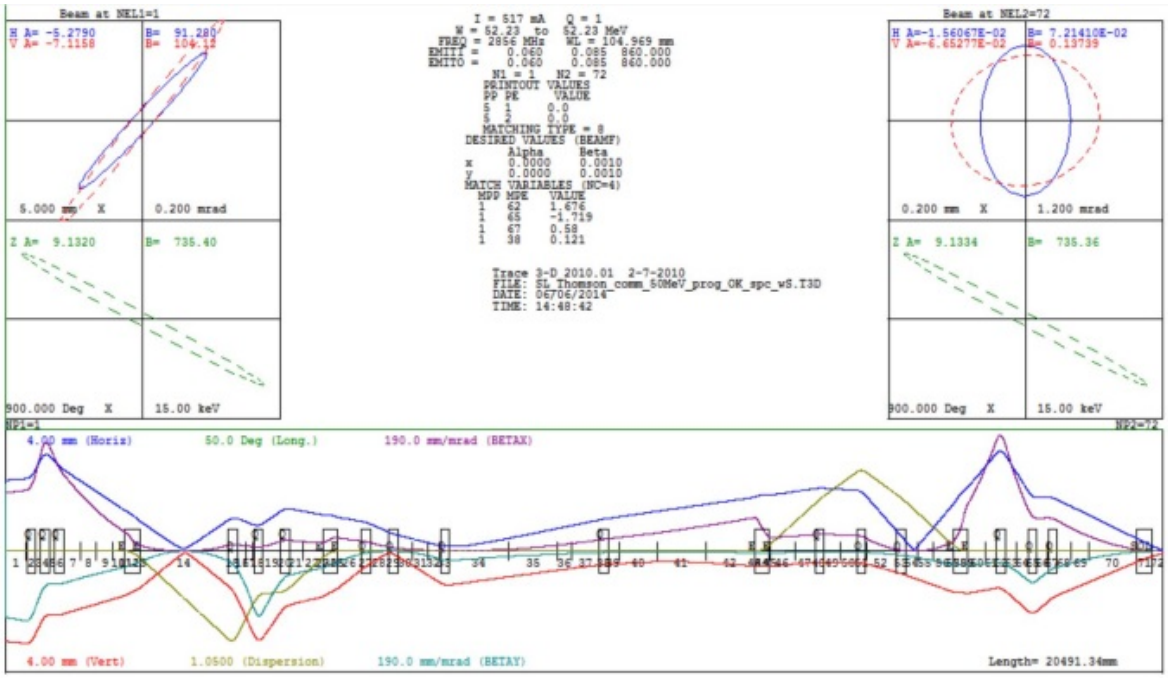


Figure 4: Twiss parameters and envelope evolution from the Linac exit to the Thomson IP obtained with the TRACE3D code

## The photon beam

The laser pulse used to drive the Thomson back scattering process with the SPARC electron beam is provided by the FLAME laser system [5]. This nominal 300 TW laser system uses 11 YAG pump lasers and 5 titanium-sapphire multi-pass amplifiers to produce linearly polarized pulses with a central wavelength $\lambda_0$=800 nm in a 60÷80 nm bandwidth. The pulse duration ranges between 25 fs $\leq \tau_L \leq$ 10 ps, and the maximum energy is E= 7J that corresponds to an energy on target $E_t \sim$ 5J, at 10 Hz repetition rate. The laser pulse is optically transported from the FLAME laser system in a shielded underground area where the compressor is located and that is adjacent to the SPARC hall. From here an optical transfer line in vacuum, (P=$10^{-6}$ Torr), carries the beam up to the parabolic mirror of the Thomson interaction chamber that focuses the beam in a 10 μm diameter (FWHM) spot at the interaction point.

The good focal spot has been obtained with the use of the adaptive optic placed inside the compressor. This mirror is used to control the phase-front of the photon beam. Fig. 5 shows two images of phase front measurement: the one on the left hand side, is the phase front measured without any correction which shows a large aberration (the rms error respect to a perfect spherical

phase front of about 2 micron) and the one on the right hand side shows a corrected phase front which shows almost no aberrations (the error this time is only 50 nm).

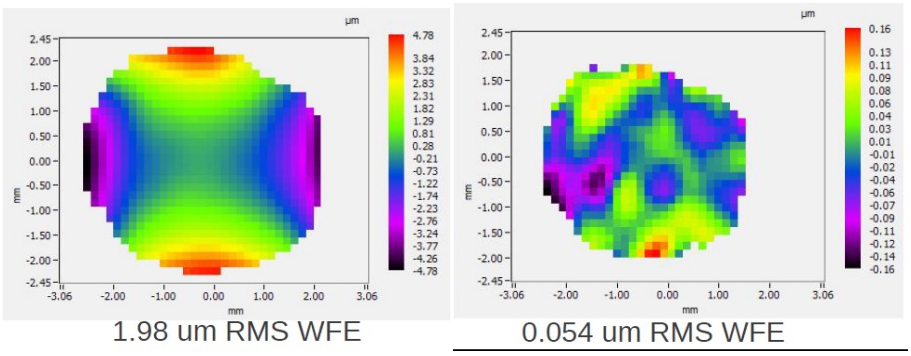


Fig. 5: Phase front error measured (a) before phase front correction and (b) after correction showing an rms error respect to a perfect spherical phase front of (a) 1.98 micron and (b) 0.054 micron.

The corresponding beam at the focus (Thomson IP) for these two different phase fronts are imaged in fig. 6. It is evident that the beam is quite oval in the case of no phase front correction and becomes nearly round when the best phase front is applied. Moreover, it is perceptible that the use of the adaptive optics is crucial also for the energy contained in the central spot (considering the $1/e^2$ diameter): in fact, when there is no phase front correction, the energy inside the central spot is only 25% while after the phase front correction, this energy is 60%.

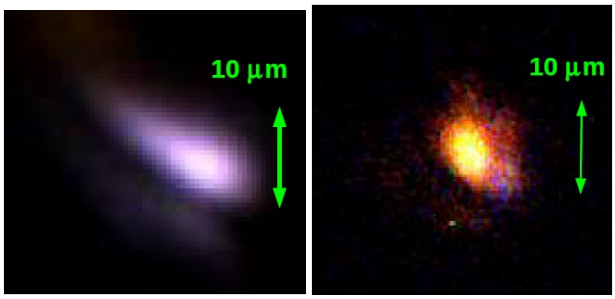


Fig. 6: FLAME focal spot (a) without phase front correction and (b) with phase front correction.

## The synchronization system

The Thomson scattering experiment needs an extremely precise synchronization between electron bunch and laser pulse. The electrons and the photons collide well inside the waist region of the laser beam final focus provided that the relative time of arrival jitter at the IP between the 2 beams is < 500 fs $_{RMS}$.

The electrons are generated by photo-emission from a copper cathode hit by an UV pulse produced by a dedicated laser system (the photo-cathode laser), then they are captured and accelerated by the RF fields of the RF gun and traveling wave accelerating sections. Then the bunch time of arrival at the IP depends on the arrival time of the laser on the photocathode and on the phase of the RF accelerating fields. The arrival time at the IP of the extremely intense IR laser pulse

depends on the starting time of the seed pulse, which is selected from a laser oscillator pulse train and then amplified, compressed and transported.

The synchronous arrival of electrons and photons at the IP is obtained by locking precisely the oscillators of the photo-cathode laser and interaction laser systems, and the phase of the RF accelerating fields to a common Reference Master Oscillator (RMO). The RMO is a low phase noise (60 $fs_{RMS}$ integrated in the 10 Hz ÷ 10 MHz range) μ–wave oscillator tuned at the Linac main frequency 2856 MHz. The laser oscillators are locked through a PLL architecture to the 36$^{th}$ sub-harmonics of the RMO, while the output RF phase of the linac klystrons is downconverted to baseband by mixing with the RMO signal, and deviations are corrected both within the 4 μs RF pulse duration (jitter feedback) and pulse-to-pulse (drift feedback).

Table 2: Measured synchronization performances of the main SPARC_Lab sub-systems

| System | Measured jitter | Note |
|---|---|---|
| Reference Master Oscillator | ≈ 60 $fs_{RMS}$ | Absolute, 10 Hz ÷ 10 MHz |
| Photo-cathode Laser Oscillator (MIRA) | ≈ 50 $fs_{RMS}$ | Absolute, 10 Hz ÷ 10 MHz |
| Interaction Laser Oscillator | ≈ 100 $fs_{RMS}$ | Absolute, 10 Hz ÷ 10 MHz |
| RF output Klystron #1,2 | ≈ 50 $fs_{RMS}$ | Relative to RMO, average over the pulse |
| Electron bunch | < 100 $fs_{RMS}$ | Relative to RF (meas. with RF deflector)<br>Relative to photocathode laser (meas. with EOS) |

The measured synchronization performances of the main SPARC_Lab sub systems are reported in Table 2. The jitter of the bunch arrival time at the end of the linac has been measured relative to the klystron RF streaking the bunch on a screen by means of an RF deflecting cavity and recording shot to shot the bunch centroid vertical position. In alternative the bunch arrival time has been measured relative to the photocathode laser using the Electro Optical Sampling technique [6]. The measured jitter of the bunch arrival time is <100 $fs_{RMS}$with both methods, that in our implementation present a similar estimated resolution of ≈ 20 $fs_{RMS}$.

Once locked to the RMO, the measured absolute integrated phase noise of the interaction laser FLAME oscillator is ≈100 $fs_{RMS}$, and we do not expect significant performance degradation by the laser amplification and transport. So the expected relative jitter of the arrival time at IP of electron bunch and laser pulse is well below the 500 $fs_{RMS}$ specification.

In Fig. 6a the control window of the PLLs implemented on the photo-cathode and interaction lasers is shown. Once locked both to the RMO, the window gives the possibility of freely phasing the 2 systems at any desired position. Fig. 6b shows the signals induced by electron and photon pulses in pick-ups placed close to the IP. Taking into account the time-of-flight from pick-up to IP, this measurement allows a coarse temporal pre-alignment of the beams, while a fine temporal superposition can be found experimentally by maximizing the flux of the Thomson radiation.

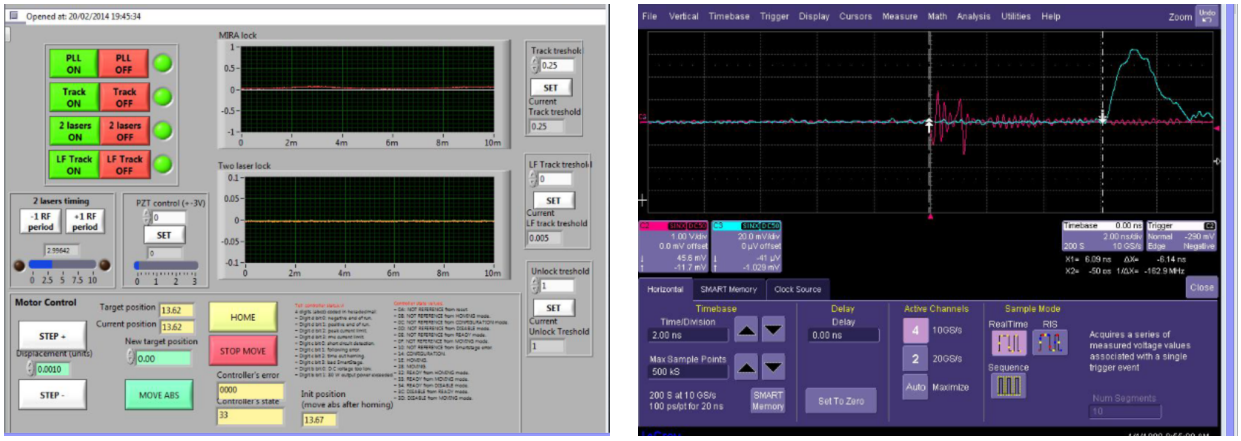


Figure 6: a) control window of PLL of the 2 lasers; b) Screenshot of signals induced by the electron and photon pulses passing near the IP

## X-ray beam diagnostic

In the commissioning phase, the x-ray detection is a fundamental diagnostic tool to verify the collision alignment and synchronisation. In this phase a detector that allows the x-ray yield measurement was required in order have a high sensitivity and a wide dynamic range to detect the potentially weak signal generated in the first non-optimised collisions. The detector we selected is a scintillator crystal coupled with a photomultiplier tube (PMT). The crystal used is a CsI(Tl) of size (20x20x2) $mm^3$, coupled with a light-guide to a PMT (Hamamatsu, mod. R329-02). The signal is acquired using both an oscilloscope and a multichannel analyser (MCA-8000, Amptek, US) connected to a PC. Due to the high intensity and short duration of the pulse, it is not possible to distinguish the signal produced by the interaction of each single photon in a pulse, as in traditional spectroscopic application, but the signal is proportional to the entire energy released in the scintillator by each pulse. Therefore, the information on the energy distribution is required to evaluate the number of photon in each pulse.

To calibrate the detector response, the signal produced by two radioactive sources: Am-241 (59.54 keV) and Cs-137 (662 keV) was performed as a function of the HV applied and the amplificator gain; adjusting the HV and gain it is possible to detect signals in a wide range. For a monochromatic radiation at 60 keV, it is possible to detect the signal produced by a single photon up to the one due to pulses containing about $10^6$ photons. The detector was placed at a distance of 4 m from the IP, aligned with the x-ray propagation direction and mounted on an *x-y* movement for the fine position adjustment. In addition to the PMT described, the beamline is equipped with a set of detectors that, together with techniques specifically developed [7-8], will allow a full characterization of the x-ray source in terms of flux, energy distribution, spatial distribution and beam stability, during the next 2015 run.

## Commissioning results

For the commissioning phase a 200 pC electron beam at 50 MeV has been selected as working point; at the Linac exit the measured normalized transverse emittance was $\varepsilon_{x\text{-}y} = 1.5 - 2.2 \pm 0.2$ mm mrad, with an energy spread $\sigma_\delta = 0.1 \pm 0.03$ %, and a rms length $\sigma_z = 3.1 \pm 0.2$ ps. In this very first four weeks shift the focusing solenoid upstream the IP was kept at 70 % of the nominal value due to a limit in the magnet cooling system for which an upgrade is foreseen in the very next. The minimum electron beam size reached was $\sigma_{x\text{-}y} \sim 90 \pm 3$ µm, nevertheless a clear Thomson photon production signature has been obtained with an electron spot size $\sigma_{x\text{-}y} \sim 240\text{-}160 \pm 10$ µm, due to a residual misalignment and a consequent poor overlap between the electron and laser beams.

Simulations of the interaction between the electron beam and the laser pulse have been made with a code based on the classical theory [9]. The 50 MeV electron beam, with 200 pC charge, 5 mm mrad of emittance, 150 µm of rms beam transverse dimension, colliding with the laser with 500 mJ and 30 µm of waist, gives a number of photons of $2\times10^5$ in a bandwidth of about 19%. The photon energy edge, given by $E_p \sim 4E_L\, g^2$, is about 63 keV.

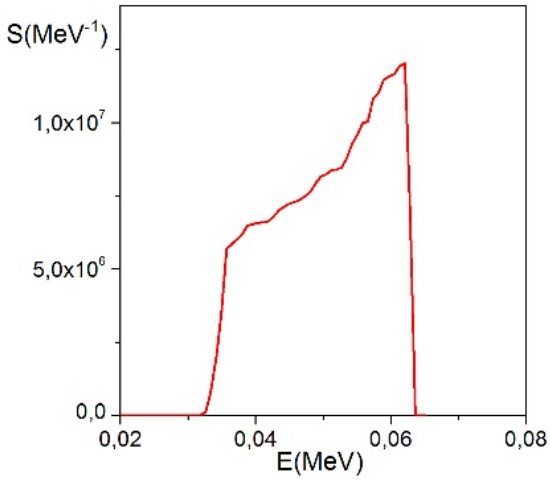


Fig 7 shows the spectral density S in $MeV^{-1}$ vs the photon energy in MeV. Fig. 7: Spectral density S ($MeV^{-1}$) versus photon energy.

The signal of the x-ray detector was measured using both a 20 GHz bw oscilloscope, for a fast response, and the multichannel analyser to acquire an integral measurement over various interactions. In Fig. 8 the results of the multichannel acquisition are shown as a histogram of the signal intensities acquired over 120 s; it is possible to distinguish the signal due to background (without interacting laser FLAME) and that due to Thomson backscattering. The pulse-to-pulse variation is due to fluctuations of the overlap region of the two beams, the relative temporal jitter between electrons and photons is ~150 fs.

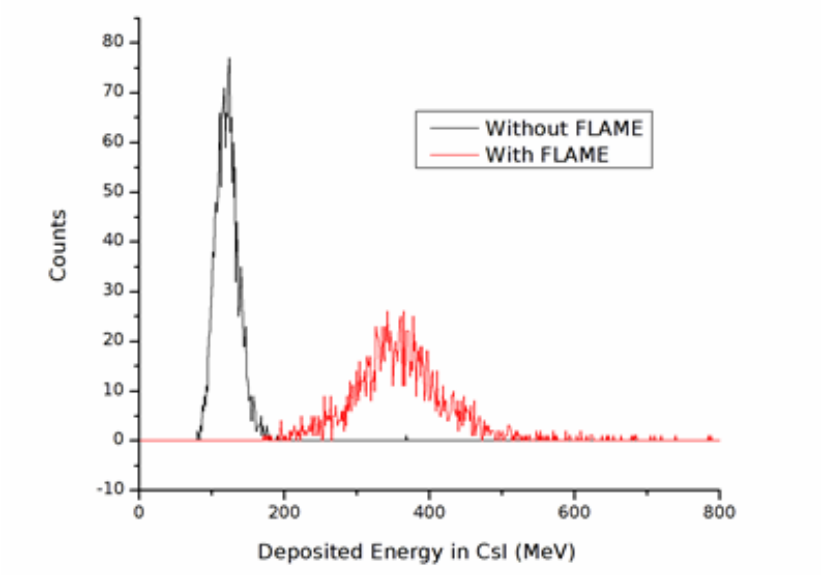


Figure 8: Thomson x-rays signal in red, in black the electron background signal (without FLAME laser), integrated over 120 s (1200 pulses).

The obtained signal is the sum of the background and the signal due to Thomson X-rays: performing a background subtraction it results in an average energy of about 235 MeV released in the crystal by each pulse. This background is synchronous to the Thomson x-rays and it is mainly due to the radiation produced in the electron beam dumping section being the dumping dipole presently located downstream the parabolic mirror vacuum chamber, i.e. too much close to the X-ray radiation extraction. In the June 2014 shutdown the insertion took place of a dumping dipole immediately after the interaction point, to avoid any background contribution from the dumping beam line.

The energy distribution of the Thomson radiation was reconstructed by CAIN simulation of the interaction and the average energy of the photons reaching the detector was 60 keV. We can then calculate that the number of photons per each pulse, nevertheless coming from poor overlap conditions, and interacting with the detector sensitive area, is in average $6.7 \times 10^3$. In the next run a full characterization of the source is planned, including also the measurement of the energy distribution and the spatial distribution of the radiation produced.

### Interaction setup upgrade

In the described first commissioning phase the electron beam dumping after the Thomson interaction was performed by means of an existing dipole magnet located downstream the X-rays extraction, due to the unavailability of the special dumping dipole projected to be inserted between the interaction cross-chamber and the parabolic mirror location. In July 2014 the final Interaction Chamber configuration has been setup with the special U-type dumping dipole insertion as it is shown in Fig. 9, and the interaction system alignment has been checked and optimized in view of the next runs.

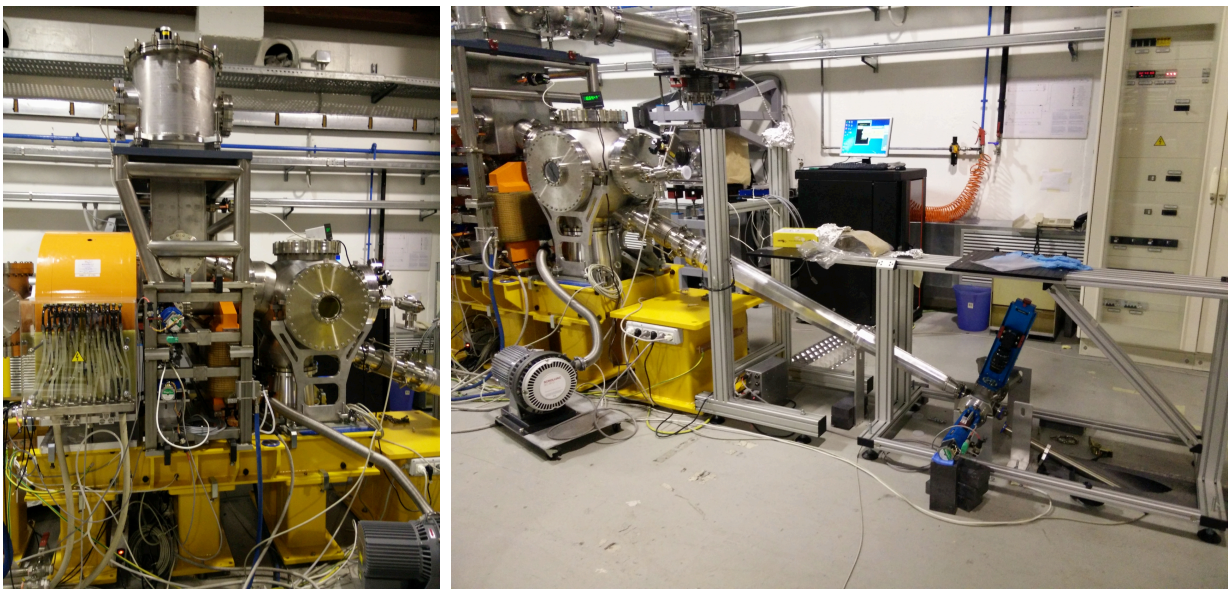

Figure 8: SL- Thomson Interaction Chamber: February shifts configuration (left) and final setup (right).

## References


[1] M. Ferrario *et al*, "Advanced Beam Dynamics Experiments with the SPARC High Brightness Photoinjector", IPAC 10, Kyoto , Japan

[2] P. Oliva *et al*, Nucl.Instr.Meth. A615 (2010) 93-99

[3] K. Flottmann, http://www.desy.de/~mpyflo/

[4] K. R. Crandall, D. P. Rusthoi, LA-UR-97-886

[5] Labate, L. *et al*, Radiat.Eff.Def.Solids 165 (2010) 787-793

[6] R. Pompili, in PhD Thesis 2013, www.infn.it/thesis/thesis_dettaglio.php?tid\=8140

[7] Cardarelli, P et al. Journal of Applied Physics, 112, 074908 (2012)

[8] Golosio, B. Applied Physics Letters, 100, 164104 (2012)

[9] V. Petrillo et al. NIMA 693,109-116 (2012)


## Papers


C. Vaccarezza *et al*., IPAC 15, Dresda, Germany

**ODRI2D: Achievements in 2014**

E. Chiadroni (Resp. Locale), M. Castellano (Ass.),
D. Di Giovenale (Tecnologo), G. Gatti (Ric.), R. Pompili (Assegnista)

ODRI2D (Optical Diffraction Radiation Interference in 2-dimensions) is the natural continuation of the ODRI one, performed at FLASH (DESY) in the past, which allows for the first time the totally non-intercepting measurement of the normalized transverse emittance [1].

When a charged particle passes through the aperture on a boundary between two media with different refraction indices, diffraction radiation (DR) is emitted both into the forward and backward direction. DR is emitted only when the extension of the transverse electromagnetic field, at given wavelength and beam energy, is larger than the aperture size. Since the beam passes through a hole, DR provides a non-intercepting diagnostics tool, and is therefore well suited for measuring parameters of high charge density beams in a parasitic way. In the traditional DR-based diagnostics, the DR angular distribution which is emitted when a charged particle beam passes a single slit aperture is detected. For ODRI measurements, an additional slit aperture with different size has been used (see Fig. 1).

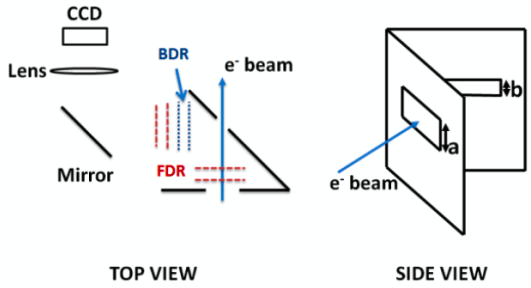


Figure 1: Experimental Setup.

The distance between the two screens is shorter than the radiation formation length such that the ODR emitted in the forward direction at the first slit (FDR) interferes with the backward radiation produced at the second slit (BDR), resulting in measurable angular intensity distribution which is recorded with a conventional optical system.

Different slit apertures are required in order to avoid signal cancellation due to destructive interference between the emitted fields. The interference pattern contains valuable information of the beam parameters: transverse size, angular divergence and relative position inside the slits can be retrieved from it. When using a single slit setup, it is not possible to distinguish the influence of beam size and beam position inside the slit, and a complementary diagnostics is needed in order to separate both contributions. We have demonstrated that this is not the case when using ODRI with non-collinear slits. This is an important difference because in our case we do not need any additional diagnostics to retrieve the beam position inside the slit, and also the contribution of beam position and beam size to the angular distribution are separated from each other.

In our experiment at the FLASH by-pass line, the ODRI angular distribution has been used for the first time to measure the transverse emittance in a non-intercepting way. The ODRI measurements were compared with measurements performed using standard intercepting OTR imaging technique, showing an excellent agreement [1].

Optical Diffraction Radiation Interference has been demonstrated to be a valuable tool for measuring the emittance with a completely not intercepting device in the vertical plane. This is a crucial point for high brightness, high repetition rate accelerators, where the usual intercepting diagnostics cannot be used.

The ODRI2D experiment consisting of a new improved experimental station, made of two sets of slits, has been installed at the end of the FLASH2 electron beam line, downstream of the undulators (Fig. 2), in order to measure the emittances both horizontally and vertically. The main goal of the ODRI2D experiment is to demonstrate that Optical Diffraction Radiation Interference is a useful tool for measuring emittances in both planes at the same position.

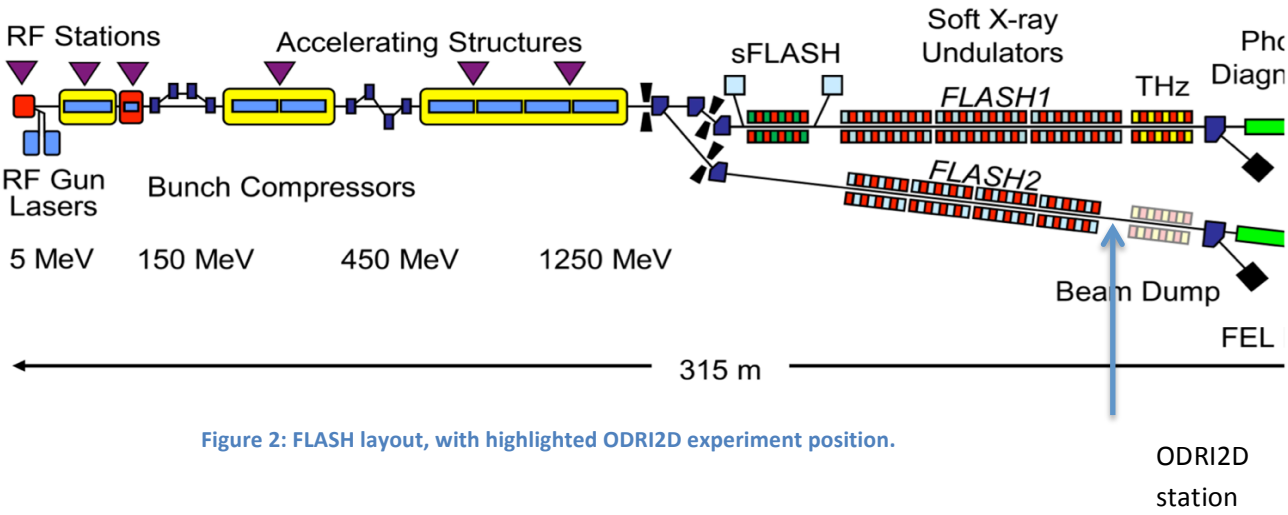


Figure 2: FLASH layout, with highlighted ODRI2D experiment position.

During the first tests in November 2014, we successfully commissioned the new hardware, and by using a standard camera we measured the beam size and the emittance at the location of our experiment as well as checked the consistency between measurements and simulations. For the actual measurements, we will install a sophisticated optical system, equipped with several lenses, interferential filters and high quantum efficiency CCD. In addition, we performed beam dynamics studies in order to test the beam transport up to the OTRFL2BURN and compare it with simulation. The beam transport has been optimized at about 1 GeV, with 300 pC bunch charge.

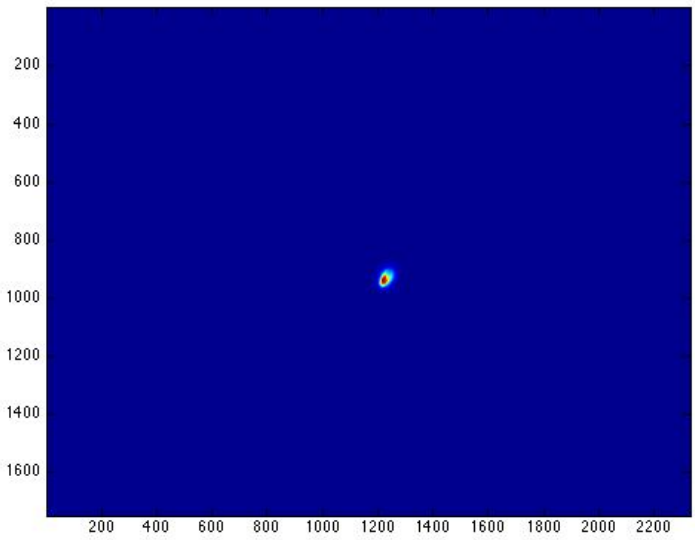


Figure 3: Optimized beam at the OTRFL2BURN: 990 MeV, 300 pC, 1 bunch, less than 100 um rms transverse size.

Normalized transverse emittance has been measured both by standard quadrupole scan at the ODRI2D station and by the DESY tool in the seed section. Analysis is ongoing in order to validate both models.

[1] A. Cianchi et al., PHYSICAL REVIEW SPECIAL TOPICS - ACCELERATORS AND BEAMS 14, 102803 (2011)

# RDH

E. Spiriti (Resp.)

Not received

# SL-COMB

M. Ferrario (Resp.)

Not received

SL_EXIN

Anania Maria Pia, Del Franco Mario, Di Giovenale Domenico, Di Pirro Giampiero, Gallo Alessandro, Ghigo Andrea, Vaccarezza Cristina, Villa Fabio

At the SPARC LAB facility [1] of INFN-LNF we are installing two transport lines for ultra-short electron bunches and an ultra-intense laser pulses, generated by the SPARC photo-injector and by the FLAME laser in a synchronized fashion at the tens of fs level, to co-propagate inside a hydrogen filled glass capillary, in order to perform acceleration of the electron bunch by a plasma wave driven by the laser pulse. The main aim of this experiment is to demonstrate that a high brightness electron beam can be accelerated by a plasma wave without any significant degradation of its quality. A 5 – 30 pC electron bunch, with an energy between 70-110 ME with 30-40 fs long is produced by SPARC and transported to injection into the capillary, which is 100 micron wide, at a gas density around $10^{17}$ $cm^{-3}$ . The laser pulse, 25 fs long, focused down to 65 microns into the capillary is injected ahead of the bunch, drives a weakly non-linear plasma wave with wavelength of about 130 microns. A proper phasing of the two pulses allows acceleration of electrons from the injection energy of 150 MeV up to about 570 MeV for a 8 cm long capillary.

In the last year we have defined the interaction chamber, it is in advanced acquisition and testing stage.fig.1

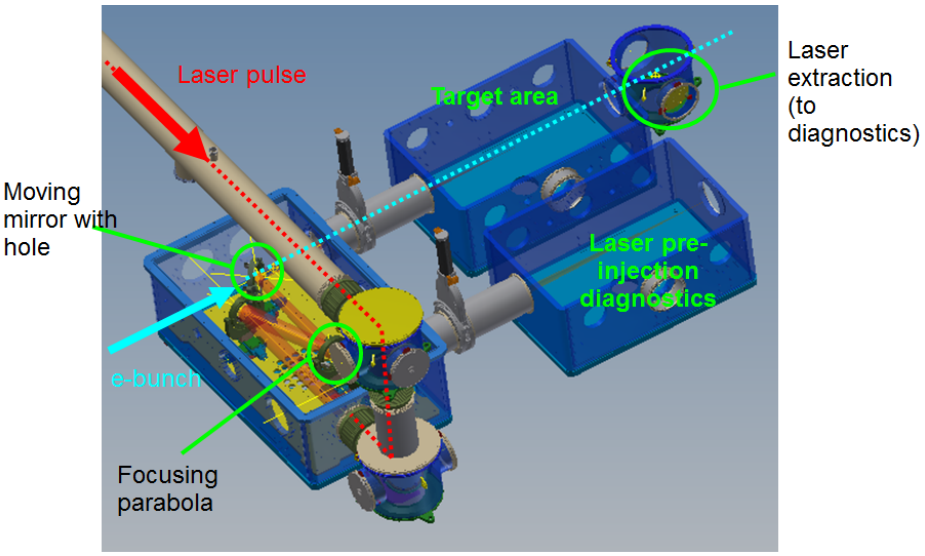


Fig.1 Interaction chamber

Installation is scheduled from October and commissioning within the current year.

Another important element necessary to the success of the experiment is completed the system synchronization between the accelerator and the Laser FLAME.

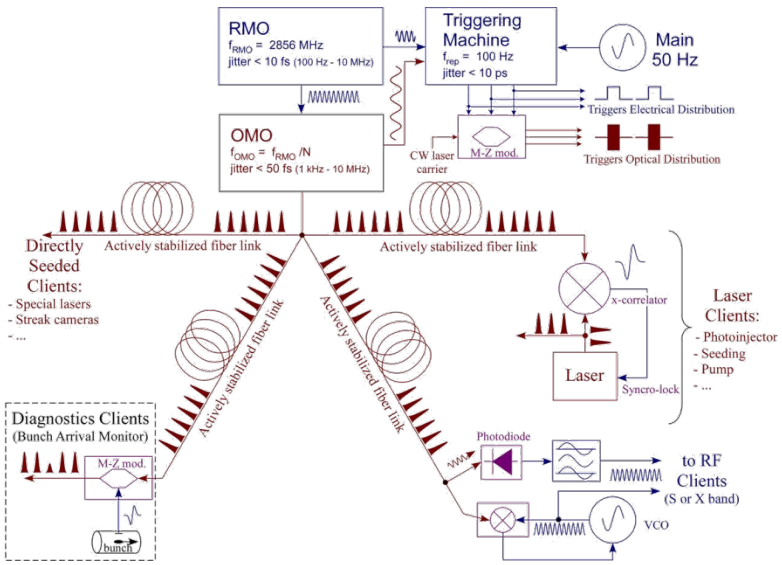


Fig.2 Typical Optcal Synchronization

The system is based on a typical optical synchronization system, this system is installed and in the test phase in SPARC.

Reference

[1] “SPARC_LAB present and future” M. Ferrario,etal.,Nuc.Instrum.MethodsPhys.Res.B309(2013)183.

**SL_Femtotera: Achievements in 2014**

E. Chiadroni (Resp. Locale), M. Cestelli Guidi (Art. 23), M. Daniele (Dottoranda), A. Nucara (Ass.), G. Gatti,
C. Ronsivalle (Ass.)

The experiment called SL_Femtotera aims at the characterization of advanced THz sources, broad-band (0.15-5 THz) and narrow-band, featuring high peak and fs pulse duration, as both linac and laser based.

The linac-based THz source is produced at SPARC_LAB through radiative phenomena based on relativistic electron bunches as short as 100 fs, produced and manipulated at the SPARC high brightness photo-injector.

Taking advantage of the advanced electron beam manipulation techniques, well-established at SPARC_LAB, both broadband and quasi-narrow band THz radiation is produced for several purposes, e.g. as electron beam longitudinal diagnostics, linear and non-linear spectroscopic applications thanks to the high electric (MV/cm) and magnetic (0.5 T) fields associated to the SPARC THz radiation.

The activity in 2014 was focused on the generation and characterization of high intensity THz radiation pulses from the SPARC high brightness electron beams, mainly dedicated to user's experiments. We succeeded to produce ultra-short, down to 100 fs, THz pulses with up to 40 uJ energy per pulse, corresponding to a peak electric fields of 1.6 MV/cm at the THz focus.

The first experiment using the THz radiation produced at SPARC_LAB has been performed to study non-linear electrodynamics properties on topological insulators, such as $Bi_2Se_3$.

The experimental apparatus used to investigate the THz properties of $Bi_2Se_3$ TI is shown in Fig.1.

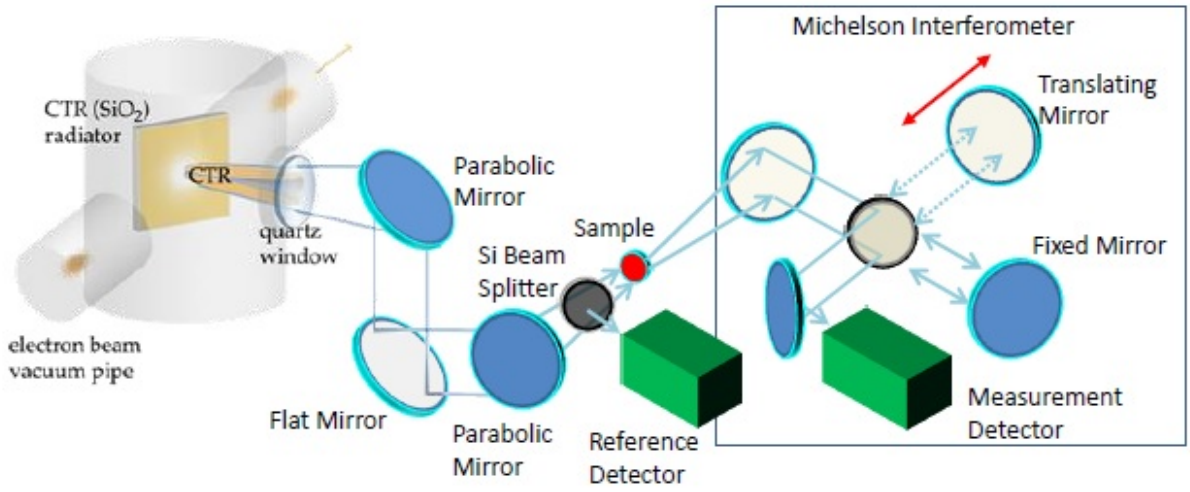


**Figure 1: Cartoon of the experimental apparatus: The CTR THz radiation extracted through the z-cut quartz window is focalized onto the sample by means of off-axis parabolic mirrors, and the spectrum measured by a Michelson interferometer.**

A strong reduction of the absorption of $Bi_2Se_3$ has been observed for the first time increasing the THz electric field from few kV/m up to 1.6 MV/m onto the sample, which determined an electromagnetic induced transparency in the material, as reported in Fig.2.

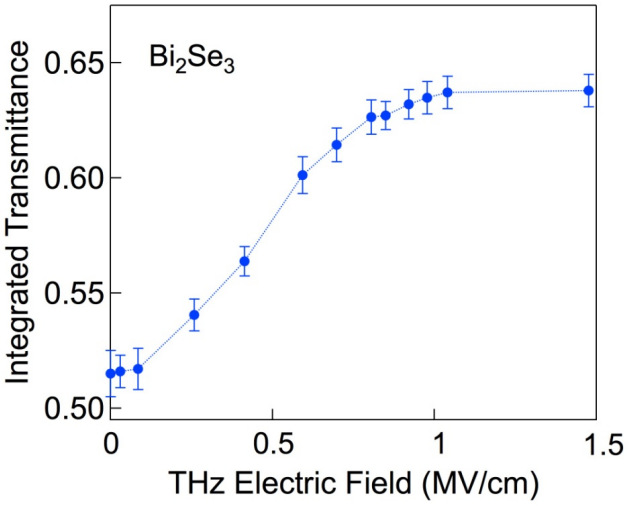


**Figure 2: Integrated transmittance through the $Bi_2Se_3$ as function of the THz electric field. In the region below few kV/m, the transmitted signal does not depend on the electric field, therefore the optical response of the $Bi_2Se_3$ is linear. As the electric field increases the transmitted signal increases of about 25%, showing an induced transparency due to the non linear response.**

The properties of coherent radiation, both transition and diffraction, have been also investigated in the near field through a pyro-sensors THz camera.

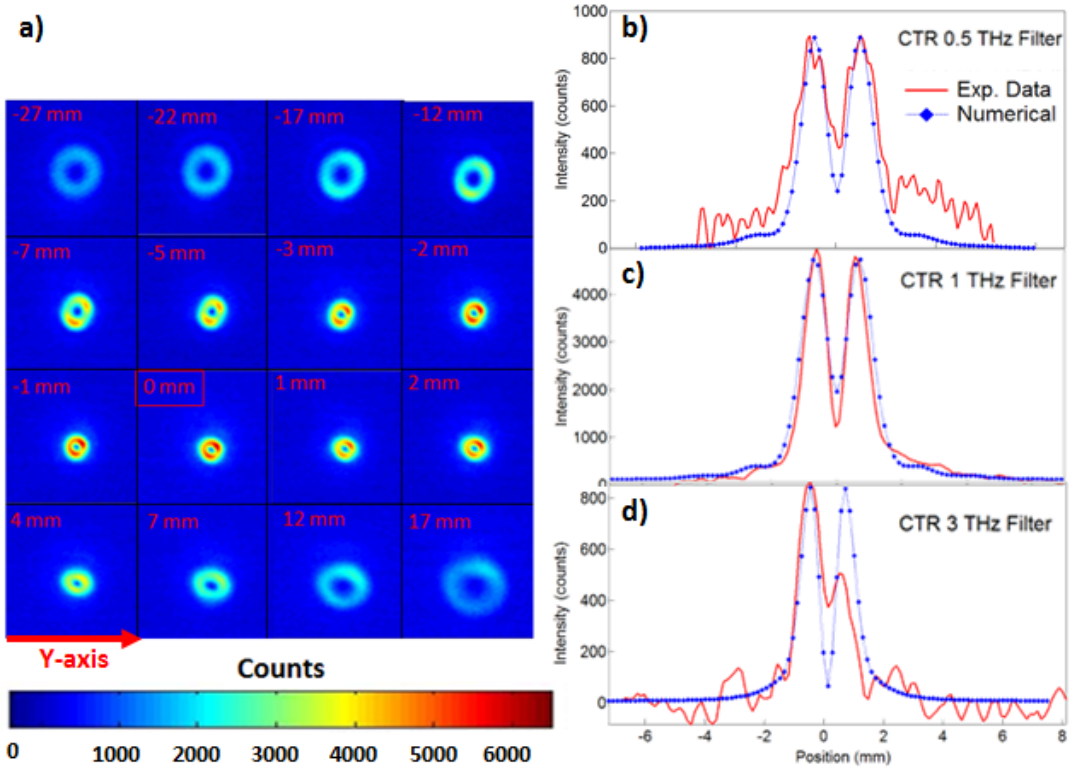


**Figure 3:** Coherent transition radiation transverse distribution in the focal plane: a) Spatial distribution of the source with a 1 THz filter at different distances from the focal plane (0 mm). Each frame has a dimension of 12x12 mm; b), c), d) Experimental data (red lines) and numerical calculation (blue dotted lines) of transverse profile at respectively 0.5, 1 and 3 THz on focus. Numerical curves have been normalized.

In Fig. 3a the CTR peculiar annular distribution at 1 THz is reported as function of the distance from the focal plane of the off-axis parabolic mirror. Each image has a dimension of 12 x 12 mm.

The vertical component of the spatial distribution in the focal plane at 0.5, 1 and 3 THz is shown

in Fig. 3b), c), d) respectively. An overall reduction of the intensity at 3 THz with respect to 1 THz is observable, depending on the high frequency cut-off given by longitudinal bunch size. At 0.5 THz instead the intensity reduction might be due to both a reduction of sensor sensitivity of the THz camera and the low frequency cut-off introduced by the finite target size. The spatial transverse asymmetry at 3 THz might be due to optical misalignment, which affects mainly the high frequency. The experimental data have been compared with numerical calculation, blue dotted lines in Fig. 3b), c), d). Peaks position and width are in agreement with experimental data, while their intensity is normalized to experimental values.

These achieved features not only demonstrate the high intensity, high quality of the SPARC_LAB THz source, but make it also of great interest for a wide range of applications.

# DAΦNE

*The DAΦNE Team*

D.Alesini, M.E.Biagini, M.Boscolo, B.Buonomo, S.Cantarella (Art. 23), A.De Santis (Art. 23), G.O.Delle Monache, A.Drago, L.Foggetta (Art. 23), O.Frasciello (Ph.D stud), A.Gallo, A.Ghigo, F.Guatieri (Bors.), S.Guiducci, C.Ligi, G.Mazzitelli, C.Milardi (Resp.),L.Pellegrino, R.Ricci, U.Rotundo, C.Sanelli, M.Serio, A.Stecchi, A.Stella, M.Zobov [INFN/LNF]
S.Bini, R.Gargana, A.Michelotti [Cabibbo Lab & INFN/LNF]

*The DAΦNE Technical Staff*

G.Baldini, P.Baldini, A.Battisti, A.Beatrici, M.Belli, B.Bolli, L.Cacciotti, F.Casarin Calenda (art.15), G.Ceccarelli, R.Ceccarelli, A.Cecchinelli, S.Ceravolo, P.Chimenti (Ass.), P.Ciuffetti, R.Clementi, O.Coiro, S.De Biase, M.De Giorgi, R.Di Raddo, G.Ermini, M.R.Ferrazza, G.Fontana, U.Frasacco, C.Fusco, F.Galletti, E.Gaspari, M.Giabbai, O.Giacinti, F.Iungo, V.Lollo, M.Marchetti, C.Marini, S.Martelli(art.15), M.Martinelli, A.Mazzenga, C.Mencarelli, M.Monteduro, M.Paris, E.Passarelli, S.Pella, D.Pellegrini, G.Piermarini, S.Quaglia, M.Rondinelli, L.A.Rossi(art.15), M.Sardone, M.Scampati, G.Sensolini, R.Sorchetti, A.Sorgi, M.Sperati, A.Sprecacenere, S.Strabioli(art.15), R.Tonus, T.Tranquilli, M.Troiani, V.Valtriani, R.Zarlenga, A.Zolla.

*International Collaborations*

M.Tobiyama (KEK, Tsukuba, Japan), D.Shatilov (BINP, Novosibirsk, Russia), A.Valischev (FermiLab, USA).

## 1 DAΦNE activities during 2014

The activities on the DAΦNE collider in the 2014 would have been completely dedicated to ensure the largest possible up-time during the KLOE-2 physics run. Nevertheless periods of machine shutdown have been caused by multiple problems:

- in January (first 2 weeks) to install skew CHV correctors in the positron ring (scheduled);
- in January (last 2 weeks) for LINAC cabling refresh (not scheduled);
- after the first decade of February until the end of March for the well known problem to the aqueduct of Grottaferrata and ENEA/LNF causing the stop of the water flow for both industrial and hygienic purposes;
- again for the water flow stop at the end of April/begin of May (~10 days);
- since May/14-th until June/11-th for cooling system maintenance, cryogenic system fault, and electric power external fault and limitation;
- in July for a week for cryogenic plant fault and vacuum loss on positron ring;
- in August for the scheduled shutdown;
- from end of August until begin of November for cryogenic plant fault;
- in November for electric blackout (few days);
- in last decade of December for LNF shutdown.

All these periods of forced inactivity do not have allowed to produce the integrated luminosity as foreseen even if some interesting result has been achieved. Indeed there is a clear evidence of a substantial continuous progress in the collider performances:

a) the instantaneous luminosity is now the highest ever achieved by DAΦNE in operations with an experimental apparatus including high field detector solenoid.

b) The limiting factors have been well understood and still many parameters can be ameliorated to further improve the collider performances.

c) The first KLOE-2 data-taking tests have been successfully done and a plan has been done for the data taking.

d) Some criticalities affecting specific subsystems have been cured during the summer shut-down.

e) Concerning up-time and reliability of the DAΦNE subsystems we hope to be on the verge of inverting the negative trend, which requires a lot of efforts, quite long time and a proper framework.

## 2 Main updates and achievements during 2014

The Interaction Region has had useful structural modifications. First of all a pair of carbon fiber composite legs have been added to the existing ones. As second point some rubber pads previously inserted below the cradle support have been removed, thus strengthening the structure and increasing its rigidity.
After this operation, the spectrum of a previously observed vertical beam oscillation got modified. The main harmonic was shifted toward higher frequencies, ~15 HZ, and its amplitude reduced by a factor four.
Moreover the spherical vacuum chamber was suffering of heating problem affecting the low-ß defocusing quadrupole downstream (e- beam) that have been fixed giving more stability to the working point during operations. Moreover new BPMs in this area allow more accurate beams overlap and transverse betatron coupling studies.
The commissioning of the linear optics started mainly by the end of January 2014, but it has been severely slowed down by the 3 main interruptions due to the external circumstances causing, in total, more than five months of inactivity.
The working points adopted are Qx-=5.098, Qy-=5.164, Qx+=5.102, Qy+=5.139.
According to LIFETRAC simulations they should provide good luminosity.
The transverse betatatron coupling with all skew quadrupoles off is ~0.4% for the positrons and ~0.6% for the electrons. This value is not yet optimal. Tuning the skew quadrupoles we achieved a value between 0.2% and 0.3% for both beams.
Dynamic apertures have been simulated by using a new tool (MADX + LIFETRACK) developed for HL-LHC and tested with the DAΦNE optics.
Considering the beam dynamics the highest currents stored, so far, are 1.85A for the electrons and 1.2A for positrons both in 98 bunches. These currents are the highest ever achieved after installing the new IR for the KLOE2 detector, based on the Crab-Waist collision scheme.
The three independent bunch-by-bunch feedback systems installed on each ring are essential for high current multi-bunch operations. The e+ vertical feedback is now using a new ultra-low noise front-end module, designed in collaboration with the SuperKEKB feedback team, aimed at reducing the noise contribution to the transverse vertical beam size in collision. An identical module is ready for the electron vertical feedback.
The beam dynamics in the e+ ring is clearly dominated by the e-cloud inducing transverse instabilities which are kept under control by:

- powerful bunch-by-bunch transverse feedback systems;
- solenoids wound all around the straight sections;
- electrodes installed inside dipole and wiggler vacuum chambers.

Electrodes effectiveness has been already proved in 2012 polarizing the stripline with a *positive* voltage in the range 0÷250V. Simulations indicate that a factor two higher voltage is required to completely neutralize the e-cloud density due to an e+ current of the order of 1A. The electrode power supplies have been replaced with devices providing a maximum *negative* voltage of 500V. The change of polarity was intended to limit the current delivered by the power supplies, nevertheless three of the twelve power supplies are not working. These are the power supplies for the striplines located in the wiggler magnets where the parasitic clouds are denser. The e-cloud induced effects have been also mitigated by lengthening the bunch by reducing the RF cavity voltage. An important and measured effect of e-cloud is also the betatron tune spread of the e+ beam limiting the luminosity performances as shown by simulations.
The peak luminosity has touched 1.8x10^32cm-2s-1 (see Fig.1) exceeding by a 13% the best luminosity ever achieved, at DAΦNE, during operations for an experimental apparatus including high field detector solenoid. The background presently has been reduced to levels almost compatible with the KLOE detector data taking. The Crab-Waist sextupoles effectiveness has been proved on the e+ ring. The strengths are 30% and 50% lower than the nominal ones for e+ and e- respectively.
Storing a test pattern of contiguous 10 bunches, the peak luminosity has achieved ~2.5x10^31cm-2s-1, demonstrating that ~2.5x10^32 cm-2 s-1 might be

achieved by using 100 bunches if the e-cloud effects can be controlled at the best (e+ beam) and the dynamical vacuum will be optimized (for both rings). Nevertheless vertical enlargement due to high currents coherent instabilities like microwave instability could still be a limiting factor to achieve the best peak luminosity.

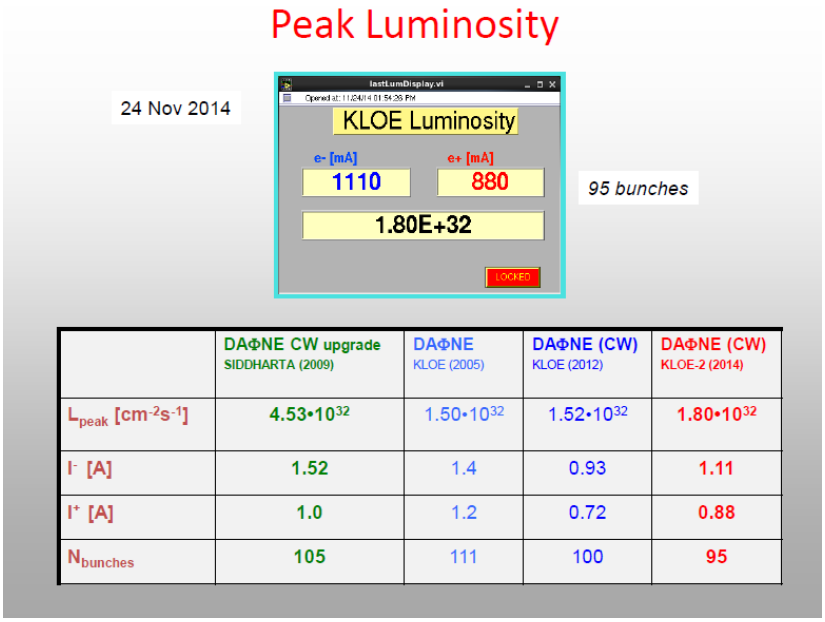


| | DAΦNE CW upgrade SIDDHARTA (2009) | DAΦNE KLOE (2005) | DAΦNE (CW) KLOE (2012) | DAΦNE (CW) KLOE-2 (2014) |
|---|---|---|---|---|
| $L_{peak}$ [$cm^{-2}s^{-1}$] | $4.53 \cdot 10^{32}$ | $1.50 \cdot 10^{32}$ | $1.52 \cdot 10^{32}$ | $1.80 \cdot 10^{32}$ |
| $I^-$ [A] | 1.52 | 1.4 | 0.93 | 1.11 |
| $I^+$ [A] | 1.0 | 1.2 | 0.72 | 0.88 |
| $N_{bunches}$ | 105 | 111 | 100 | 95 |

Fig.1 – Peak luminosity achieved in the past and present runs.

In conclusion the best integrated luminosity per hour was 485 nb-1 that extrapolated to 24h give a daily integrated luminosity for KLOE of 11 pb-1. Integrated luminosity trend in the last 30 days of 2014 is in Fig.2 where the dotted line shows what is the goal in the next months for KLOE.

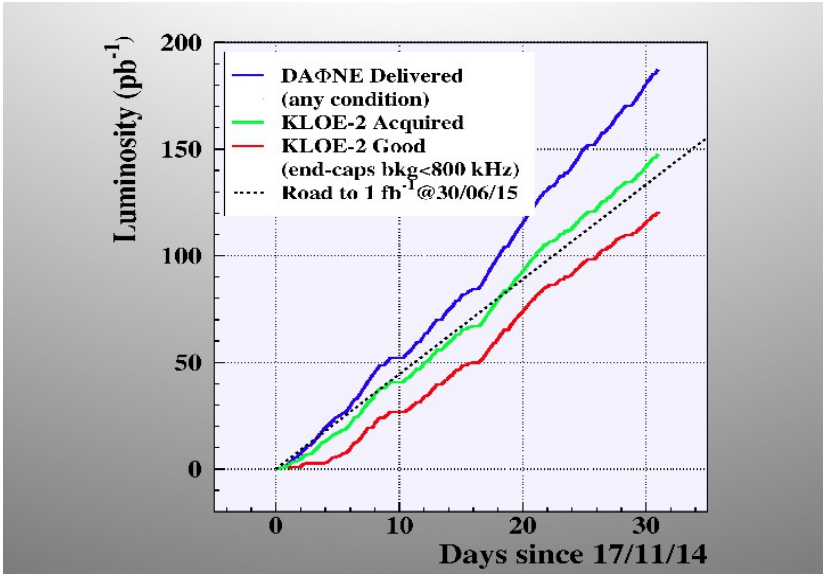


Fig.2 – Integrated luminosity acquisition rate in the last 30 days of 2014. Dotted line shows the rate required to accumulate 1fb-1 by the end of June 2015.

## 2014 Reference

C. Milardi, et al., "DAΦNE General Consolidation and Upgrade". Proc. Of IPAC'14, Dresden, Germany.

A. De Santis, et al.,"DAΦNE Transfer Line for KLOE-2 Physics Run". Proc. Of IPAC'14, Dresden, Germany.

C. Milardi, et al., "DAΦNE Operation with the Upgraded KLOE-2 Detector". Proc. Of IPAC'14, Dresden, Germany.

# BTF

P. Valente (Ass., Resp.), B. Buonomo, L. Foggetta (art. 23)

In collaboration with DAΦNE LINAC:

M. Belli, R. Ceccarelli A. Cecchinelli, R. Clementi, M. Martinelli, G. Piermarini, S. Strabioli, L.A. Rossi and R. Zarlenga

The BTF provides electron and positron beams since 2002. Since 2004 the operation of the facility in parallel with the DAΦNE collider is possible. Since 2008 the installation of a dedicated pulsed magnet allows running in a completely parasitic mode also during DAΦNE injections. Beam time is usually allocated in slots of one week, from Monday to Monday, with a few hours of overlap for installation and de-installation, as well as BTF quick maintenance, clean up and routine checks (especially for safety purposes). Beam is provided 24/7, thanks to the DAFNE shift crew, managing the LINAC and collider experiments, as well as BTF and Synchrotron light facilities. In the last years the BTF user access has been, on average, 220 days/year. Considering short machine development periods and the usual summer shutdown, in 2014 BTF has delivered 261 beam-days (including three shifts in co-user) [7-12].

In May 2014, the first BTF Users Workshop [1] took place at LNF, with the participation of more than 30 experimental groups, with several presentations on the results – mainly obtained in the previous two or three years – and with one session dedicated to future developments and upgrades of the facility. The discussions were very lively and interesting, especially from the point of view of improving the quality of the facility, in order to match as much as possible the users needs.

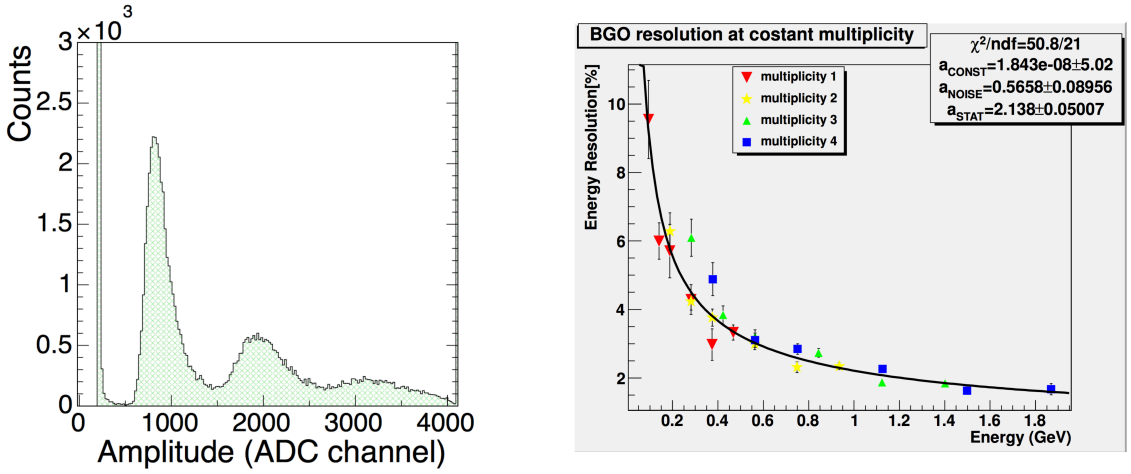


***Figure**: Example of single electron tests: MCP readout of scintillator planes at 491 MeV, from Ref. [10], i-MCP group (left); energy resolution vs. energy of BTF beam of BGO calorimeter, from Ref. [8], BGO-OD collaboration.*

Also a very interesting new proposal came up, for a new experimental research activity using the BTF extraction line and the LINAC positron/electron beam for dark matter searches, in particular the so-called hidden or dark photon (vector portal) [2]. This class of experiments are essentially electron/positron fixed target set-ups, thus posing new requirements for the beam, in particular modulating and controlling the BTF pulse length both in low and high intensity phase.

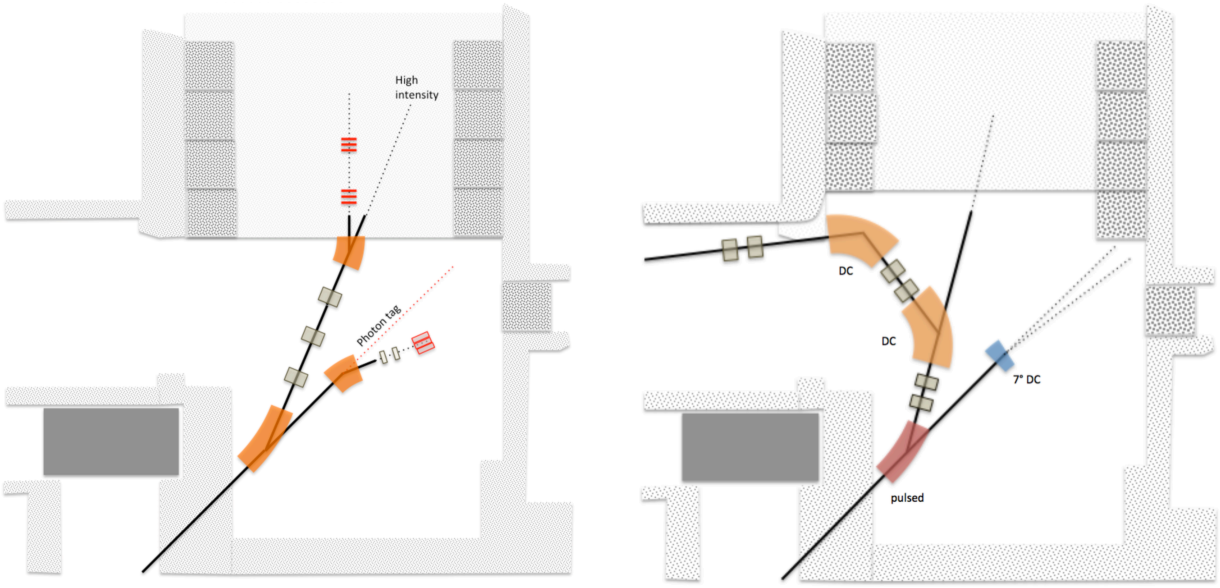


***Figure**: Two possible layouts for the doubling of the BTF beam line [3].*

For the main task of providing beam for HEP and astro-particle detector testing several possible improvements have been identified [3]: increasing the LINAC energy, increasing the repetition rate, doubling the BTF extraction lines, new optics setup and a new BTF hall, are few examples of the options under study. Finally, the good results with the R&D activities on the neutron photo-production target [4], suggested to step from the study phase, to the implementation of a real facility, in connection with the increase of the beam intensity and radio-protection assessment. Part of this upgrade has been presented in the framework of the AIDA-2020 project, submitted in Horizon 2020 European Commission funding.

It is worth mentioning that in the last year also some foreign institutions (international and European) asked to BTF staff to show the entire BTF system layout in order to have possibility for developing BTF-like infrastructures, in particular collaborations with LAL, Orsay and SLRI, Thailand [5], have been started.

In order to achieve a better beam stability of the primary LINAC delivered beam, the BTF and LINAC groups have performed a number of activities, in particular a new LINAC gun hardware has been deployed allowing to tune the beam pulse width from 1.5 to 40 ns in 0.5 ns steps (when not running in parallel with injections).

## BTF facility improvements and upgrades:

A number of improvements and modifications were performed in order to have better customizable services and easier user experience with the BTF beam(s):

- **Gas system**: the gas lines in the BTF area have been upgraded and fully tested. Now four different gas lines are fully operational: low pressure hydrocarbons, high pressure hydrocarbons, two lines for $CO_2$/Ar/N/He and similar gases. An additional inert gas line is also planned. Dried compressed air pipes to manage actuator from BTF control room were also installed.

- **BTF beam conditioning/magnet system:** The DHPTB101 pulsed magnet and the BTF scrapers were subject to a thorough maintenance due to aging of the electronics. The last scrapers software was perfectly integrated in a very stable configuration in the virtual machine BTF subsystem. A new C-shaped magnet has been installed at the neutron target exit in order to sweep charged particles from the neutron flight path.

- **BTF Cooling system:** The BTF cooling sub-system was linked with the LINAC one, thus allowing a continuous operation even in case of DAFNE shut-down. This strategy was extremely important in assuring beam time in 2014, since the DAFNE complex suffered a long down-time due to exceptionally bad weather conditions, in particular several long stoppages of the main water supply from the local aqueduct. The existing strong collaboration and common activities with the LINAC staff also was fundamental to minimize the BTF down-time to a couple of weeks.

- **Vacuum system**: The BTF pipes operate to LINAC-Transfer lines vacuum, i.e. down to ~$10^{-10}$ mbar. The vacuum pipe ends with 500 μm-thick Be flange in order to minimize the multiple scattering. The overall BTF vacuum is provided via 60-120 l/s ion pumps. In order to connect to the users experimental vacuum, we design the pipe-end with internal gating valves equipped with pre-vacuum service for different line extensions, We also built some mylar windows for a level of pre-vacuum of $10^{-6}$ mbar. The pumping system was also improved and now we are able to get a stable value of (average) $2\times10^{-9}$ mbar on all the sections of the BTF vacuum pipes. A new passive protection system for the thin vacuum exit window of the bent line has been designed in order to house the wall current monitor (WCM) detector as well as protecting the ceramic pipe and the Beryllium window with a removable polycarbonate window spacer. Finally, all of the BTF vacuum subsystem has been moved under the control of the DAFNE vacuum supervisor program.

## Detector, diagnostic, scientific instrumentation and DAQ improvements:

A complete new design of the BTF networking service offered to the users has been performed, in accordance to the recent developing of the DAFNE network service:

- The serial bus-controlled apparatus (I.e. BTF scrapers, HVGEM CANBUS, remote trolley table and others) have been migrated to a MOXA serial to Ethernet switches in order to standardize, via serial virtualization, the basic BTF slow control low-level communications.

- Network switches and wireless access point has been improved and access to a BTF VLAN is now offered to non-LNF/INFN users. A BTF-dedicated DHCP server has been implemented.

- After having fixed these hardware development steps, we have migrated the software in a virtual machine environment in order to strengthen the reliability of the software services needed by the BTF equipment and the ones given to the users for BTF beam run-time control.

- The DELL based virtual machine subsystem (VMS) improved the efficiency of all BTF systems, also allowing some software development during the users run-time in a common environment.

- A BTF live data collecting system has been developed in conjunction with the DAFNE control system upgrades. It is based in MEMCACHED technology with a dead time completely negligible in comparison with loop time of BTF asynchronous data chunk repetition rate.

- It has been implemented a complete redundancy on BTF DAQ boards, VMIC control machine and crates.

- User-friendly BTF PTU environmental sensors have been implemented, providing temperature, humidity and pressure in real time, very useful information for detector calibration purposes.

The BTF data format has been completely revised, maintaining the DAQ modular flexibility, with a substantial improvement of timing issues (especially synchronization problems with users DAQ systems). The BTF data acquisition is working in a very straightforward and stable way, collecting and displaying data to the users via the DAFNE slow control environment. The data caching of BTF-DAQ has been doubled also on the BTF MEMCACHED server in order to permit a full collection of BTF data sources. Some improvement to the BTF-DAQ code and bug fixing allowed to stably run the system at the full LINAC repetition rate. The overall system stability is assured by the BTF internal network, that reached a very good stable configuration even if the weekly stress due to different users requirements.

The assembly and test of GEM service elements (gas system, electronics, installation systems) has been performed. The installation and test of the new software, design and implementation of a hand manageable fixed installation of the operative TPC GEM support has been completed.

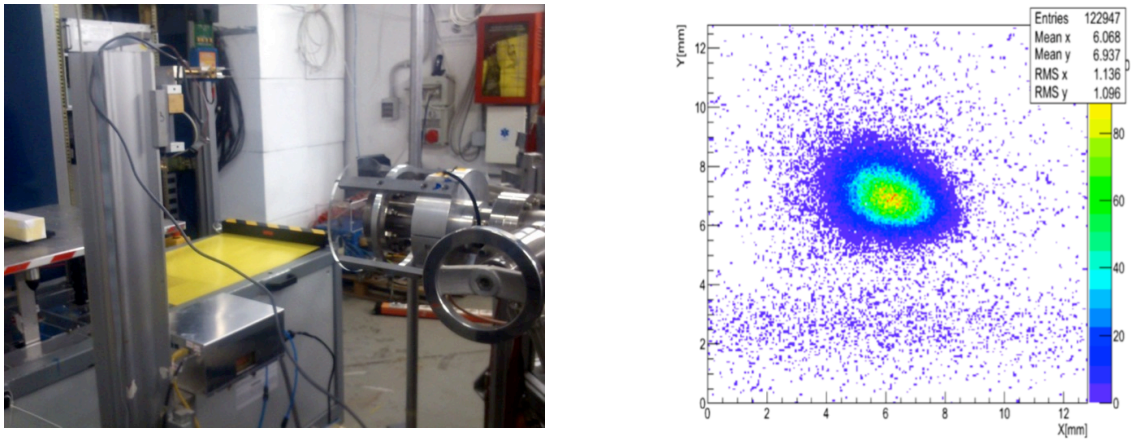


***Figure**: Left: the mechanical support on the left of the photograph holds both the TIMEPIX (top) and GEM TPC (bottom), that can be put alternatively on the BTF beam line; Right: Typical beam spot reconstructed by the TIMEPIX detector.*

The GEM detectors are now completely integrated in the BTF data caching, timing and virtual machine subsystem with newly private gas pipes for gas supply. A easy automated calibration software has been developed to improve detectors reliability. A resolution in the direction of the drift of 120 $\mu$m has been measured and the detector was the main tool for low-energy positron channelling experiments [6].

In order to accomplish the user need for a fast silicon transverse beam imaging, a TIMEPIX® detector with BLUEbox has been integrated in the BTF timing and virtual machine sub-systems and is now available to the users for fast beam transverse diagnostics purposes. TIMEPIX® has a square pixel size of *55 μm* side length in a 256×256 pixels layout for a square sensitive area of about 2 $cm^2$. The timing feature of TIMEPIX detector easily fit the BTF experimental needs.

## References


[1] First BTF Users Workshop, https://agenda.infn.it/conferenceDisplay.py?confId=7359.

[2] M. Raggi and V. Kozhuharov, Adv. in HEP (2014) 959802.

[3] P. Valente *et al*., Possible upgrades of the DAFNE Beam-Test Facility (BTF), INFN-14-06/LNF.

[4] M. Prata *et al*., Eur. Phys. J. Plus (2014) **129**: 255.

[5] K. Kittimanapun *et al*., https://indico.cern.ch/event/346743/session/2/contribution/10/material/slides/1.pdf

[6] M. Andreotti *et al*., Performance of beamline and infrastructure, Deliverable Report AIDA-D8.9, http://cds.cern.ch/record/1983581.


**Recent users papers:**


[7] R. Carbone *et al*., 2015 *JINST* **10** C03007.

[8] B. Bantes *et al*., Journal of Physics: Conference Series **587** (2015) 012042.

[9] F. Happacher and M. Martini, Commissioning of the new calorimeters of the KLOE-2 experiment, arXiv:1501.05442 [physics.ins-det].

[10] L. Brianza *et al*., Response of microchannel plates to single particles and to electromagnetic showers, arXiv:1504.02728 [physics.ins-det].

[11] F. Burkart et al., IPAC 2014 Proc., THPME172.

[12] R. De Sangro et al., Eur. Phys. J. C (2015) 75:137.

# DAΦNE-Light Laboratory and Activity

M. Angelucci (Ass. Ric.), A. Balerna (Resp.), M. Cestelli Guidi, R. Cimino, A. Grilli (Tecn.), R. Larciprete (Ass.), G. Mohamed (Art. 23), E. Pace (Ass.), M. Pietropaoli (Tecn.), A. Raco (Tecn.), V. Sciarra (Tecn.), V. Tullio (Tecn.), G. Viviani (Tecn.).

## 1 Summary

The scientific activity at the DAΦNE-Light laboratory, in 2014, was performed using conventional sources and for some specific researches, when available, the DAΦNE synchrotron radiation beam. The experimental teams that got access to the DAΦNE-Light laboratory were from Italian Universities and research Institutions, and some of them also from EU countries within the EU CALIPSO project.
The experimental activities, performed in 2014, were also dedicated to some alignments and upgrades of the beamlines, and also to the installation of new instruments.

## 2 Activity

### 2.1 SINBAD - IR beamline

The experimental activity on the SINBAD IR beamline mainly concerns micro-imaging and FTIR (Fourier transform InfraRed) spectroscopy in different research areas, including material science, biology, radiobiology, live cell imaging, cultural heritage and geophysics. All these studies are possible owing to the imaging capabilities of the IR microscope coupled to the synchrotron source. Due to different problems occurred in 2014, the DAΦNE activity has some stops, and researches on the IR beamline were carried out also using conventional sources.
The institutions involved were Italian and the some International teams funded be the EU-FP7 transnational access project CALIPSO. The biological clean chamber laboratory was used to grow cell cultures for some CALIPSO experimental proposals that required sample preparation in situ. Some of the scientific results obtained at the SINBAD-IR beamline are here summarized:

1. *IR and Raman spectroscopy and mapping at DAΦNE-Light: advanced tools to support the rational design of functional nanostructures.*

   *Institute for Complex Systems, National Research Council (ISC-CNR), Rome*

   It is nowadays clear that present developments in the field of nanostructured materials and nanotechnology will have a profound impact in several areas, from energy technologies to biotechnological and medical applications. The current efforts and findings will probably lead to a drastic change of methodologies, analytical instruments and diagnostic tools, and will modify the way we approach the problems of environmental and clinical monitoring, energy storage and tissue engineering, biomarking and drug delivery. In this context, Principal Component Analysis (PCA) applied to spectral mapping constitutes a powerful tool, allowing a rapid and reliable classification of hybrid samples, which is fundamental to improve the design of the nanostructure and to optimize the preparation procedure for the specific application.
   In particular, some results are related to the application of the method to Raman maps of single wall carbon nanotubes (Fig. 1) treated with different fluorescent dyes and different coupling approaches, to verify the efficiency of the functionalization procedure, to compare the effects of various labels, to study the homogeneity of the final sample and to perform

dosing and toxicology studies for bio-imaging and delivery applications. The results, obtained thanks to a fruitful collaboration between DAΦNE-Light, the Institute of Complex Systems at CNR and the Department of Molecular Biotechnology and Health Science of the University of Torino, demonstrates the potentiality of the approach for the rational design of functional nanostructures.

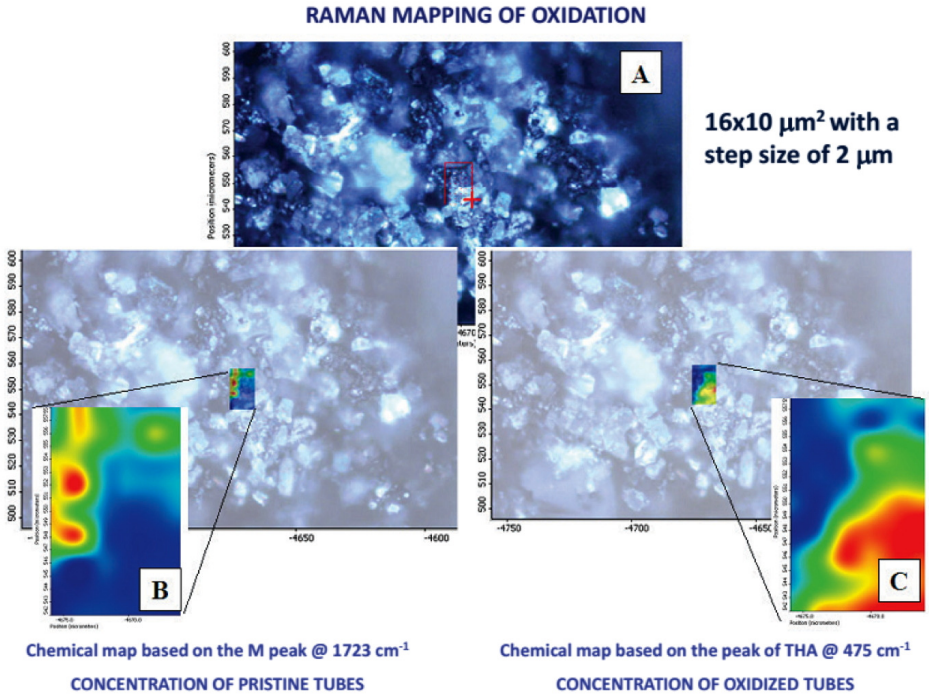


Figure 1: Raman mapping of the oxidation of a CNTs (Carbon NanoTubes) sample to study the homogeneity or compare differently oxidized samples in order to optimize the preparation protocol or to adapt it to specific applications.

2. *Development of novel techniques for in-situ HT-FTIR study of minerals.*

   *University of Roma Tre - Dipartimento di Geologia*

   Many minerals when exposed to high temperatures (HT), loose $H_2O$ or other molecular groups ($CO_2$, $SO_4{}^{2-}$, $CO_3{}^{2-}$, etc.), and may undergo different processes such as phase-transitions or dehydroxylation/decarbonation. In the case of amphiboles (a family of fibrous silicates with general formula $[AB_2C_5T_8O_{22}(OH,F)_2$, where A = Na, K; B = Na, Ca; C = Mg, Fe, Al; T = Si,Al], a loss of structural protons typically occurs coupled to oxidation reactions of $Fe^{2+}$ to $Fe^{3+}$ at the hydroxyl-coordinated sites. In addition, this process has been speculated to be responsible of the increasing electrical conductivity in subducted rocks at convergent margin zones.
   Therefore, a proper definition of the mechanism whereby these common rock-forming minerals behave at high-T is crucial in geophysical studies. In order to study the deprotonation process and its kinetics, several isothermal high-temperature FTIR experiments (Fig. 2) were carried out on selected samples of an almost pure end-member riebeckite

$(Na_2(Fe^{3+})_2(Fe^{2+})_2Si_8O_{22}(OH)_2)$ from Malawi.
An interpretation of such trends, which is still underway being a function of several parameters (time, sample size, structure orientation etc.) will allow to point out the mechanism responsible for the dehydration process, by defining the best fitting equation available in literature. Samples of the rare iron-sulfate hohmannite $(Fe_2[O(SO_4)_2]8H_2O)$ were also analyzed with HT-FTIR; the data obtained, coupled with those coming from in situ HT X-ray powder diffraction, allowed to define the thermal behavior of this notable compound (these minerals are recognized as water carrier on Mars, and are important in industrial processes) and its phase transformations as a function of T.

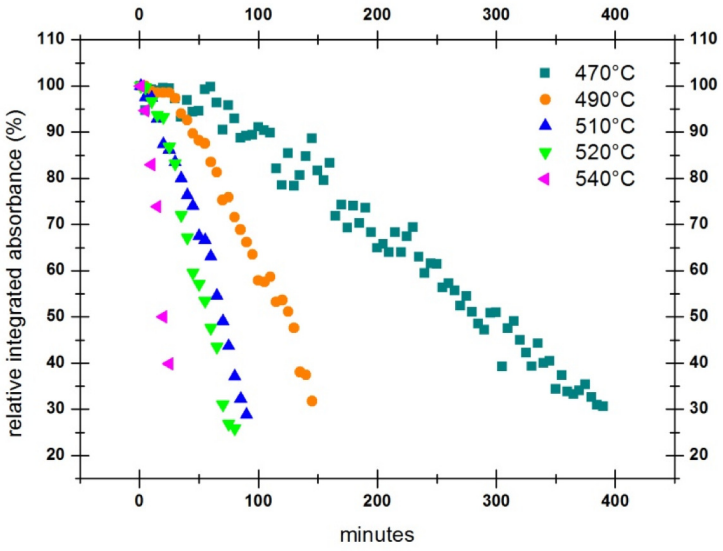


Figure 2: Evolution with time of the OH stretching IR band reported as a function of temperature.

3. *FTIR spectral imaging advances for the detection of degradation products in artwork cross-sections: a multivariate statistical approach to generate high contrast images.*

   *CISTEC University La Sapienza, Dep. Ingegneria Chimica*

   Establishing the distribution of materials and that of their degradation products in historical monuments is fundamental to understand their conservation status. Among the different analytical techniques, FTIR imaging provides information on the molecular composition of the material on a micrometric-scale in a nondestructive way.
   When thin sections of the material are not available for transmission, and when ATR imaging mode is not suitable due to possible damages on the sample surface, FTIR imaging is performed in reflection mode on thick polished, matrix embedded samples.
   Even if many efforts have been done in the optimization of the sample preparation, surface quality is a critical issue that can prevent the achievement of good infrared images. Moreover, spectral artifacts due to volume and surface effects can give ambiguous results in standard data treatment.
   A multivariate statistical data analysis was addressed as an alternative and complementary approach to obtain high contrast FTIR images from reflection spectra. The case study of Septimius Severus's Arch (Fig. 3) is presented to validate the model and to show new per-

spectives for FTIR imaging (Fig. 4) in art conservation.

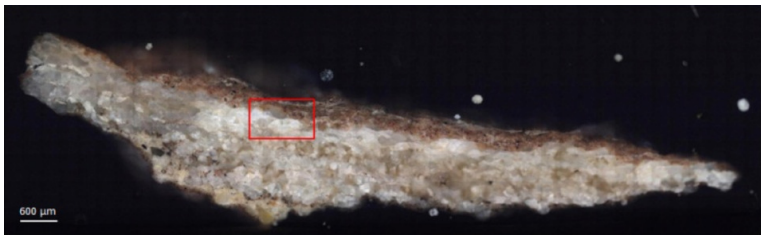


Figure 3: Fragment of Septimius Severus's Arch.

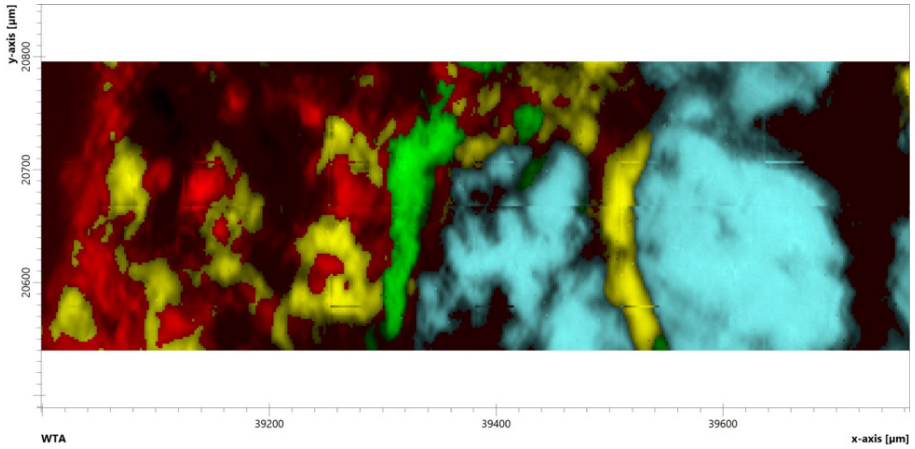


Figure 4: Distribution of four components: oxalate (green); gypsum (yellow); calcite (light blue) and silicates (light red).

4. *Apoptosis Modulation in A549 Lung Cancer Cells investigated by FTIR-Microspectroscopy. University of Bordeaux*

   FTIR microspectroscopy of biological cells and tissues is a rapidly growing area of biomedical research, especially, in cancer research. The technique sheds the brightest light on the dynamics of the molecular contents, and their changes over time. Those signs, of crucial importance for diagnostic and/or therapeutic studies. It has been found useful for detecting single-cells apoptotic changes induced in human lung cancer cells at micron-level resolution. Apoptosis is a preferable way to induce tumor cell death, as it is an alternative path to other toxic chemical or radiative therapeutic approaches. But, depending on the way apoptosis is mediated, the process can be fully efficient or not. FTIR microspectroscopic study at DAΦNE-Light Facility for micron scale analysis of nuclear and cytosolic locations on lung cancer cells with/without the action of a target protein (Calretinin) is running to investigate its role in modulating the cancerous cells apoptosis. This in turn, opens the door to promising drug targets and new therapies. Lung cancer is one of the most common malignant tumors all over the world, and the non-small cell lung cancer (NSCLC) accounts for 80% of all reported cases. A549 cell line was chosen for this study, cell cultures (Fig. 5), and the

cryofixed cellular sets, were prepared at the cell biology Laboratory, and the FTIR image acquisitions and data analysis will be accomplished at SINBAD beamline.
This project is performed in collaboration with the Bordeaux University, and is financially supported through the Transnational Access Activity within the CALIPSO project.

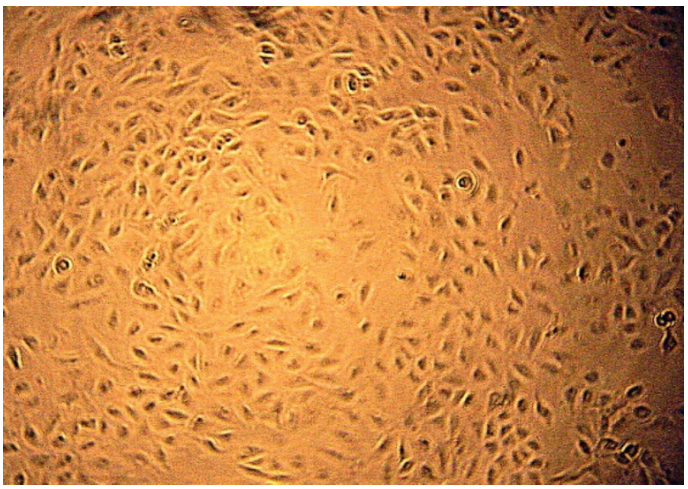

Figure 5: Adherent A549 cell culture micrograph (magnification 20x).

5. *Application of Infrared Spectroscopy as a Probe of Nanostructured Noble Metal Film Morphology.*

   *Czestochowa University of Technology, Poland*

   Disordered arrays of metallic nanostructures are relatively easy to fabricate and can provide remarkable enhancement of EM radiation due to nanoscale plasmonic phenomena. Ultrathin silver films, also known as silver island films, or SIFs, are well-known examples of this materials class. The absorption intensity in ultra-thin nanostructured films depends significantly on the morphological characteristics of the film. IR spectroscopy and electrical impedance spectroscopy are suggested the most appropriate tools to explore the interaction of EM field with the nanostructured noble metal film as a function of morphology and other factors.
   Several milestones were assigned to eventually develop sensitive structures for environmental monitoring, that exploit the Surface Plasmon Resonance effect, and that operate at ambient conditions. Also this research was performed in the framework of the CALIPSO project.

During 2014 a student performed part of her Master Thesis activity at the SINBAD beamline: Deborah Schierano from University of Florence continued her Master Thesis on ″Atmospheres in a test tube″, on the setup of the instrumentation to realize a database of FTIR spectra of gas atmospheres in different pressure and temperature conditions, to be used for comparison with the spectra collected by existing and future space missions.

## 2.2 DXR1 - Soft X-ray Beamline

The DAΦNE soft X-ray beamline, DXR-1, is mainly dedicated to soft X-ray absorption spectroscopy. The X-ray source of this beamline is one of the 6-poles equivalent planar wiggler devices installed on the DAΦNE electron ring (0.51 GeV) for the vertical beam compaction. The 6 wiggler poles and the high storage ring current (higher then 1 Ampere) give a useful X-ray flux for

measurements well beyond ten times the critical energy. The useful soft X-ray energy range is 900 eV - 3000eV where the lower limit is given by the Beryl crystals used in the double-crystal monochromator and the higher limit is given by the wiggler working conditions.
In 2014, when the beam conditions became more stable an alignment of the beamline and of the experimental chamber had to be performed to go back to effective flux values, because as observed also in 2013 the photon flux was quite lower than in the past. In order to control the new working conditions some XANES measurements were performed in the presence of good and stable beam conditions (Fig. 6).

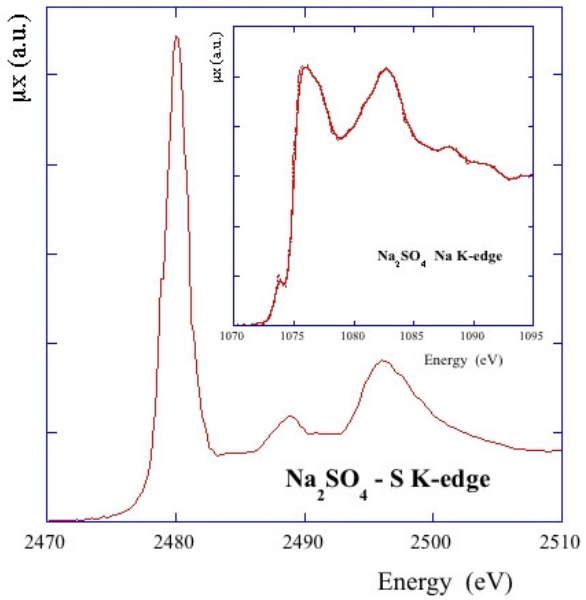


Figure 6: Normalized XANES spectra of a $Na_2SO_4$ sample at the S and Na K-edges.

The soft X-ray beamline was equipped in 2013 with a microfocus W x-ray source to test samples and also to perform X-ray fluorescence (XRF) measurements using the available SDD detector. A vacuum compatible experimental chamber to test samples containing low Z materials has been completed and aligned in 2014. Using this experimental chamber, some XRF tests were performed on nineteenth century optical prisms (study proposed by E. Bernieri (LNF) and INAF Museum) to check differences in their chemical composition. In Fig. 7 the presence, at low energy, of the Si contributions and the big differences between the two prisms are clearly visible. The old flint glass contains a big amount of lead (Pb): this kind of glasses are also known as lead glasses. On the other hand, the old crown glass contains a bigger amount of potassium and calcium oxide.
In 2014 the experimental project ARDESIA (ARray of DEtectors for Synchrotron radIation Applications), for the development of a new detection system for XAFS measurements in fluorescence mode, based on arrays of SDD (Silicon Drift Detector) with high energy resolution and able to handle high count rates, has been approved by the INFN National Scientific Committee V and will start its activity in 2015.

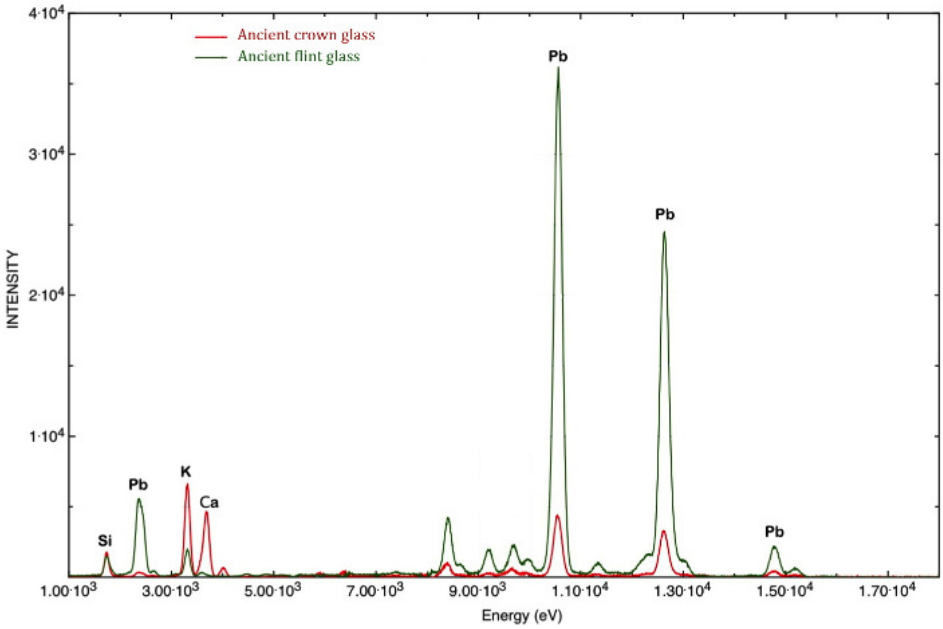


Figure 7: XRF tests on nineteenth century prisms of very old telescopes to control differences in their atomic compositions.

### 2.3 DXR2 -UV branch Line

The DXR2 beamline at DAΦNE- Light operates with UV radiation on an extended spectral range from 120 nm to 650 nm. The UV radiation can be used in a wide range of experiments such as reflectance/transmittance, ageing and response of optical systems and detectors. The UV light has been used at the DXR2 branch-line in many and different research fields from biological to high energy physics experiments, to study solar-blind UV diamond-based detectors or FOAM for space missions. Furthermore, coupling the UV radiation and IR spectroscopy it is possible to study the evolution of analyzed samples in real time, measuring the variation of IR spectra during UV exposure. The facility operates with UV radiation obtained as synchrotron radiation (SR) or standard sources (HgXe lamp in the 200-650 nm range and Deuterium lamp for the Deep UV 120-250 nm); furthermore the facility is equipped with a SEM (Scanning Electron Microscope) microscope, for morphological characterization, coupled with EDS (Energy Dispersive X-ray Spectroscopy), for elemental analysis. During 2014, different activities were performed:

1. *Characterization of light sources in order to upgrade the setup for UV-IR measurements.*
2. *Study of diamond response under Deep UV light.*
3. *Characterization of different crystals for high energy physics experiment.*
4. *Elemental characterization with SEM coupled to EDS.*
5. *SEM characterization of UV-irradiated FOAM.*

Some of the scientific results obtained at the DXR2 -UV beamline are here summarized:

1. *Study of diamond response under Deep UV light.*

   Diamonds have high carrier mobility, wide band gap, high thermal conductivity and an extremely high radiation hardness and these properties suggest that this material is an excellent candidate for a new generation of UV detectors. This kind of detector has very low noise, due to the 5.5 eV band gap. Diamond-based Deep UV (120-240 nm) and soft x-ray detectors have been developed in the last few years. In this contest, the analysis of the behavior of these devices in the DUV range is a basic starting point to their optimization. At the DXR2 beamline at DaΦne-Light, the DUV radiation can be obtained with synchrotron radiation (SR) or with standard vacuum deuterium (D2) sources. The behavior of a diamond-based detector illuminated by a D2 lamp has been observed, measuring the photo generated electric current (Fig.8).

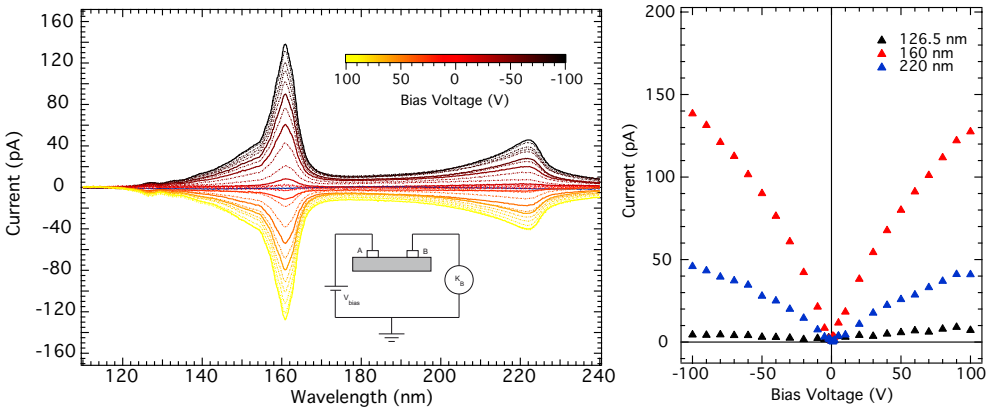


Figure 8: Diamond detector photo generated electric current as a function of wavelength and bias voltage.

2. *Characterization of scintillators.*

   The Mu2e ( muon-to-electron-conversion) experiment, that involves the INFN- National Laboratories of Frascati, is looking for Charged Lepton Flavor Violation by studying the coherent neutrinoless muon-to-electron conversions in the field of an atomic nucleus. The produced electrons will be measured in a calorimeter using the fluorescence produced of $BaF_2$ or CsI crystals. The main fluorescence emissions of the crystals are centered at 220 and 310 nm for $BaF_2$ and CsI respectively. In this context, the DXR2 UV beamline aims to characterize and test the crystals that will compose the calorimeter.
   The transmittance is an important parameter to check the quality of the crystals and can be measured using the continuum spectrum produced by synchrotron radiation in the UV range between 120 and 600 nm. The same radiation can be used also to stimulate the fluorescence emission, in order to estimate the efficiency of the crystals. Furthermore, the emitted light from the CsI crystals can be measured using a Hamamatsu Multi-Pixel Photon Counter (MPPC) to characterized it in the UV range below 300 nm.
   So far, some preliminary studies (Fig.9) have been done on the transmittance of $BaF_2$, CsI and LYSO crystals and on the the fluorescence of LYSO crystals with UV radiation using a 500 W HgXe Hamamatsu lamp in the range of 220-600 nm. The results confirmed the good quality of the $BaF_2$ and LYSO crystals and highlighted the very good transmittance behavior of a new CsI crystal.

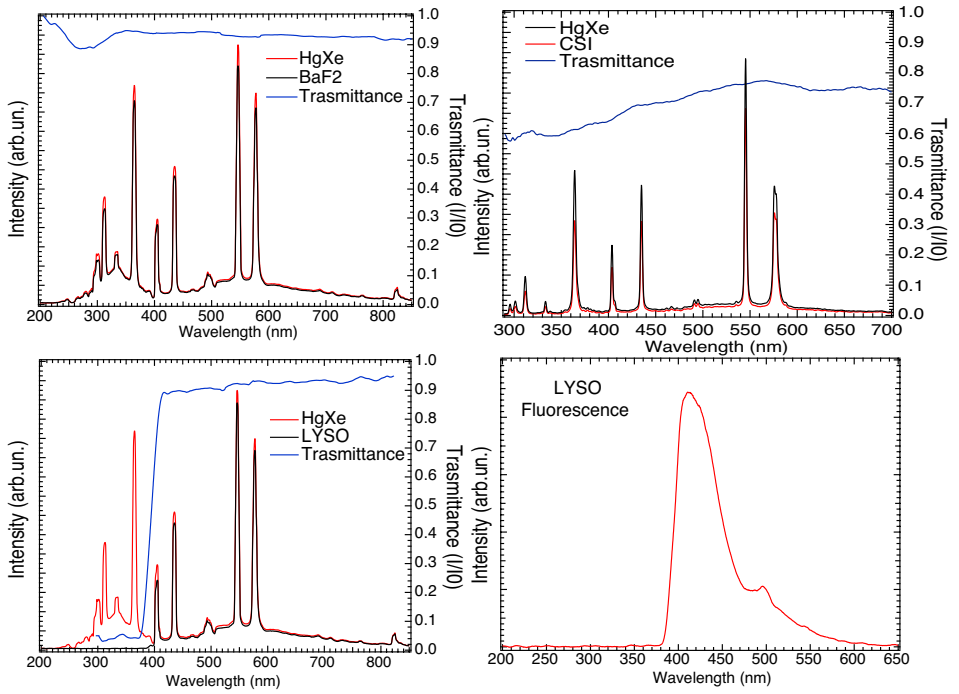


Figure 9: UV transmittance of $BaF_2$, CsI and LYSO crystals and fluorescence of a LYSO crystal.

3. *SEM and EDS characterization of a meteorite sample.*

   The installation of a SEM apparatus with EDS analysis gives the possibility to obtain morphological and elemental information. With elemental analysis it is possible to discriminate the elements content in a meteorite sample (Fe, Si, Mg, Al, O) or due to external contaminations (Zr, K, Ca, Cu, C). The different concentrations of Fe, Al, Mg, O and C atoms in different areas of the sample (in Figure 10 blue and red spectra in EDS analysis correspond to data acquired in the blue and red squares reported in SEM image) confirm the formation of spinels and their iron-based structure.

4. *SEM on irradiated FOAM.*

   FOAM is a new material developed for space application. Memory FOAM materials can be modified, stretched, pressed and turned, for specific applications and recover the original configuration under specific condition, generally being warmed up to 100°C. The study of this material, using UV radiation, is important to understand its behavior under solar-UV radiation in space. A FOAM sample has been irradiated with UV light, with a power of 60 $mW/cm^2$, for several hours (from 1 to 14 hours) and analyzed with the SEM microscope at different steps. The morphological characterization shows a standard degeneration of the system, according with previous results. Differently, analyzing the surface quality in the same area before and after 14h exposure, there is no evidence of breaking points at a micro scale.

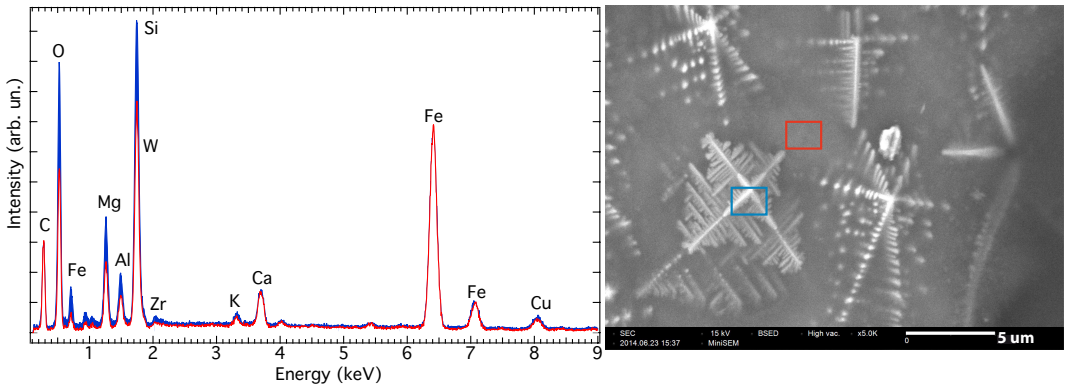


Figure 10: A meteorite sample studied using SEM and EDS: the blue and red squares reported in SEM microscope image correspond to the blue and red spectra recorded in the EDS analysis.

## 2.4 XUV beamlines and laboratory

Aim of this laboratory is to host two bending magnet beamlines covering the photon energy range from 30 eV to 1000 eV. One beam line will cover the low energy part of this interval (30-200 eV) and is called LEB (Low Energy Beam line), the other will cover the range from 60 eV to 1000 eV and is called HEB (High Energy Beam line). Both beam lines are in UHV and directly connected to the vacuum of the main DAΦNE ring. All the safety protocol and control systems are ready and tested. Since the beginning of last year, the two beam lines are ready to start commissioning with light. Such initial commissioning was not even started due to the lack of a stable orbit and beam from DAΦNE in 2013 and 2014. The complex procedures of commissioning of the two XUV beamlines (usually 6 months at full time operation) will start as soon as the necessary beam conditions and a long term schedule will become available.
Meanwhile, the implementation and successful use of the two *state of the art* end stations, whose construction was nearly completely funded without using resources from the DAΦNE-L laboratory, is going on. Both experimental set-ups, are equipped with commercial laboratory sources (X-ray lamp and He-discharge lamps), electron sources and all the needed tools to perform experiments for some INFN granted projects (see IMCA and Garfield reports) which shares some resources and space.
A *state of the art* micro-Raman station is routinely being used to perform the necessary runs on approved experiments. Fig. 11 shows the capability of Raman spectroscopy in providing fast and direct information on the electronic and structural properties of C-based materials.
Fig.8a compares the spectra measured on highly oriented pyrolytic graphite (HOPG) and on monolayer graphene grown on Cu foils and then transferred on a $SiO_2$ substrate. For graphitic materials the Raman spectra consists mainly of an intense G band (around 1585 $cm^{-1}$) due to stretching of the C-C bonds, a D band (around 1350 $cm^{-1}$) whose intensity is related to the density of defects in the hexagonal rings and a 2D band (around 2700 $cm^{-1}$) due to a second-order two-phonon process in the $sp^2$ lattice. Fig.11a indicates that although graphene is a single foil of graphite the two materials can be easily distinguished by Raman spectroscopy due to specific fingerprints, that are 2D/G ratio higher for graphene than for graphite (see inset), and more important, a different 2D line shape, which in monolayer graphene is a single component and in graphite becomes a structured peak due to the contributions of several layers. It should be noted that graphene exhibits also a weak D peak due to the presence of structural defects likely arising during the transfer

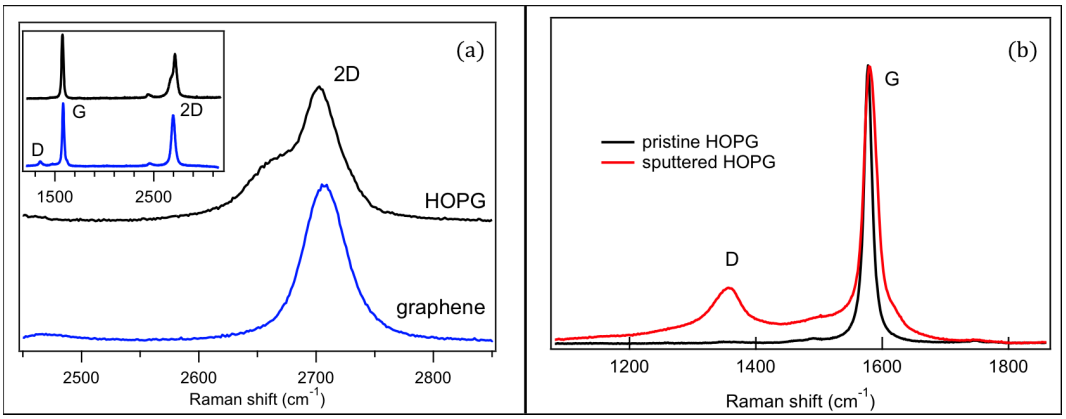


Figure 11: a) Raman spectra measured on highly oriented pyrolytic graphite (HOPG) and on graphene/$SiO_2$. b) Comparison between the Raman spectra measured on HOPG before and after the bombardment with $Ar^+$ ions at 500 eV

process.
Raman spectroscopy has been used also to follow the nucleation of lattice defects induced in HOPG by bombardment with $Ar^+$ ions with kinetic energy of 500 eV. This study was performed to investigate the nucleation of defects in graphitic materials of interest for high particle accelerators exposed to aggressive radiation. Fig.11b shows the Raman spectra measured on HOPG before and after the exposure to the $Ar^+$ beam for 3 hours. The comparison indicates the appearance of the defect peak D and of a spectral background due to inelastic photon-phonon scattering which is enhanced in the $Ar^+$ bombarded sample as the higher density of defects contributes to break the momentum selection rules.
The Raman spectroscopy set-up, besides being a useful tool to develop our internal research, attracts also, whenever possible and compatible with our time schedule, external users. The laboratory has been recently equipped with an in air scanning tunneling microscope (STM), which in 2014 has been upgraded to be used at variable temperature and in UHV, incrementing the analysis capabilities for funded studies as well as the general appeal and the available techniques of the laboratory.

## 3 List of Conference Talks

1. A. Balerna ″La fisica per la cristallografia: evoluzione delle sorgenti di raggi X, dai tubi ai FEL. ″, 100° Congresso Nazionale SIF, Pisa, 22 - 26 Settembre 2014.

## 4 Lectures

1. A. Balerna, ″Introduction to Synchrotron Radiation″, Scuola per Dottorato ″LNF Test Labs″ (LTL 2014), LNF, 16-19 Giugno 2014
2. A. Balerna, ″Synchrotron radiation applications with X-rays″, Scuola per Dottorato ″LNF Test Labs″ (LTL 2014), LNF, 16-19 Giugno 2014
3. M. Cestelli-Guidi, ″Synchrotron radiation applications with IR radiation″, Scuola per Dottorato ″LNF Test Labs″ (LTL 2014), LNF, 16-19 Giugno 2014

4. E. Pace, ″Synchrotron radiation applications with UV radiation″, Scuola per Dottorato ″LNF Test Labs″ (LTL 2014), LNF, 16-19 Giugno 2014

5. M. Cestelli-Guidi, ″La generazione di immagini spettrali. Dalla teoria alla pratica″, Scuola di Spettroscopia IR Applicata alla Diagnostica dei Beni Culturali: III edizione - Venaria Reale (TO), 3-6 Novembre 2014.

## 5 Publications

1. G. Bellisola, S. Caldrer, G. Cinque, M. Cestelli Guidi, B. M. Assael, P. Melotti, C. Sorio, ″The identification of cystic fibrosis (CF) cells and their pharmacological correction by mid-infrared microspectroscopy and unsupervised data analysis methods.″, ScienceJet, **3**, 51 (2014)

2. M. Cestelli Guidi, C. Mirri, E. Fratini, V. Licursi, A. Marcelli″ FT-IR imaging spectroscopy as a complementary analytical technique to monitor lipids as biomarkers to high-LET (linear energy transfer) radiation.″, Rend. Fis. Acc. Lincei , **25** (Suppl 1) 75-79 (2014)

3. V. Licursi , E. Fratini, B. Benassi, M. Cestelli Guidi, C. Consales, A. Marcelli, C. Mirri, R. Negri, R. Amendola, ″A proposed integrated systems approach to the radiation biology of cosmic interest: biophysics and molecular characterization of tissues irradiated with 14 MeV neutrons.″, Rend. Fis. Acc. Lincei , **25** (Suppl 1), 23-27 (2014)

4. I. Rago, C. R. Chandraiahgari, M. P. Bracciale, G. De Bellis, E. Zanni, M. Cestelli Guidi, D. Sali, A. Broggi, C. Palleschi, M. S. Sarto, D. Uccelletti, ″Zinc Oxide Microrods and Nanorods: Differential Antibacterial Activity and their Mode of Action against Gram-positive Bacteria.″, RSC Advances, **4**, 56031-56040 (2014)

5. A. Balerna (on behalf of the DAΦNE-Light Group), ″DAΦNE-Light Facility Update.″, Synchrotron Radiation News, **27:1**, 21-24 (2014)

6. L. Di Mario, S. Turchini, N. Zema, R. Cimino, F. Martelli, ″Electronic properties of Si hollow nanowires″, J. of Appl. Phys., **116**, 174310 (2014)

# Computing Service

S. Angius (Tec.), C. Bisegni (Art. 15), D. Maselli (Tec.), R. Orru' (Ass. Ric.),
M. Pistoni (Resp.), C. Soprano (Tec.), D. Spigone (Art. 15), T. Tonto (Tec.)

In collaboration with LNF-DA:
R. Gargana (Art. 23), M. Tota (Ass. Ric.)

## 1. Summary

The Computing Service of LNF deals with the configuration and administration of data transmission network, of the IT infrastructure and of the computing resources of LNF and AC (Central Administration). Furthermore, it also plays a relevant role for INFN by managing several IT services, relevant at national level, even if they are centralized at LNF. In detail, the Computing Service manages:

- *The network infrastructure:* the structured cabling system, both copper and optic fiber, the Local Area Network equipment (Layer 2 and Layer 3 switches), the wireless network equipment, the Wide Area Network connections and access routers, the devices for the management of information security;
- *The following Storage infrastructures and Mass Storage resources:* Storage Area Network, Network Attached Storage, Distributed File System (Andrew File System), Tivoli Storage Manager to provide backup and archiving services through the magnetic tape libraries;
- *A virtualization system infrastructure:* a set of machines based on Intel processor, used to manage several virtualization environments leveraging open source software technologies (Linux O-Virt or Xen);
- *A set of infrastructure services for ensuring the functionalities of the network:* the Dynamic Host Configuration Protocol and the Domain Name System servers, security servers (Log and Audit recording, monitoring system), virtual servers for providing the national infrastructure of authentication and authorization, etc...;
- *A set of critical and virtual IT services:* the Mail system (ie mail relays, inbox server, webmail, Antivirus and Antispam), the Database Servers (Oracle and MySQL), the web and streaming servers, the printing servers, etc .;
- *The scientific computing resources:* computing farms of some experiments, the Windows domain, Linux virtual systems for general users access;
- *Computing management resources for ERP (Enterprise Resource Planning):* the Information System for staff management and payroll, for documents and protocol administration;
- *The web hosting services for INFN, AC and LNF:* web servers and portals, database and application servers.

Moreover, the Computing Service provides also support to:

- facilities and experiments which autonomously manage their computing resources and in particular to the IT infrastructure based on the computational grid of the Atlas experiment and to the virtualization systems for Daϕne control within the Accelerators Division;

- configuration and administration of workstations and personal computers used by employees, associates, graduate students, undergraduates, guests, LNF services and/or INFN experiments;
- the use of IT resources exported or shared and of distributed devices and peripherals.

## 2. Activities developed in 2014

During 2014, the Computing Service has collaborated to the development of a new room devoted to scientific computing. The new room is about 100m$^2$ and is prepared to house about 24 standard racks with total energy consumption not exceeding 150KW. Currently, the room hosts Tier-2 GRID for the Atlas experiment.

The Computing Service has also updated the local area network switches, due to the old age and obsolescence of the models installed and operational until few years before. In particular, within the machine room, a network infrastructure based on a 10Gb/s Ethernet protocol was implemented and is used to support the growing data flows coming from the experiments and from the Grid infrastructure. The 10Gb/s ethernet network is currently extended to the slow control room of the particle accelerator.

The Computing Service has updated the Storage Area Network, either by replacing the pair of old central Fibre Channel switches with a new and more powerful model (with 16Gb/s interfaces), and by removing an old Storage System, implementing a new system mainly devoted

to the AFS server volumes, but also to provide storage space to the new virtualized services that will be implemented in the future.

The Computing Service has also contributed to the development of the !Chaos project (aimed to the realization of a prototype of Control as a Service open platform, suited for a large number of applications in science, industry and society); and more in detail both to Work Package 2, for the development of the software and of the common framework, and to Work Package 5, for the implementation of a cloud infrastructure aimed to deploy IT resources based on IaaS (Infrastructure as a Service) and PaaS (Platform as a Service) models.

In 2014, driven by the needs of the !Chaos project, the Computing Service has started to plan the study and implementation of an IT Cloud infrastructure for the supply of generic services delivered on demand to all users. The R&D activities developed by the Computing Service are based on the open source “Openstack platform” to create a testing environment meeting the requirements of high reliability, availability and scalability.

# ACTIVITY REPORT 2014

## Communication and Outreach

D. Babusci (Resp till April 2014), R. Centioni (Resp. from April 2014), D. Bifaretti, A. Cupellini, G. Di Giovanni, C. Federici, A. Mecozzi, S. Reda (Bors.), M. Scudieri (Art. 15), E. Santinelli (Art. 15), B. Zuaro (Bors.)

## SIDS - Scientific Information and Documentation Service

Throughout the year the LNF provides basic education in physics by means of a vast outreach program for the general public, teachers and students.

These activities are made possible by the enthusiastic involvement of the INFN-LNF personnel: graduate students, postdocs, researchers, engineers and technicians.

The events are organized both at the LNF (Visits, Open Day, Public Lectures, European Researchers Night and special appointments addressed to high school teachers and students such as Incontri di Fisica and Stages) and outside the Laboratories (Seminars at schools, local libraries, etc).

1) **Visits** www.lnf.infn.it/edu/visite to LNF are a well-established tradition. They consist of a brief historical presentation of the Laboratories and their activities, on site and abroad, and of a guided tour of the experimental areas and the open air museum. Visits are organized for both students in their last high school year and pupils (age: 10-14) and they usually last about 3 hours. In 2014 the pupils' program, named Quasar Project, hosted about 700 kids.
Not just Italian schools but also schools from all over the world book visits. During 2014 about 5200 people visited the LNF.
*(Coordinator: M. Mascolo and B. Sciascia for the Quasar Project)*

2) The **Open Day** www.lnf.infn.it/edu/openday/ consists of a full day program of guided tours inside the LNF, conferences, public lectures, expositions and scientific videos. Most of the LNF employees are then in action to present their research centre, answer questions and take care of their guests. This year's the LNF Open Day, "LNF is Open!" was, for the first time, organized on the day of Saturday. About 1400 people visited the LNF on May 17th, 2014. *(Care of Servizio Informazione e Documentazione Scientifica - SIDS)*


*Open Day 2014 (INFN-LNF Photo)*


*Open Day 2014 Studenti in Staff (INFN-LNF Photo)*

4) **Seminars and Public Lectures** www.lnf.infn.it/edu/seminaridivulgativi/ aimed to high school students and the general public are held every couple of months by important personalities of the scientific field at the LNF's Bruno Touschek Auditorium.

The 2014 saw the LNF host an extremely appreciated seminar, attended by a huge audience:
David Blair from the School of Physics, University of Western Australia, talked about changing the paradigm of school physics education by introducing the language of modern physics at an early age; Teresa Montaruli from the University of Ginevra presented a talk on the Ice cube experiment for the detection of neutrinos from astrophysical sources;
Antonio Masiero (INFN Vice President, Professor at Padova University) presented a talk on the link between the primordial universe and LHC physics.

Upon request, many LNF researches will also hold lessons in schools and libraries. A special agreement exists with the Frascati's library and the IKEA store.

In 2014 the Seminars programs involved about 1600 students from all over Italy.

**BTML – Bruno Touschek Memorial Lectures** held on December 4$^{th}$, 2015.

The **Bruno Touschek Memorial Lectures (BTML)** were established in 1987 to honor the life and works of Bruno Touschek. The Lectures saw in the last few years the participation of distinguished scientists lecturing on important innovative research topics and historical perspectives. In 2014, the BTML were dedicated to muon colliders and Higgs factories, with Carlo Rubbia's talk "A complete

demonstrator of a muon cooled Higgs factory". The close 40th anniversary of the observation of the J/ψ particle in Frascati has also been mentioned by Giorgio Bellettini, director of the Laboratory at the time. The event closed with a lecture, in Italian, addressed to the general public, given by Giovanni Bignami, President of INAF, who talked about the "Gamma Ray Universe".


*BTML 2014 Carlo Rubbia (INFN-LNF Photo)*

6) **European Researchers' Night** http://www.frascatiscienza.it/ organized by FrascatiScienza. SIDS is involved in setting up guided tours at the LNF and public lectures.
The European Researchers' Night took place on September 26th, 2014, and hosted about 500 people with a program of guided tours, conferences and performances.

7) High school teachers course - **Incontri di Fisica** www.lnf.infn.it/edu/incontri/ has been organized since 2001. The event is a three-days course for high school teachers and INFN people involved in scientific research dissemination. About 200 participants from all over Italy attend this event every year. The goal is to stimulate the teachers' professional training and provide an occasion for interactive and hands-on participation in the latest developments in physics.

The program consists of plenary lessons, presentations of INFN-LNF activities, visits to LNF experimental area and discussions. The peculiarity of this course is represented by the group work, focused on a theoretical lesson followed by hands-on activity or data analysis of a real experiment. This way, teachers have a direct contact with researchers and get to use typical experimental instrumentation employed in contemporary physics.

Teachers, authorized by the Minister of Education, receive a certificate of participation.
All the programs are published on the LNF web site (lessons, videos, photos).
LNF October 8th -10th, 2014.
*(Organizing Committee: D. Babusci, R. Centioni, C. Curceanu (Chair), P. Di Nezza, U. Dosselli, R. Fabrianesi (AIF), R. Faccini, C. Gatti, – Secretariat: D. Bifaretti E. Santinelli, M. Scudieri; webmaster S. Reda)*

8) **Stages for students** www.lnf.infn.it/edu/stagelnf have been organized since 2000 for high school students in their last years. Students are selected by their teachers on the basis of their curriculum but, above all, on the basis of their interest and motivation.
In direct contact with their tutors (1 tutor / 2 students), students are involved in theoretical lessons and practical operations. They acquire knowledge and understanding of INFN research activities in an interactive modality.

At the end of the stage they get a Certificate of Participation.

The LNF offers a number of different stages:

**- The Winter Stages** take place during the school year and they consist of 9 appointments, once a week; 36 student – February 10th – May 22, 2014
Students are divided into various experimental groups: Electronics, Informatics, Modern Physics, Mechanics and this year, for the first time, also Administrative activities.
*(Scientific Coordinator: C. Curceanu)*

**- The Stage Masterclass** is organized in partnership with the IPPOG Masterclasses International Project. It lasts 5 full days, in March. Students, in one group of 43, follow lessons on modern physics and analyze data from the ALICE experiment at CERN.
This year's Stage Masterclass was at LNF between February 25nd and March 1 *(Scientific Coordinators: D. Domenici (Resp), P. Di Nezza)*

**- The International Masterclass** is open for 50 of the best students in their last year(s) of high school/college, from every European country. It lasts 5 days and it involves lectures on Modern Physics and its applications in our society and activities to be performed in laboratories. Participants have, as well, the opportunity to visit the main experiments and accelerating facilities of the LNF. *(Scientific Coordinator: C. Curceanu)*

**- The Summer Stages** are organized in June, at the end of the school year, and last 10 days. Summer Stages – 129 students - LNF June 16th -27th, 2014. The students, divided in small groups, joined 10 different experimental activities (Quantum Mechanics, Superconductivity, Cosmic Rays, Electronics, Informatics, Mechanics, Data Analysis, Theoretical activities, Bio-Nanotechnology, Scientific Communication). *(Scientific Coordinator: D. Babusci)*

-**Mini-stage** organized by the LNF for students (age:13-18) as a 2 days camp, that took place on 4-5 August 2014, involving 10 students (also from abroad) in a program of conferences, guided tours and experimental activities. More info http://www.lnf.infn.it/edu/stagelnf/2014/summer-mini-stage/ *(Scientific Coordinator: C. Curceanu)*

Participation in the stages program has increased over the last 10 years: since 2000, 2308 students attended the stages. As shown in Tab. 1, in the year 2000 LNF hosted only 12 students from one

local school, while in the year 2014, 395 students from over 93 different schools all over Italy and from abroad came to Frascati.

Tab. 1

| Year | Students | Females | Males | School | INFN Tutors |
|---|---|---|---|---|---|
| 2000 | 12 | 1 | 11 | 1 | 7 |
| 2001 | 14 | 3 | 11 | 1 | 14 |
| 2002 | 57 | 15 | 42 | 8 | 50 |
| 2003 | 56 | 11 | 45 | 14 | 22 |
| 2004 | 114 | 34 | 80 | 21 | 25 |
| 2005 | 154 | 42 | 112 | 29 | 56 |
| 2006 | 161 | 48 | 113 | 46 | 58 |
| 2007 | 163 | 45 | 118 | 51 | 55 |
| 2008 | 161 | 47 | 114 | 51 | 63 |
| 2009 | 177 | 40 | 137 | 54 | 67 |
| 2010 | 166 | 36 | 130 | 60 | 60 |
| 2011 | 184 | 61 | 184 | 60 | 70 |
| 2012 | 206 | 59 | 147 | 72 | 59 |
| 2013 | 288 | 78 | 210 | 90 | 84 |
| 2014 | 395 | 144 | 251 | 93 | 86 |

The LNF monitor the success of the various initiatives proposed, mostly through questionnaires (each one specific to the event) and keep track of the progresses using dedicated databases, thanks to whom it is possible to perform simple statistical analysis.

## 9) **Web page**

On the LNF web site are reported all the events organized: tutors' lessons, videos, photos, reports that, together with the educational material and the general information about the LNF research activities, introduce the general public and schools to modern physics and INFN-LNF research, so to bridge the gap between science and society.

Tab. 2 - Number of participants to LNF events during 2013

| **EVENTS (2014)** | **PARTICIP ANTS** |
|---|---|
| Visits | 5200 |
| Open Day | 1400 |
| Seminars and Public Lectures (at the LNF and outside) | 1600 |
| European Researchers' Night | 370 |
| Incontri di Fisica for high school teachers | 222 |
| Stages for high school students | 395 |

**Acknowledgements**

Many thanks to the LNF Director and the Heads of the Accelerator, Research and Technical Divisions. Special thanks to all LNF Tutors and Services LNF.

## CONFERENCES, WORKSHOPS and MEETINGS

International conferences, workshops and meetings hosted and/or organized by LNF:

1. *"Is quantum theory exact ? The endeavor for the theory beyond standard quantum mechanics" - FQT2014*, April 28-30, 2014.
2. *New frontiers for Majorana fermions from condensed to dark matter*, May 5-6, 2014.
3. *XVII LNF Spring School "Bruno Touschek*, S. Juan (Puerto Rico), May 12-16, 2014.
4. *Investigating Strangeness: from Accelerators to Compact Stellar Object*, May 14, 2014.
5. *Vulcano Workshop 2014*, Vulcano, May 18-24, 2014.
6. *Panda Hadron Physics Workshop 2014*, September 08-12, 2014.
7. *4th Low Emittance Rings Workshop (LOW?RING 2014)*, September 17-19, 2014.
8. *MesonNet2014*, September 29 - October 1, 2014.
9. *Channeling 2014*, Capri, October 5-10, 2014.
10. *Nanoscienze e nanotecnologie 2014*, October 6-7, 2014.
11. *LNF Mini-Workshop Series: Stato e Prospettive dell'Adroterapia in Europa*, October 15, 2014.
12. *What next LNF: Perspectives of fundamental physics at the Frascati Laboratory*, November 10-11, 2014.
13. *4th International Workshop on Nucleon Structure at Large Bjorken x - HiX2014*, November 17-21, 2014.
14. *3rd FLUKA Advanced Course and Workshop*, December 1-5, 2014.
15. *Bruno Touschek Memorial Lectures - BTML2014*, December 4, 2014.
16. *Topical Workshop: Rethinking Naturalness*, December 17-19, 2014.
17. *Quantum theory and Gravity: which way?*, December 18-19, 2014.

**INFN INTERNAL NOTES**

**INFN-14-01/CCR**
F. Serafini et al., *Integrazione Single Sign on su JASPERSERVER PER INFN AAI*

**INFN-14-02/CNAF**
S. Dal Pra, *Accounting Data Recovery. A Case Report from INFN-T1*

**INFN-14-03/LNF**
D. Di Gioacchino et al., *The NORCIA Experiment*

**INFN-14-04/LNF**
M. Raggi et al., *Proposal to search for a dark photon in e+ on target collisions at DAFNE linac*

**INFN-14-05/LNF**
A.A. Babaev et al., *Deflection of Proton Beams by Crystal Miscut Surface*

**INFN-14-06/LNF**
P. Valente et al., *Possible upgrades of the DAFNE Beam-Test Facility (BTF)*

**INFN-14-07/LNF**
D. Alesini et al., *DAFNE Gamma-Rays Factory*

**INFN-14-08/LNF**
M. Beretta et al., *Electrons diffusion and signal noise contributions on electron clusters detection efficiency*

**INFN-14-09/LNF**
M. Pullia et al., *Progetto della nuova facility di irraggiamento al CNAO*

**INFN-14-10/GE**
M. Sanguineti et al., *Direct measurment of antares detector angular resolution with moon shadow effect*

**INFN-14-11/LNF**
E. Vilucchi et al., *Review del Tier-2 di ATLAS dei Laboratori Nazionali di Frascati*

**INFN-14-12/LNF**
O. Ciaffoni et al., *PORFIDO on the NEMO phase 2 and KM3 phase 1 towers*

**INFN-14-13/LNF**
L. Benussi et al., *Properties of potential eco-friendly gas replacements for particle detectors*

**INFN-14-14/LNF**
L. Benussi et al., *A study of HFO-1234ze (1,3,3,3-Tetrafluoropropene) as an eco-friendly replacement in RPC detectors*

**INFN-14-15/LNF**
F. Antonucci et al., *!CHAOS: a cloud of controls – MIUR project proposal*

**INFN-14-16/LNF**
S.V. Abdrashitov et al., *Hybrid Scheme of Positron Source at SPARC_Lab LNF Facility: Channeling Radiation and Amorphous Photon Converter*

**INFN-14-17/CCR**
M. Michelotto et al., *Aspetti di Sicurezza nella Programmazione di Siti WEB in Ambiente Accademico*

**INFN-14-18/CCR**
M. Michelotto et al., *Aspetti di Sicurezza nella Gestione di Siti WEB in Ambiente Accademico*

**INFN-14-19/CCR**
S. Dal Pra, *Job Packing: Optimized Configuration for Job Scheduling*

**INFN-14-20/GE**
M. Anghinolfi et al., *The Electronic Design and the Layout of Central Logic Board (CLB) for the KM3NET Experiment*

**INFN-14-21/GE**
A. Orzelli et al., *CLB Test Report*

## POPULAR PHYSICS NOTES

**INFN-DIV-14-01/LNF**
D. Di Gioacchino, *Il fenomeno della superconduttività*

**INFN-DIV-14-02/LNF**
C. Gatti, *Il Plasma di Quark e Gluoni e la Fisica con Ioni Pesanti ad ATLAS*

# SEMINAR

M. Boscolo (Resp.)

Not received

# The General Services and Technical Division 2014

F. Angeloni (Art. 15), M. Arpaia, G. Bisogni, F. Bocale, M. Campoli, S. Cantarella (Art. 23), A. Cassarà, P. Celli, O. Cerafogli, A. Chiarucci, A. Clozza, V. Crisanti, A. Delle Piane (Art. 23), A. De Paolis, A. Donkerlo, G. Ferretti, M.A. Franceschi, C. Fusco, M. Giorgi, E. Iacuessa, S. Incremona (Art. 23), M. Marchetti, U.Martini, M Matteo (Art. 15), M. Maestri (borsista), .G.A. Monacelli, M. Monteduro, T. Napolitano, E. Passarelli, R. Ricci, A. Riondino, M. Rondinelli, U. Rotundo, M. Ruggeri, C. Sanelli*, F. Sanelli, M. Santoni, A. Sorgi, A. Tacchi, R. Tonus, R. Valtriani

*Retired in December 2014

## 1 Introduction

The facility management of the Frascati Laboratories and support to experiments and accelerating machines (mechanics, electric systems, and HVAC systems) are the main tasks of the Division.

During 2014, collaboration, support and consultancies were supplied to the following experimental activities: ALICE, ATLAS, CCR, CIGS, CMS, CNAO, CUORE, DAFNE, ELI-NP, FLAME, JEM-EUSO, JLAB12, KAONNIS, KLOE2, LHCb, MU2E, NA62, NEURAPID, PANDA, SCF_LAB, SPARC, VIP2.

In December 2014, U. Rotundo was appointed Head of the Division, succeeding C. Sanelli who retired.

The next Figure shows the Division's OBS:

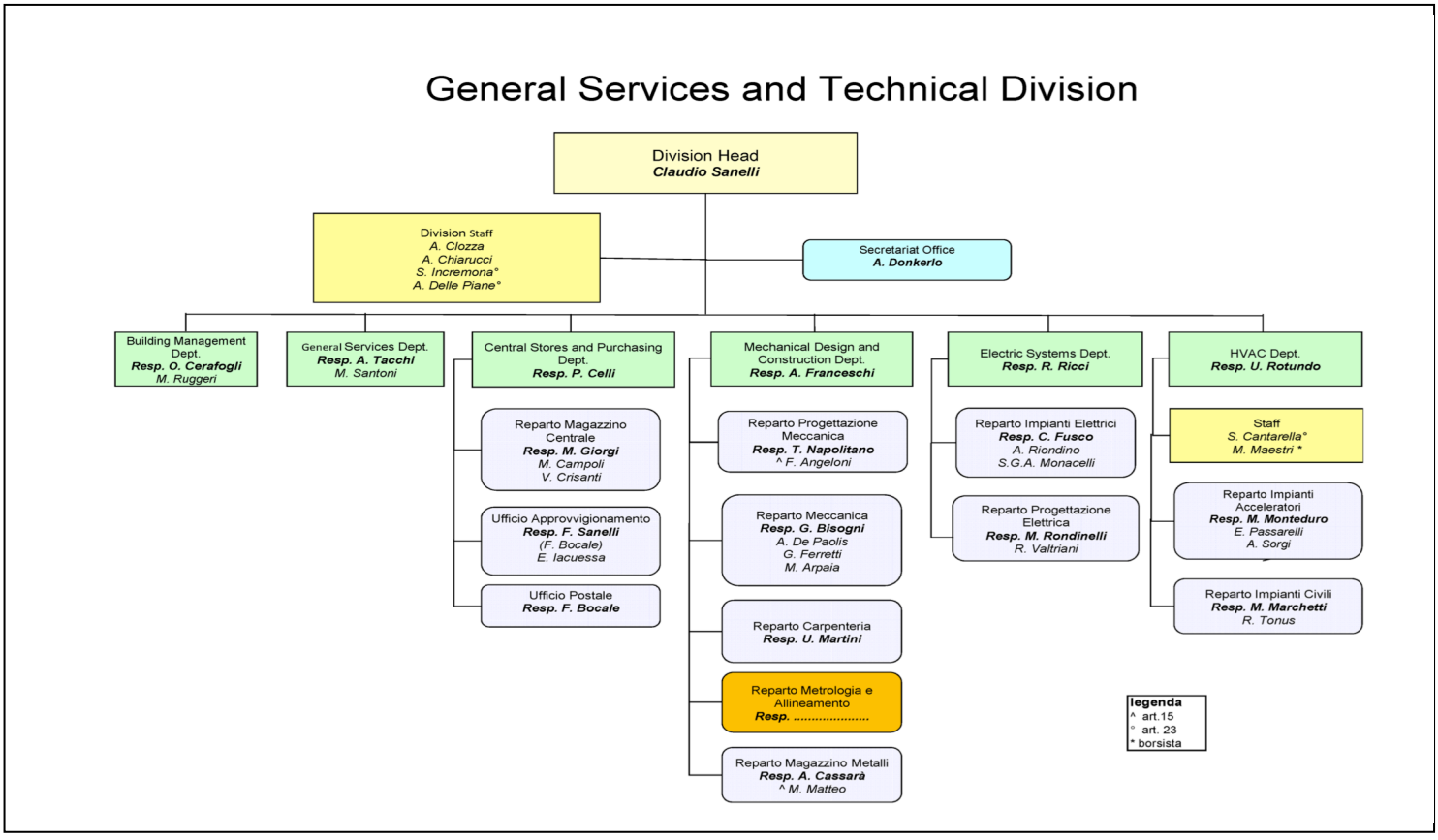

## 2 General Services Dept.

The General Services Dept. of the LNF deals with the organization and management of the general operational activities of the LNF and the Central Administration of the INFN, such as:

1. Bar/Canteen LNF
2. Cleaning Service
3. Guards Service
4. Gardening Service
5. Porterage
6. Reuse of discarded furniture
7. Child care center
9. Coffee breaks and lunches
10. Derattization and pest control
11. Purchase of hygienic materials and rental of no-dust carpets
12. Purchase and cleaning of work clothes
13. Drink water dispensers rental
14. Microbiological analyses of LNF bar food & equipment
15. Lease, insurances, maintenance and documentation of LNF vehicles
16. Support to scientific secretariats in the organization of events
17. Liaising with the City of Frascati for licenses, authorizations and taxes
18. Liaising with the ENEA Frascati Center
19. Public tenders for large service contracts.

In addition to routine activities, during 2014 the Dept. has dealt with:

- handling of the consequences of the water supply pollution emergency (drinking water for canteen & offices);
- reorganization of various rooms, offices and workshops, including relocation & cleaning;
- handling of the contract for cleaning services of LNF, AC & Head Quarters;
- organization of services for big events: Open Day and Researchers' Night: logistics, access, gardening, portering, coordination of the restoration of some apparatus and monuments;
- handling of the aftermath of the "water bomb" event: pumping of various inundated areas, clearing out of the inundated Library, Aula Touschek and basement areas of blg. 36, including disposal of the resulting rubbish to the dump; disassembly and reassembly of Aula Touschek seats.

Beyond dealing with these emergencies, the following activities were carried out:

- pruning of the pine trees, and recovery of some abandoned green areas.
- organization of meetings and conferences: coffee breaks, work lunches, meeting rooms preparation, shuttle buses (Summer Internships, Spring School, Researchers' Night, BTML2014, Panda Hadron Physics W. 204, Physics Encounters , NN2014, etc.)

## 3 Central Stores and Purchasing Dept.

The Central Stores and Purchasing Dept. supervises the purchasing and stocking of goods of the Central Stores as well as those of the Metals Stores, and incoming and outgoing articles; development and extension of the stocked articles. The LNF, the Central Administration and some INFN Sections and groups have access to the LNF Stores.

Moreover, the Dept. carries out market researches upon request of the users for the extension and upgrade of the articles in stock, maintains quality standards of stocked articles, and performs maintenance and updating of its web pages, including the online General Catalogue database for the general users. Extensive use of Consip, mainly through MEPA, has been made.

During the 2014 accounting period the Central Stores and Purchasing Dept. has transferred a total amount of € 145.000,00 for stock materials replenishment as follows:

- € 52.500,00 on Cap. 130110 (standard consumables),
- € 92.800,00 on Cap. 130120 (research consumables).

Furthermore, the Dept. has spent approx.. € 70.000,00 for its ordinary activities, including mail handling services and management of small services such as the fork lift and small office equipment.

These activities have entailed the preparation and emission of over 100 PO, to which should be added approx. 100 orders to contacted firms for minor purchases.

## 4 Building Management Dept.

In the course of the year 2014, routine maintenance and repairs as well as extraordinary maintenance has been executed on the LNF buildings in order to preserve the value of the LNF assets. Other repair and maintenance works involving modifications, adaptations and renovations on LNF buildings have been carried out upon requests of the various LNF experimental groups. In June, damage caused by the “water bomb” has been repaired.

## 5 Mechanical Design and Construction Group

The Mechanical Design and Construction Group (SPCM) is composed of five Units: Mechanical Design, Carpentry and Soldering, Machine Shop, Metrology and Alignment, Metals Store.

In previous years, the SPCM has lost several staff units due to retirement or internal relocation; Metrology in particular continued to suffer lack of personnel and its activity is stopped since June 2012.

The SPCM performs the following tasks:

- mechanical design of experimental apparatus and detectors, using CAD/CAE software and FEM analysis;
- construction of prototypes and structures with the support of various soldering techniques and numeric control machine tools;
- production of high precision mechanical components, relying on manual and numeric control machine tools equipped with CAM control;
- high precision dimensional check, material strength test, large structures and apparatus optical alignment;
- acquisition and storing of mechanical components, tooling, metallic and plastic materials for common workshop use.

During 2014, SPCM supported some experimental activities, playing a role of direct responsibility in the design, production, construction or installation of CUORE (Cryogenic Underground Observatory for rare Events) at LNGS for the study of Neutrinoless Double Beta Decay (engineering coordination and integration of the whole experimental apparatus), and of JEM-EUSO (Extreme Universe Space Observatory) to be installed aboard the International Space Station or satellite for the study of Ultra High Energy Cosmic Rays (photo detector module and focal surface layout and mechanics).

Many other activities were supported as well, though with no direct involvement in terms of responsibility: ALICE, ATLAS, BELLE2, JEM-EUSO, KAONNIS, LHCb, MU2E, NA62, NEURAPID, PANDA, SCF_LAB were supported in terms of mechanical design or construction.

To conclude, some 60 short-term actions were taken by the SPCM personnel to support experimental activities, in case of unplanned production, interventions or urgent repairs.

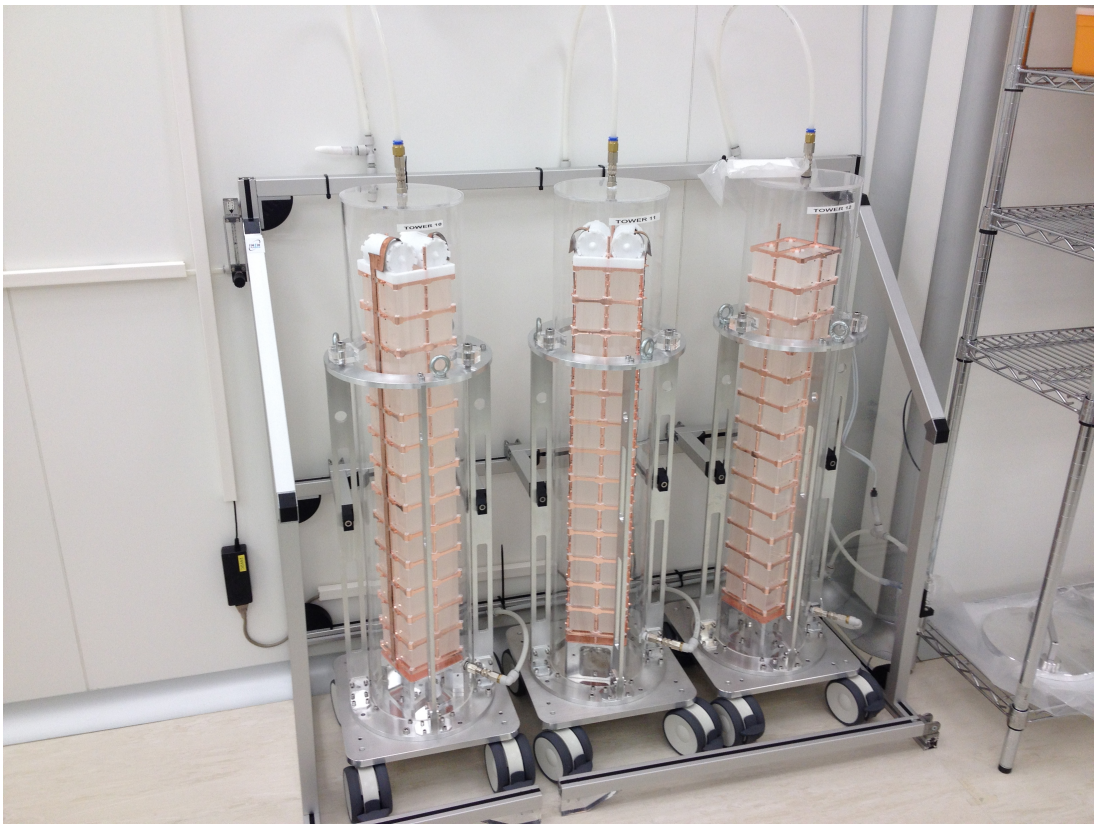

CUORE: Detector Towers (19 over 19), stored @LNGS

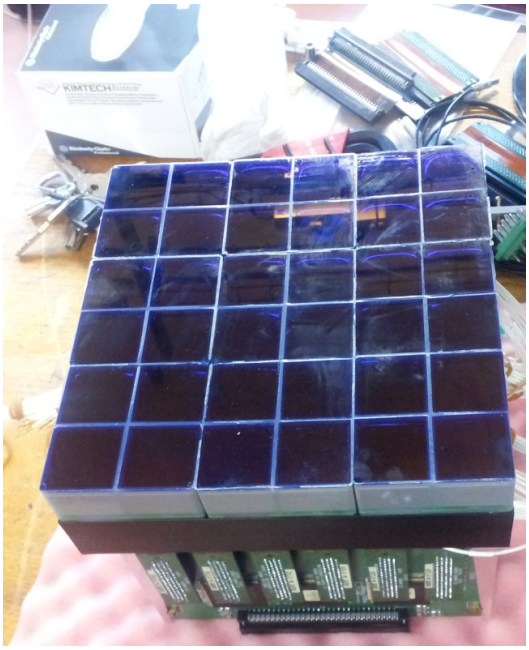

JEM-EUSO: Photo Detector Module prototype, ready for test on board a stratospheric balloon @Timmins base (Ontario, Canada).

## 6 Heating, Ventilation, Air Conditioning Department

The Dept. is in charge of the operation and maintenance of the auxiliary plants, comprising water cooling plants, water treatment facilities, compressed air and other gases production and distribution systems, HVAC plants for accelerators and experimental halls.
The group is also in charge of the HVAC Building Management (civil plants), and tap water distribution for the whole Lab.
Procurements for new installations, from technical specifications definition to the follow-up of tender procedures, construction, commissioning, start-up, performance tests and standard operations constitute part of the work scope of the Dept.
In 2014 the group has provided support to DAFNE, KLOE2, BTF, SPARC_LAB, FLAME, CNAO, ATLAS and the LNF Data Center.
During the year, the Dept. supported the design activities of cooling plants and compressed air distribution system for the ELI-NP project to be built in Magurele, Bucharest (Romania), bearing the responsibility of the related work package within the WBS. The project is ongoing and it should commit the Dept. up until the end of 2018.
Consultancy was given for the development of the cooling plants of the new CNAO experimental line, the XPR, which should be installed in the next couple of years.
At the beginning of the year the Dept. had to cope with a severe lack of tap water due to damage of some part of the ancient Roman waterworks, still used to convoy water to the Lab. Lot of interface activities had to be carried out with Local Authorities because during this period the Dafne accelerating complex had to be turned down. Sparc_Lab and the LNF Central Data Center along with the Atlas TIER2 could be operated, the latter thanks to the upgrade of the facility infrastructure operated during 2013.
The design phase for heat recovery from the Dafne Cooling Station, with the aim of supplying warm water for the building's HVAC systems, has been completed along with the procurement for the installation works, which should start at the end of the winter season, in April 2015.

## 7 Electric Systems Department

The Dept. manages the LNF electrical installations from the high voltage power supply to end users and the lighting. The150 kV substation and the 8 cabins are operated by staff, who also cover emergency calls and fault fixing. Routine safety and functional maintenance activities are usually performed by external contractors under the Dept.'s supervision. Maintenance involves several skilled scheduled activities on switchboards, transformers, medium voltage devices, safety lighting, UPS, emergency generating sets and electrical devices of Dafne and Sparc cooling system, but also small repairs or changes requested by users. LNF phone service is also taken care of.

The Dept. takes care also of the Dafne auxiliaries automation and control system after the revamping performed in the previous years.
The technical direction of the electrical power supply contract involves continuous contact with public utility and ever more accurate load and budget forecasts. 25,6 GWh were used in the 2014, with a bill of 4,57 M€.
Energy saving activities have been carried out both in the civil and in the particle accelerator installation.
The Department takes care of the INFN Rome Headquarters offices installation too.
ELI-NP project involves a big effort of graduates, in the design and coordination of the electrical installation.

## 8 Other technical-scientific support activities

The experimental activities of the PED4PV project, started in 2013, continued in 2014 too. The PED4PV project aims to demonstrate that the Pulsed Electron Deposition (PED) technique is a valid and innovative method to realize thin film based Photo Voltaic (PV) cells. Scope of the task, performed at the LNF, is the deposition of Molybdenum thin film as back contact on several substrates of various nature, such as: glass, stainless steel, copper, bronze, ceramic, cement. A dedicated thin film deposition system, realized in 2013, is now working with good performance. Besides the deposition of the molybdenum back contact, a successful activity on the deposition of the Transparent Conductive Oxides (TCO) aluminum doped zinc oxide (AZO), has been carried out. We were able to cover an area of 160 by 160 $mm^2$ with a thickness of about 250 nm of AZO, with a good homogeneity and a very good adhesion. More recently we have been testing the feasibility to deposit the CdS heterojunction layer through a sputtering technique, instead of through the traditional chemical bath deposition technique. The work is going on.

## 9 Some Statistics

During 2014, a total number of 612 registered requests reached the Technical and General Services Division, either through the General Users Form, the SPCM ‘small jobs request procedure’, or through a ‘flash mail’ system for several standard requests (illumination repairs, conference coffee breaks requests, HVAC repairs, and tenocode modifications).

| ORIGIN OF REQUESTS | N. | % |
|---|---|---|
| Research Division | 287 | 47% |
| Technical Division | 111 | 18% |
| Accelerator Division | 121 | 20% |
| Central Administration | 23 | 4% |
| FISMED | 23 | 4% |
| Directorate | 21 | 3% |
| Administration | 8 | 1% |
| Safety and Protection Dept. | 7 | 1% |
| SPARC-lab | 6 | 1% |
| Human Resource | 5 | 1% |
| **TOTAL** | **612** | **100%** |

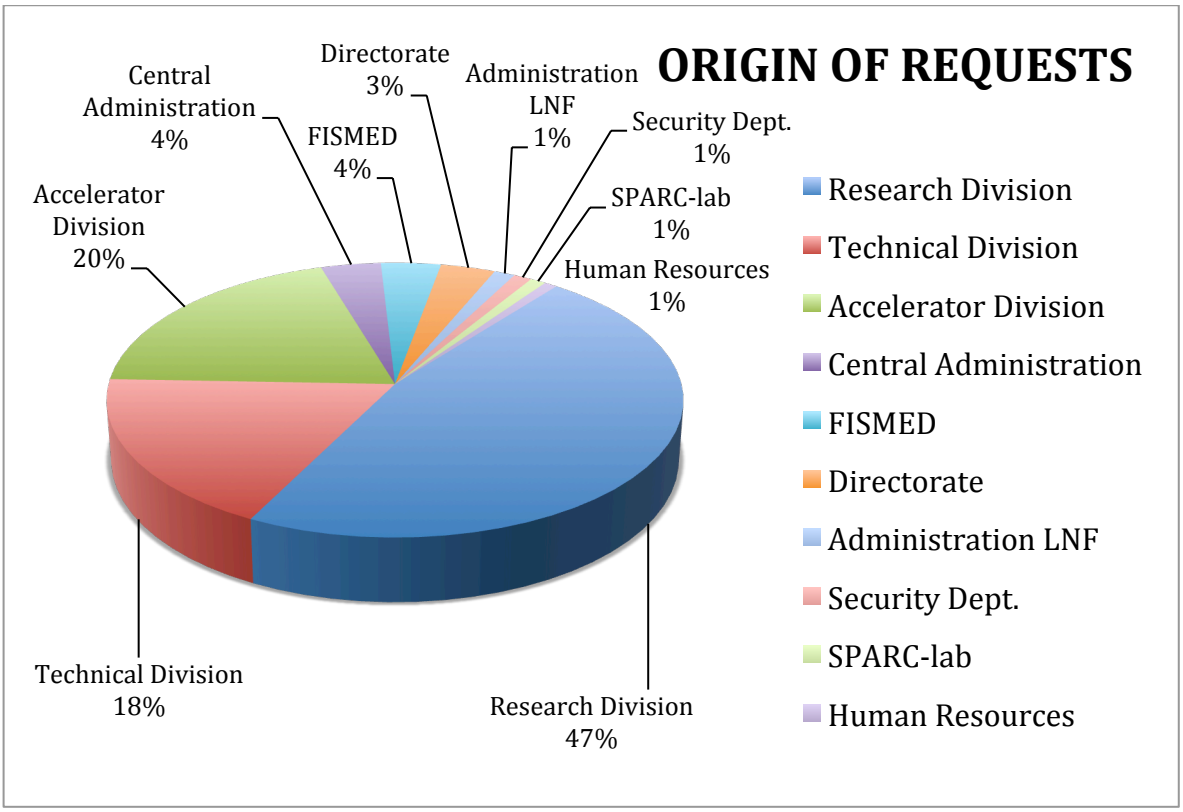

The following departments were involved in the requests:

| DEPTS INVOLVED | n. |
|---|---|
| General Services | 200 |
| Building Management | 123 |
| SPCM | 119 |
| Telephone Dept. | 86 |
| Electricity Dept. | 51 |
| HVAC | 29 |
| SMCA | 4 |
| **TOTALE** | **612** |

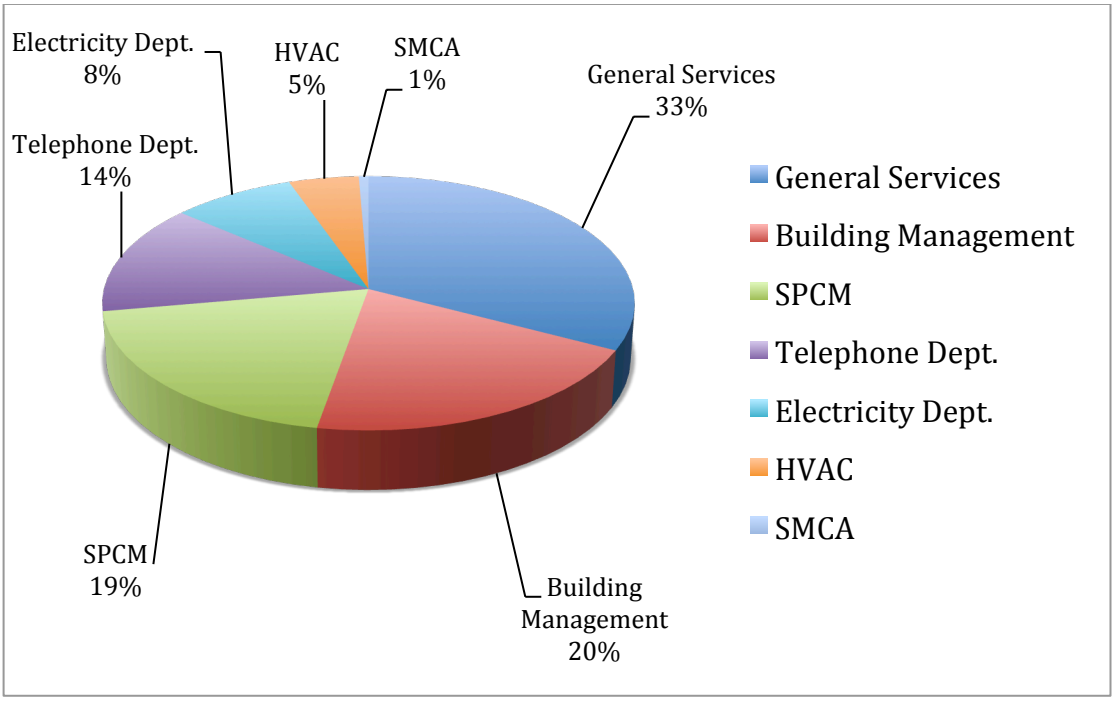


Beyond these requests, the normal scheduled maintenance activities on the research and general facilities of the LNF and electrical maintenance of the INFN Head Quarters in Rome took place.

## FINANCE

In 2014 the Technical Division spent over €4.500.000 (2013: €3.989.290,20), between the General Stores' budget, the Division's main budget, other TD-budgets (e.g. water supplies, insurances, phone bills, cleaning services, guards services, ...) and non TD-budgets (e.g. Accelerator Division, Infrastrutture Sperimentali,...), with a total of 331 Purchase Orders issued by its own Departments.

| **Budget** | **2014** | **2013** |
|---|---|---|
| General Stores | €88.633,52 | €74.917,37 |
| TD Main | €1.312.190,98 | €1.331.975,44 |
| Other TD | €2.409.884,38 | €2.326.855,16 |
| Other non TD | €721.532,64 | €255.542,23 |
| **TOTAL** | **€4.532.242,52** | **€3.989.290,20** |